Contract REPORT

Naval Facilities Engineering Service Center, Port Hueneme, CA 93043-4328

CR 94.003-SHR
June 1994

TRIAXIAL AND TORSIONAL SHEAR TEST RESULTS FOR SAND

An Investigation Conducted by:

Bruce L. Kutter
Yie-ruey Chen
C. K. Shen
Department of Civil and Environmental Engineering
University of California, Davis

Sponsored by

Office of Naval Research
Arlington, VA

Abstract This report presents the results of the laboratory tests conducted in triaxial and torsional apparatus. The purposes of this report are not only to support the calibration and verification of the bounding surface hypoplasticity model for granular soil but to provide a valuable data base for further research in numerical model simulation and design.

Under this contract, two experiments were carried out: (1) laboratory samples in the triaxial apparatus and hollow cylinder torsional apparatus, and (2) centrifuge model tests including two and three-dimensional structures subjected to static and dynamic loadings.

This report presents the results of triaxial tests including drained and undrained, monotonic and cyclic, and stress and strain controlled tests. The maximum stress ratio achieved in drained triaxial tests was significantly larger than that in undrained triaxial tests. Results of six hollow cylinder torsional and rotational shear tests are also presented. The results from different types are compared. Finally, the conclusions of these laboratory tests are also discussed.

The test results indicate that the shape of phase transformation and failure surfaces were different when viewed in the π-plane. It was also found that samples subject to rotational shear may be less likely to develop larger strain during undrained cycling than samples in triaxial compression/extension cyclic tests at similar stress ratios.

In the cyclic torsional simple shear test, the maximum stress ratio is between values obtained from triaxial compression and extension tests. In rotational shear tests, the stable cycling of effective stress ratios are bounded by the values of triaxial compression and extension failure stress ratios. The maximum stress ratio observed in the rotational shear tests for both compression and extension agree reasonably well with the stress ratio in the undrained triaxial tests.

METRIC CONVERSION FACTORS

Approximate Conversions to Metric Measures

Symbol	When You Know	Multiply by	To Find	Symbol
		LENGTH		
in	inches	*2.5	centimeters	cm
ft	feet	30	centimeters	cm
yd	yards	0.9	meters	m
mi	miles	1.6	kilometers	km
		AREA		
in^2	square inches	6.5	square centimeters	cm^2
ft^2	square feet	0.09	square meters	m^2
yd^2	square yards	0.8	square meters	m^2
mi^2	square miles	2.6	square kilometers	km^2
	acres	0.4	hectares	ha
		MASS (weight)		
oz	ounces	28	grams	g
lb	pounds	0.45	kilograms	kg
	short tons (2,000 lb)	0.9	tonnes	t
		VOLUME		
tsp	teaspoons	5	milliliters	ml
Tbsp	tablespoons	15	milliliters	ml
fl oz	fluid ounces	30	milliliters	ml
c	cups	0.24	liters	l
pt	pints	0.47	liters	l
qt	quarts	0.95	liters	l
gal	gallons	3.8	liters	l
ft^3	cubic feet	0.03	cubic meters	m^3
yd^3	cubic yards	0.76	cubic meters	m^3
		TEMPERATURE (exact)		
°F	Fahrenheit temperature	5/9 (after subtracting 32)	Celsius temperature	°C

*1 in = 2.54 (exactly). For other exact conversions and more detailed tables, see NBS Misc. Publ. 286, Units of Weights and Measures, Price $2.25, SD Catalog No. C13.10:286.

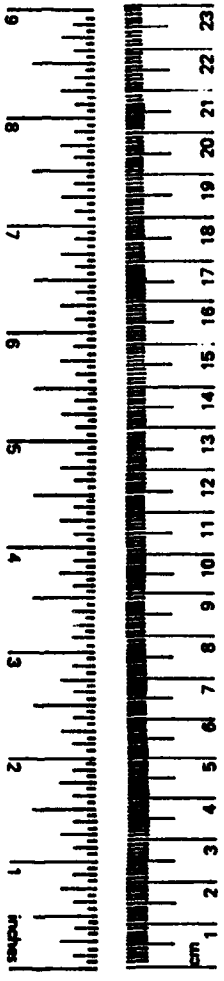

Approximate Conversions from Metric Measures

Symbol	When You Know	Multiply by	To Find	Symbol
		LENGTH		
mm	millimeters	0.04	inches	in
cm	centimeters	0.4	inches	in
m	meters	3.3	feet	ft
m	meters	1.1	yards	yd
km	kilometers	0.6	miles	mi
		AREA		
cm^2	square centimeters	0.16	square inches	in^2
m^2	square meters	1.2	square yards	yd^2
km^2	square kilometers	0.4	square miles	mi^2
ha	hectares (10,000 m^2)	2.5	acres	
		MASS (weight)		
g	grams	0.035	ounces	oz
kg	kilograms	2.2	pounds	lb
t	tonnes (1,000 kg)	1.1	short tons	
		VOLUME		
ml	milliliters	0.03	fluid ounces	fl oz
l	liters	2.1	pints	pt
l	liters	1.06	quarts	qt
l	liters	0.26	gallons	gal
m^3	cubic meters	35	cubic feet	ft^3
m^3	cubic meters	1.3	cubic yards	yd^3
		TEMPERATURE (exact)		
°C	Celsius temperature	9/5 (then add 32)	Fahrenheit temperature	°F

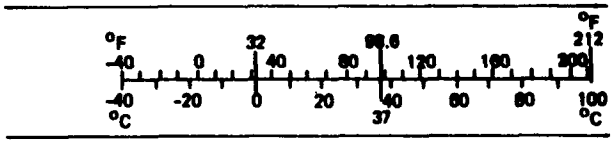

REPORT DOCUMENTATION PAGE

Form Approved
OMB No. 0704-018

1. AGENCY USE ONLY *(Leave blank)*	2. REPORT DATE	3. REPORT TYPE AND DATES COVERED
	June 1994	Final; October 1990 - June 1994

4. TITLE AND SUBTITLE

TRIAXIAL AND TORSIONAL SHEAR TEST RESULTS FOR SAND

5. FUNDING NUMBERS

PE - 61153N
C - N47408-89-C-1058
WU - DN666342

6. AUTHOR(S)

Bruce L. Kutter; Yie-ruey Chen; and C. K. Shen

7. PERFORMING ORGANIZATION NAME(S) AND ADDRESSE(S)

Department of Civil and Environmental Engineering
University of California, Davis

8. PERFORMING ORGANIZATION REPORT NUMBER

CR 94.003

9. SPONSORING/MONITORING AGENCY NAME(S) AND ADDRESSES

Office of Naval Research
Arlington, VA 22170-5000

10. SPONSORING/MONITORING AGENCY REPORT NUMBER

11. SUPPLEMENTARY NOTES

12a. DISTRIBUTION/AVAILABILITY STATEMENT

Approved for public release; distribution is unlimited.

12b. DISTRIBUTION CODE

13. ABSTRACT *(Maximum 200 words)*

This report presents the results of the laboratory tests conducted in triaxial and torsional apparatus. The purposes of this report are not only to support the calibration and verification of the bounding surface hypoplasticity model for granular soil but to provide a valuable data base for further research in numerical model simulation and design.

Under this contract, two experiments were carried out: (1) laboratory samples in the triaxial apparatus and hollow cylinder torsional apparatus, and (2) centrifuge model tests including two and three-dimensional structures subjected to static and dynamic loadings.

This report presents the results of triaxial tests including drained and undrained, monotonic and cyclic, and stress and strain controlled tests. The maximum stress ratio achieved in drained triaxial tests was significantly larger than that in undrained triaxial tests. Results of six hollow cylinder torsional and rotational shear tests are also presented. The results from different types are compared. Finally, the conclusions of these laboratory tests are also discussed.

The test results indicate that the shape of phase transformation and failure surfaces were different when viewed in the π-plane. It was also found that samples subject to rotational shear may be less likely to develop larger strain during undrained cycling than samples in triaxial compression/extension cyclic tests at similar stress ratios.

In the cyclic torsional simple shear test, the maximum stress ratio is between values obtained from triaxial compression and extension tests. In rotational shear tests, the stable cycling of effective stress ratios are bounded by the values of triaxial compression and extension failure stress ratios. The maximum stress ratio observed in the rotational shear tests for both compression and extension agree reasonably well with the stress ratio in the undrained triaxial tests.

14. SUBJECT TERMS

Soil consititutive material models, bounding surface plasticity, cohesionless soil, sand, laboratory test data, triaxial test data, torsional test data, granular soil, cyclic test data, geotechnical models, finite element technology

15. NUMBER OF PAGES

204

16. PRICE CODE

17. SECURITY CLASSIFICATION OF REPORT	18. SECURITY CLASSIFICATION OF THIS PAGE	19. SECURITY CLASSIFICATION OF ABSTRACT	20. LIMITATION OF ABSTRACT
Unclassified	Unclassified	Unclassified	UL

TABLE OF CONTENTS

		Page No.
LIST OF FIGURES		3
LIST OF TABLES		5
ABSTRACT		6
1.	INTRODUCTION	7
	1.1 Background and Scope	11
	1.2 Soils Tested	11
	1.3 Testing Program	12
	1.4 Units, Stresses and Strains	21
2.	TRIAXIAL TESTS	23
	2.1 Sample Preparation	23
	2.2 Undrained, Strain Controlled, Constant p, Monotonic Tests	24
	2.3 Drained, Strain Controlled, Constant p', Monotonic Tests	27
	2.4 Undrained, Stress Controlled, Cyclic Tests	33
	2.5 Triaxial Consolidation Tests	34
3.	HOLLOW CYLINDER TORSIONAL TESTS	36
	3.1 Sample Preparation and General Observations	36
	3.2 Torsional Shear Tests	38
	3.3 Rotational Shear Tests	41
4.	SUMMARY COMPARISONS OF TRIAXIAL, TORSIONAL AND ROTATIONAL SHEAR TEST RESULTS	45
5.	CONCLUSIONS	50
6.	ACKNOWLEDGEMENTS	51
7.	REFERENCES	52

LIST OF FIGURES

Figure 1.2.1 : Grain Size Distribution Curve for Nevada Sand

Figure 1.3.1 : Schematic of Triaxial Apparatus

Figure 1.3.2 : Typical Stress Path for Triaxial Tests

Figure 1.3.3 : Schematic of Hollow Cylinder Torsional Apparatus

Figure 1.3.4 : Stress Paths for Hollow Cylinder Torsional Tests

Figure 2.2.a : Summary Plot for Deviatoric Stress Versus Mean Normal Effective Stress in Triaxial Undrained Tests Under Different Confining Pressure

Figure 2.2.b : Summary Plot for Deviatoric Stress Ratio Versus Mean Normal Effective Stress in Triaxial Undrained Tests Under Different Confining Pressure

Figure 2.2.1
↓ : Triaxial, Undrained, Strain Controlled, Constant p Test
Figure 2.2.26

Figure 2.3.a : Photograph of the Colored Sand After Triaxial Test N70D100A

Figure 2.3.b : Sketch of the Vertical Offset of the Sample After Triaxial Test

Figure 2.3.c : Measurements of the Vertical Offset from Photograph of Sample (N70D100A)

Figure 2.3.d : Comparisons of Data Measured from Load Cells Mounted on Both Inside and Outside of Triaxial Chamber

Figure 2.3.1
↓ : Triaxial, Drained, Strain Controlled, Constant p' Test
Figure 2.3.10

Figure 2.4.1
↓ : Triaxial, Undrained, Stress Controlled, Cyclic Test
Figure 2.4.35

Figure 2.5.1
↓ : Triaxial Consolidation Test
Figure 2.5.8

Figure 3.2.1
↓ : Hollow Cylinder Cyclic Torsional Shear Test
Figure 3.2.20

Figure 3.3.1
↓ : Hollow Cylinder Rotational Shear Test
Figure 3.3.10

Figure 4.1 : Summary Data for Cyclic Stress Ratio Versus Number of Cycles to Cause 3% Strain in Triaxial, Torsional and Rotational Shear Tests

Figure 4.2 : Relationship Between Cyclic Strain and Number of Cycles in Hollow Cylinder Cyclic Torsion Shear Tests

Figure 4.3 : Relationship Between Stress Ratio and Angle in π Plane for Hollow Cylinder Cyclic Torsion Shear Tests

Figure 4.4. : Summary Plot for Peak Stress Ratio Versus Angle in π Plane in Triaxial and Cyclic Simple Shear Tests with Stress Paths of the Last Cycle of Torsional and Rotational Shear Tests

Figure 4.5 : Summary Plot for Stress Ratio Versus Mean Normal Effective Stress in Triaxial Compression and Extension Tests

LIST OF TABLES

Table 1.1 : Summary of Some Earlier Studies in Triaxial Tests

Table 1.2 : Summary of Some Earlier Studies in Hollow Cylinder Apparatus

Table 1.2.1 : Summary of Specific Gravity, Dry Density and Void Ratio for Nevada Sand

Table 1.2.2 : Summary of Permeability Test Results for Nevada Sand

Table 1.2.3 : Summary of Sieve Analysis for Nevada Sand

Table 1.3.1 : Nomenclature Used for Designation of Triaxial Tests

Table 1.3.2 : Nomenclature Used for Designation of Data Files

Table 1.3.3 : Nomenclature Used for Designation of Hollow Cylinder Torsional Tests

Table 2.2.1 : Summary of Triaxial, Undrained, Strain Controlled, Constant p Test Data for Nevada Sand

Table 2.3.1 : Summary of Triaxial, Drained, Strain Controlled, Constant p' Test Data for Nevada Sand

Table 2.4.1 : Summary of Triaxial, Undrained, Stress Controlled, Cyclic Test Data for Nevada Sand

Table 2.5.1 : Summary of Triaxial, Consolidation and Rebound Test Data for Nevada Sand

Table 2.5.2 : Summary of Compression Index λ and Rebound index κ for Nevada Sand

Table 3.2.1 : Summary of Hollow Cylinder Undrained, Stress Controlled, Cyclic Torsional Shear Test Data for Nevada Sand

Table 3.3.1 : Summary of Hollow Cylinder Undrained, Stress Controlled, Rotational Shear Test Data for Nevada Sand

1. INTRODUCTION

In geotechnical engineering practice, laboratory tests play an important role. In the past 30 years, a variety of apparatuses for laboratory shear tests such as triaxial, simple shear and hollow cylinder torsional shear tests have been developed. In conventional triaxial tests, the intermediate principal stress is equal to either the major or minor principal stress. A 90° jump in the major principal stress may occur, but continuous rotation is not possible in a triaxial apparatus. In most field problems, however, the principal stress directions rotate continuously. Table 1.1 lists the summary of some earlier studies in the conventional triaxial tests for sand. Most of the hollow cylinder torsional shear test apparatuses have the capability of rotating the major principal stress directions with different magnitude of stress ratio. Table 1.2 lists a summary of some earlier studies of sand behavior in a torsional hollow cylinder apparatus.

In spite of its limited ability to rotate principal stresses, the triaxial test is a relatively simple and accurate testing method. In the field problems involving soil strength and deformation behavior, the effects of the magnitude of the stress ratio are more important than those of the rotation of principal stress directions. Therefore, triaxial tests are extremely useful.

In this study, the results of laboratory testing of granular soil for the calibration and verification of the bounding surface hypoplasticity model for granular soils (Wang and Dafalias 1990 and Li 1992) are presented. These tests included general tests (e.g. particle size analysis, maximum and minimum dry density and permeability test), triaxial tests and hollow cylinder torsional tests. All of the laboratory test results reported were performed at The University of California in Davis (UCD). Several types of triaxial tests including both drained and undrained, monotonic and cyclic tests were performed. In the hollow cylinder test samples, both cyclic torsional and rotational shear tests which involved rotation of principal stress directions were performed.

This report is compiled in two parts. The first part is written in five sections including the introduction (Section 1), triaxial tests (Section 2), hollow cylinder torsional tests (Section 3),

summary comparisons (Section 4) and conclusions (Section 5). Afterward, summary tables of test conditions, plots of all laboratory test results and summary plots of comparisons are presented in sequence in the appendix of this report. Figures and tables presented in the first part are directly related to the contents of the text.

The background of this research, the material used in the laboratory tests and the laboratory programs are introduced in Section 1.1, Section 1.2 and Section 1.3, respectively. Finally, the units and the stress and strain definitions used in this report are described in Section 1.4.

Table 1.1: List of Some Earlier Studies in Triaxial Tests

Reference	Test Program	Subject of Investigation
Bishop & Green (1965)	Compression	Influence of end restraint
Seed & Lee (1966)	Cyclic	Liquefaction
Arthur & Menzies (1972)	Compression	Inherent anisotropy
Castro (1975)	Cyclic	Liquefaction and cyclic mobility
Ishihara et al. (1975)	Cyclic	Undrained deformation and liquefaction
Townsend (1978)	Cyclic	Factors affecting triaxial test
Seed (1979)	Cyclic	Liquefaction
Shankariah & Ramamurthy (1980)	Compression / Extension	Anisotropy of sand
Hettler & Vardoulakis (1984)	Compression	Behavior of dry sand
Vaid & Chern (1985)	Cyclic	Undrained response of sand
Lam & Tatsuoka (1988)	Compression / Extension	Effects of initial anisotropy and deformation of sand
Gilbert & Marcuson (1988)	Cyclic	Density variation in specimen
Riemer et al. (1990)	Compression	steady state strength
Chu et al. (1992)	Compression	Strain-softening behavior in strain-path test

Table 1.2: List of Some Earlier Studies in Hollow Cylinder Apparatus

Reference	Rotation of Principal Stress Direction	Subject of Investigation
Kirkpatrick (1957)	No	Influence of σ_2 on failure of sand
Whitman & Luscher (1962)	No	Strength characteristics of hollow cylinders of sand
Wu et al (1963)	No	Failure envelope
Broms & Jamal (1965)	No	Analysis of triaxial test on sand
Ersig & Bemben (1965)	No	Failure condition in sand
Barden & Proctor (1971)	No	Drained strength of granular material
Jamal (1971)	No	Shear Strength of sand
Ishibashi & Sherif (1974)	Yes	Effect of K_0 on liquefaction
Ishihara & Yasuda (1975)	Yes	Liquefaction of sand under irregular cyclic loading
Lade (1975)	Yes	Influence of stress reorientation on stress-strain behavior
Ishihara et al. (1980)	Yes	Effect of principal stress rotation on liquefaction
Dusseault (1981)	No	Tunneling and pressuremeter testing in sand
Muramatsu & Tatsuoka (1981)	Yes	Cyclic undrained stress-strain behavior
Saada & Townsend (1981)	Yes	Strength of soil
Tatsuoka et al. (1982)	Yes	Cyclic undrained stress-strain behavior of dense sand
Hight et al. (1983)	Yes	Effects of principal stress rotation
Yamada & Ishihara (1983)	Yes	Undrained deformation of sand
Towhata & Ishihara (1985)	Yes	Undrained strength of sand
Alarcon et al. (1986)	Yes	Stress-strain characteristic of sand
Miura et al. (1986)	Yes	Deformation of anisotropic sand
Saada (1988)	Yes	Advantage / Limitation of devices
Vaid et al. (1990)	Yes	Generalized stress-path-dependent soil behavior
Pradel et al (1990)	Yes	Yielding and flow of sand
Wijewickreme & Vaid (1991)	Yes	Stress Nonuniformity
Gutierrez et al. (1991)	Yes	Flow theory for sand
Gutierrez & Ishihara (1993)	Yes	Deformation of sand
Yamashita & Toki (1993)	Yes	Anisotropy of sand

(Note: part of this list is obtained from Hight et al. 1983)

1.1. Background and Scope

A three year research program entitled "Validation of A Proposed Rational Material Characterization for Granular Soil" has been conducted at the University of California, Davis. The overall objective was to develop and validate the proposed hypoplasticity model for sand (Wang and Dafalias 1990). The objective of the present research focused on developing an experimental data base as follows:

Conduct a variety of triaxial and hollow cylinder torsional tests. These involved monotonic and cyclic drained and undrained tests. In the hollow cylinder torsional tests, the effects of rotation of principal stress direction were also to be investigated.

Parallel studies existed as follows:

(1) Determine the parameters of the hypoplasticity model using the data obtained in triaxial and hollow cylinder torsional tests report by Chen and Kutter (1993).

(2) Conduct variety of centrifuge model tests involving static and dynamic loading of saturated and dry sand to obtain data from boundary value problems for comparison with dynamic finite element analysis. The results of these model studies are described in separate reports (Wilson and Kutter, 1993).

1.2. Soils Tested

Nevada sand was used to perform the laboratory tests. This sand was the same material used throughout the VELACS (Verification of Liquefaction Analysis by Centrifuge Studies) project (Arulanandan and Scott, 1993).

Saturated fine grained Nevada sand was used in all of the reported triaxial and torsional tests. Attempts were made to also study the behavior of a coarse sand, but difficulty arose due to effects of membrane penetration, therefore, the results of the tests in coarse sand are not presented.

1.3. Testing Program

The laboratory tests in this report are divided into three groups: general tests, triaxial tests and hollow cylinder torsional tests.

1. General tests:

The general tests included maximum and minimum dry density tests, permeability tests and particle-size analysis. The maximum and minimum dry densities represent the densest and loosest packing of particles without crushing the grains. The standard test methods ASTM D4253-83 and D4254-83 were used to determine the maximum and minimum dry densities, respectively.

Void ratio is the ratio between the volume of voids and the volume of solid particles in a mass of soil. The amount of void space within a soil has an important effect on its characteristics. The specific gravity is the ratio between the mass of dry solids and the mass of distilled water displaced by the dry soil particles. The summary of specific gravity, dry density and void ratio for Nevada sand is shown in Table 1.2.1.

The permeability of a soil is a measure of its capacity to allow the flow of a fluid through it. The fluid concerned in this report is water. Permeability depends on a number of factors (i.e. particle size, shape, void ratio, degree of saturation, type of flow and temperature). It is, however, an important parameter for analysis of flow of water in boundary value problems. The permeability of Nevada sand, measured in the vertical direction, is summarized in Table 1.2.2 for various relative densities

Particle size analysis is used for classification of granular soil's particles into a separate range. Summaries of sieve analysis and grain size distribution for Nevada sand are shown in Table 1.2.3 and Figure 1.2.1, respectively.

Table 1.2.1 : Summary of Specific Gravity, Dry Density and Void Ratio for Nevada Sand

Gs	γ_{dmax}(kN/m³)	γ_{dmin}(kN/m³)	e_{max}	e_{min}
2.67	17.33	13.87	0.887	0.551

Table 1.2.2 : Summary of Permeability Test Results for Nevada Sand

RELATIVE DENSITY (%)	PERMEABILITY (cm/sec)
91.0	$2.3*10^{-3}$
60.1	$5.6*10^{-3}$
40.2	$6.6*10^{-3}$

(Data Source: Earth Technology Co., 1991)

Table 1.2.3 : Summary of Sieve Analysis for Nevada Sand

Sieve #	30	40	60	100	140	200
Percentage Passing	99.7	98.4	91.1	40.4	17.1	5.4

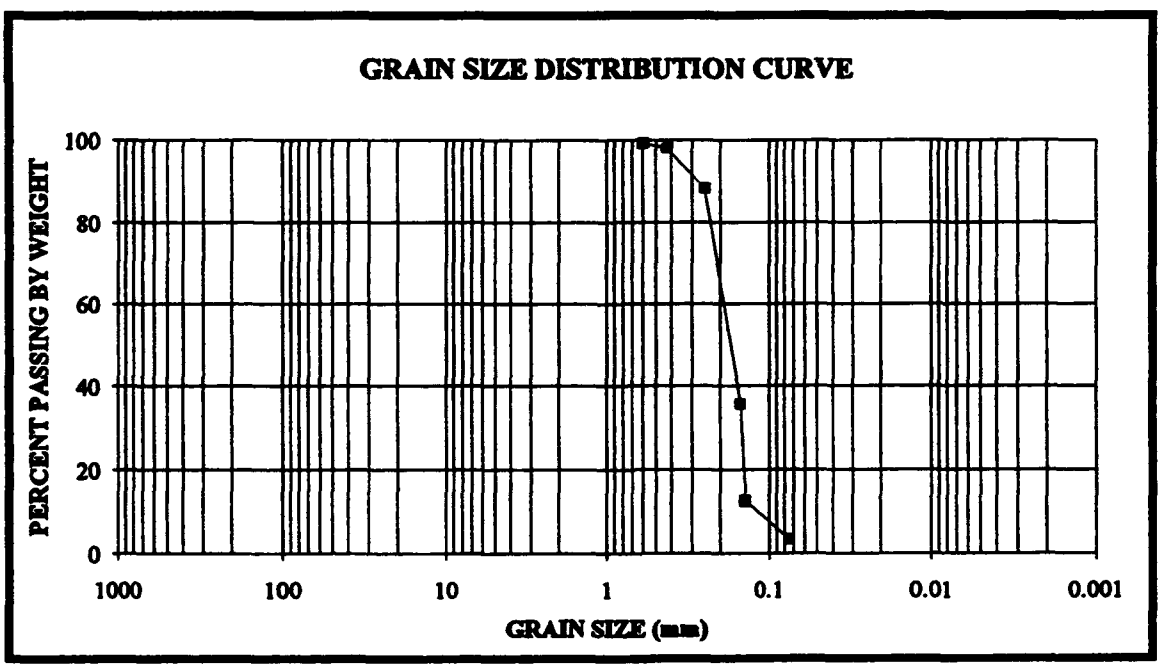

Figure 1.2.1 : Grain Size Distribution Curve for Nevada Sand

2. Triaxial tests:

Several types of tests were performed in a computer controlled triaxial apparatus. They included both undrained and drained, monotonic and cyclic tests. The triaxial test is a standard test in geotechnical engineering research. It consists of loading a cylindrical sample of soil with variable lateral pressure and an axial load. A schematic of the triaxial apparatus is shown in Figure 1.3.1. Table 1.3.1 shows the nomenclature used for designation of the triaxial tests, and Table 1.3.2 indicates the nomenclature used for computer data files. Diskette copies of the test data will be made available to interested readers. They can be obtained by contacting the first author of this report. Schematic stress paths for triaxial tests are illustrated in Figure 1.3.2 to assist the reader in understanding of the nomenclature.

The procedures of triaxial tests can be related to numerous types of practical problems. The triaxial apparatus can control the magnitude (not the orientation) of the principal stresses, the drainage and the measurement of pore water pressure. Test results derived from triaxial tests can provide valuable information for the understanding of soil behavior as well as soil properties for use in numerical model simulation and practical design.

3. Hollow cylinder torsional tests:

The torsional shear tests were performed in the UCD hollow cylinder torsional apparatus. They included torsional shear and rotational shear tests. Figure 1.3.3 shows the schematic of the hollow cylinder torsional apparatus. The nomenclature used for designation of data files and torsional tests are shown in Tables 1.3.2 and 1.3.3, respectively.

During the past 30 years, many experimental and analytical procedures have been developed for evaluating the liquefaction potential of soil deposit. Generally, procedures developed in early days were formulated on unidirectional basis by simplifying the soil condition during earthquake shaking. The triaxial test (explained in previous section) is widely used to characterize soil in the field and to provide the data base for soil constitutive laws. However, it is known that triaxial testing can not account for multi-directional shear which has been recognized

to represent the real field conditions. Rotational shear, a special case of non-proportional loading, can only take place under multi-directional loading conditions. Rotational shear is defined in this report as a stress path for which the second invariant of the deviatoric stress tensor, J, is constant while the directions of the principal stress rotate. Figure 1.3.4 shows different stress paths used for torsional tests. The hollow cylinder torsional apparatus has the capability of controlling the three normal stresses (σ_z σ_r and σ_θ) independently, and in addition, it can apply a shear stress, $\sigma_{z\theta}$, which the triaxial apparatus can not apply. For tests presented in this report, σ_r and σ_θ were held equal to each other.

Table 1.3.1 : Nomenclature Used for Designation of Triaxial Tests

NO.	NOMENCLATURE	DESCRIPTION
1	CIUC/E	Isotropically-consolidated one cycle undrained compression and reversed extension triaxial test.
2	CIUE/C	Isotropically-consolidated one cycle undrained extension and reversed compression triaxial test.
3	CIUC	Isotropically-consolidated monotonic undrained compression triaxial test.
4	CIUE	Isotropically-consolidated monotonic undrained extension triaxial test.
5	CIDC/E (p'=Constant)	Isotropically-consolidated one cycle drained compression and reversed extension triaxial test.
6	CIDE/C (p'=Constant)	Isotropically-consolidated one cycle drained extension and reversed compression triaxial test.
7	CIDC (p'=Constant)	Isotropically-consolidated monotonic drained compression triaxial test.
8	CIDE (p'=Constant)	Isotropically-consolidated monotonic drained extension triaxial test.
9	CIUCyclic	Isotropically-consolidated stress-controlled undrained cyclic test.

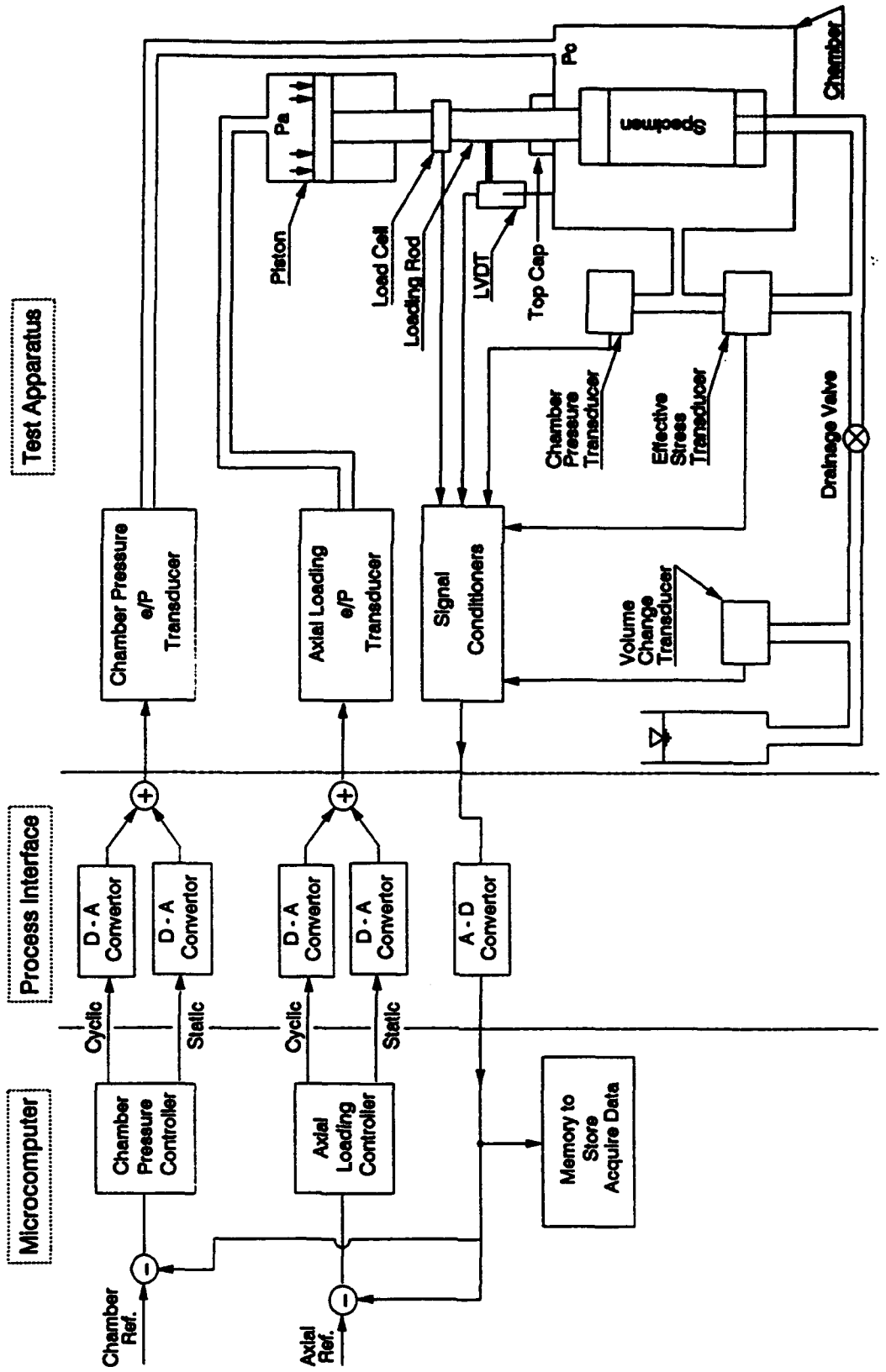

Figure 1.3.1 : Schematic of Triaxial Apparatus

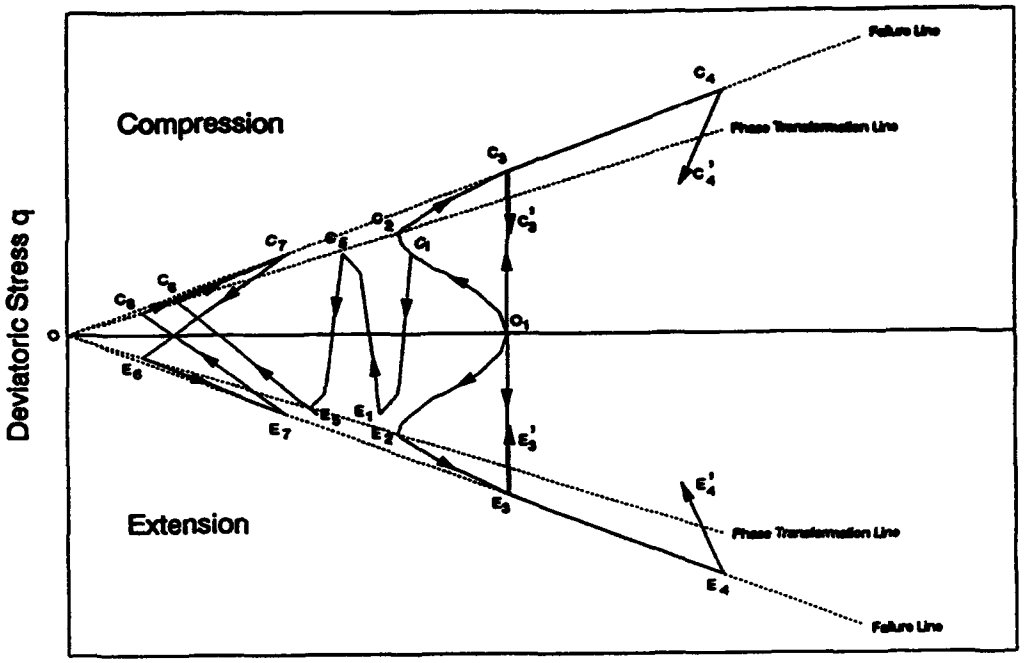

TEST	PATH
CIUC/E	O O_1 C_1 C_2 C_4 C_4'
CIUE/C	O O_1 E_2 E_4 E_4'
CIUC	O O_1 C_1 C_2 C_4
CIUE	O O_1 E_2 E_4
CIDC/E (p'=Const.)	O O_1 C_3 E_3 O_1
CIDE/C (p'=Const.)	O O_1 E_3 C_3 O_1
CIDC (p'=Const.)	O O_1 C_3 C_3'
CIDE (p'=Const.)	O O_1 E_3 E_3'
CIUCylic	O O_1 C_1 E_1 C_5 E_5 C_6 C_7 E_6 E_7 C_8 ····· O

Figure 1.3.2 : Typical Stress Paths for Triaxial Tests

Table 1.3.2 : Nomenclature Used for Designation of Data Files

NOMENCLATURE	DESCRIPTION
N60Uxy	Normally consolidated, undrained, strain controlled, constant p test. 60 : intended relative density x : effective confining pressure y : test number
O60Uxy	Over consolidated, undrained, strain controlled, constant p test. 60 : intended relative density x : effective confining pressure y : test number
N70Dxy	Normally consolidated, drained, strain controlled, constant p' test. 70 : intended relative density x : effective confining pressure y : test number
CYxNy	Normally consolidated, undrained, stress controlled, cyclic test. x : effective confining pressure y : test number
CYxOy	Over consolidated, undrained, stress controlled, cyclic test. x : effective confining pressure y : test number
NRxCUy	Hollow cylinder anisotropically consolidated, undrained, stress controlled, rotational shear test. x : $(J_{2d}^{1/2})$ y : test number
NKxCUy	Hollow cylinder anisotropically consolidated, undrained, stress controlled, cyclic torsional shear test. x : (σ_θ/σ_z) y : test number

Table 1.3.3 Nomenclature Used for Designation of Hollow Cylinder Torsional Tests

NO.	NOMENCLATURE	DESCRIPTION
1	HCCAUTSCyclic	Hollow cylinder anisotropically consolidated, undrained, cyclic torsional shear tests.
2	HCCAURS	Hollow cylinder anisotropically consolidated, undrained, rotational shear tests

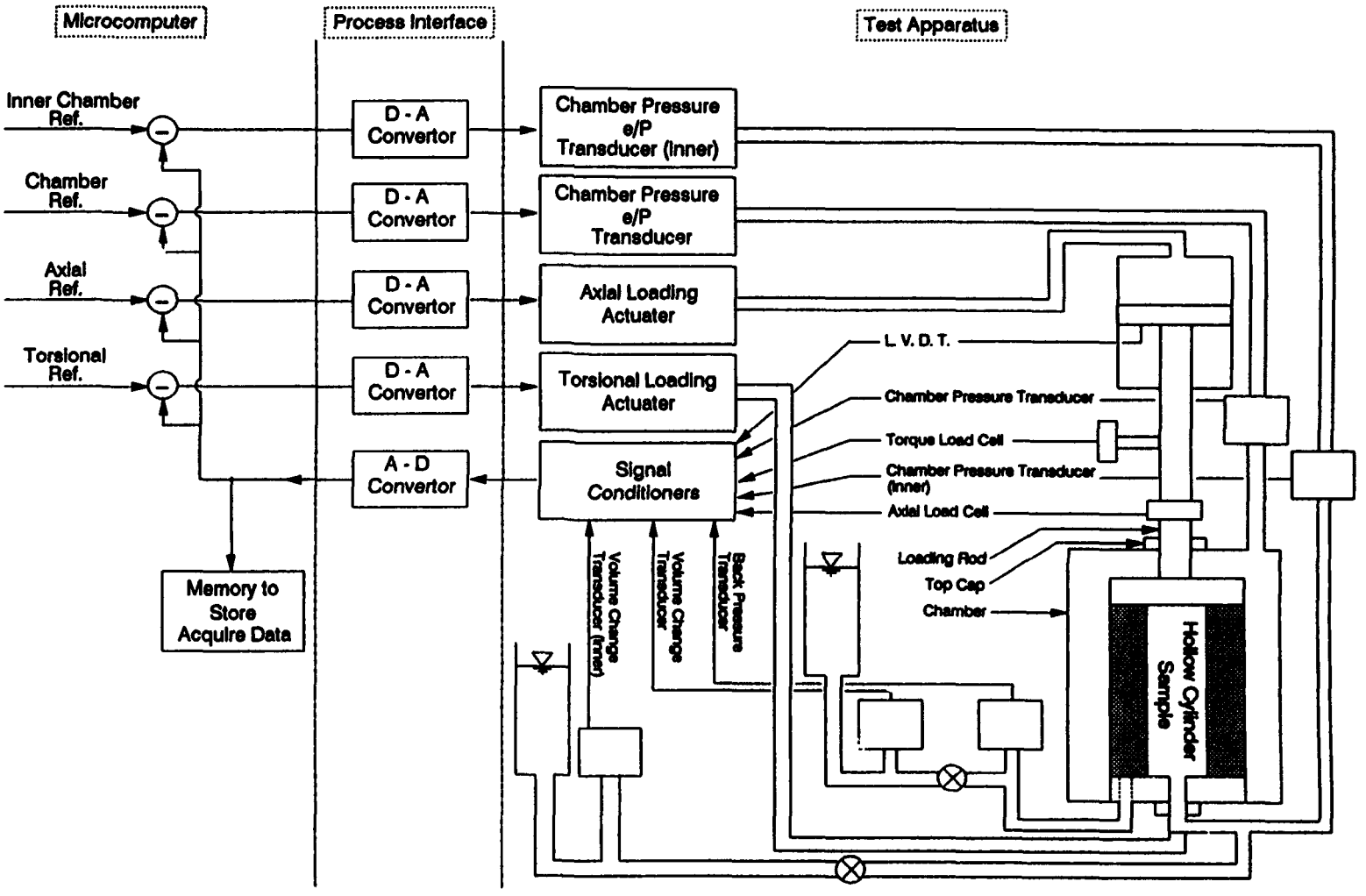

Figure 1.3.3 : Schematic of Hollow Cylinder Torsional Apparatus

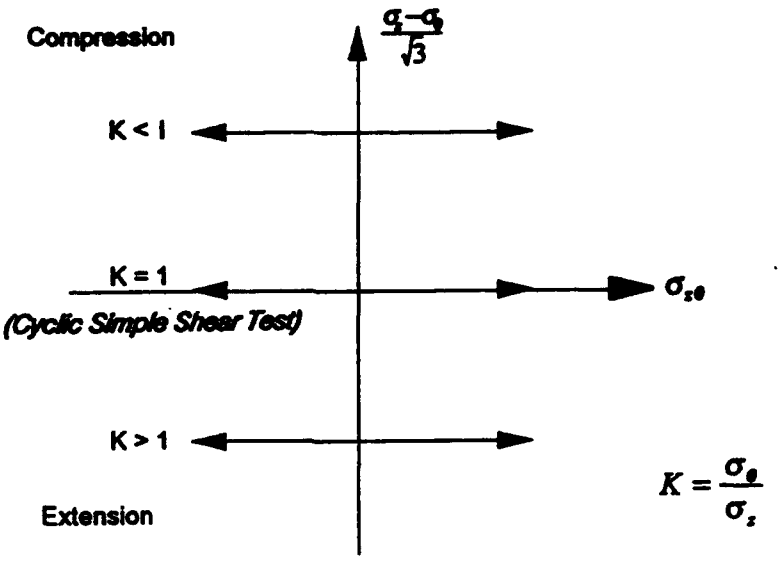

Cyclic Torsional Shear Test Paths

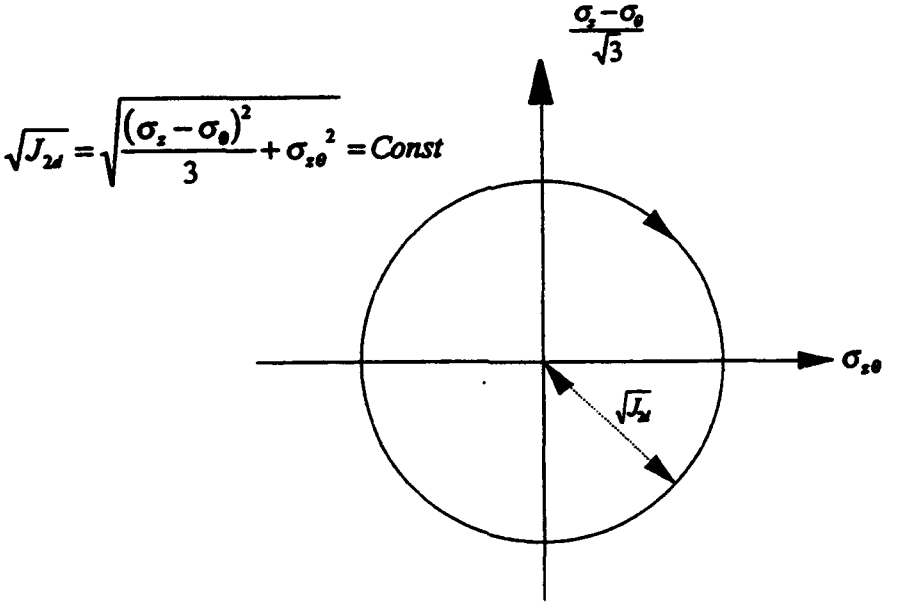

Rotational Shear Test Path

Figure 1.3.4 : Stress Paths for Hollow Cylinder Torsional Tests

1.4. Description of Units, Stresses and Strains

1. Units: The SI system of units are used in this report.

2. Stresses and strains:

$J_{2d} = \frac{1}{2} S_{ij} S_{ij}$	: second invariant of deviatoric stress tensor
$S_{ij} = \sigma_{ij} - p\delta_{ij}$	: deviatoric stress tensor
δ_{ij}	: Kronecker delta
$p = \sigma_{ii}/3$	: mean normal stress
p'	: mean normal effective stress
$J = \sqrt{J_{2d}}$	: isotropic invariant of deviatoric stress
$R = J/p'$	: stress ratio invariant
$\theta = \frac{1}{3} Cos^{-1}\left[3\sqrt{3}/2\left(J_{3d}/J_{2d}^{3/2}\right)\right]$	: Angle in π plane (Lode angle + 30°)
$J_{3d} = \frac{1}{3} S_{ij} S_{jm} S_{mi}$	: third invariant of stress tensor
$c = R_{extension}/R_{compression}$	: shape parameter in deviatoric plane

In the above definition, the summation convention for repeated indices is assumed.

For triaxial tests: $(\sigma_1 \neq \sigma_2 = \sigma_3)$

σ_1	: total vertical stress
σ_1'	: effective vertical stress
$\sigma_2 = \sigma_3$	: total lateral stresses
σ_2', σ_3'	: effective lateral stresses
u	: pore water pressure
σ_c'	: confining pressure
$p' = (\sigma_1' + 2\sigma_3')/3$	: mean normal effective stress
$p = p' + u$	: mean normal stress

$q = \sigma_1 - \sigma_3$	: deviatoric stress
ε_1	: axial strain
$\varepsilon_2 = \varepsilon_3$	: lateral strains
$\varepsilon_v = \varepsilon_1 + 2\varepsilon_3$	: volumetric strain
$\varepsilon_q = 2(\varepsilon_1 - \varepsilon_3)/3$	: deviatoric strain

For all cyclic torsional and rotational shear tests in this report, the internal and external cavity pressures were equal, thus $\sigma_\theta = \sigma_r$ and various stress and strain quantities are defined below:

$\sigma_{z\theta}$	: torsional shear stress
$J = \sqrt{J_{2d}} = \sqrt{(\sigma_z - \sigma_\theta)^2/3 + \sigma_{z\theta}^2}$	: second invariant of stress
$p = (\sigma_z + 2\sigma_\theta)/3$	: mean normal stress
$\varepsilon_{z\theta}$	: torsional shear strain
$\varepsilon_q = 2(\varepsilon_z - \varepsilon_\theta)/3$	: triaxial deviatoric strain
$K = \sigma_\theta/\sigma_z$	: coefficient of lateral pressure

For frictional materials, the ratio of shear to normal stress is known to be most important parameter in characterizing the proximity of the stress state to a failure condition. $R = J/p'$ is a parameter which characterizes the ratio of shear to normal stress in principal stress space. It is known that the value of R at failure, R_f, depends on the angle in the π plane, θ. The value of R at which phase transformation occurs is also a function of θ. This report will use f, p, c and e as subscripts to indicate failure, phase transformation, compression ($\theta = 0$) and extension ($\theta = \pi/6$), respectively.

2. TRIAXIAL TESTS

This section provides all triaxial test information in this project. Sample preparation is described in Section 2.1 and test results accomplished from different types of triaxial tests are presented in Section 2.2 to 2.5. These tests include undrained and drained strain controlled constant p tests (Section 2.2 and 2.3), undrained stress controlled cyclic tests (Section 2.4) and isotropic consolidation tests (Section 2.5). In addition, the typical stress paths for different types of triaxial tests are shown in Figure 1.3.2.

2.1. Sample Preparation

The samples for this study were prepared by pluviation through a 20 inch high Plexiglas cylinder. The sand was fed by hand using a funnel through a #16 sieve at the top of the cylinder. For most of the tests, the relative density was approximately 70%. In a few tests, the sand was tested at much lower densities. The diameter and height of sample were about 71 mm and 150 mm, respectively. The top and bottom sides of sand sample were covered by the Plexiglas pedestals. In order to allow drainage of sample and measurement of pore water pressure, these Plexiglas pedestals were inlaid with porous stones (diameter = 0.5 inches).

2.2. Triaxial Undrained Strain Controlled Constant p Tests (CIUC/E, CIUE/C, CIUC or CIUE)

The results of 26 undrained strain controlled triaxial tests are reported. These results (q vs. p', q vs. ε_1 and p' vs. ε_1) are shown in Figure 2.2.1 to Figure 2.2.26. These tests were performed with various combinations of Overconsolidation Ratio (OCR), confining pressure, compression/extension or back pressure. To check the saturation of the soil specimens, the pore pressure coefficient (B value) was measured. The B value is the ratio of the increase in pore pressure to increase in total stress p during isotropic compression while the sample is undrained. The increase of pore pressure was recorded while the cell pressure was increased by 50 kPa for all B value measurements. The summary table for these tests is shown on Table 2.2.1.

Some important observations are:

1. The stress ratios $\left(R = \sqrt{J_{2d}}/p'\right)$ at failure (peak stress ratio) and phase transformation were obtained from the average of several test results (Figure 2.2.a and 2.2.b) as listed in the following:

For undrained compression tests:

phase transformation stress ratio : R_{pc}=0.556

failure stress ratio : R_{fc}=0.853

For undrained extension tests:

phase transformation stress ratio : R_{pe}=0.467

failure stress ratio : R_{fe}=0.524

The phase transformation is the line corresponding to the transformation from compression to dilation behavior due to deviatoric loading (see Figure 1.3.2).

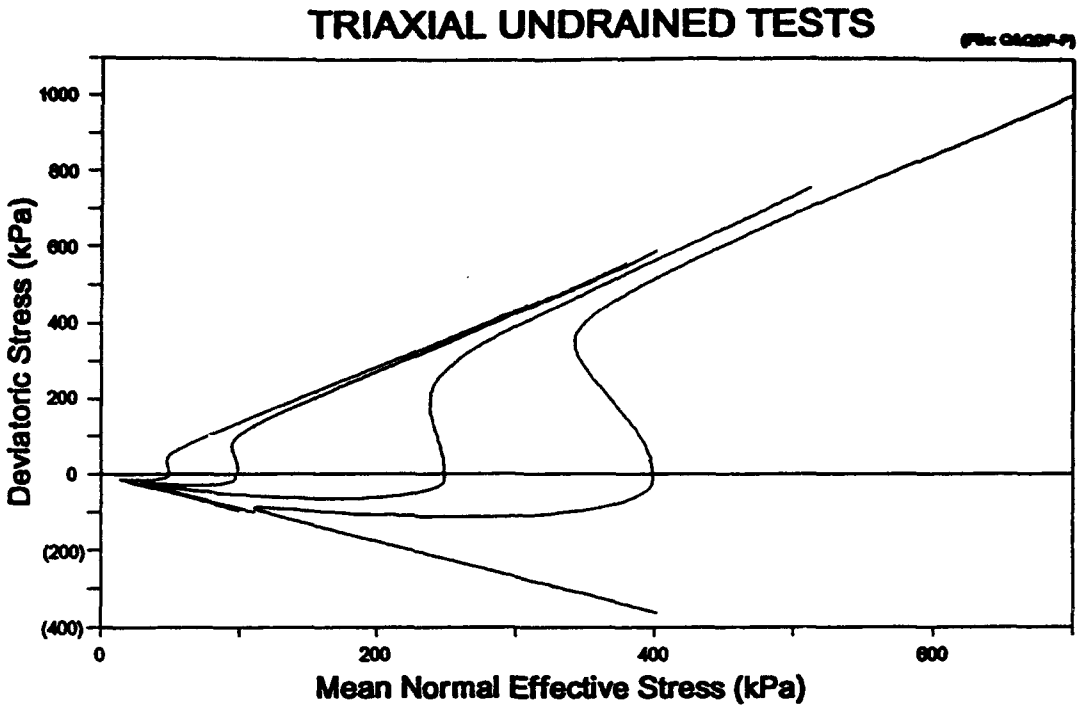

Figure 2.2.a : Summary Plot for Deviatoric Stress Versus Mean Normal Effective Stress in Triaxial Undrained Tests Under Different Confining Pressure

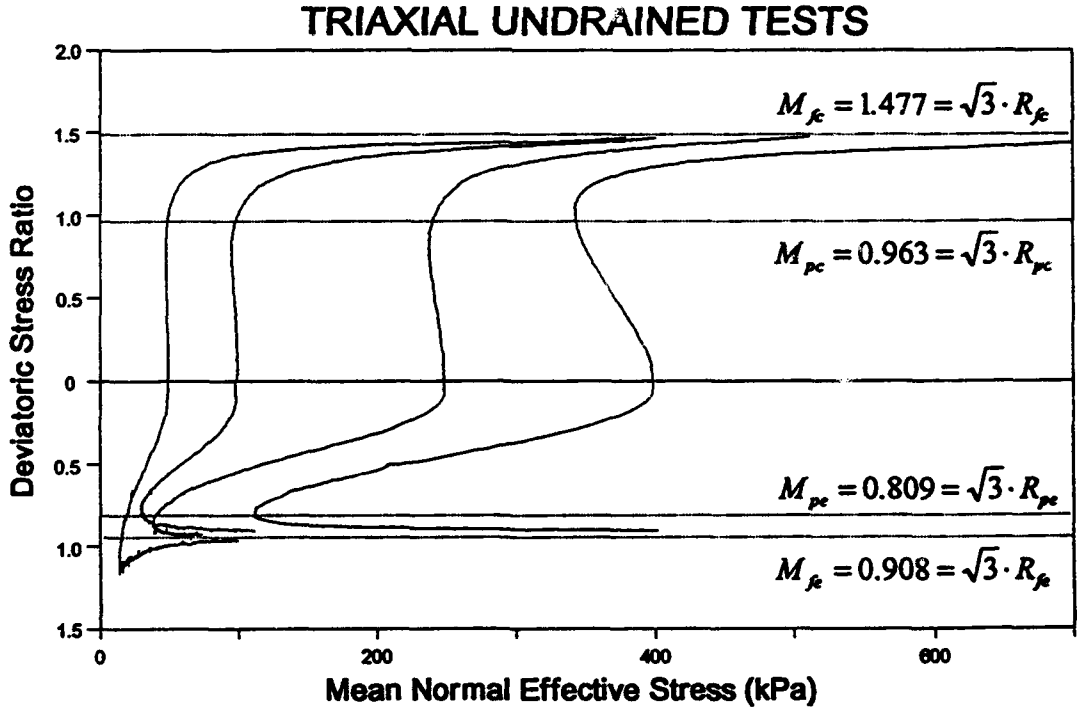

Figure 2.2.b : Summary Plot for Deviatoric Stress Ratio Versus Mean Normal Effective Stress in Triaxial Undrained Tests Under Different Confining Pressure

2. The ratio $R_{pe}/R_{pc}=c_p=0.84$ is different from the ratio at failure $R_{fe}/R_{fc}=c_f=0.61$. This is significant because the hypoplasticity model assumes that $c_f=c_p=c$.

3. Reasonable repeatability of results for tests which had similar testing conditions was obtained. In this report, for OCR=1, the CIUC/E tests at confining pressure = 100 kPa were repeated three times (Figure 2.2.2, 2.2.3 and 2.2.4), and repeated two times at both confining pressures = 250 kPa (Figure 2.2.5 and 2.2.6) and 400 kPa. (Figure 2.2.7 and 2.2.8) In addition, the CIUE tests (OCR=1) were repeated three times at confining pressure = 100 kPa (Figure 2.2.11, 2.2.12 and 2.2.13).

4. In almost every undrained test, the deviatoric stress increased until cavitation occurred. After cavitation, the deviatoric stress stabilized, but the stress ratio was observed to increase. In fact, after cavitation occurs the test essentially becomes a drained test.

Summary of important observations:

1. The hypoplasticity model shape parameter c ($c = R_{extension}/R_{compression}$) for failure and phase transformation are found to be different.

2. In triaxial undrained test, after cavitation the deviatoric stress stabilized but the stress ratio was observed to increased.

2.3. Triaxial Drained Strain Controlled Constant p' Tests (CIDC/E, CIDE/C, CIDC or CIDE)

The results of 10 drained, strain controlled, constant p' triaxial tests are reported. These results (ε_v vs. ε_1, q vs. ε_1 and q vs. ε_v) are shown in Figure 2.3.1 to Figure 2.3.10. To study shear band phenomena, 3 samples (N70D100A, B and C) were prepared with thin horizontal layers of dark sand. The thickness of dark sand layer was about 1 mm and the distance between two dark sand layers was about 25 mm. In addition, to determine the effects of friction in the apparatus on measurements made by the external load cell, 6 tests (N70D100A, B, C, P Q and R) were performed with a second load cell inside the triaxial chamber. The summary table for testing conditions of each test is shown on Table 2.3.1.

Some important observations are:

1. The maximum "failure" stress ratio R_f observed in drained tests was significantly larger than that in undrained tests. The average stress ratios $\left(R=\sqrt{J_{2d}}/p'\right)$ on failure line were 1.04 and 0.63 in drained compression and extension tests respectively. The ratio (i.e. shape factor in deviatoric plane) at failure c_f (c_f=R_{fe}/R_{fc}=0.6) in drained tests is closed to that in the undrained tests. The hypoplasticity model assumes that the shape parameter, c, is a unique value for both undrained and drained test conditions.

2. Most of the drained test results showed a peak followed by a drop of deviatoric stress. The drop began when the axial strain reached 6 to 8 % depending on the confining pressure. The drop was sometimes sudden and sometimes gradual, occurring while the axial strain increased by an additional 0.2 (Figure 2.3.8) to 3% (Figure 2.3.6). The drop in stress corresponded to a drop in the dilatancy rate and the formation of a shear band.

3. The samples with colored sand were dissected to observe any shear bands. From tests interrupted at 3.6% strain, prior to the drop in stress no shear band was apparent. From tests stopped at 8.5% strain after the drop was complete, it appears that the shear band was completely developed. A photograph of the colored sand is shown in Figure 2.3.a for test N70D100A.

4. An example sketch which indicates the offset of the sample after triaxial test (N70D100A) is presented in Figure 2.3.b. From results of three tests N70D100A, B and C, the thickness of the shear band appears to be about 10 to 12 times D_{50} (mean grain size). The failure planes were inclined at the angles between 63° and 65°. Figure 2.3.c shows the example measurements of the vertical offset from the photograph of sample N70D100A. The offset at the ends of the sample were measured to be 3.7 mm at the top and 9.15 mm at the bottom of the sample. From Figure 2.3.4, the axial strain at the end of test, ε_e, was 8.4%. Once the shear band is formed, it may be assumed that all of the deformation occurs on the shear band. Therefore, the axial strain corresponding to the formation of the shear band, ε_i, can be calculated by

$$\varepsilon_i = \varepsilon_e - \frac{\Delta}{\ell_0}$$

where, Δ is the offset across the shear band and ℓ_0 is the initial length of sample. Thus, the shear band formed at the bottom of the sample at ε_i = 0.084 - 9.15 / 147.6 = 2.2%, and the shear band formed at the top of the sample when ε_i = 0.084 - 3.7 / 147.6 = 5.9%.

5. Based on the test results (Figure 2.3.d) measured from load cells mounted on both inside and outside of triaxial chamber, a small offset of the initial reading (about -5 kPa in compression and +5 kPa in extension) was observed. The maximum offset of test results was less than 2 kPa in compression test (N70D100A, C and R) and reached about 8 kPa in extension test (N70D100R). This may be the result of friction induced between the

loading rod and the bearing of the top cap (see figure 1.3.1). The results for compression suggest that friction is relatively small. For extension, the friction appears to be more important. However, these results are only preliminary investigations and more data is needed to verify this.

Summary of important observations:

1. The maximum "failure" stress ratio R_f in drained tests was found to be significantly larger than that in undrained tests.

2. Most of the triaxial drained test results showed a peak followed by a drop of deviatoric stress. The drop in stress corresponded to a drop in the dilatancy rate and the formation of a shear band.

3. The thickness of shear band was observed to be about 10 to 12 times mean grain size of the Nevada sand. The failure planes were inclined at the angles between 63° and 65°.

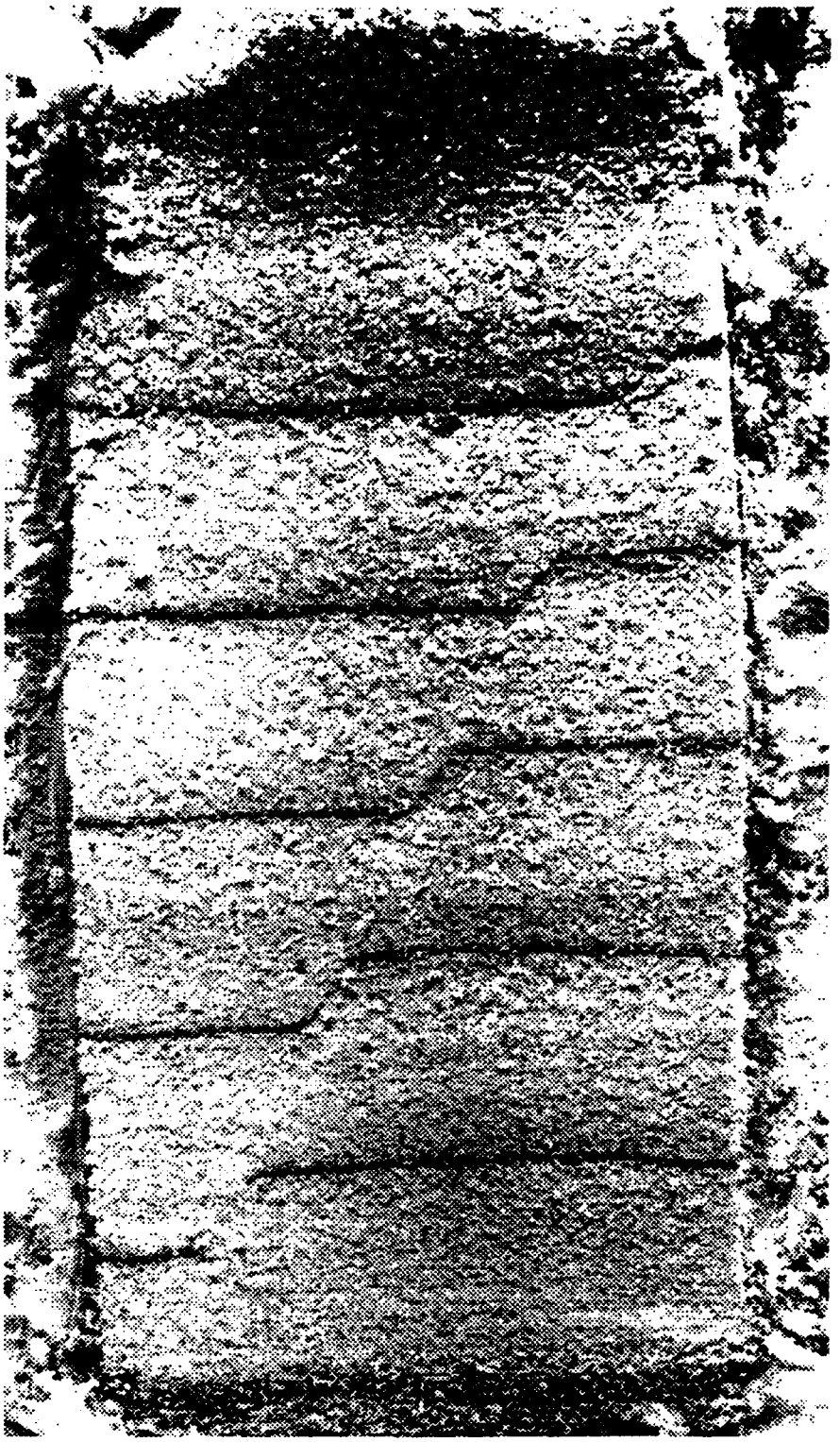

Figure 2.3.a : Photograph of the Colored Sand After Triaxial Test N70D100A

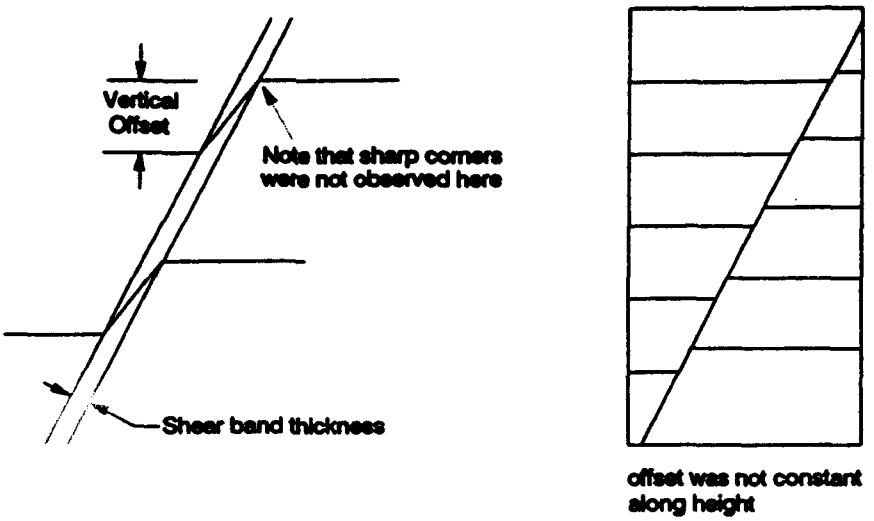

Figure 2.3.b : Sketch of the Vertical Offset of the Sample After Triaxial Test

Depth (mm)	0	25	50	75	100	125	147.6
Vertical Offset at End of Test N70D100A (mm)	Top	4.4	5.7	7.0	7.2	8.1	Bottom

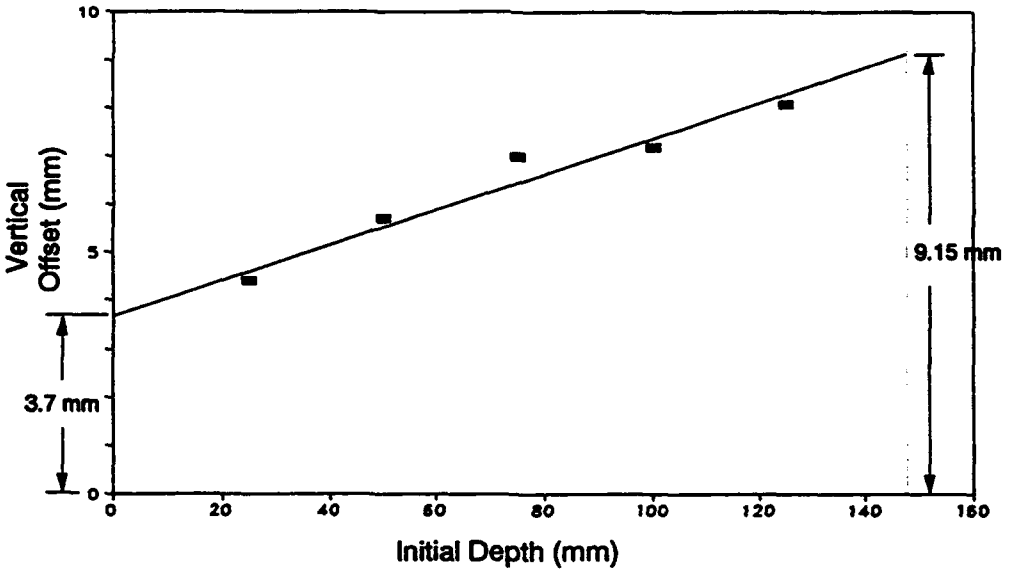

Figure 2.3.c : Measurements of the Vertical Offset from Photograph of the Sample (N70D100A)

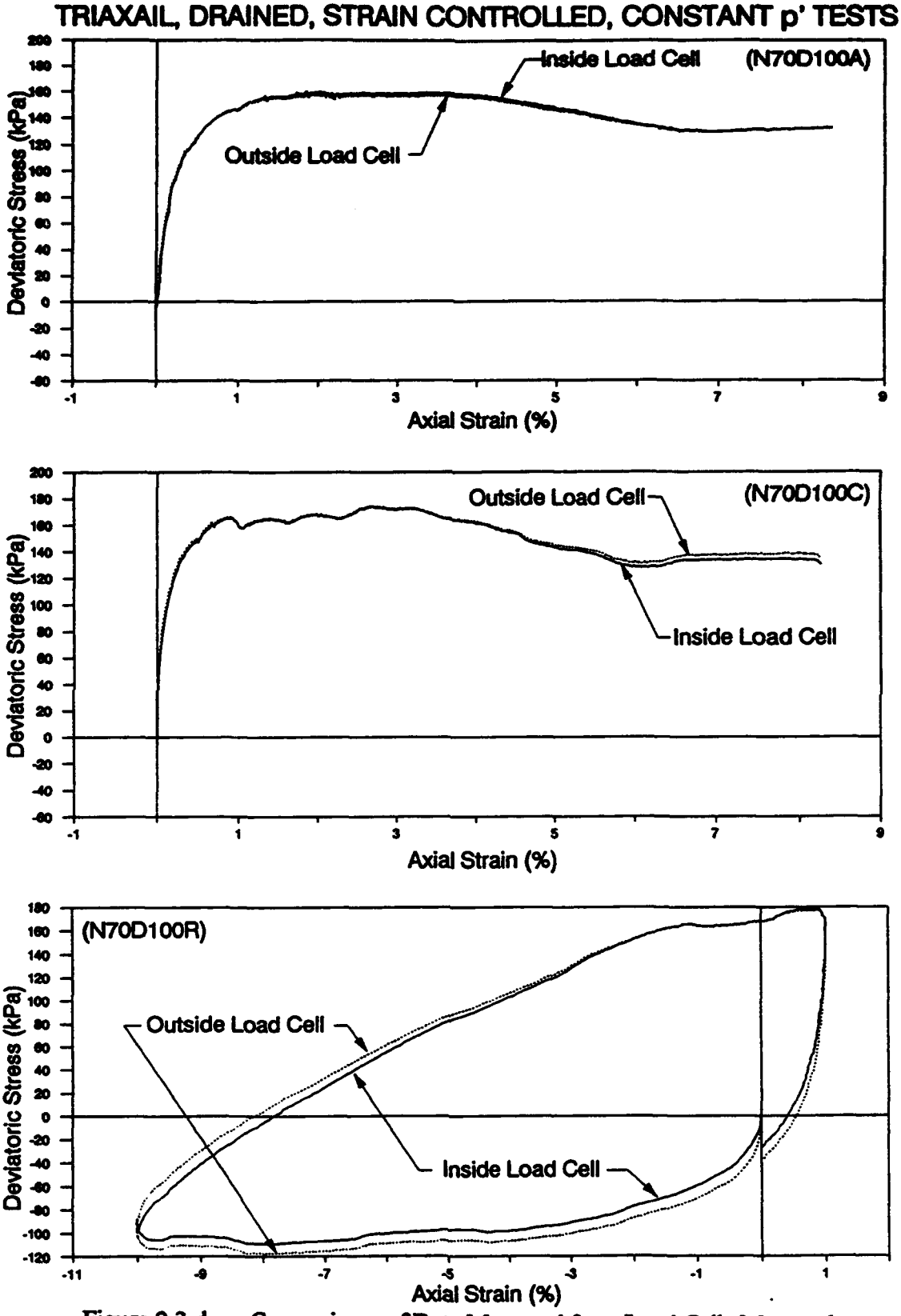

Figure 2.3.d : Comparisons of Data Measured from Load Cells Mounted on Both Inside and Outside of Triaxial Chamber

2.4. Triaxial Undrained Stress Controlled Cyclic Tests (CIUCyclic)

The results of 35 cyclic undrained stress controlled triaxial tests are reported in Figure 2.4.1 to Figure 2.4.35 (q vs. p', q vs. ε_1 and p' vs. ε_1). These tests were performed with varying cyclic stress ratio, over-consolidation ratio, confining pressure and testing frequency. For most of the tests, the testing period were 300 sec. The summary table for these tests is Table 2.4.1.

Some important observations are:

1. The number of cycles to cause 3% strain for different stress ratios was observed and is discussed later in connection with Figure 4.1. The liquefaction of dense sand is normally considered to develop when the pore water pressure ratio builds up to a value of 100% and the strains of the order of about 5% (Seed and Idriss, 1982). In this report, however, 3% strain is adopted due to the useful comparisons to hollow cylinder torsional shear tests for which the strains only reach around 3%.

2. The observed slopes of phase transformation lines and failure lines agreed reasonably well with those measured in undrained monotonic tests.

3. Some test results show mean normal effective stress slightly less than zero. This is the result of an incorrect zero offset in the pressure transducers.

2.5. Triaxial Consolidation Tests

Results of 8 isotropic consolidation tests are reported in Figure 2.5.1 to Figure 2.5.8. Table 2.5.1 summarized the test data.

Some important observations are:

1. The compression index λ and rebound index κ for critical state soil mechanics (Schofield and Wroth 1968) were obtained and are presented in Table 2.5.2. Here, $\lambda = \Delta e / \Delta \ell n(p')$ for virgin compression and $\kappa = \Delta e / \Delta \ell n(p')$ for rebound. λ and κ were not found to be constant. Constant λ and κ values may apply to a limited range of confining pressures. In any constitutive modeling efforts, these parameters must be experimentally determined over the pressure range of interest.

2. The hypoplasticity model (Wang and Dafalias 1990) assumes that compression index λ^* and rebound index κ^* are constants. Here, $\lambda^* = de / d(p'/p_a)^{1/2}$ for virgin compression and $\kappa^* = de / d(p'/p_a)^{1/2}$ for rebound, in which p_a and p' are atmospheric pressure and mean normal effective pressure respectively. It is interesting to point out that the values of λ^* and κ^* (Table 2.5.2) appear to be somewhat better "constants" than λ and κ. For example λ varies from 0.0031 to 0.0091, whereas λ^* only varies from 0.0037 to 0.0071.

Summary of important observations:

1. The compression index λ ($\lambda = \Delta e / \Delta \ell n(p')$) and rebound index κ ($\kappa = \Delta e / \Delta \ell n(p')$) for critical state soil mechanic were found to be not constant. Constant values of λ and κ may apply to a limit range of confining pressure.

2. Hypoplasticity model compression index λ^* ($\lambda^* = de/d(p'/p_a)^{1/2}$) and rebound index κ^* ($\kappa^* = de/d(p'/p_a)^{1/2}$) appear to be better "constants" than λ and κ.

3. HOLLOW CYLINDER TORSIONAL TESTS

Two different types of tests (cyclic torsional shear and rotational shear tests) were performed in the hollow cylinder apparatus at University of California, Davis.

The cyclic torsional shear test was performed by initially applying the axial loading σ_z on an isotropically consolidated sample until the desired coefficient of lateral pressure, K ($K = \sigma_\theta/\sigma_z$), was reached. Shear stress, $\sigma_{z\theta}$, was than cyclically applied.

The stress path of a rotational shear test was performed by initially applying the axial loading σ_z on an isotropically consolidated sample until the desired value of J ($J = \sqrt{J_{2d}} = \sqrt{(\sigma_z - \sigma_\theta)^2/3 + \sigma_{z\theta}^2}$) was reached. The sample was then sheared with a constant value of J. The mean normal stress p was held constant while $\sigma_{z\theta}$ and $(\sigma_z - \sigma_\theta)$ were varied in such a way that J was constant.

Sample preparation and general observations of hollow cylinder samples are illustrated in Section 3.1. *Cyclic torsional and rotational* shear test results are presented in Sections 3.2 and 3.3, respectively.

3.1. Sample Preparation and General Observations

The samples used in the hollow cylinder torsional tests were prepared by pluviation through a 20 inch high Plexiglas cylinder. The sand was fed by hand using a funnel through a #16 sieve at the top of the cylinder. The inside and outside diameters of samples were about 4 inches and 6 inches, respectively. The height of samples was about 6 inches. The range of relative density was 68% to 74%. The sample was covered with top and bottom pedestals and vacuumed along the inner and outer vertical surfaces by two separate membranes (thickness = 0.012 inches). The inner membrane was fixed by two Plexiglas ring wedges setting on the top and bottom side of

pedestal individually. The outer membrane was fixed by o-rings. To avoid slippage and transfer shear stress from pedestals to the sample, an epoxy coated sand was provided to the pedestals. In addition 12 blades (6 blades on each pedestal) were placed perpendicular to the epoxy coated sand surfaces. To allow drainage of sample and measurement of pore water pressure, total 6 porous stones (diameter = 0.5 inches) were inlaid on both top and bottom pedestals.

Most of test results showed a slight overshoot in deviatoric stress, $(\sigma_z - \sigma_\theta)/\sqrt{3}$, during the initial axial loading condition before application of torsional shear stress. This is the result of friction induced between loading rod and bearing of top cap and backlash of controller. In preliminary tests, significant binding was observed in the piston, resulting in excessive errors in the measurements of stresses applied to the sample. This problem was resolved by loosening certain parts of the axial and torsional load measurement system, but introduced some backlash in the torsional displacement measuring system. The data was "corrected" to eliminate the observed backlash. Figures 3.2.2, 3.2.17 and 3.3.2 illustrate how the data was corrected. An internal load cell has been designed and implemented to eliminate these problems, but the results presented in this report were all obtained before the internal load cell was implemented.

3.2. Cyclic Torsional Shear Tests (HCCAUTSCyclic)

This report contains the results of four cyclic torsional shear tests performed in the UCD hollow cylinder torsional apparatus (Figure 1.3.3). These results are shown in Figures 3.2.1 to 3.2.20. The tests were conducted with the following values for coefficient of lateral pressure: K= σ_θ/σ_z = 0.41, 0.63, 1.0 and 1.38. During a given torsional simple shear test σ_θ and σ_z were held constant while the shear stress $\sigma_{z\theta}$ (56 kPa) was cycled, $\sigma_{z\theta} = \pm 56$ kPa. The summary table for these tests is shown on Table 3.2.1. The relationship between stress ratio ($\sqrt{J_{2\sigma}}/p'$) and angle θ in π plane for these four cyclic torsional shear tests will be presented later in Figure 4.2.

Some important observations are:

1. At the same stress ratio, the number of cycles to cause 3% strain for cyclic torsional shear tests was larger than that in cyclic triaxial tests. Furthermore, the number of cycles to cause 3% strain consistently increased as K decreased. K is the initial ratio of σ_θ/σ_z. The relationship between cyclic stress ratio (i.e. $(\sigma_z - \sigma_\theta)/(\sqrt{3}\cdot\sigma_\theta')$ for triaxial test and $\sigma_{z\theta}/\sigma_c'$ for torsional shear test) and the number of cycles to cause 3% strain will be explained later in Section 4.

2. The mean normal effective stress (shown in Figures 3.2.5 and 3.2.10) exhibited the phenomenon of stable cycling in stress space between phase transformation and failure after certain number of cycles in the conditions of K<1. During this cycling, the magnitude of strains continued to increase. It is interesting to note that the changes in mean normal effective stress during stable cycles were about 27% and 9% of the cyclic shear stress, $\sigma_{z\theta}$, for K=0.63 and K=0.41, respectively. For the cyclic simple shear test (K=1), the mean normal effective stress gradually approached zero at $\sigma_{z\theta}$=0 (i.e. sample

liquefied) after a certain number of cycles (shown in Figure 3.2.15). For the case of K>1 (shown in Figure 3.2.20), stable cycling between phase transformation and failure was also observed, but cyclic change in effective mean normal stresses during these cycles was almost equal to the magnitude of shear stress $\sigma_{z\theta}$, and the mean normal effective stress was much larger than zero at $\sigma_{z\theta}$=0.

3. During the stable cycling of stresses the shear strains, $\varepsilon_{z\theta}$, cycled in the range of ±0.25% and ±0.3% for K=0.41 and K=0.63, respectively (shown in Figures 3.2.4 and 3.2.9). The shear strains $\varepsilon_{z\theta}$ in cyclic simple shear test (K=1, i.e. the major principal stress ±45° relative to the vertical in Figure 3.2.14) were ±3% in both directions and gradually increased as the number of stress cycles increased. It is interesting to point out that as K approaches one, the initial stress approaches an isotropic state (i.e. the initial deviatoric stress, σ_z-σ_θ, decreases) yet the cyclic shear strains, $\varepsilon_{z\theta}$, increase. The shear strains increased in the order K=0.41, 0.63, 1.0 and 1.38.

4. For the cyclic simple shear test, the maximum (failure) stress ratio $R_f = J/p'$ is 0.737 and phase transformation is observed to occur at $R_p = J/p' = 0.4$. The maximum stress ratio is in between values obtained from undrained triaxial compression (R_{fc}=0.853) and extension (R_{fe}=0.524). The stress ratio at phase transformation appears to be less than that in both triaxial compression (R_{pc}=0.556) and extension (R_{pe}=0.467) tests. A detailed explanation of model parameters for the hypoplasticity model will be discussed in the report "Calibration and Testing of the Proposed Hypoplasticity Model for Sand" (Chen and Kutter, 1993).

5. The maximum stress ratios, $R = \sqrt{J_{2d}}/p'$, were about 0.71, and 0.56 for the cases of K<1 and K>1, respectively.

Summary of important observations:

1. At the same stress ratio, the number of cycles to cause 3% strain for cyclic torsional shear tests was larger than that in cyclic triaxial tests. The number of cycles to cause 3% strain consistently increased as the initial ratio of σ_θ/σ_z decreased.

2. The effective stress path exhibited the phenomenon of stable cycling between the phase transformation and failure stress ratios for the cases of K<1 and K>1 after a number of cycles. For the cyclic simple shear test (K=1), the mean normal effective stress gradually approached zero at $\sigma_{z\theta}$=0 (i.e. sample liquefied) after a number of cycles.

3. In the cyclic torsional shear tests, the cyclic shear strain amplitude ($\varepsilon_{z\theta}$) seems to increase as the ratio of σ_θ/σ_z increases.

4. In the cyclic simple shear test, the maximum stress ratio, R_f is between values obtained from triaxial compression and extension tests, and the stress ratio at phase transformation was less than that in both triaxial compression and extension tests.

3.3. Rotational Shear Tests (HCCAURS)

The results of two rotational shear tests are reported as follows.. Test results are presented in Figures 3.3.1 to 3.3.10. Each stress cycle of the rotational shear tests was accomplished by continuous rotation of principal stress axes at constant values of J. The direction of the major principal stress rotated from compression (angle θ=0°) to simple shear (θ =30°), then continuously rotated to extension (θ=60°) and finally turned back to compression through another simple shear condition.

In these figures, the filled square, empty square and plus sign symbols represent the conditions of compression, extension and simple shear, respectively. These symbols were found to be useful for mapping and cross referencing from one plot to another. The two tests were conducted using different values of J (Figures 3.3.1 and 3.3.6). The chosen values of J (56 kPa and 40 kPa) corresponded to stress ratios that were 33% and 24% of the stress ratio at failure in triaxial compression tests, respectively. The summary table for these tests is shown on Table 3.3.1.

Some important observations are:

1. The relationship between cyclic stress ratio, $\sqrt{J_{2d}}/p_i$, and the number of cycles to cause 3% strain will be explained in later section and is shown in Figure 4.1. The inclination of curve in the rotational tests appear to be higher than that in the triaxial tests. More data is required to define the relationship.

2. For both rotational tests, the stress ratios, $(\sigma_z - \sigma_\theta)/(\sqrt{3}\cdot p')$ and $\sqrt{J_{2d}}/p'$, stabilized after reaching a large strain (shown in Figures 3.3.4 and 3.3.9). Although the phenomenon of stabilization of stress ratio was observed, the mean normal effective stress, p', continued to change cyclically. Figures 3.3.3 and 3.3.8, show the change of mean

normal effective stress, p', with the shear strain, $\varepsilon_{z\theta}$. Initially, the mean normal effective stress gradually decreased resulting in an increase in stress ratio until the "stabilization" of stress ratio occurred. During the "stable" cycles, p' tended to increase as the direction of stress moved from compression (θ=0°) to simple shear (θ=30°), to extension (θ=60°) and p' tended to decrease as direction of loading rotated from extension to simple shear, to compression. The minimum value of p' occurred at θ=0° (triaxial compression). The maximum value of p' occurred at θ=60° (triaxial extension). The value of p' was nearly constant as θ reduced from 60° to 30°.

3. The relationship between shear stress, $\sigma_{z\theta}$, and shear strain, $\varepsilon_{z\theta}$, for both rotational shear tests are shown in Figures 3.3.2 and 3.3.7. For θ increasing from 0° to 60° and θ decreasing from 60° to 0°, the relationship between $\sigma_{z\theta}$ and $\varepsilon_{z\theta}$ appears to be symmetrical. The maximum shear strain ($\varepsilon_{z\theta,max}$) occurs after the peak value of $\sigma_{z\theta}$ when $\sigma_{z\theta}$ is about half of the peak $\sigma_{z\theta}$. The deviatoric strains $2(\varepsilon_z-\varepsilon_\theta)/3$ were not symmetrical, extension strains were three or four times greater than compression strains in both tests. The deviatoric strain consistently returned to near zero when the deviatoric stress, $\sigma_z-\sigma_\theta$, was a maximum (θ=0°). Similar to the relationship between $\sigma_{z\theta}$ and $\varepsilon_{z\theta}$, the maximum deviatoric strains occurred after the maximum deviatoric stress when the magnitude of the deviatoric stress was about half of its maximum value.

4. Although the shear stress and deviatoric stress ratios stabilized near their phase transformation and failure surfaces, the magnitude of shear strain, $\varepsilon_{z\theta}$, and deviatoric strain, $2(\varepsilon_z-\varepsilon_\theta)/3$, increased as the numbers of stress cycles increased. The stabilization of stress ratio is clear in the repeatable loop in the plot of $(\sigma_z-\sigma_\theta)/(\sqrt{3}p')$ vs. $\sigma_{z\theta}/p'$ (Figures 3.3.4 and 3.3.9). The increasing rate of strain is also clear in the spiral shape in

the plot of $2(\varepsilon_z-\varepsilon_\theta)/3$ vs. $\varepsilon_{z\theta}$ (Figures 3.3.4 and 3.3.9) In test NR40CU50 (J=40 kPa), while the shear strain reached about 3%, a sudden increase of shear strain was observed.

5. The cycling of stress ratios, $R=\sqrt{J_{2d}}/p'$ and $(\sigma_z-\sigma_\theta)/(\sqrt{3}\cdot p')$ (Figures 3.3.5 and 3.3.10), from compression (θ=0°) to extension (θ=60°) through the simple shear state (θ =30°) are shown for tests NR40CU50 (J=40 kPa) and NR56CU50 (J = 50 kPa), respectively. These results revealed that the stress ratios stabilized after a certain number of cycles. The maximum stress ratios, R_{max}, are about 0.85 in compression and 0.6 in extension for both tests. It is interesting to point out that the ratio, $R_{max,ext}/R_{max,comp}$, is equal to 0.7 which is between the value c_p and c_f determined from undrained triaxial tests. In the triaxial tests, the ratio c_p was 0.84 ($c_p=R_{pe}/R_{pc}$ on phase transformation line) and c_f was 0.61 ($c_f=R_{fe}/R_{fc}$ on failure line). The values of R_{fc} (0.853), R_{fe} (0.524), R_{pc} (0.556) and R_{pe} (0.467) determined from undrained triaxial tests as indicated on Figure 3.3.5 and 3.3.10 for reference, the stable cycling of stress ratio are bounded by the values of R_{fc} and R_{fe}.

Summary of important observations:

1. The stress ratios, $(\sigma_z-\sigma_\theta)/(\sqrt{3}\cdot p')$ and $\sqrt{J_{2d}}/p'$, traced a stable loop after reaching a larger strain. Although the phenomenon of stabilization of stress ratio was observed, the mean normal effective stress, p', continued to change cyclically. The maximum value of p' occurred at θ=60° (triaxial extension).

2. Although the shear stress and deviatoric stress ratios stabilized near their phase transformation and failure surfaces, the magnitude of shear strain and deviatoric strain increased as the numbers of stress cycles increased.

3. In rotational shear tests, the relationship between $\sigma_{z\theta}$ and $\varepsilon_{z\theta}$ was found to be symmetrical but the deviatoric strains, $2(\varepsilon_z-\varepsilon_\theta)/3$ in extension were three or four times greater than those in compression.

4. In rotational shear tests, the stable cycling of stress ratios are bounded by the values of triaxial compression and extension failure stress ratios.

4. SUMMARY COMPARISONS OF TRIAXIAL, TORSIONAL AND ROTATIONAL SHEAR TEST RESULTS

Figure 4.1 shows the summary data for cyclic stress ratio versus number of cycles to cause 3% strain in triaxial, torsional and rotational shear tests. It should be noted that $\sqrt{J_{2d}} = \sqrt{(\sigma_z - \sigma_\theta)^2/3 + \sigma_{z\theta}^2}$ for rotational shear tests and $\sqrt{J_{2d}} = \sqrt{(\sigma_z - \sigma_\theta)^2/3}$ for triaxial tests, (i.e. $\sigma_{z\theta}$=0 for triaxial tests). For torsional shear tests, $\sigma_{z\theta}$ was cycled with constant values for $(\sigma_z - \sigma_\theta)$, which depended on the values for coefficient of lateral pressure K ($K=\sigma_\theta/\sigma_z$). Thus, these cyclic stress ratios were calculated by $(\sigma_z - \sigma_\theta)/(\sqrt{3}\cdot\sigma_\theta')$, $\sigma_{z\theta}/\sigma_c'$ and $\sqrt{J_{2d}}/p_i$ for triaxial, torsional and rotational shear tests, respectively. These results indicate that the soil samples which have similar relative density are more resistant to cyclic loading for the rotational tests than for symmetric cyclic compression/extension triaxial tests. Note that triaxial tests with unsymmetrical loading with a larger magnitude of compression than extension never developed large strains (for example, CY250N1, see Table 2.4.1). At the same stress ratio, the number of cycles to cause 3% strain in the torsional shear tests was larger than that in the cyclic triaxial tests. Based on these results, liquefaction potential appears to be overestimated by conventional symmetrical triaxial cyclic test results. This appears to be inconsistent with observations of Towhata and Ishihara (1985). Further investigation is required.

The consistent picture which emerges is that the occurrence of triaxial extension states of stress is damaging. In the torsional shear tests, $\sigma_{z\theta}$ was cycled while σ_z-σ_θ was held constant corresponding to four different initial values of $K=\sigma_\theta/\sigma_z$. For K>1, the initial state is one of triaxial extension, and for K<1 the initial state is triaxial compression, and for K=1 the initial state is isotropic. For K=1 the cycling of $\sigma_{z\theta}$ corresponds to simple shear. A summary plot for the relationship between cyclic strain, $\varepsilon_{z\theta}$, and number of cycles is shown in Figure 4.2. For K=1.38 (extension), 3% strain developed in 4 cycles, for K=1, 3% strain developed in 7 cycles but for K=0.41, only 0.25% strain and for K=0.63, only 0.3% strain developed when the tests were terminated after 15 cycles.

Figure 4.3 shows the relationship between stress ratio, $\sqrt{J_{2d}}/p'$, and the angle θ in π plane for cyclic torsional shear tests performed with different values of coefficient of lateral pressure K. For the cyclic simple shear test (K=1) ($\sigma_z=\sigma_r=\sigma_\theta$ and $\sigma_{z\theta}$ was cycled) the angle θ was approximately constant (θ=30°). For $K=\sigma_\theta/\sigma_z<1$ (i.e. $\sigma_z>\sigma_r=\sigma_\theta$ and $\sigma_{z\theta}$ was cycled) the angle θ was started at 0° and cycled with the cycling of shear stress $\sigma_{z\theta}$. The maximum stress ratios for both K=1 and K<1 were about 0.71. For the case of K> 1, the pattern is similar to that for K<1 but the angle θ was started at 60°, and the maximum stress ratio was observed to be 0.56.

Figure 4.4 shows a summary plot of stress ratio versus angle θ in the π plane for undrained and drained triaxial, torsional shear and rotational shear tests. The data points plotted in this figure represent the failure points in varying conditions of triaxial tests, the maximum point in torsional shear test with K=1 (cyclic simple shear). The lines in Figure 4.4 show the last cycle of cyclic torsional and rotational shear tests. This plot might be thought of as a map of the failure surface. Note that the data points at drained and undrained triaxial tests represent average values from more than one test. The angles of 0°, 30° and 60° represent the triaxial compression ($\sigma_z>\sigma_r=\sigma_\theta$, $\sigma_{z\theta}=0$), simple shear ($\sigma_z=\sigma_r=\sigma_\theta$, $\sigma_{z\theta}\neq0$) and triaxial extension ($\sigma_z<\sigma_r=\sigma_\theta$, $\sigma_{z\theta}=0$) tests, respectively. The path for rotational shear tests is a loop between 0° and 60°. The torsional shear tests for the cases of $K=\sigma_\theta/\sigma_z>1$ begin from θ=0° and the angle θ increases as $|\sigma_{z\theta}|$ increases. For K<1, the test path starts on θ=60° and θ decreases as the magnitude of $\sigma_{z\theta}$ increases.

These results (Figure 4.4) show that the maximum stress ratio, $\sqrt{J_{2d}}/p'$, in triaxial drained compression tests is significantly larger than that in undrained compression tests. This finding also can be concluded from the data plotted in Figure 4.5. In Figure 4.5 the filled square and empty circle symbols represent the maximum and ultimate stress ratios, q/p', in drained triaxial tests respectively, and the solid lines represent the undrained triaxial stress paths under different confining pressures. Note that the error bar for the drained tests represents the scatter in stress ratios in drained triaxial compression and extension tests. The maximum stress ratio, q/p', in

drained triaxial tests is larger than that in undrained tests in both compression and extension. The difference in maximum stress ratio for triaxial undrained and drained tests appears to be decreasing as the mean normal effective stress increases. The larger stress ratios at failure in drained tests are also apparent in undrained tests after cavitation occurs. The upward hook at the end of the undrained stress path corresponds to cavitation.

Based on the results plotted in Figure 4.4, the maximum stress ratios in the rotational shear tests for both compression (θ=0°) and extension (θ=60°) are also found to agree reasonably well with the stress ratios in the undrained triaxial tests. It was observed that the maximum stress ratio in the torsional shear test (K=1) was larger than that in rotational shear tests in simple shear direction (θ=30°).

Several types of laboratory tests involving general tests, triaxial shear tests and hollow cylinder torsional and rotational shear tests were conducted on samples of Nevada sand using different facilities and apparatus at the University of California, Davis. Regarding the results obtained from these tests, the following enumerated observations were made.

1. In triaxial tests, the shape parameter, c ($c = R_{extension} / R_{compression}$), for phase transformation (c_p) and failure (c_f) are observed to be different. However, the hypoplasticity model assumes that $c=c_f=c_p$ (Figure 2.2.a and 2.2.b).

2. The maximum "failure" stress ratio R_f observed in drained triaxial tests was significantly larger than that in undrained triaxial tests. The difference appears to be decreasing as the mean normal effective stress increases (Figure 4.4). The larger stress ratios at failure in drained triaxial tests are also apparent in undrained tests after cavitation occurs (Figure 4.5).

3. By measuring the deformed shape of colored sand layers in some drained triaxial samples, the thickness of shear bands was observed to be about 10 to 12 times mean grain

size of the Nevada sand (Figure 2.3.a and 2.3.b) or about 1.7 to 2.0 mm. The failure planes were observed to be inclined at angles between 63° and 65°. A drop in deviatoric stress (strain softening) was observed to occur as the failure plane developed (e.g., Figure 2.3.8).

4. Over a limited range of confining pressure, values for the compression index λ^* and rebound index κ^* in the hypoplasticity model appear to be more closely a constant than values for λ and κ for the critical state soil mechanics model (Table 2.5.2). However, the hypoplasticity model assumes that λ^* and κ^* are constants.

5. At the same stress ratio, the number of cycles to cause 3% strain for cyclic torsional shear tests was larger than for cyclic triaxial tests (Figure 4.1). Also, soil samples tested in rotational shear appear to be more resistant to cyclic loading than samples subject to symmetrical cyclic triaxial tests. Thus, the liquefaction potential appears to be overestimated by conventional symmetrical triaxial cyclic test results. This conclusion needs to be further verified since it contradicts the well-known observation by Towhata and Ishihara (1985).

6. For the cyclic simple shear test ($K=\sigma_\theta/\sigma_z=1$), the mean normal effective stress gradually approached zero at $\sigma_{z0}=0$ (Figure 3.2.15). The effective stress path exhibited the phenomenon of stable cycling between the phase transformation and failure stress ratios for the cases of $K<1$ and $K>1$ after a number of cycles (Figure 3.2.5, 3.2.10 and 3.2.20).

7. In the cyclic simple shear test, the maximum stress ratio is between values obtained from triaxial compression and extension tests (Figure 4.4).

8. In the series of cyclic torsional shear tests, the rate of change of cyclic shear strain amplitude seems to increase as the ratio of σ_θ/σ_z increases (Figure 4.2).

9. In rotational shear tests, the stress ratios, $(\sigma_z - \sigma_\theta)/(\sqrt{3}\cdot p')$ and $\sqrt{J_{2d}}/p'$, traced a stable loop after a number of cycles (Figure 3.3.4 and 3.3.9). The stress ratios appeared to oscillate between the phase transformation and failure surfaces.

10. In rotational shear tests, although the shear stress and deviatoric stress ratios stabilized near their phase transformation and failure surfaces, the magnitude of shear strain, $\varepsilon_{z\theta}$, and deviatoric strain, $2(\varepsilon_z-\varepsilon_\theta)/3$, increased as the numbers of stress cycles increased (Figure 3.3.4 and 3.3.9).

11. In rotational shear tests, θ increasing from 0° to 60° and θ decreasing from 60° to 0°, the relationship between $\sigma_{z\theta}$ and $\varepsilon_{z\theta}$ appears to be symmetrical but the deviatoric strains $2(\varepsilon_z-\varepsilon_\theta)/3$ were not symmetrical (Figure 3.3.2 and 3.3.7). The deviatoric strains in extension were three or four times greater than those in compression.

12. In rotational shear tests, the stable cycling of stress ratios are bounded by the values of triaxial compression failure stress ratio R_{fc} and extension failure stress ratio R_{fe} (Figure 3.3.5 and 3.3.10).

13. The maximum stress ratio observed in the rotational shear tests for both compression and extension are found to agree reasonably well with the stress ratios in the undrained triaxial tests (Figure 4.4).

5. CONCLUSIONS

The major accomplishment of this research has been the generation of a wide diversity of laboratory test data. These test data not only can be used to support the calibration and verification of the bounding surface hypoplasticity model for granular soil but also provide a valuable data base for further research in constitutive model studies. Summary comparisons are also made between triaxial, cyclic torsional and rotational shear tests. The test results indicate that the rotations of principal stress directions have very important effects on the soil deformation and strength characteristics.

Regarding the results obtained from these tests, soil samples tested in rotational shear were found to be more resistant to cyclic loading than samples in symmetrical triaxial cyclic tests. The maximum "failure" stress ratio in drained triaxial tests was significantly larger than that in undrained triaxial tests. Also, the shape of phase transformation and failure surfaces were different when viewed in the π-plane.

In the cyclic simple shear test, the stress ratio on the failure line is between values obtained from triaxial compression and extension tests. In rotational shear tests, although the shear stress and deviatoric stress ratios stabilized near their phase transformation and failure surfaces, the magnitude of shear and deviatoric strains still increased as the numbers of stress cycles increased. Also, the stable cycling of stress ratios are found to be bounded by the values of triaxial compression and extension failure stress ratios. In addition, The maximum stress ratio observed in the rotational shear tests for both compression and extension are found to agree reasonably well with the maximum stress ratio in the undrained triaxial tests.

6. ACKNOWLEDGEMENTS

This research reported herein was conducted under Naval Civil Engineering Laboratory contract number N47408-89-C-1058. This support is gratefully acknowledge. Dr. Ted Shugar provided valuable advice and review comments at several stages of this research.

In this research, forty-five triaxial tests were conducted by James Wickstrom, fifteen triaxial tests were conducted by Shiyo Chen and six torsional tests were accomplished by Chi-Wen Lin.

The technical assistance and computer programs from Dr. Xiang-Song Li in all aspects of the experimental work are appreciated very much.

Many thanks to Mr. Bill Sluis and Mr. Tom Kohnke, the development technicians, for their valuable suggestions and excellent contributions to improve the test apparatus.

Thanks are also due to Dr. Han-Wei Yang and Dr. S. Jafroudi for their previous developments of the hollow cylinder torsional apparatus at U. C. Davis.

6. REFERENCES

Alarcon, A., Chameau, J. L. and Leonards, G. A., "A New Apparatus for Investigating the Stress-Strain Characteristics of Sands", Geotechnical Testing Journal, Vol. 9, No. 4, 1986, PP204-212

Arthur, J. R. F. and Menzies, B. K., "Inherent Anisotropy in a Sand", Geotechnique, Vol. 22, No. 1, 1972, PP115-129

Arulanandan, K. and Scott, R. F., "Project VELACS - Control Test Results", Journal of Geotechnical Engineering, ASCE, Vol. 119, No. 8, August 1993, PP1276-1292.

Arulanandan, K. and Scott, R. F., "Verification of Numerical Procedures for the Analysis of Soil Liquefaction Problems", Proceedings of the International Conference, Davis, California, Vol. 1, October, 1993.

Arulmoli, K., Muraleetharan, K. K., Hossain, M. M. and Fruth, L. S., "VELACS Laboratory Testing Program", preliminary data report to National Science Foundation, The Earth Technology Corporation, September, 1991.

Castro, G., "Liquefaction and Cyclic Mobility of Saturated Sands", Journal of Geotechnical Engineering Division, ASCE 101(GT6), 1975, PP551-569

Chen, Y.-R. and Kutter, B. L., "Calibration and Testing of the Proposed Hypoplasticity Model for Sand", report to Naval Civil Engineering Laboratory, Department of Civil and Environmental Engineering, University of California, Davis, 1994.

Chu, J., Lo, S.-C. R. and Lee, I. K., "Strain-Softening Behavior of Granular Soil in Strain-Path Testing", Journal of Geotechnical Engineering, ASCE, Vol. 118, No. 2, 1992, PP191-208

Dasseault, M. B., "A Versatile Hollow Cylinder Triaxial Device", Can. Geotech. J. 18, 1981, PP1-7

Desai, C. S. and Siriwardane, H. J., "Constitutive Laws for Engineering Material With Emphasis on Geologic Materials", Prentice Hall, 1984.

Gilbert, P. A. and Marcuson, W. F., "Density variation in Specimen Subjected to Cyclic and Monotonic Load", Journal of Geotechnical Engineering, ASCE, Vol. 114, No. 1., 1988, PP1-20.

Gutierrez, M, Ishihara, K. and Towhata, I. "Flow Theory for Sand During Rotation of Principal Stress Direction", Soils and Foundations, Vol. 31, No. 4, Dec. 1991, PP121-132.

Gutierrez, M, Ishihara, K. and Towhata, "Model for the Deformation of Sand During Rotation of Principal Stress Directions", Soils and Foundations, Vol. 33, No. 3, Sept. 1993, PP105-117.

Hight, D. W., Gens, A. and Symes, M. J., "The Development of a New Hollow Cylinder Apparatus for Investigating the Effects of Principal Stress Rotation in Soils", Geotechnique, 33, No. 4, 1983, PP355-383.

Head, K. H., "Manual of Soil Laboratory Test", Volume 1, 2 and 3, ELE International Limited, 1985.

Hettler, A. W., and Vardoulakis, I., "Behavior of Dry Sand Tested in a Larger Triaxial Apparatus", Geotechnique, Vol. 34, No. 2, 1984, PP183-198.

Ishihara, K., Tatsuoka, F. and Yasuda, S., "Undrained Deformation and Liquefaction of Sand Under Cyclic Stresses", Soils and Foundations, Vol. 15, No. 1, March, 1975, PP29-44.

Lam, W.-K. and Tatsuoka, F., "Effects of Initial Anisotropic Fabric and σ_2 on Strength and Deformation Characteristics of Sand", Soils and Foundations, Vol. 28, No. 1, 1988, PP89-106.

Li, X. S., "Free Field Soil Response Under Multi-directional Earthquake Loading", Ph.D. dissertation, University of California, Davis, 1990.

Li, X. S., Chan, C. K. and Shen, C. K., "An Automatic Triaxial Testing System", Advanced Triaxial Testing of Soil and Rock, ASTM, STP77, 1988, PP95-106.

Miura, K., Miura, S. and Toki, S., "Deformation Behavior of Anisotropic Dense Sand Under Principal Stress Axes Rotation", Soils and Foundations, Vol. 26, No. 1, Mar. 1986, PP36-52.

Pradel, D., Ishihara, K. and Gutierrez, M., "Yielding and Flow of Sand Under Principal Stress Axes Rotation", Soils and Foundations, Vol. 30, No. 1, Mar. 1990, PP87-99.

Riemer, M. F., Seed, R. B., Nicholson, P. G. and Jong, H. L., "Steady State Testing of Loose Sands: Limiting Minimum Density", Journal of Geotechnical Engineering, ASCE, Vol. 116, No. 2, 1990, PP332-337.

Saada, A. S. and Townsend, F. C., "State of the Art: Laboratory Strength Testing of Soils", Laboratory Shear Strength of Soil, ASTM STP 740, 1981, PP7-77.

Saada, A. S., "State of the Art Paper - Hollow Cylinder Torsional Devices: Their Advantages and Limitations", Advanved Triaxial Testing of Soil and Rock, ASTM STP 977, 1988, PP766-795.

Schofield, A. N. and Wroth, C. P., "Critical State Soil Mechanics", Mcgraw-Hill Publishing Company, Great Britain, 1968.

Seed, H. B. "Soil Liquefaction and Cyclic Mobility Evaluation for Level Ground During Earthquake", Journal of Geotechnical Engineering Division, ASCE, Vol. 105, No. GT2, 1979, PP201-255.

Seed, H. B. and Idriss, I. M., "Ground Motions and Soil Liquefaction During Earthquake", Earthquake Engineering Research Institute, 1982.

Shankariah, D. B. and Ramamurthy, T., "Axisymmetric Compression and Extension of Anisotropic Sand", Indian Geotechnical Journal, Vol. II, 1980, PP77-81.

Tatsuoka, F., "Some Recent Developments in Triaxial Testing Systems for Cohesionless Soils", State-of-the-Art Paper, Advanced Triaxial Testing of Soil and Rock, ASTM, STP77, 1988, PP7-67.

Tatsuoka, F., Muramatsu, M. and Sasaki, T., "Cyclic Undrained Stress-Strain Behavior of Dense Sands by Torsional Simple Shear Test", Soils and Foundations, Vol. 22, No. 2, June 1982, PP55-70.

Towhata, I. and Ishihara, K., "Undrained Strength of Sand Undergoing Cyclic Rotation of Principal Stress Axes", Soils and Foundations, Vol. 25, No. 2, June, 1985.

Townsend, F. C., "A review of Factors Affecting Cyclic Triaxial Tests", Dynamic Geotechnical Testing, ASTM, STP 654, 1978, PP356-383.

Vaid, Y. P. and Chern, J. C., "Cyclic and Monotonic Undrained Response of Saturated Sands", Advances in the Art of Testing Soils Under Cyclic Conditions, Proceedings, ASCE 1985, PP120-147.

Vaid, Y. P., Sayao, A., Hou, E. and Negussey, D., "Generalized Stress-Path-Dependent Soil Behavior with a New Hollow Cylinder Torsional Apparatus", Can. Geotech. J. 27, 1990, PP601-616.

Wang, Z. L., "Bounding Surface Hypoplasticity Model for Granular Soils and its Application", Ph.D. dissertation, University of California, Davis, 1990.

Wang, Z. L., Dafalias, Y. F. and Shen, C. K., "Bounding Surface Hypoplasticity Model for Sand", Journal of Engineering Mechanics, ASCE, Vol. 116, No. 5, May 1990, PP983-1001.

Wijewickreme, D. and Vaid, Y. P., "Stress Nonuniformities in Hollow Cylinder Torsional Specimens", Geotechnical Testing Journal, ASTM, Vol. 14, No. 4. Dec. 1991, PP349-362.

Wilson, D. and Kutter, B. L., "Centrifuge Tests on Circular and Rectangular Model Foundations", report to Naval Civil Engineering Laboratory, Department of Civil and Environmental Engineering, University of California, Davis, 1994.

Yamada, Y. and Ishihara, K., "Undrained Deformation Characteristics of Sand in Multi-Directional Shear", Soils and Foundations, Vol. 23, No. 1, Mar. 1983, PP61-79.

Yamashita, S. and Toki, S. "Effects of Fabric Anisotropy of Sand on Cyclic Undrained Triaxial and Torsional Strength", Soils and Foundations, Vol. 33, No. 3, Sept. 1993, PP92-104.

Yang, H. W., "Deformation Behavior of Granular Material Under Non-proportional Loading", Ph.D. dissertation, University of California, Davis, 1992.

SUMMARY TABLES AND SOME RESULTS
ON
TRIAXIAL, TORSIONAL AND ROTATIONAL SHEAR TESTS

Table 2.2.1 : Summary of Triaxial, Undrained, Strain Controlled, Constant p Test Data for Nevada Sand

Table 2.3.1 : Summary of Triaxial, Drained, Strain Controlled, Constant p' Test Data for Nevada Sand

Table 2.4.1 : Summary of Triaxial, Undrained, Stress Controlled, Cyclic Test Data for Nevada Sand

Table 2.5.1 : Summary of Triaxial, Consolidation and Rebound Test Data for Nevada Sand

Table 2.5.2 : Summary of Compression Index λ and Rebound index κ for Nevada Sand

Table 3.2.1 : Summary of Hollow Cylinder Undrained, Stress Controlled, Cyclic Torsional Shear Test Data for Nevada Sand

Table 3.3.1 : Summary of Hollow Cylinder Undrained, Stress Controlled, Rotational Shear Test Data for Nevada Sand

Table 2.2.1 : Summary of Triaxial, Undrained, Strained Controlled, Constant p Test Data for Nevada Sand

OCR = 1

File	Stress Path	Sample Diameter (mm)	Sample Height (mm)	Relative Density (%)	Back Pressure (kPa)	B Value (%)	Confining Pressure σ_{3c}'(kPa)	Remark
N50U1	CIUC	70.5	146.8	70	250	98.9	50	** p-q plot in early stage
N60U1001	CIUC/E	70.7	148.3	66	250	95.1	100	PWP always decrease; 1 hr BP sat. @ 200 kPa then 20 min BP sat. @ 250 kPa
N60U1002	CIUC/E	70.8	144	63	250	96	100	** 40 min BP sat. @ 200 kPa then 20 min BP sat. @ 250 kPa
N60U1003	CIUC/E	70.7	144.1	66	250	97.7	100	** 2hrs @ BP=0; then 30 min BP sat. @ 250kPa
N60U2501	CIUC/E	71.0	147.6	65	250	95.5	250	** 30 min BP sat. @ 250 kPa
N60U2502	CIUC/E	70.8	149.2	67	300	93	250	Low B value, but, BP=300kPa; 4 hrs BP sat. @ 200 kPa then 5 min BP sat. @ 300 kPa
N60U4001	CIUC/E	71.2	151.6	65	250	97.7	400	Tri. consol. exe. before shear; 30 min BP sat. @ 250 kPa
N60U4002	CIUC	70.7	148.6	66	250	97.3	400	** 2 hrs @ BP=0; 2 hr2 BP sat. @ 250 kPa
N60U4501	CIUC/E	70.8	149.1	62	200	99	450	Low density, 2 hrs BP sat. @ 200 kPa
N50U2	CIUE	70.9	147.5	71	250	98.6	50	** 15 hrs @ BP=0, cell pre=50 kPa; then 4 min BP sat @ 250 kPa
N60U1006	CIUE	69.4	144.4	71	200	97.1	100	12 hrs BP sat. @ 200 kPa
N60U1008	CIUE	71.2	149.4	71	250	98.7	100	12 hrs BP sat. @ 250 kPa
N60U1009	CIUE	70.9	150.4	64	250	98.4	100	** 16 hrs @ BP=0, cell pre=100 kPa; then 8 min BP sat @ 250 kPa

N60U2506	CIUE/C	70.6	147.4	71	250	100	250	** Diff. rate; Tri. consol exe. before shear; then 8 min BP sat. @ 100 kpa; then 1.5 hrs BP sat. @ 250 kPa; B value greater than 1;
N60U4006	CIUE	71.2	152.1	66	250	99	400	** Tri consol exe before shear; then 4 hrs BP sat. @ 250 kPa
10N400U1	CIUC	71.0	149.8	18	200	99	400	Loose sample
40N25OU1	CIUC/E	71.0	150.3	47	250	99	250	Loose sample

** : used in the calibration of hypoplasticity model parameters

OCR = 2

File	Stress Path	Sample Diameter (mm)	Sample Height (mm)	Relative Density (%)	Back Pressure (kPa)	B Value (%)	Confining Pressure σ_{3c}'(kPa)	Remark
O50U3	CIUC	70.9	151.7	73	250	97.1	50	16 hrs @ BP=0, cell pres.=100 kPa; then 20 min BP sat. @ 250 kPa; PWP always decrease
O60U2001	CIUC/E	71.2	149.3	69	250	95.5	200	Tri. consol exe. before shear; then 2 hrs BP sat. @ 250 kPa; PWP always decrease
O50U2	CIUE	70.9	150.5	67	250	98.7	50	1.5 hrs @ cell pres.=100 kPa, BP=0; then 23 hrs BP sat. @ 250 kPa
O60U2006	CIUE	71.2	151.9	69	250	97	200	Tri consol exe. before shear; then 18 min BP sat. @ 250 kPa

OCR = 4

File	Stress Path	Sample Diameter (mm)	Sample Height (mm)	Relative Density (%)	Back Pressure (KPa)	B Value (%)	Confining Pressure σ_{3c}'(KPa)	Remark
O50U1	CIUC	70.9	151.4	64	250	99.2	50	2.5 hrs @ cell pres.=200 KPa, BP=0; then 33 min BP sat. @ 250 kPa
O60U1001	CIUC	71.3	151	68	250	94	100	Bad result, because the ram screw was still tighten during test
O60U1002	CIUC/E	71.1	149.1	66	250	96.7	100	Tri. consol. exe. before shear; 25 min BP sat. @ 250kPa
O50U4	CIUE	70.8	150.2	69	250	97.5	50	20 hrs @ cell pres=200kPa, BP=0; then 6 min BP sat. @ 250 kPa
O60U1006	CIUE	71.3	152.4	66	250	97.2	100	Tri consol. exe. before shear; then 13 min BP sat. @ 250 kPa

Table 2.3.1 : Summary of Triaxial, Drained, Strained Controlled, Constant p' Test Data for Nevada Sand

OCR=1

File	Stress Path	Sample Diameter mm)	Sample Height (mm)	Relative Density (%)	Back Pressure (kPa)	B Value (%)	Confining Pressure σ_{3c}'(kPa)	Remark
N70D501	CIDC	71.1	149	74	250	98.1	50	** Test stop @ axi. stn=9.5%
N70D1001	CIDC/E	71.2	148.4	72	250	98.6	100	** Dev. sts suddenly drop @ dev. stn=9% & axi. stn=8%
N70D2501	CIDC/E	71.3	147.7	75	250	99.1	250	** Dev. sts suddenly drop @ dev stn=8.5% & axi stn=7.5%
N70D100A	CIDC	70.9	147.6	76	200	100.0	100	Inside load cell exe.; dark sand inside sample(each 1" distance)
N70D100B	CIDC	71.4	149.5	82	200	98.3	100	Inside load cell exe.; dark sand inside sample (each 1" distance); axial strain reach 3.6% (expected max. dev. strs.)
N70D100C	CIDC	71.3	149.4	85	200	99.0	100	Inside load cell exe.; dark sand inside sample (each 1" distance); sts data not smooth
N70D1005	CIDE/C	71.2	148.9	77	250	99.0	100	** Dev. sts suddenly drop @ dev stn=7.5% & axi stn=8%
N70D2505	CIDE/C			76		100.0	250	** Dev. sts suddenly drop @ dev stn=6% & axi stn=6.2%
N70D100P	CIDE/C	71.3	143.9	76	200	99.6	100	Inside load cell exe; bad results because damper was closed during shear
N70D100Q	CIDE/C	71.9	140.7	73	200	99.5	100	Inside load cell exe.;poor result, plot not given
N70D100R	CIDE/C	69.2	144.5	70	200	100.0	100	Inside load cell exe.

** : used in the calibration of hypoplasticity model parameters

Table 2.4.1 : Summary of Triaxial, Undrained, Stress Controlled, Cyclic Test Data for Nevada Sand

OCR = 1 (Normal Consolidated Samples

File	Sample Diameter (mm)	Sample Height (mm)	Relative Density (%)	Back Pressure (kPa)	B Value (%)	Confining Pressure σ_{3c}'(kPa)	Stress Ratio	Maximum Deviatoric Sts (kPa)	Minimum Deviatoric Sts (kPa)	Period (sec)	N (5% stn)	N Tot.	Remark
CY50N1	70.8	149.6	65	250	98.6	50	0.13	13	-13	300	15	13	** P' reach negative value; 22.5 hrs @ BP=0 ceel pre=50kPa
CY100N1	70.9	146.7	62	250	97.9	100	0.15	30	-30	300	4	2	11.5 hrs @ BP=0 cell=100kPa
CY100N2	70.9	152.1	75	250	96.1	100	0.13	26	-26	300		50+	no lique.; 17 hrs @ BP=0, cell pre=100 kPa; noisy sts-stn curve
CY100N3	70.2	145.4	65	250	97.1	100	0.825	165	0	300		50+	Cyclic compression (660*0.25); 16.5 hrs @ BPO=0, cell pre=100 kPa; 50 min BP sat. @ 250 kPa
CY100N4	70.8	151.4	65	250	99.1	100	0.35	230	0	300		50+	Cyclic compression (660*0.35); 18.5 hrs @ BP=0, cell pre=100 kPa; 20 min BP sat. @ 250 kPa
CY100N5	70.8	148.6	66	250	97.8	100	0.075		0	300		50+	Cyclic compression (660*0.075); 20.5 hrs @ BP=0, cell pre=100 kPa; noisy sts-stn curve
CY100N6	70.1	151.8	65	250	97.8	100	0.15	30	-30	300	8	3	** 12.5 hrs @ BP=0, cell pre=100 kPa
CY250N1	71.2	152.3	65	250	97.5	250	--	225	-16.25	300	20	14	Dev sts from ult Strgth; 15 hrs BP sat. @ 250 kPa, cell pre=450 kPa

CY250N2	70.9	151.1	66	250	98.5	250	0.35	70	-22.75	60		50+	Dev sts from yld strgth; noisy sts-stn curve; stn only reach 0.09%; 2.5 hrs @ BP=0, cell pre=250 kPa
CY250N3	71.2	153.7	56	250	89.4	250	0.25	125	-125	60	2	1	Poor B value;
CY250N4	71.1	149.2	59	250	96.6	250	0.15	75	-75	60	10	10	1.5 hrs @ BP=0, cell pre=250 kPa;17 hrs BP sat . @250 kpa
CY250N5	70.9	146.7	69	250	97.3	250	0.15	75	-75	60	11	9	** 17 hrs BP sat. @ 250kPa, cell pre=500 kPa
CY250N6	70.8	150.8	68	250	97.2	250	0.15	75	-75	300	10	8	17 hrs @ BP=0, cell pre=250 kPa
CY250N7	71.1	150.8	71	250	99.9	250	0.125	62.5	-62.5	300	50+	50+	21 hrs @ BP=0, cell pre=250 kPa; noisy sts-stn curve
CY250N8	71.2	147.2	63	250	96.3	250	0.25	125	-125	300	3	1-	2 hrs @ BP=0, cell pre=250 kPa
CY250N9	70.8	150.6	68	250	96.1	250	0.2	100	-100	300	3	1-	2.5 hrs @ BP=0, cell pre=250 kPa; 15 hrs BP sat. @ 250 kPa
CY250N10	70.8	147.1	66	250	97.8	250	0.17	85	-85	300	9	8	** 2 hrs @ BP=0, cell pre=250 kPa;
CY250N11	70.8	147.3	65	250	97.1	250	0.14	70	-70	300	6	4	P' didn't reach zero; 2.5 hrs @ BP=0, cell pre=250 kPa
CY250N12	70.8	146.2	66	250	94.5	250	0.13	65	-65	300	30	27	20.5 hrs @ BP=0, cell pre=250 kPa;
CY250N13	71.0	150.5	69	250	96.1	250	0.18	90	-90	300	11	8	11.5 hrs @ BP=0, cell pre=250 kPa; p' did not reach 0
CY250N14	70.7	146.9	66	250	97.9	250	0.19	85	-85	300	3	1-	8 hrs @ BP=0, cell pre=250 kPa

**: used in the calibration of hypoplasticity model parrameters

OCR = 2

File	Sample Diameter (mm)	Sample Height (mm)	Relative Density (%)	Back Pressure (kPa)	B Value (%)	Confining Pressure σ_{3c}'(kPa)	Stress Ratio	Maximum Deviatoric Sts (kPa)	Minimum Deviatoric Sts (kPa)	Period (sec)	N Tot.	Remark
CY50O1	70.9	150.6	65	250	98.1	50	0.15	15	-15	300	16	19.5 hrs BP sat. @ 250 kPa, cell pre=350 kPa
CY100O1	70.7	148.2	67	250	97.1	100	0.15	30	-30	300	37	18 hrs @ BPO=0, cell pre=200 kPa then reach BP=250 kPa, cell pre=450 kPa
CY100O21	71.0	151.6	69	250	98.1	100	0.18	36	-36	300	30	Tri. consoli. exe. before shear;
CY100O22	71.1	151.3	68	250	98.6	100	0.19	38	-38	300	19	Tri. consoli. exe. before shear
CY200O1x	70.9	152.3	68	250	97.7	200	0.17	68	-68	300	10	Tri consoli. exe. before shear
CY200O21	71.2	150.7	65	250	98.4	200	0.2	80	-80	300	11	Tri. consoli. exe. before shear

OCR=4

File	Sample Diameter (mm)	Sample Height (mm)	Relative Density (%)	Back Pressure (kPa)	B Value (%)	Confining Pressure σ_{3c}'(kPa)	Stress Ratio	Maximum Deviatoric Sts (kPa)	Minimum Deviatoric Sts (kPa)	Period (sec)	N Tot.	Remark
CY100O2	71.0	149.8	67	250	96.1	100	0.17	34	-34	300	50+	Tri. consoli. exe. before shear; noisy sts-stn curve; axial strain only reach -0.09%
CY100O3x	71.0	149.6	66	250	97.1	100	0.2	40	-40	300	23	Tri. consoli. exe. before shear
CY100O4	71.1	150.9	69	250	98	100	0.21	42	-42	300	50+	Tri. consoli. exe. before shear; noisy sts-stn curve; axial strain only reach -0.07% and +0.05%
CY100O46	70.9	150.5	67	250	98.1	100	0.25	50	-50	300	4	Tri. consoli. exe. before shear;
CY100O47	70.8	149.5	66	250	98	100	0.24	48	-48	300	4	Tri. consoli. exe. before shear
CY100O48	70.7	149.3	64	250	98.6	100	0.23	46	-46	300	3	Tri. consoli. exe. before shear
CY100O49	70.9	150.5	66	250	98.3	100	0.22	44	-44	300	22	Tri. consoli. exe. before shear

OCR = 8

File	Sample Diameter (mm)	Sample Height (mm)	Relative Density (%)	Back Pressure (kPa)	B Value (%)	Confining Pressure σ_{3c}'(kPa)	Stress Ratio	Maximum Deviatoric Sts (kPa)	Minimum Deviatoric Sts (kPa)	Period (sec)	N Tot	Remark
CY50O2	70.9	149.8	69	250	99	50	0.2	20	-20	300	50+	Tri. consoli. exe. before shear; noisy sts-stn curve; axial strain only reach -0.09% and +0.09%

Table 2.5.1 : Summary of Triaxial, Consolidation and Rebound Test Data for Nevada Sand

File	Sample Diameter mm)	Sample Height (mm)	Relative Density (%)	Initial pressure (kPa)	Maximump ressure (kPa)	Rebound pressure (kPa)	Initial void ratio
CY50O2C	70.9	149.8	67	50	400	50	0.631
CY100O3C	71.0	149.6	66	50	400	100	0.634
CY100C46	70.9	150.5	67	100	400	100	0.631
CY100C48	70.7	149.3	64	100	400	100	0.641
CY100C49	70.9	150.5	66	100	400	100	0.634
O60C1001	71.3	151.0	68	100	400	100	0.627
O60C1002	71.1	149.1	66	100	400	100	0.634
O60C1006	71.3	152.4	66	100	400	100	0.634

Table 2.5.2 : Summary of Compression Coefficient λ and Rebound Coefficient κ for Nevada Sand

Sample	p (kPa)	λ^*	κ^*	λ	κ
CY50O2C	50-100	0.00444	0.003838	0.00317	0.00274
	100-200	0.003782	0.003356	0.00382	0.00339
	200-300	0.004614	0.002654	0.0073	0.0042
CY100O3C	50-100	0.005253		0.00375	
	100-200	0.004574	0.003851	0.00462	0.00389
	200-300	0.005144	0.002648	0.00814	0.00419
CY100C46	100-200	0.006138	0.003574	0.0062	0.00361
	200-300	0.004361	0.002648	0.0069	0.00419
CY100C48	100-200	0.006237	0.003287	0.0063	0.00332
	200-300	0.004835	0.002496	0.00765	0.00395
CY100C49	100-200	0.006287	0.003138	0.00635	0.00317
	200-300	0.004367	0.002806	0.00691	0.00444
O60C1001	50-100	0.005855		0.00418	
	100-200	0.004861	0.003574	0.00491	0.00361
	200-300	0.005144	0.002496	0.00814	0.00395
O60C1002	50-100	0.007074		0.00515	
	100-200	0.005069	0.004425	0.00512	0.00447
	200-300	0.004677	0.002806	0.0074	0.00444
O60C1006	50-100	0.005463		0.0039	
	100-200	0.004495	0.004	0.00454	0.00404
	200-300	0.00577	0.002029	0.00913	0.00321

Table 3.2.1 : Summary of Hollow Cylinder Undrained, Stress Controlled, Cyclic Torsional Shear Test Data for Nevada Sand

File	Sample I. D. (mm)	Sample O.D. (mm)	Sample Height (mm)	Relative Density (%)	Back Pressure (kPa)	B Value (%)	Cell Pressure (kPa)	$\sigma_{zθ}/p_{in}$	K Value $\sigma_θ/\sigma_z$	Number of Cycles	Remark
NK41CU50	101.1	150.6	153.5	72	200	98.5	400	0.28	0.41	15	correction of 0.1% for shear strain
NK63CU50	101.1	150.7	153.4	68	100	97.4	300	0.28	0.63	15	correction of 0.1% for shear strain
NK10CU50	101.1	150.7	153.7	71	100	99.2	300	0.28	1.0	7.5	
NK138U51	101.1	150.7	153.5	71	200	99.2	400	0.28	1.38	4.75	correction of 0.3% for shear strain

Table 3.3.1 : Summary of Hollow Cylinder Undrained, Stress Controlled, Ratational Shear Test Data for Nevada Sand

File	Sample I. D. (mm)	Sample O.D. (mm)	Sample Height (mm)	Relative Density (%)	Back Pressure (kPa)	B Value (%)	Cell Pressure (kPa)	p_{in} (kPa)	$J_{γn}^{1/2}$ (kPa)	Remark
NR40CU50	101.1	150.7	153.3	74	200	98.7	400	200	40	correction of 0.1% for shear strain
NR56CU50	101.1	150.7	153.6	73	200	94.8	400	200	56	correction of 0.1% for shear strian

TEST RESULTS
ON
TRIAXIAL UNDRAINED, STRAIN CONTROLLED, CONSTANT P TESTS

Figure 2.2.1 : Triaxial, Undrained, Strain Controlled, Constant p Test (N50U1)
Figure 2.2.2 : Triaxial, Undrained, Strain Controlled, Constant p Test (N60U1001)
Figure 2.2.3 : Triaxial, Undrained, Strain Controlled, Constant p Test (N60U1002)
Figure 2.2.4 : Triaxial, Undrained, Strain Controlled, Constant p Test (N60U1003)
Figure 2.2.5 : Triaxial, Undrained, Strain Controlled, Constant p Test (N60U2501)
Figure 2.2.6 : Triaxial, Undrained, Strain Controlled, Constant p Test (N60U2502)
Figure 2.2.7 : Triaxial, Undrained, Strain Controlled, Constant p Test (N60U4001)
Figure 2.2.8 : Triaxial, Undrained, Strain Controlled, Constant p Test (N60U4002)
Figure 2.2.9 : Triaxial, Undrained, Strain Controlled, Constant p Test (N60U4501)
Figure 2.2.10 : Triaxial, Undrained, Strain Controlled, Constant p Test (N50U2)
Figure 2.2.11 : Triaxial, Undrained, Strain Controlled, Constant p Test (N60U1006)
Figure 2.2.12 : Triaxial, Undrained, Strain Controlled, Constant p Test (N60U1008)
Figure 2.2.13 : Triaxial, Undrained, Strain Controlled, Constant p Test (N60U1009)
Figure 2.2.14 : Triaxial, Undrained, Strain Controlled, Constant p Test (N60U2506)
Figure 2.2.15 : Triaxial, Undrained, Strain Controlled, Constant p Test (N60U4006)
Figure 2.2.16 : Triaxial, Undrained, Strain Controlled, Constant p Test (10N400U1, Dr=18%)
Figure 2.2.17 : Triaxial, Undrained, Strain Controlled, Constant p Test (40N250U1, Dr=47%)
Figure 2.2.18 : Triaxial, Undrained, Strain Controlled, Constant p Test (O50U3)
Figure 2.2.19 : Triaxial, Undrained, Strain Controlled, Constant p Test (O60U2001)
Figure 2.2.20 : Triaxial, Undrained, Strain Controlled, Constant p Test (O50U2)
Figure 2.2.21 : Triaxial, Undrained, Strain Controlled, Constant p Test (O60U2006)
Figure 2.2.22 : Triaxial, Undrained, Strain Controlled, Constant p Test (O50U1)
Figure 2.2.23 : Triaxial, Undrained, Strain Controlled, Constant p Test (O60U1001)
Figure 2.2.24 : Triaxial, Undrained, Strain Controlled, Constant p Test (O60U1002)
Figure 2.2.25 : Triaxial, Undrained, Strain Controlled, Constant p Test (O50U4)
Figure 2.2.26 : Triaxial, Undrained, Strain Controlled, Constant p Test (O60U1006)

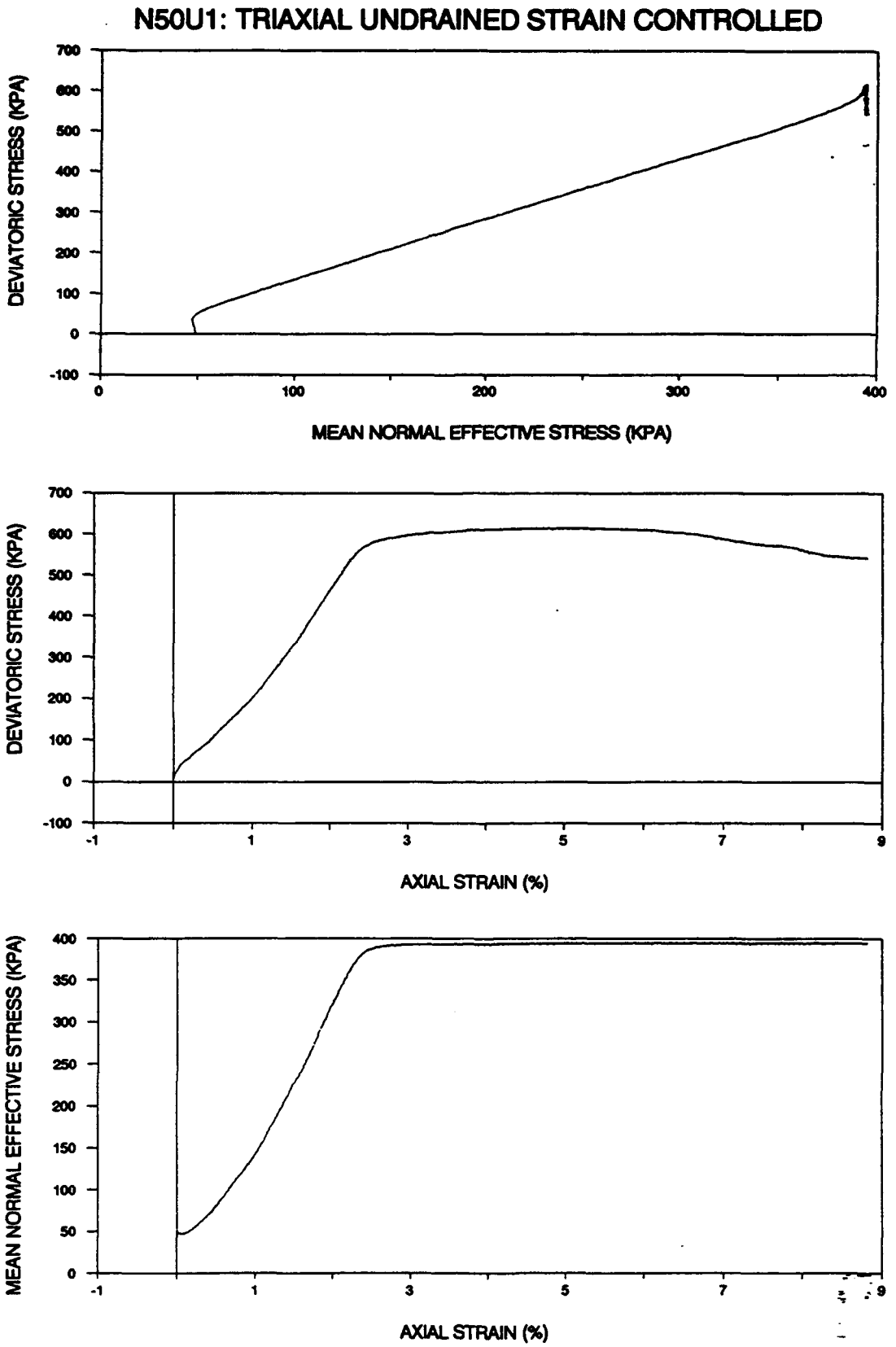

Figure 2.2.1 : Triaxial, Undrained, Strain Controlled, Constant p Test (N50U1)

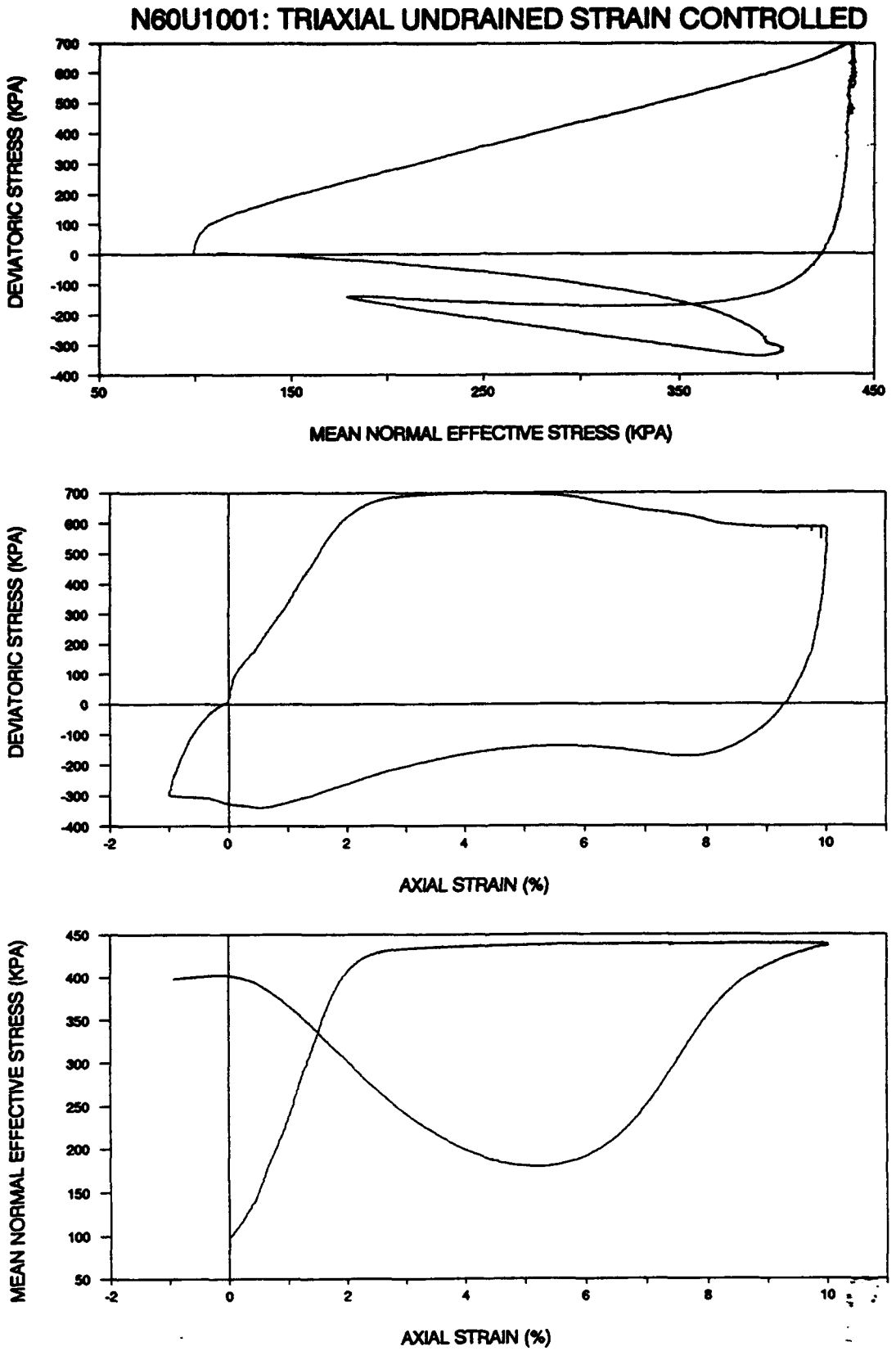

Figure 2.2.2 : Triaxial, Undrained, Strain Controlled, Constant p Test (N60U1001)

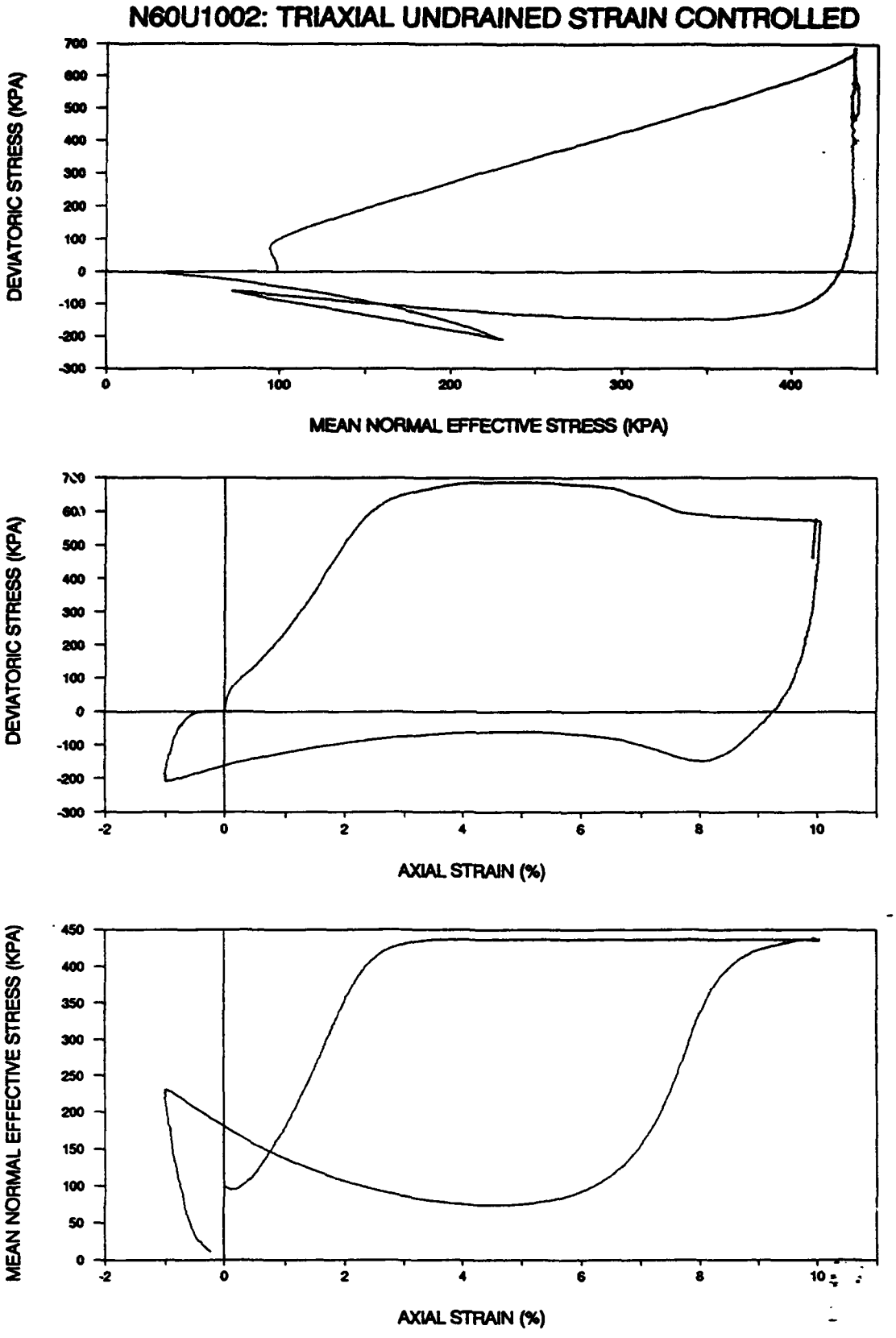

Figure 2.2.3 : Triaxial, Undrained, Strain Controlled, Constant p Test (N60U1002)

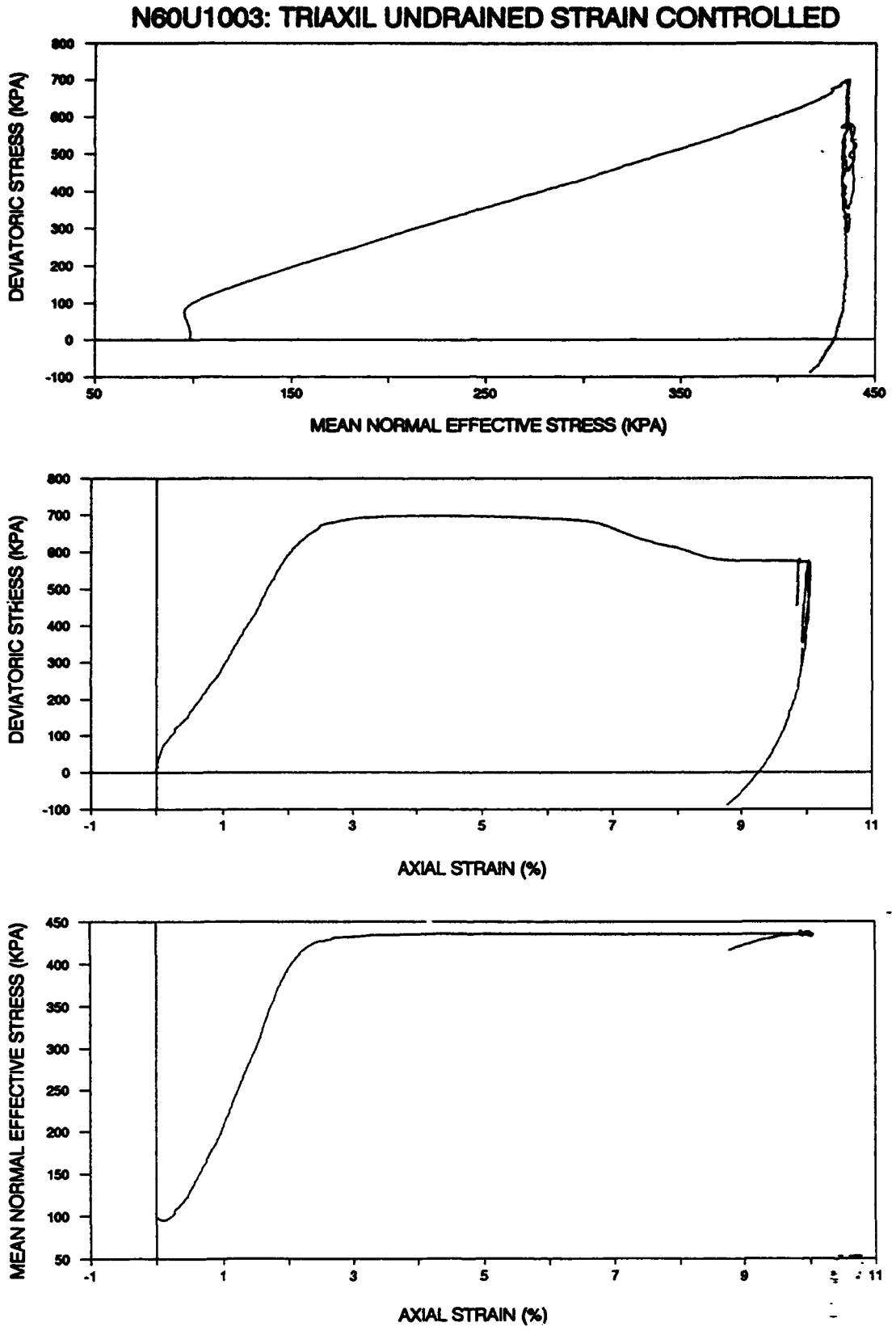

Figure 2.2.4 : Triaxial, Undrained, Strain Controlled, Const. Test (N60U1003)

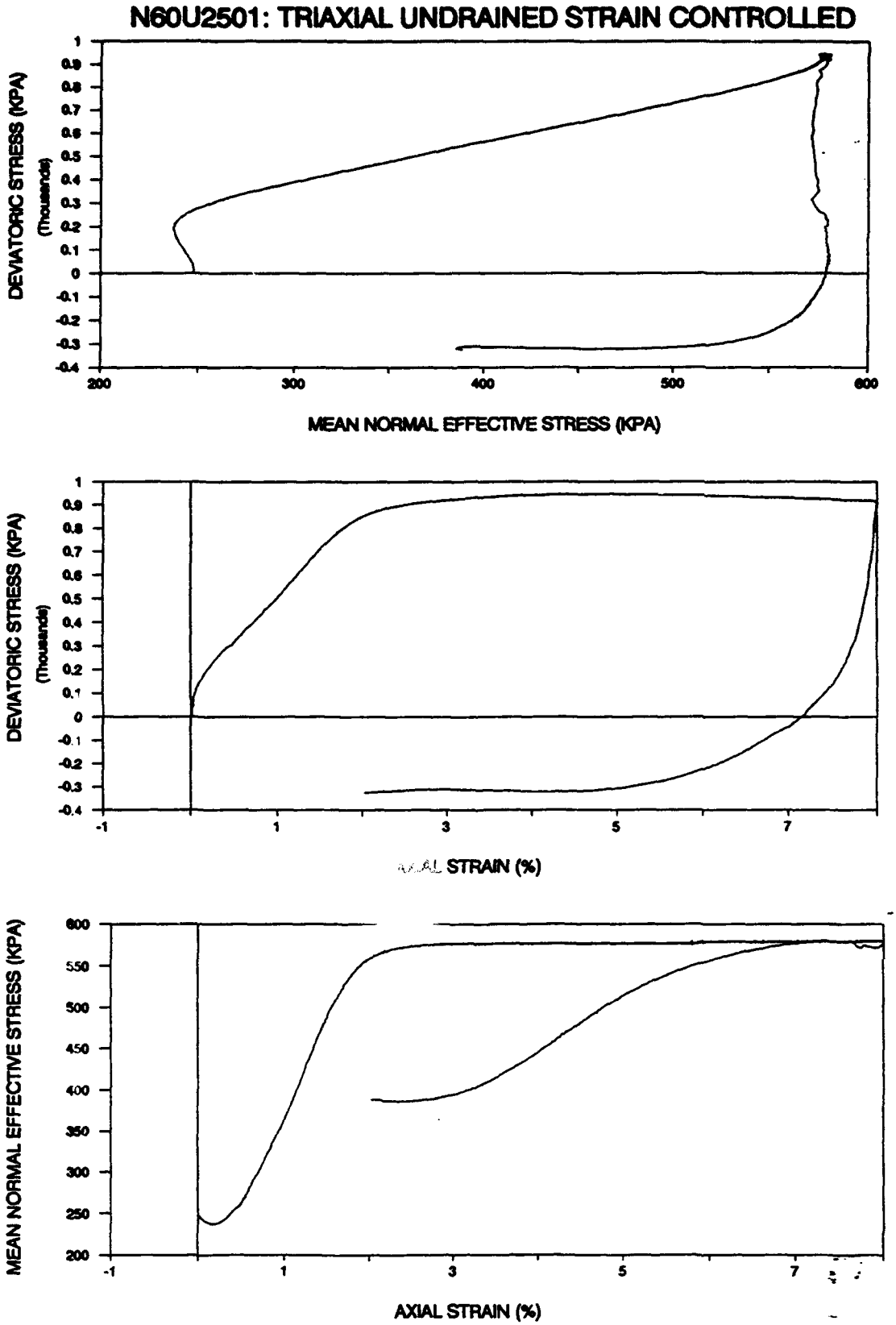

Figure 2.2.5 : Triaxial, Undrained, Strain Controlled, Constant p Test (N60U2501)

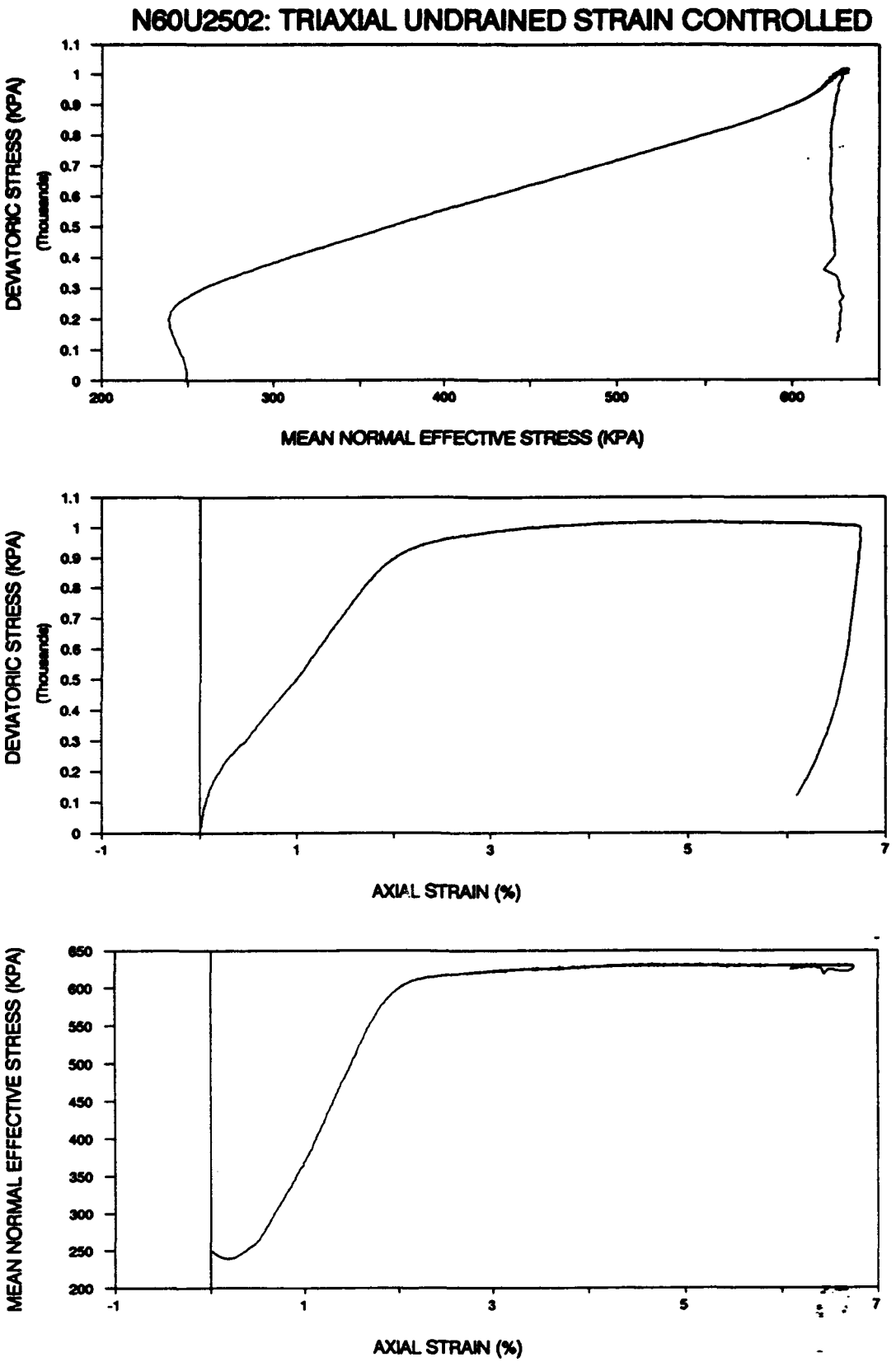

Figure 2.2.6 : Triaxial, Undrained, Strain Controlled, Constant p Test (N60U2502)

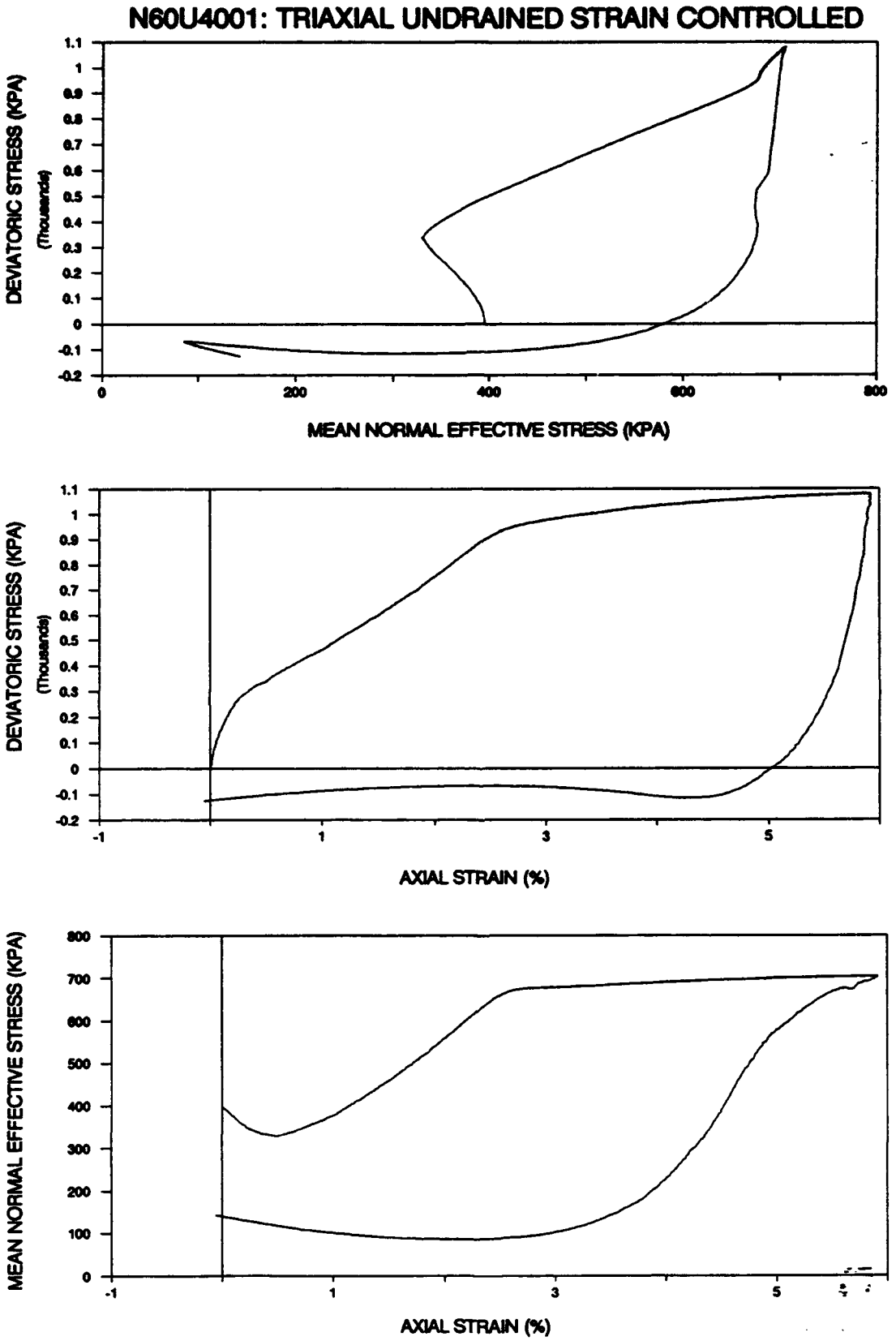

Figure 2.2.7 : Triaxial, Undrained, Strain Controlled, Constant p Test (N60U4001)

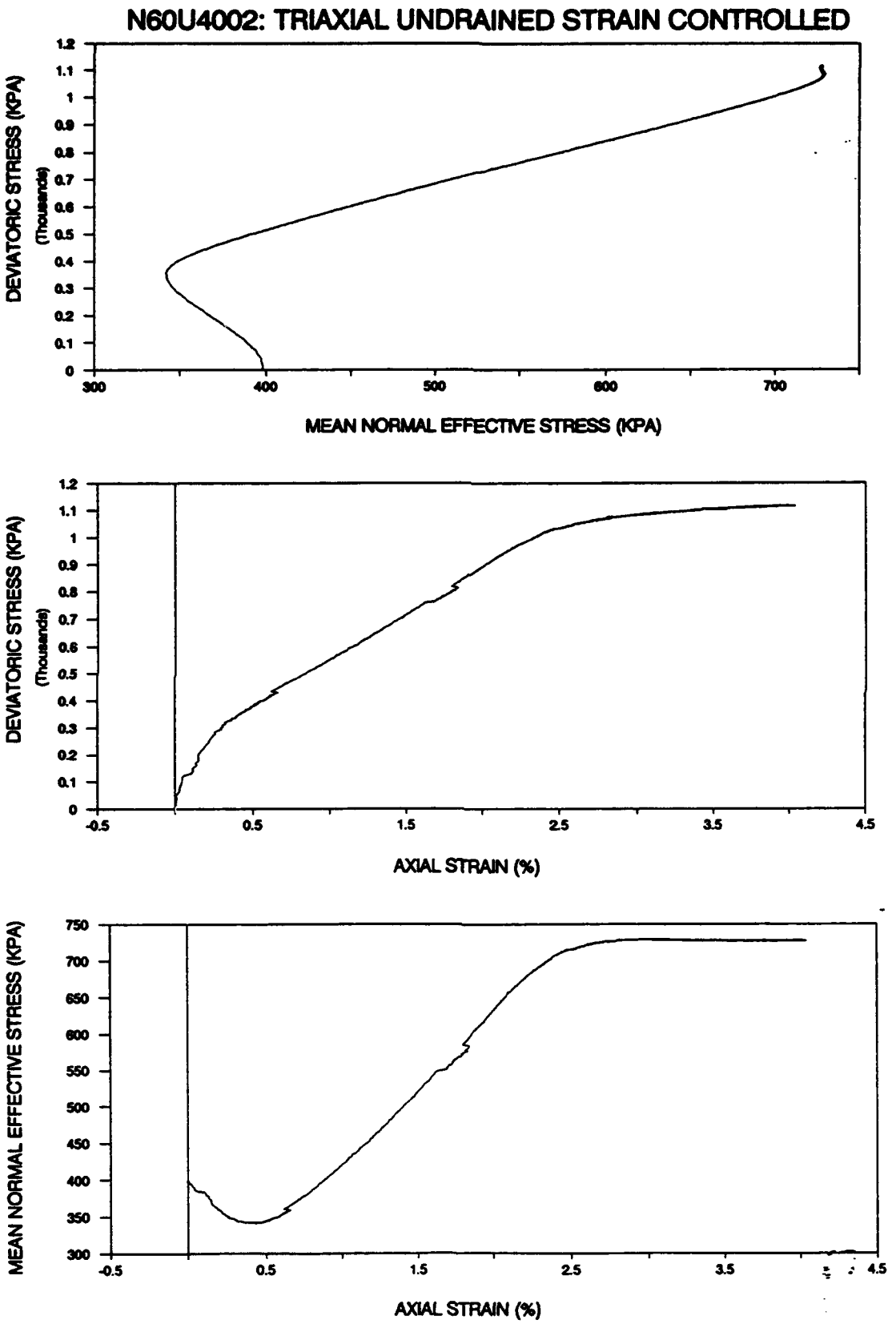

Figure 2.2.8 : Triaxial, Undrained, Strain Controlled, Constant p Test (N60U4002)

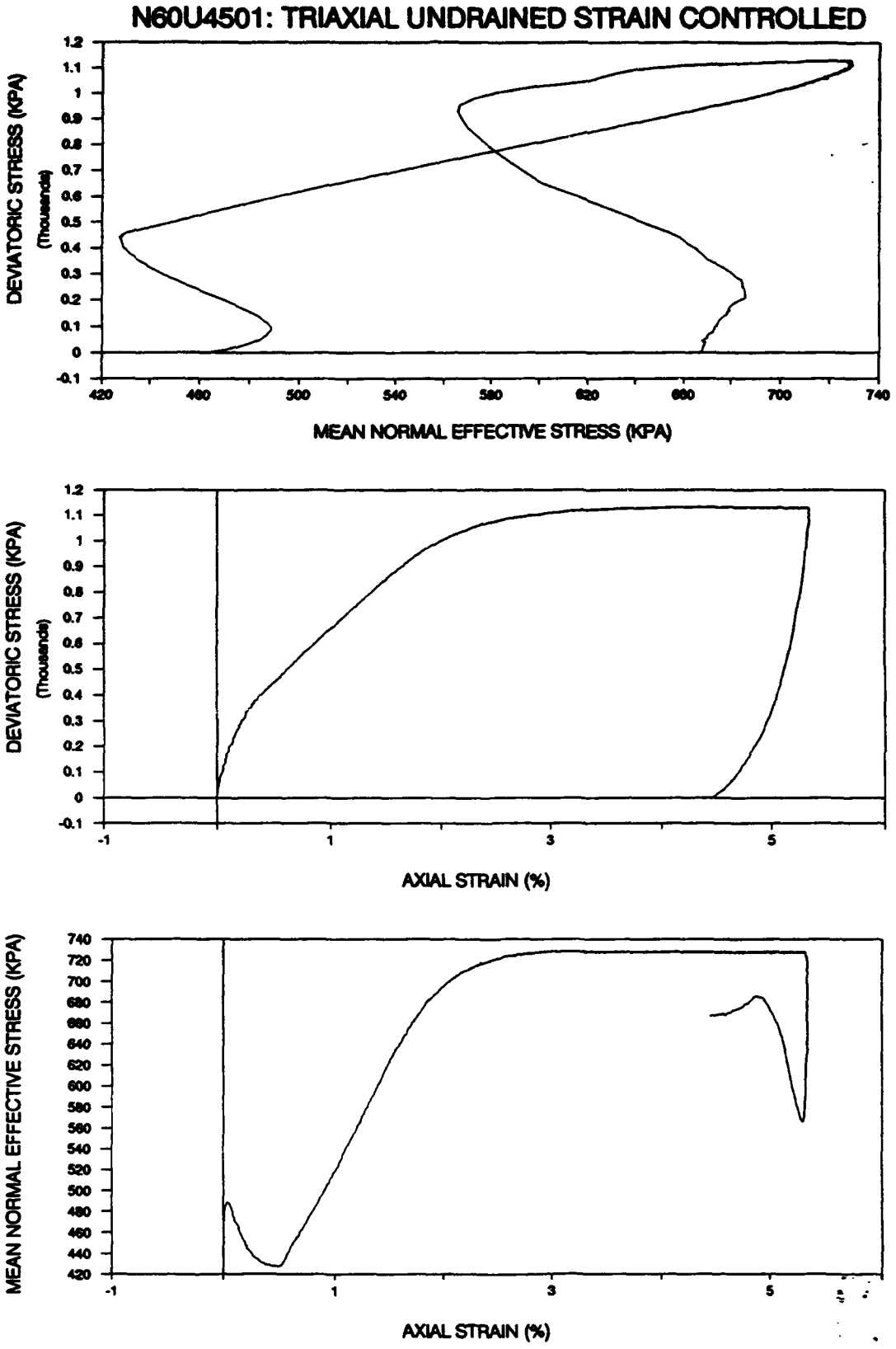

Figure 2.2.9 : Triaxial, Undrained, Strain Controlled, Constant p Test (N60U4501)

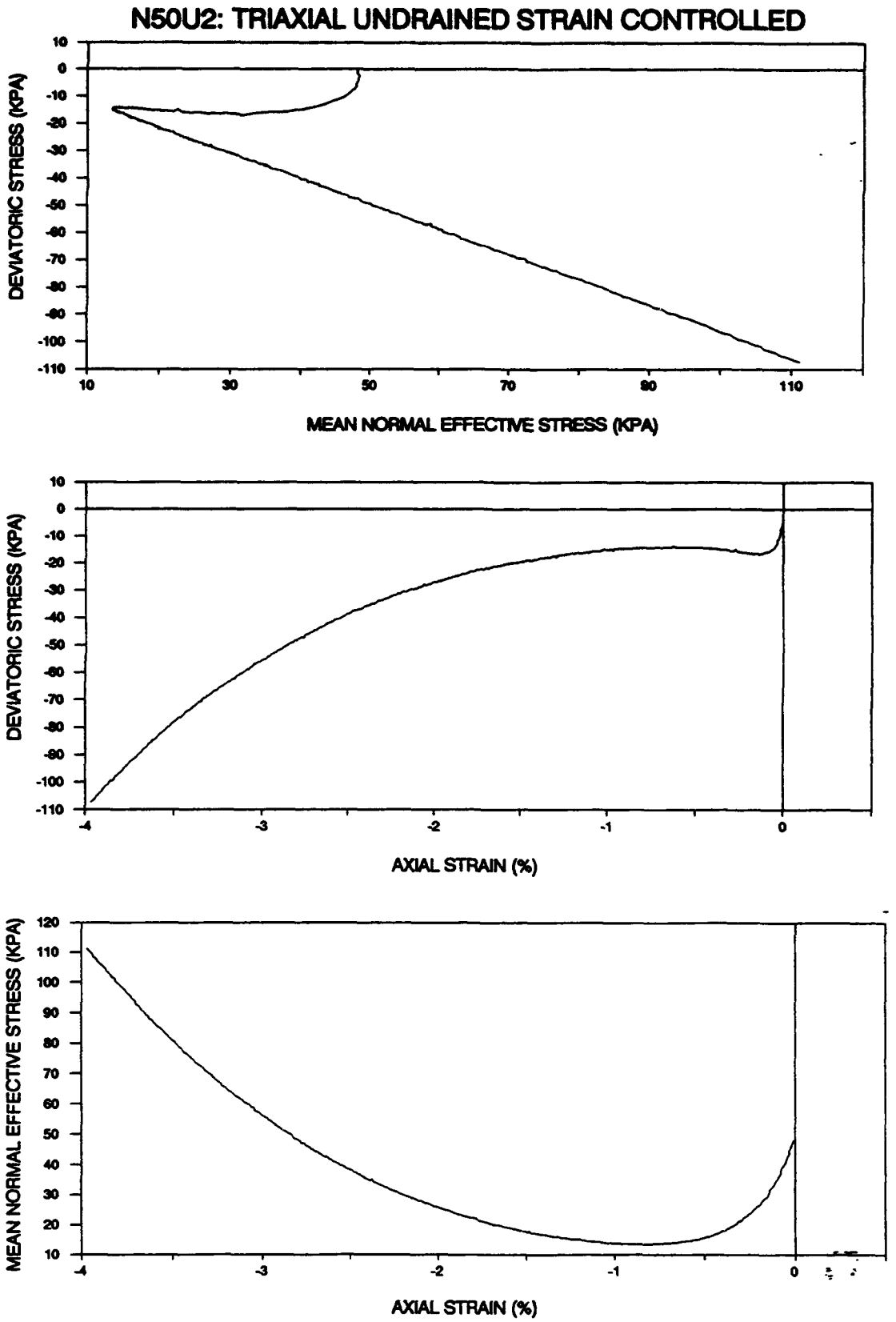

Figure 2.2.10 : Triaxial, Undrained, Strain Controlled, Constant p Test (N50U2)

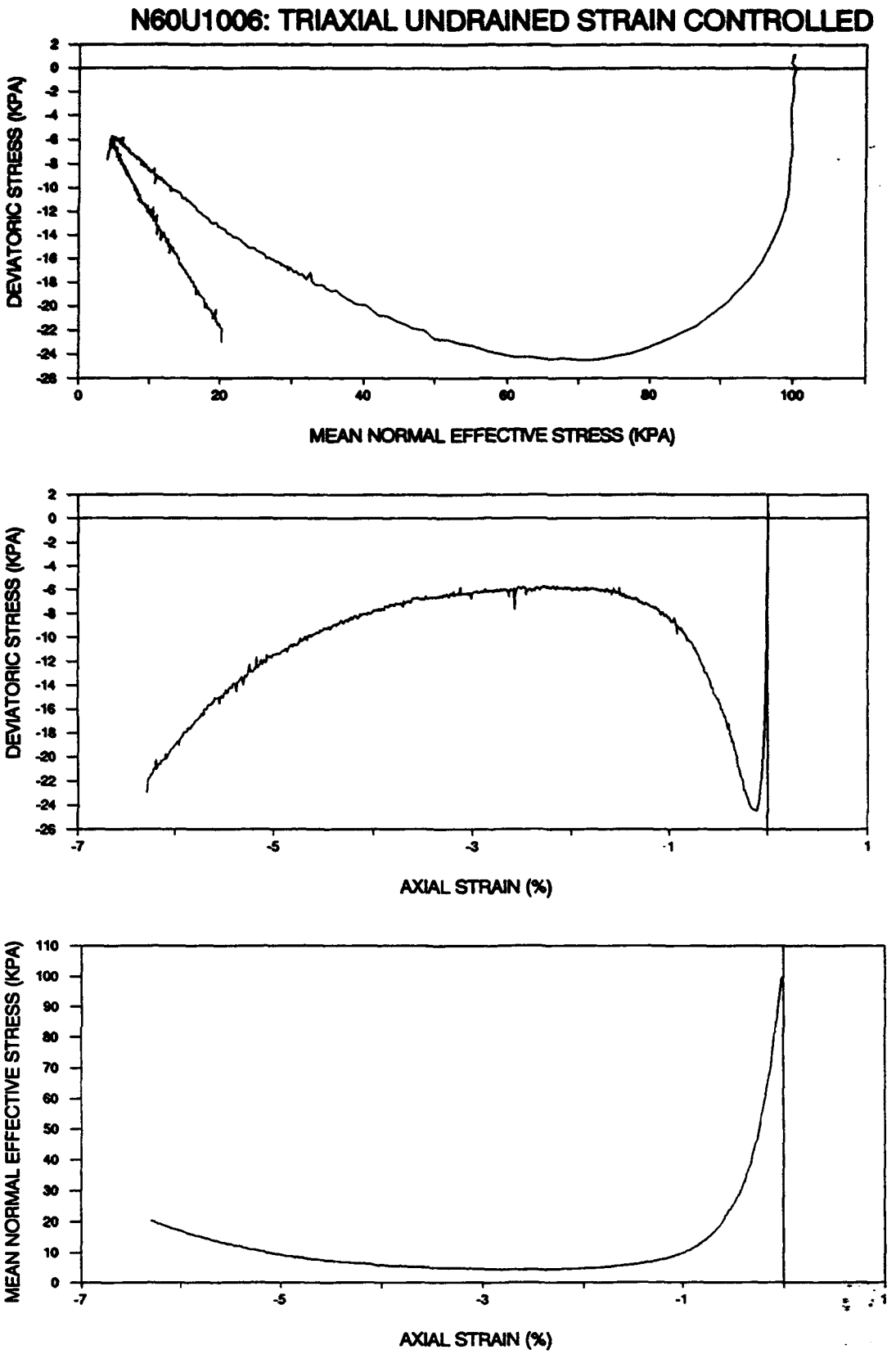

Figure 2.2.11 : Triaxial, Undrained, Strain Controlled, Constant p Test (N60U1006)

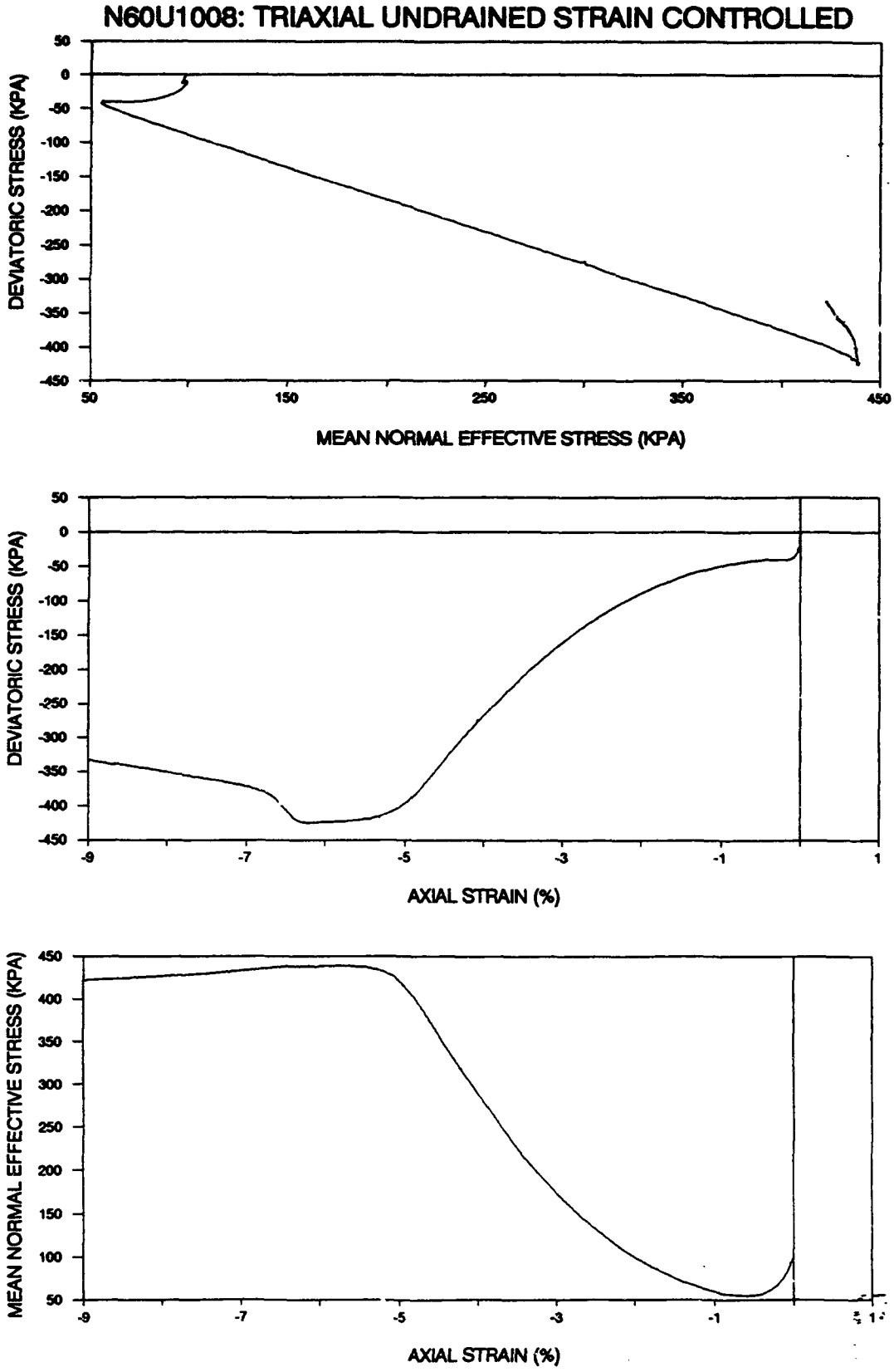

Figure 2.2.12 : Triaxial, Undrained, Strain Controlled, Constant p Test (N60U1008)

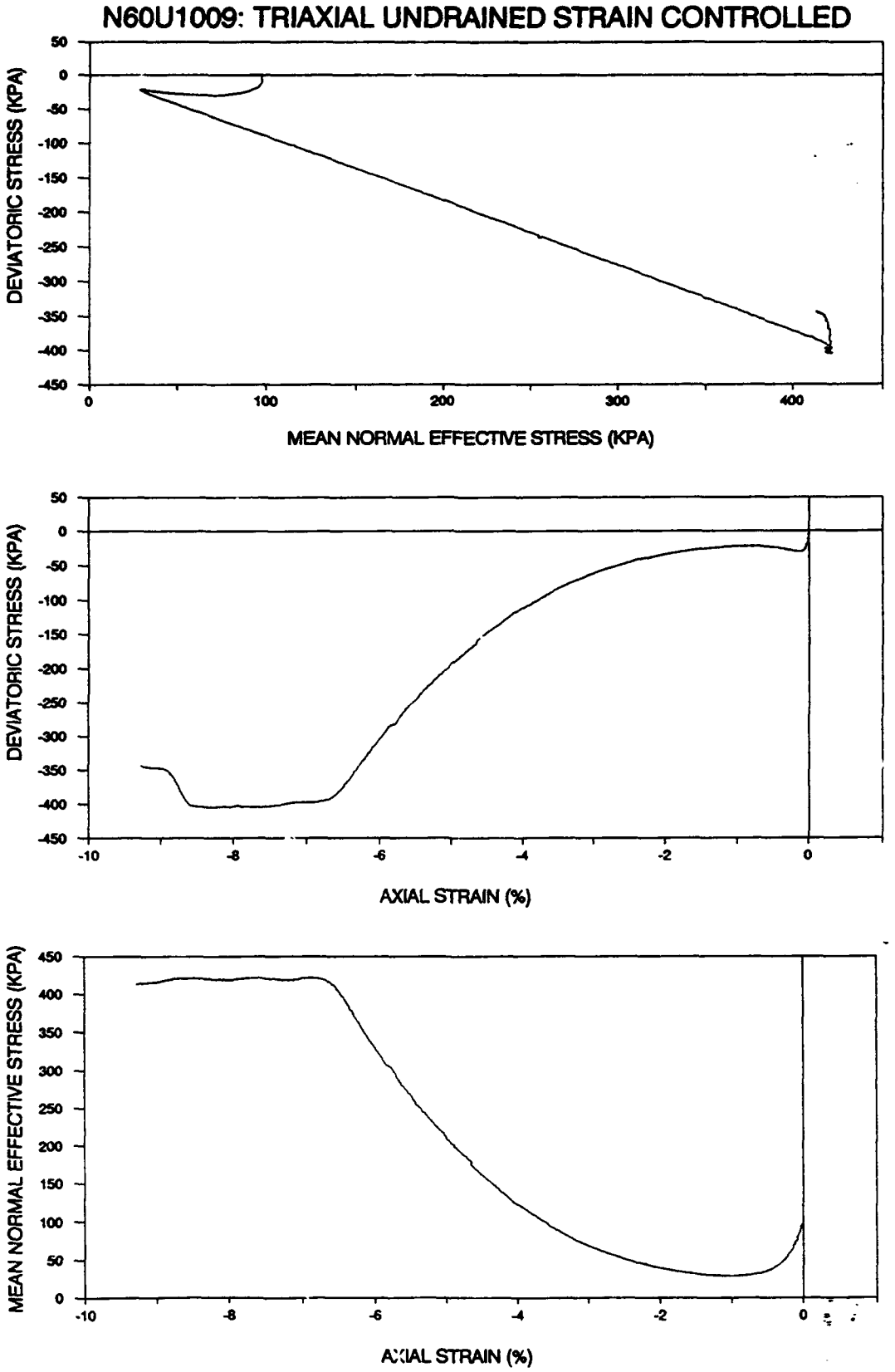

Figure 2.2.13 : Triaxial, Undrained, Strain Controlled, Constant p Test (N60U1009)

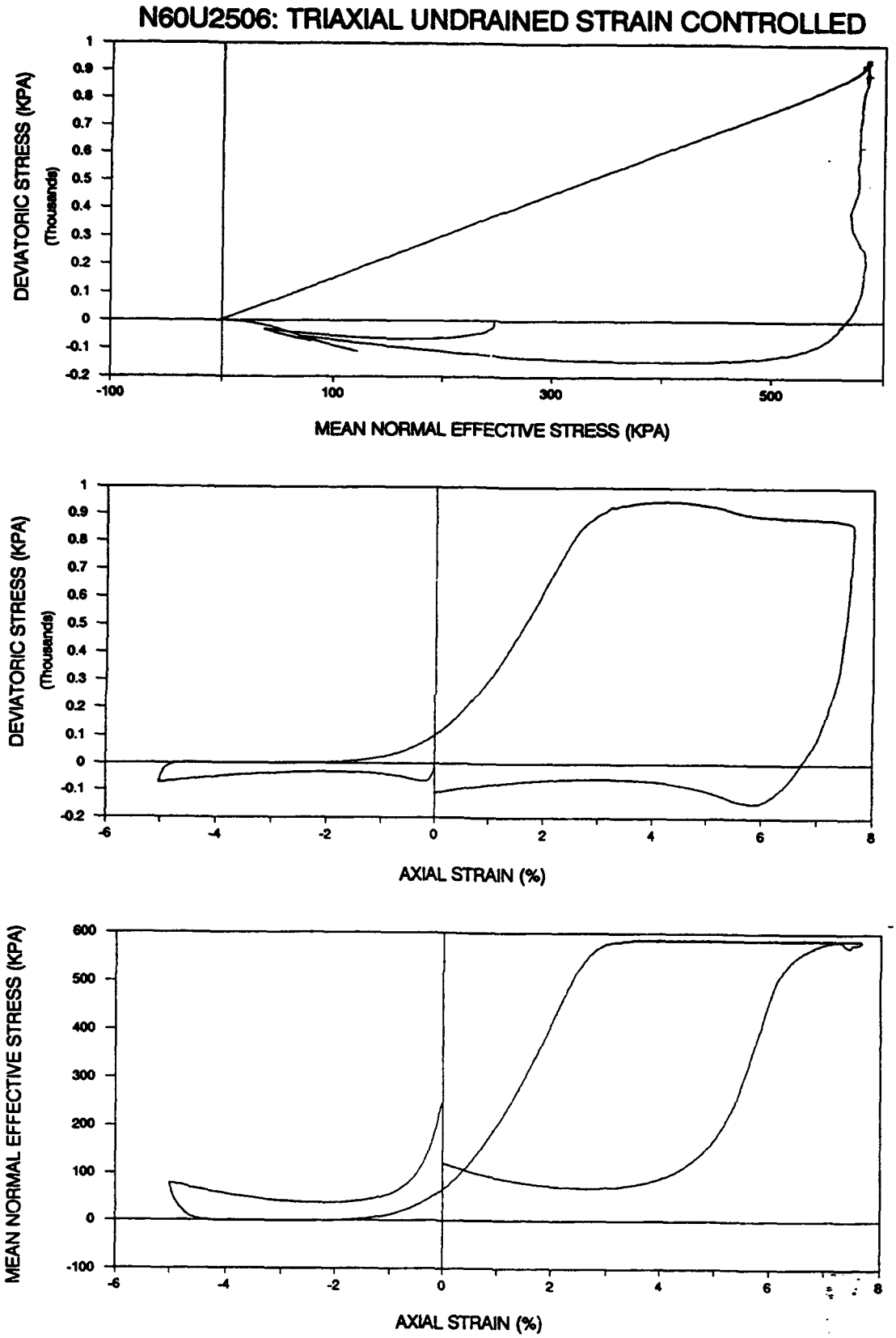

Figure 2.2.14 : Triaxial, Undrained, Strain Controlled, Constant p Test (N60U2506)

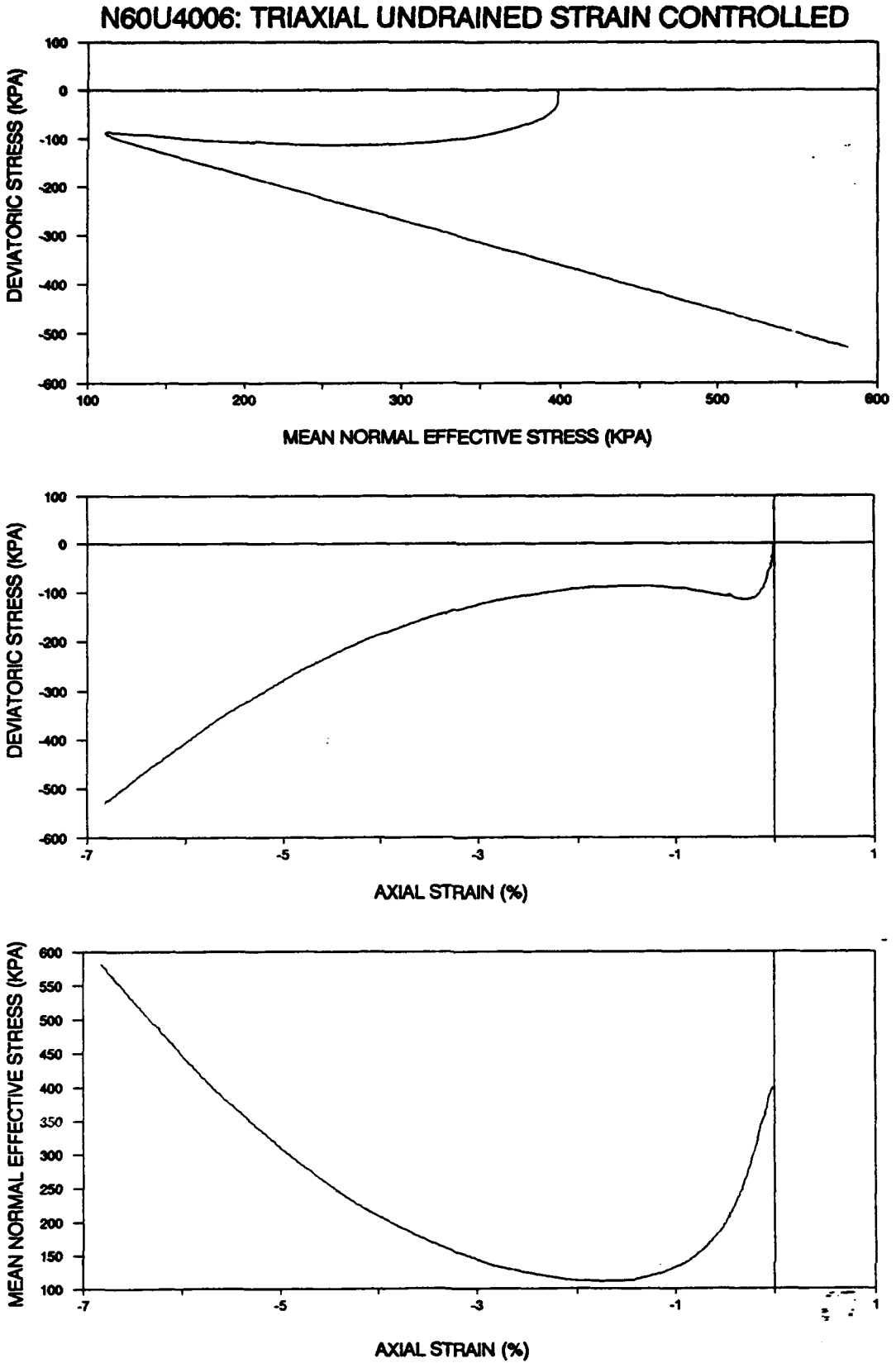

Figure 2.2.15 : Triaxial, Undrained, Strain Controlled, Constant p Test (N60U4006)

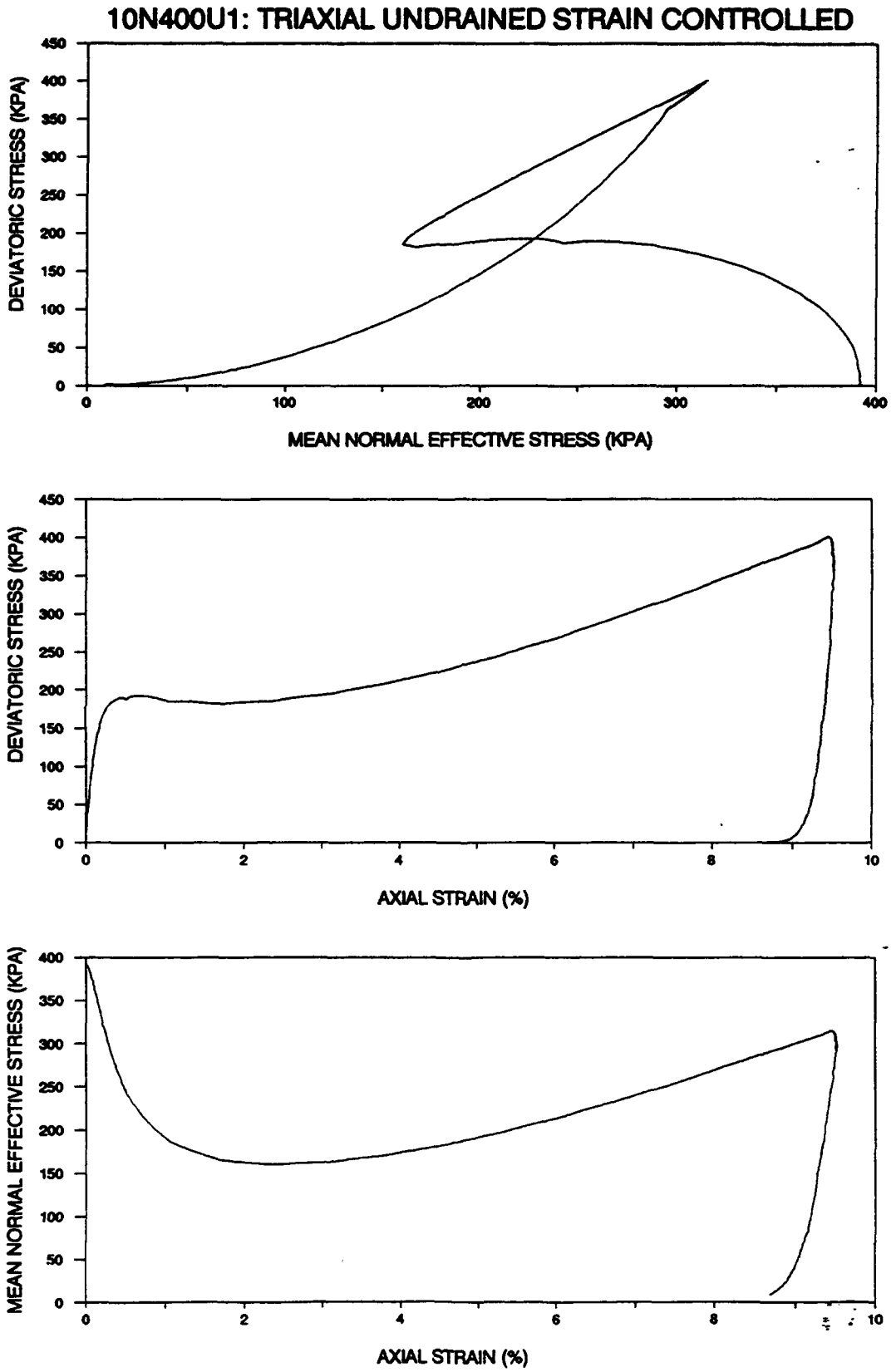

Figure 2.2.16 : Triaxial, Undrained, Strain Controlled, Constant p Test (10N400U1, Dr=18%)

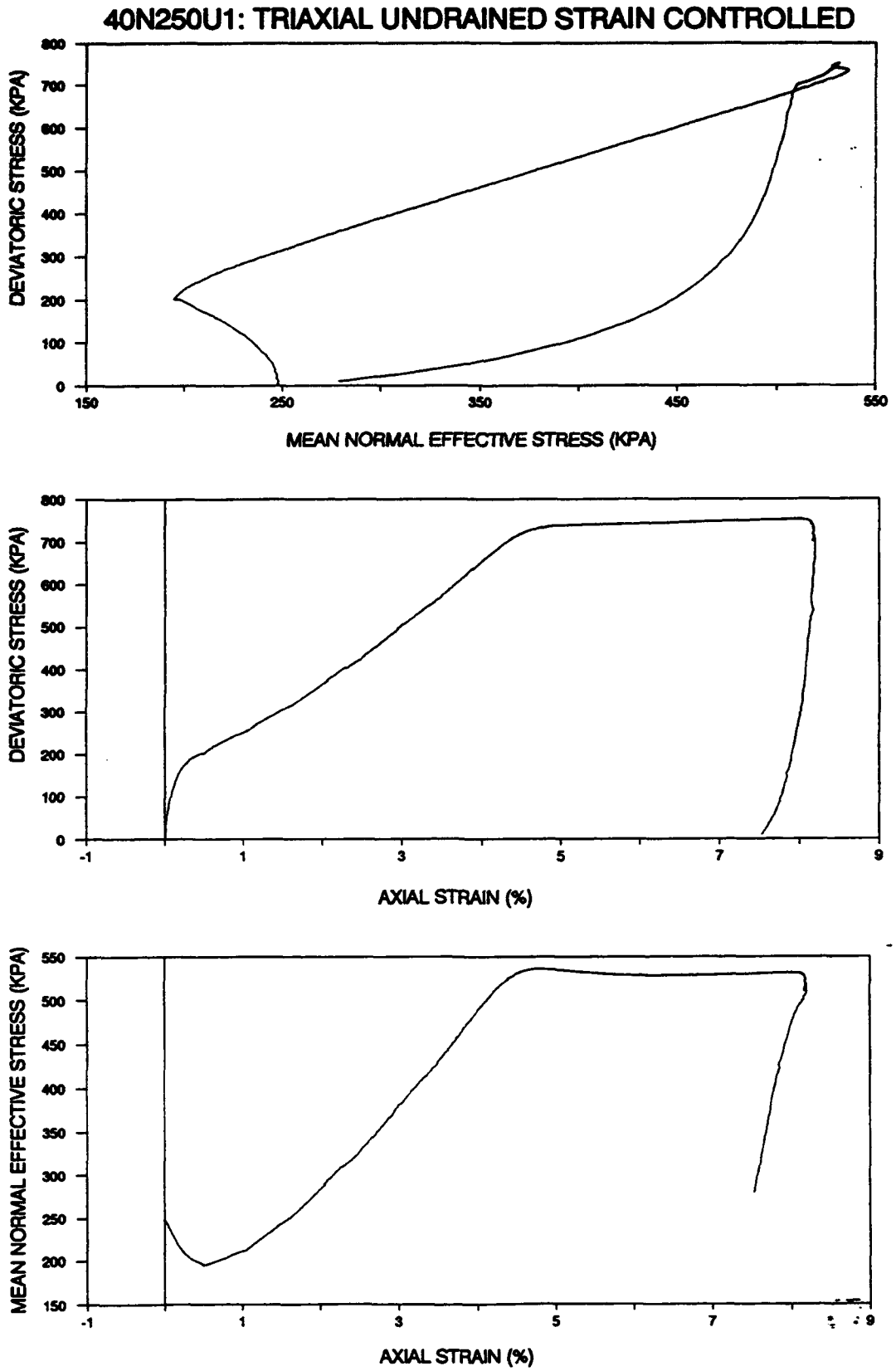

Figure 2.2.17 : Triaxial, Undrained, Strain Controlled, Constant p Test (40N250U1, Dr=47%)

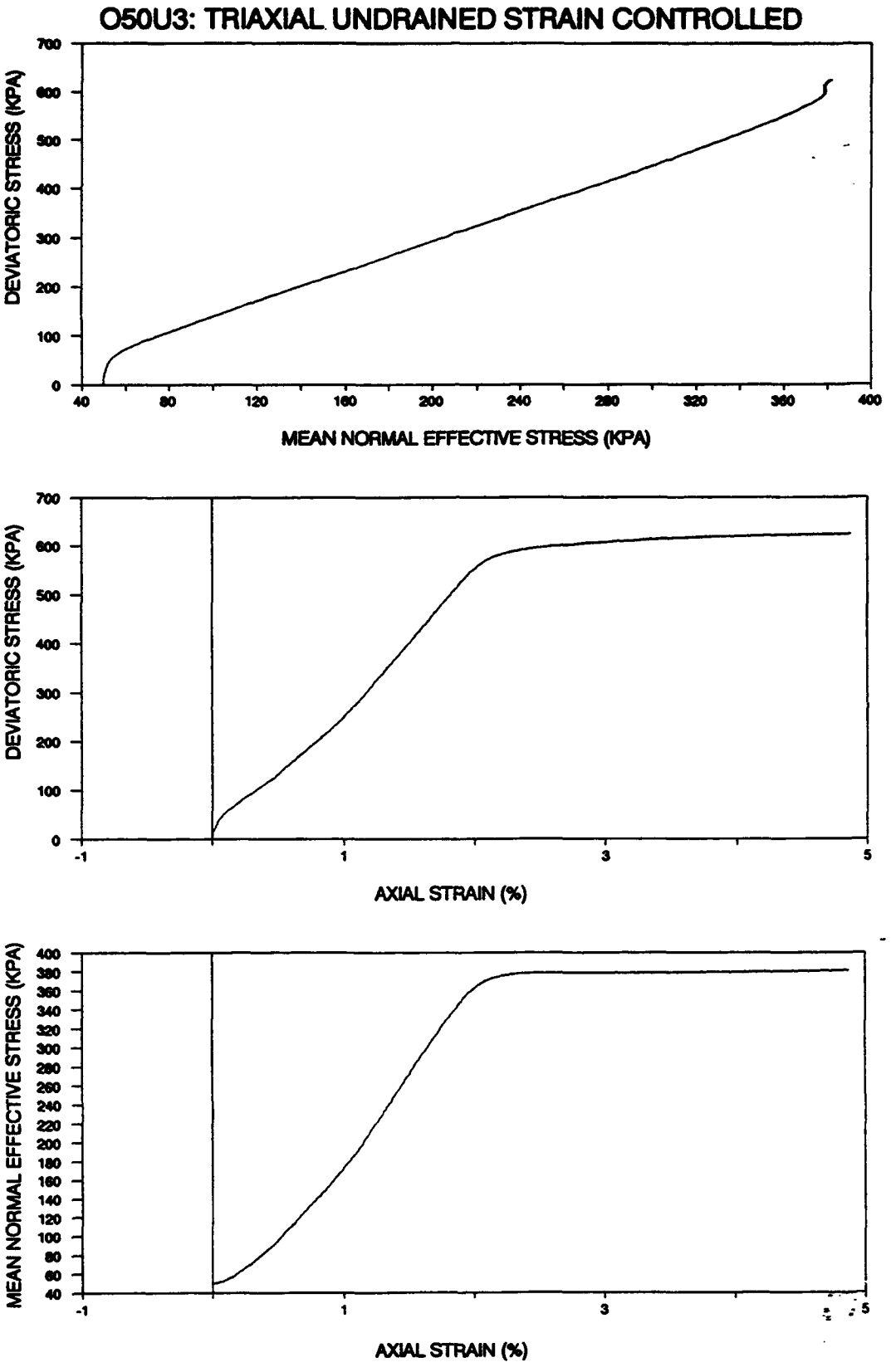

Figure 2.2.18 : Triaxial, Undrained, Strain Controlled, Constant p Test (O50U3)

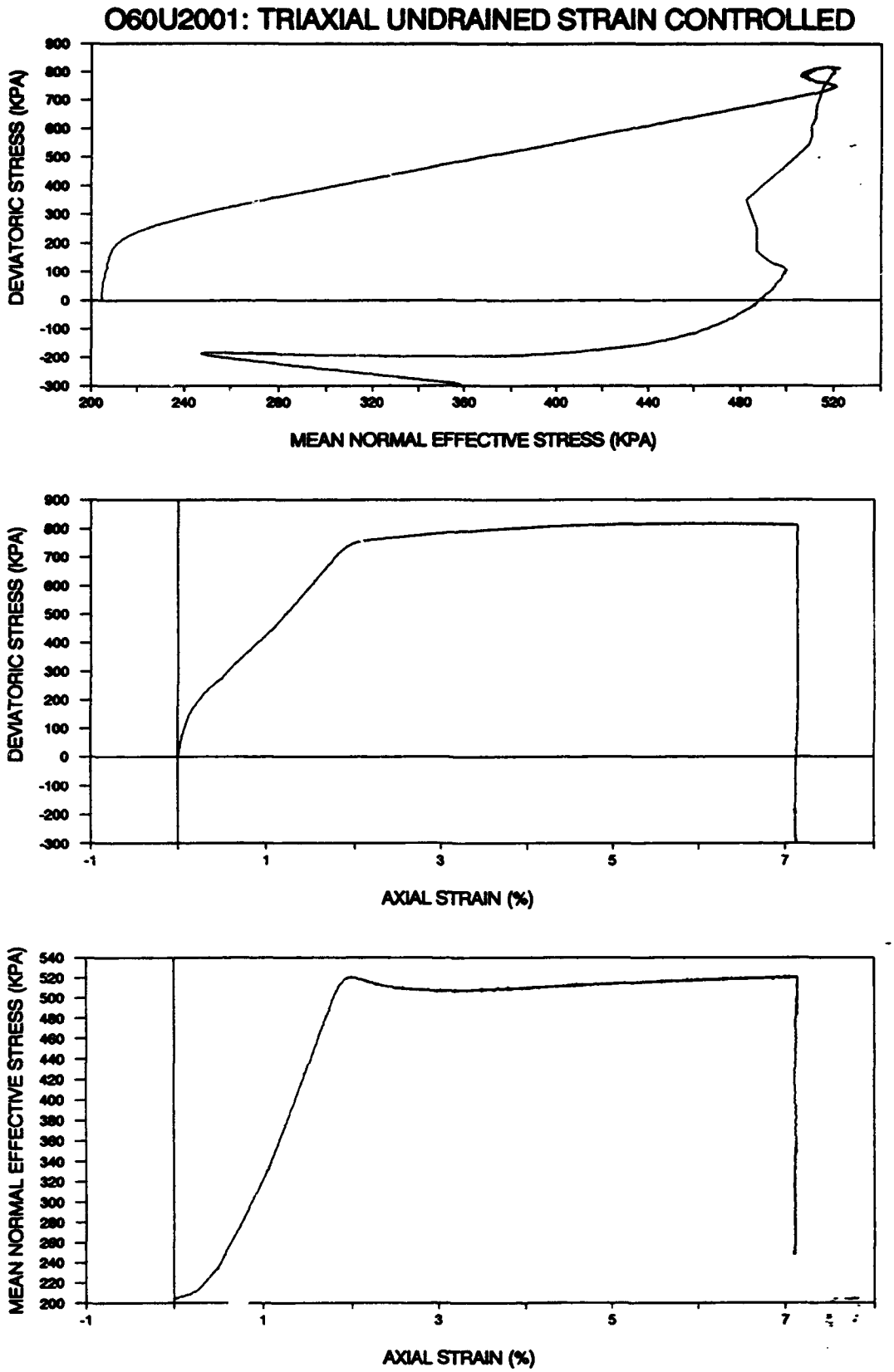

Figure 2.2.19 : Triaxial, Undrained, Strain Controlled, Constant p Test (O60U2001)

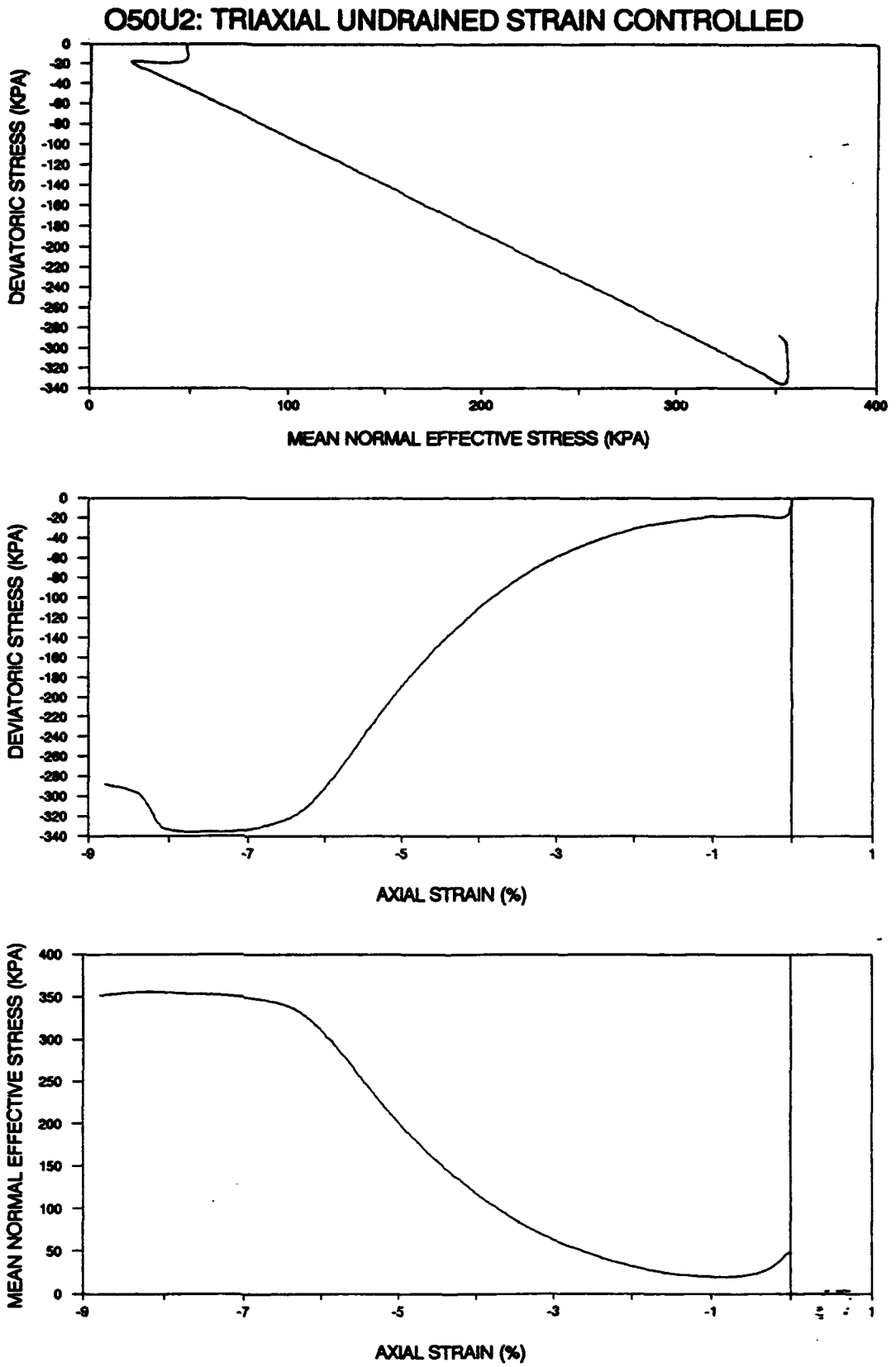

Figure 2.2.20 : Triaxial, Undrained, Strain Controlled, Constant p Test (O50U2)

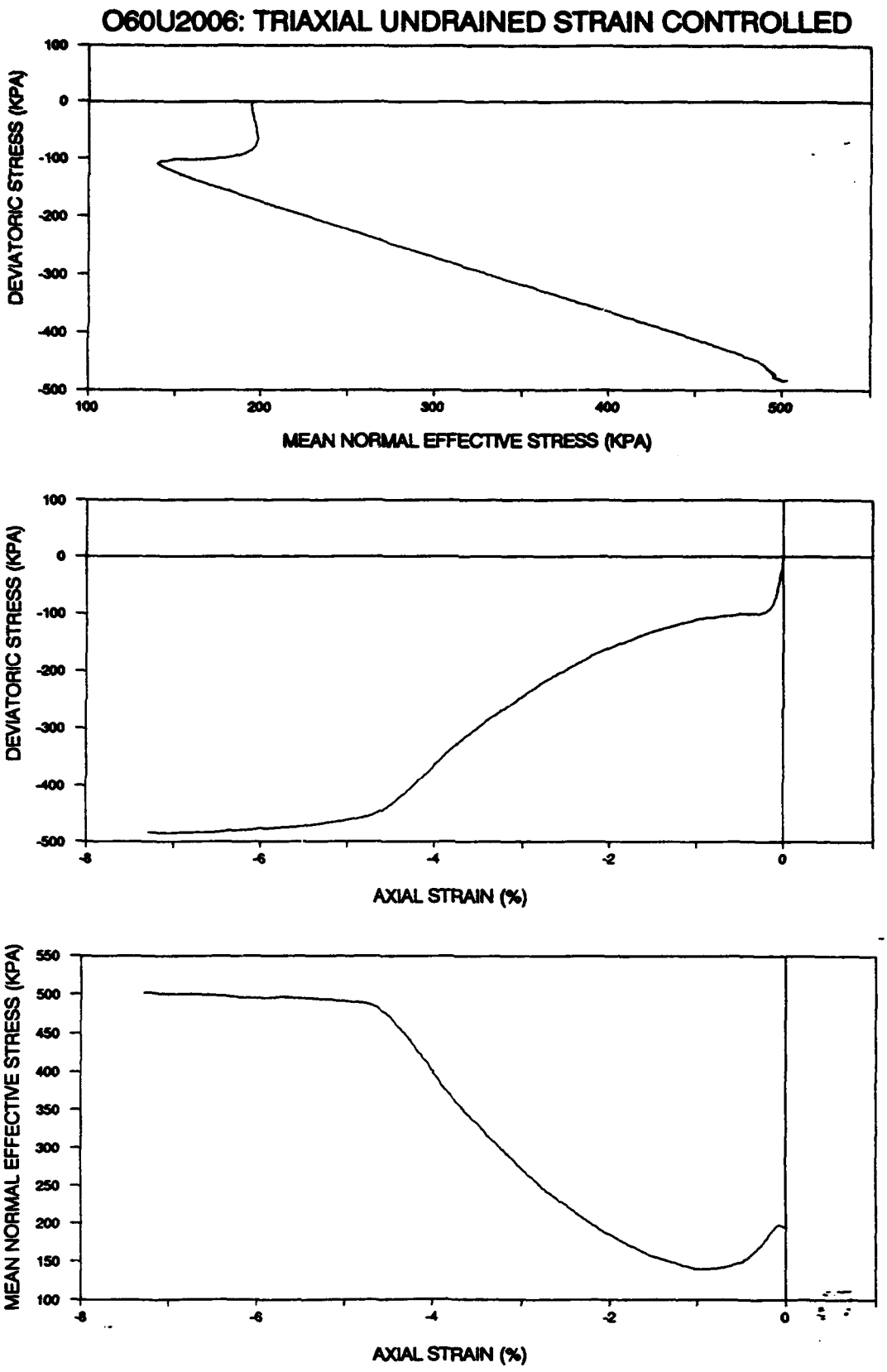

Figure 2.2.21 : Triaxial, Undrained, Strain Controlled, Constant p Test (O60U2006)

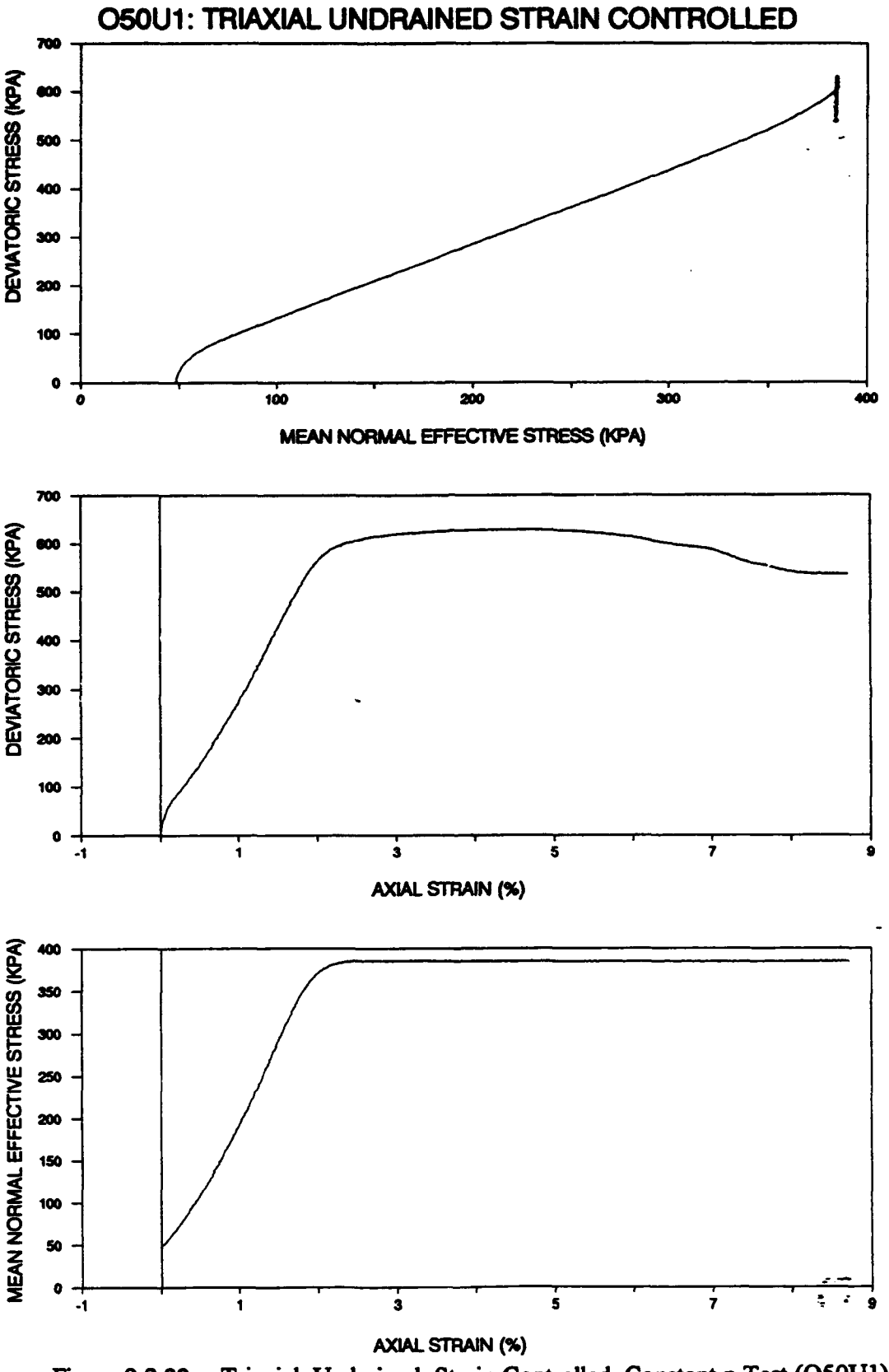

Figure 2.2.22 : Triaxial, Undrained, Strain Controlled, Constant p Test (O50U1)

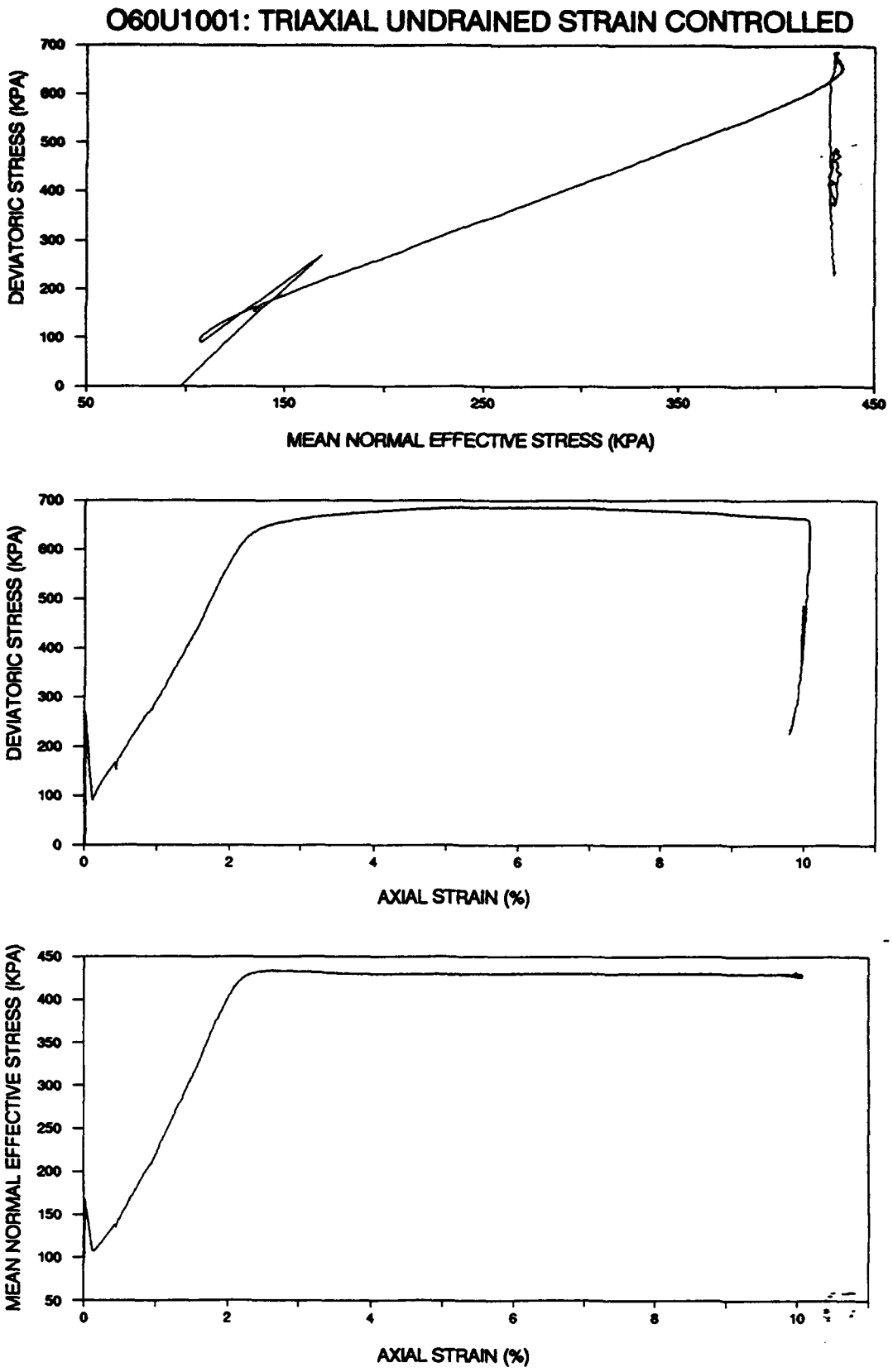

Figure 2.2.23 : Triaxial, Undrained, Strain Controlled, Constant p Test (O60U1001)

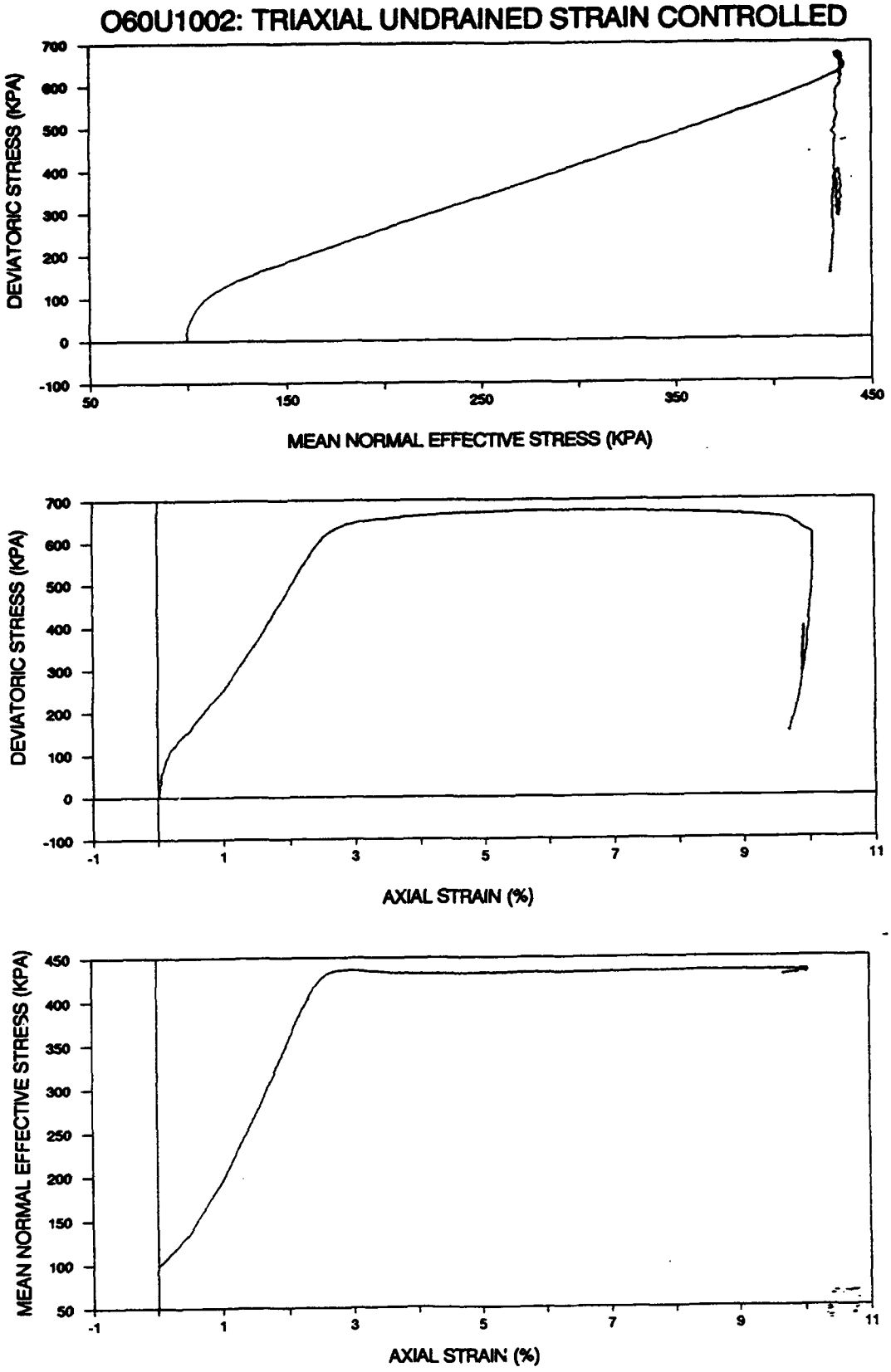

Figure 2.2.24 : Triaxial, Undrained, Strain Controlled, Constant p Test (O60U1002)

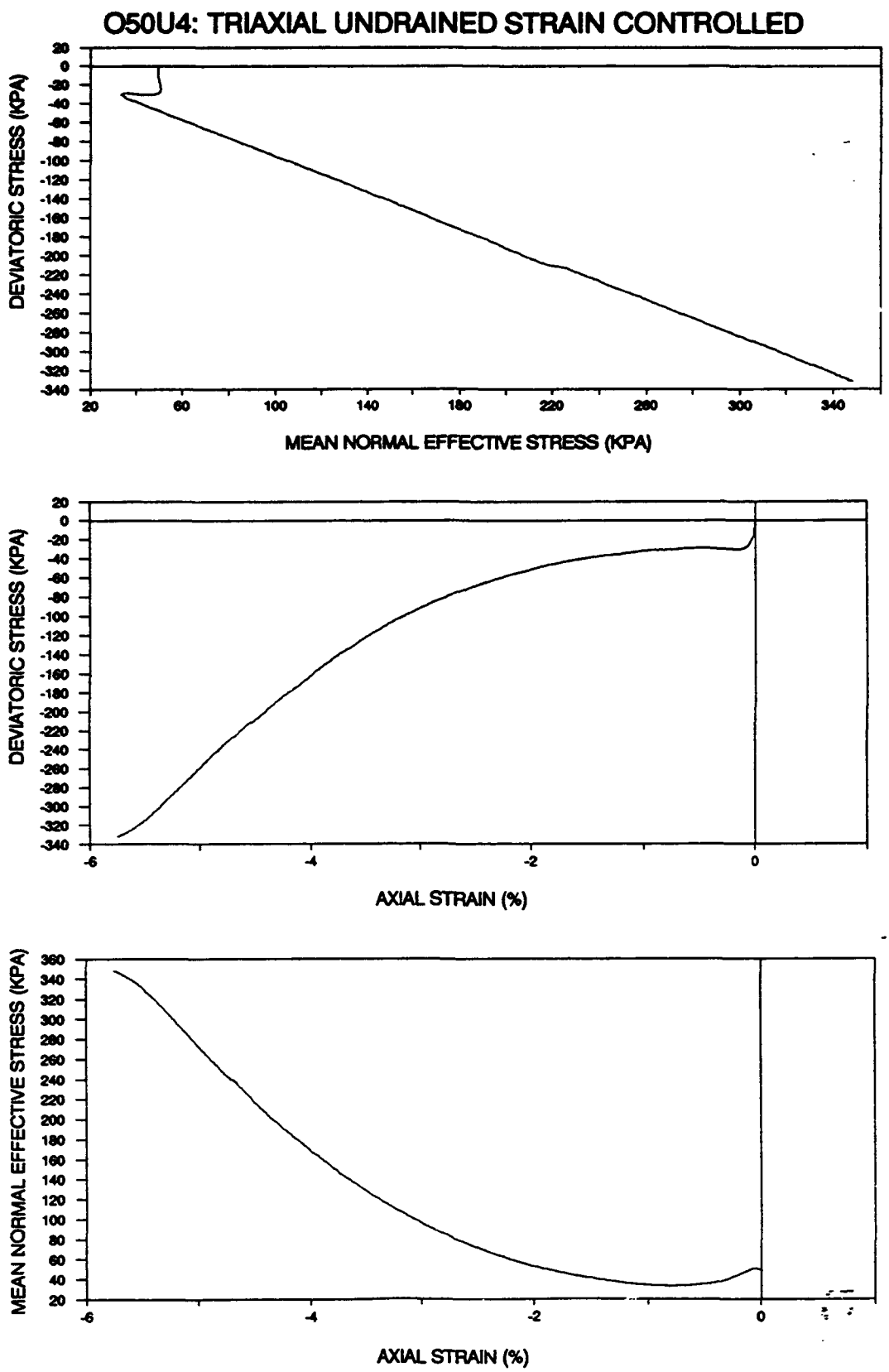

Figure 2.2.25 : Triaxial, Undrained, Strain Controlled, Constant p Test (O50U4)

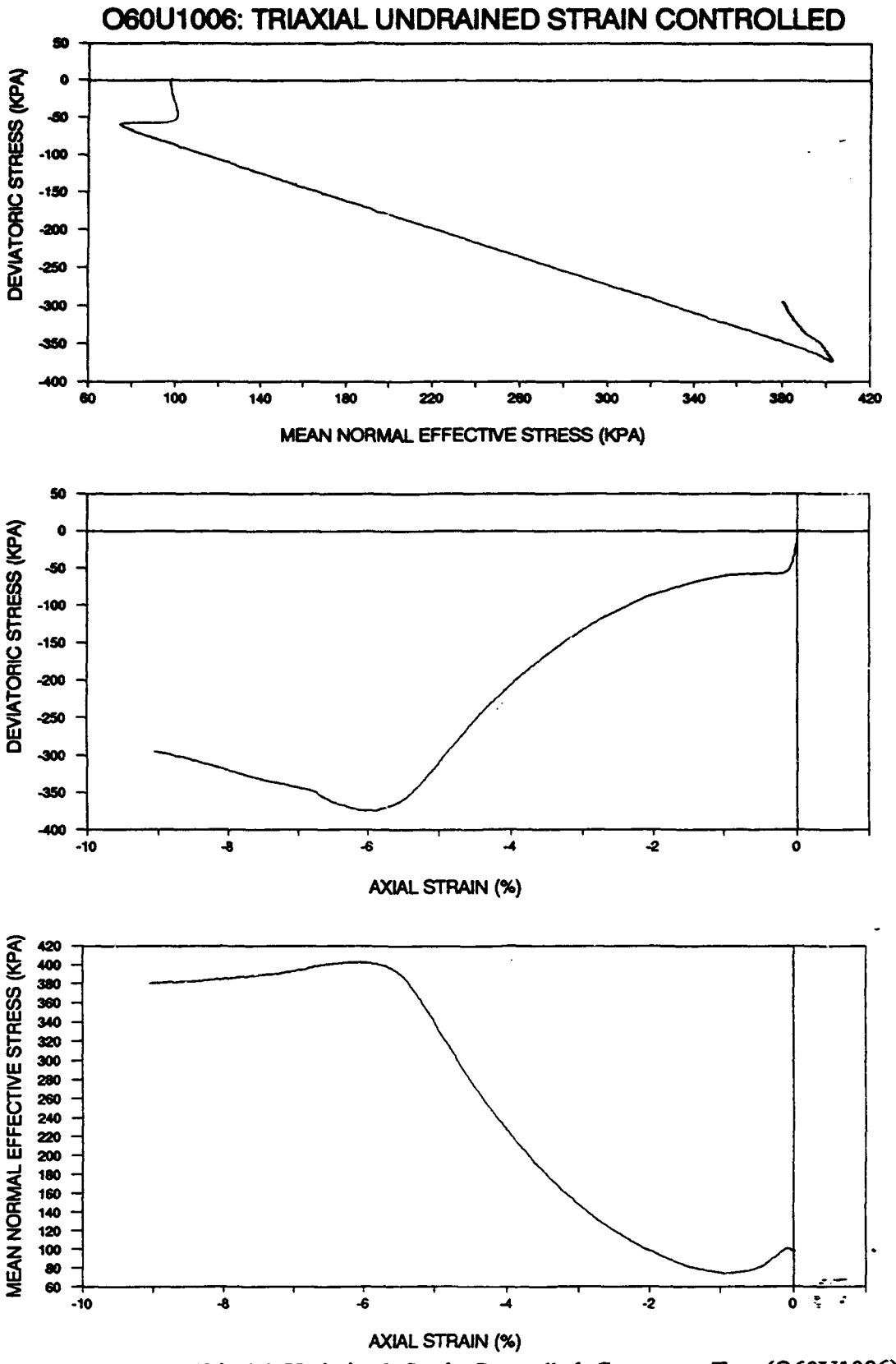

Figure 2.2.26 : Triaxial, Undrained, Strain Controlled, Constant p Test (O60U1006)

TEST RESULTS
ON
TRIAXIAL DRAINED, STRAIN CONTROLLED, CONSTANT P' TESTS

Figure 2.3.1 : Triaxial, Drained, Strain Controlled, Constant p' Test (N70D501)

Figure 2.3.2 : Triaxial, Drained, Strain Controlled, Constant p' Test (N70D1001)

Figure 2.3.3 : Triaxial, Drained, Strain Controlled, Constant p' Test (N70D2501)

Figure 2.3.4 : Triaxial, Drained, Strain Controlled, Constant p' Test (N70D100A)

Figure 2.3.5 : Triaxial, Drained, Strain Controlled, Constant p' Test (N70D100B)

Figure 2.3.6 : Triaxial, Drained, Strain Controlled, Constant p' Test (N70D100C)

Figure 2.3.7 : Triaxial, Drained, Strain Controlled, Constant p' Test (N70D1005)

Figure 2.3.8 : Triaxial, Drained, Strain Controlled, Constant p' Test (N70D2505)

Figure 2.3.9 : Triaxial, Drained, Strain Controlled, Constant p' Test (N70D100P)

Figure 2.3.10 : Triaxial, Drained, Strain Controlled, Constant p' Test (N70D100R)

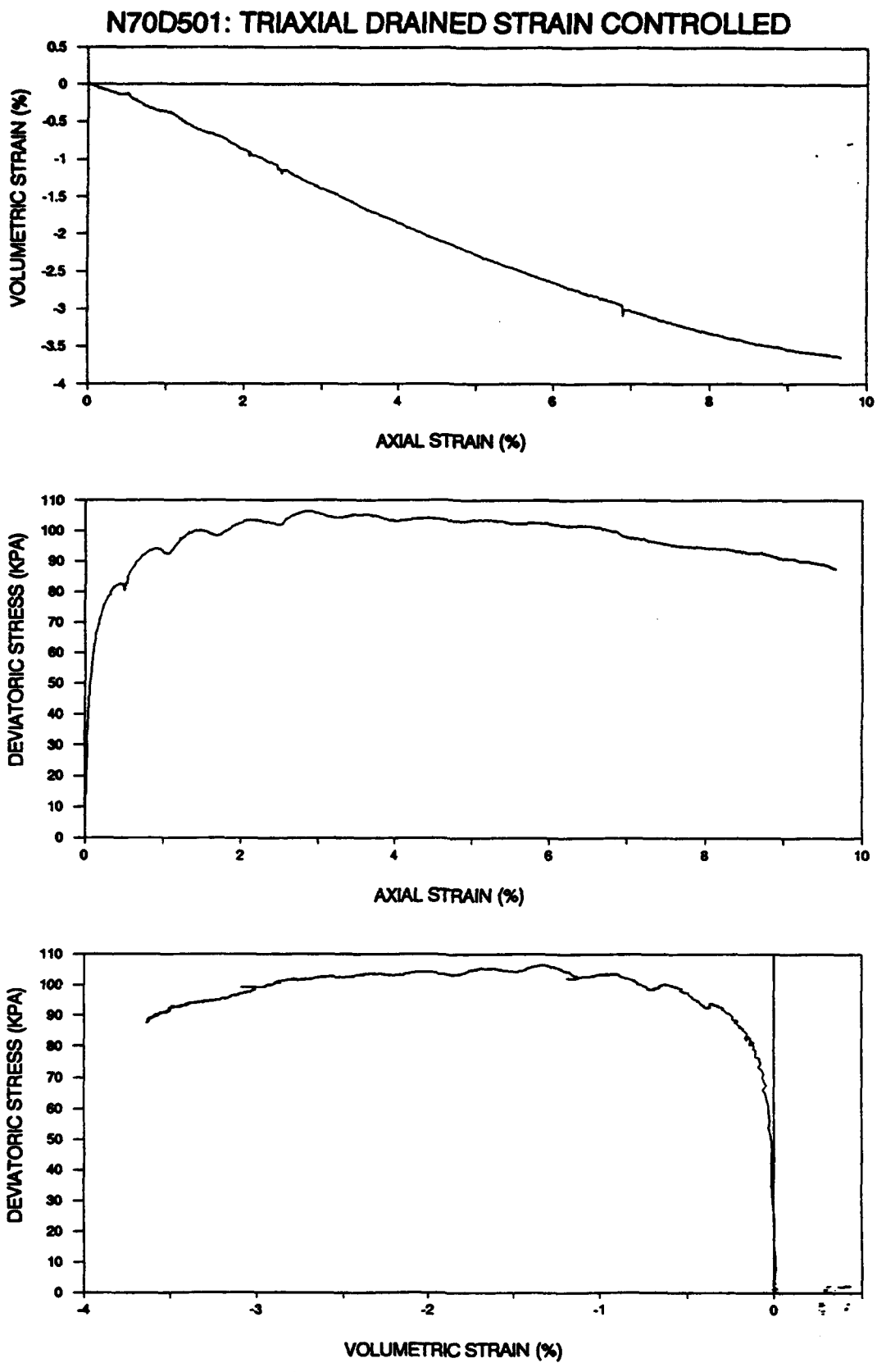

Figure 2.3.1 : Triaxial, Drained, Strain Controlled, Constant p' Test (N70D501)

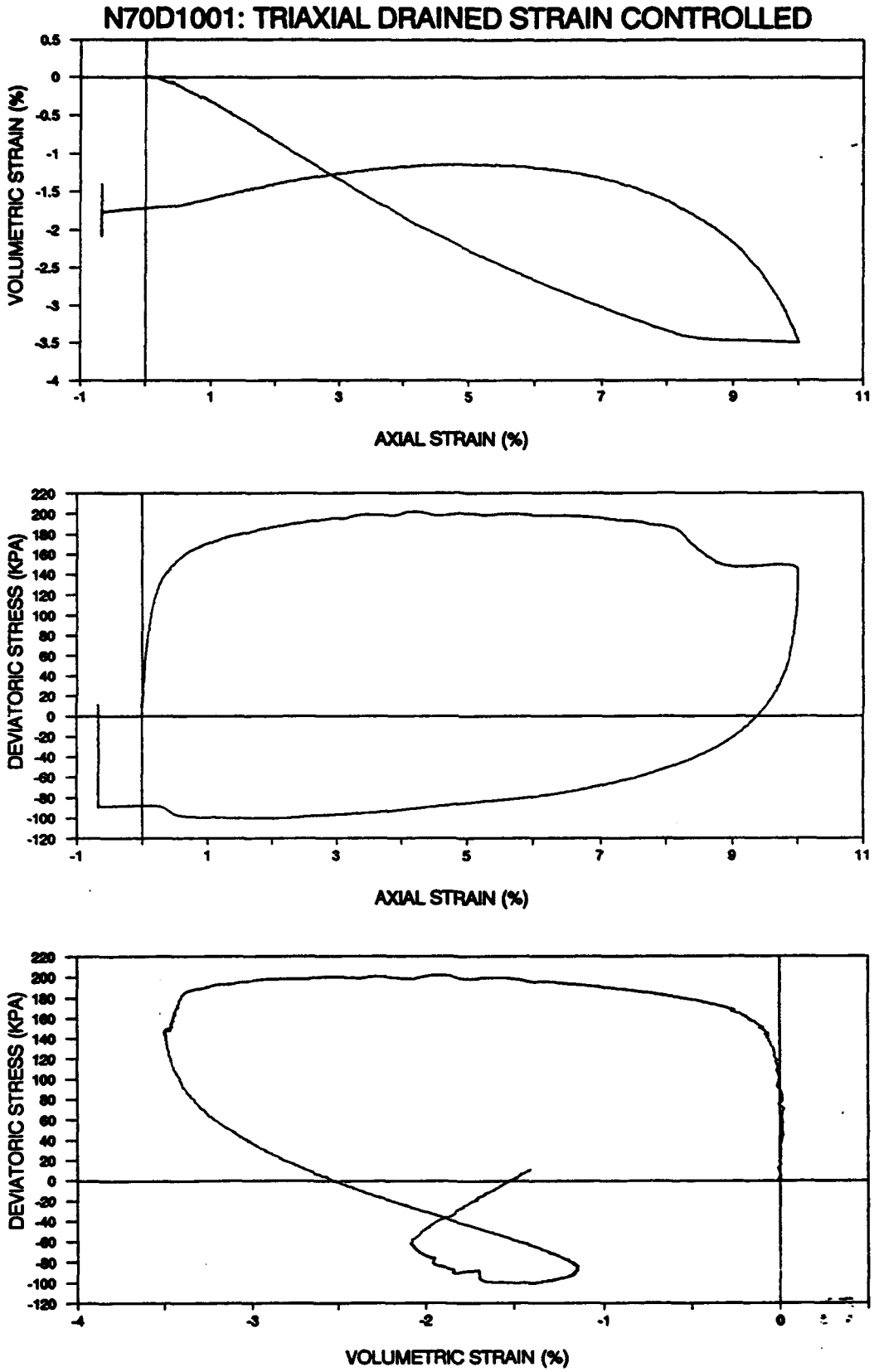

Figure 2.3.2 : Triaxial, Drained, Strain Controlled, Constant p' Test (N70D1001)

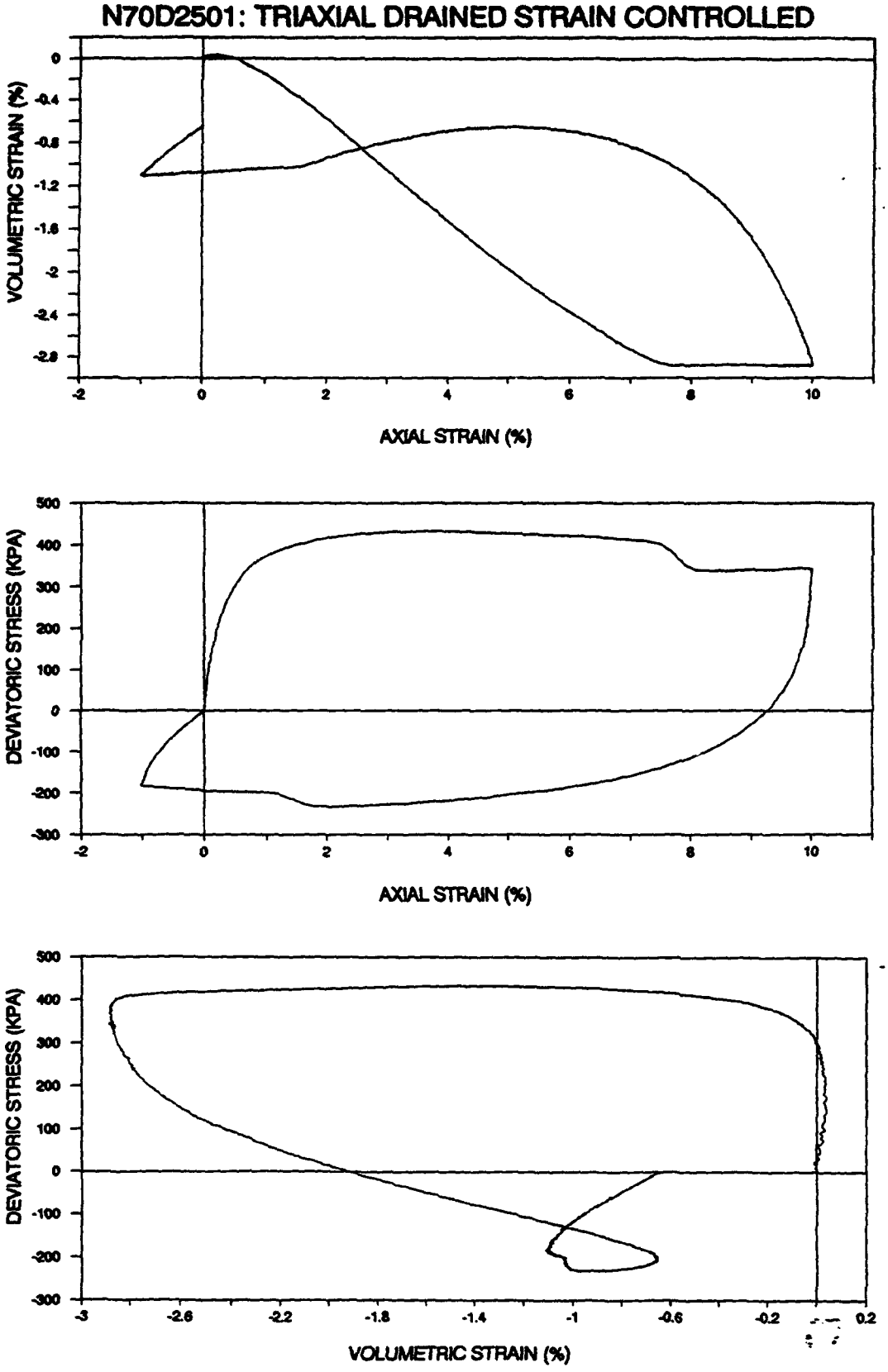

Figure 2.3.3 : Triaxial, Drained, Strain Controlled, Constant p' Test (N70D2501)

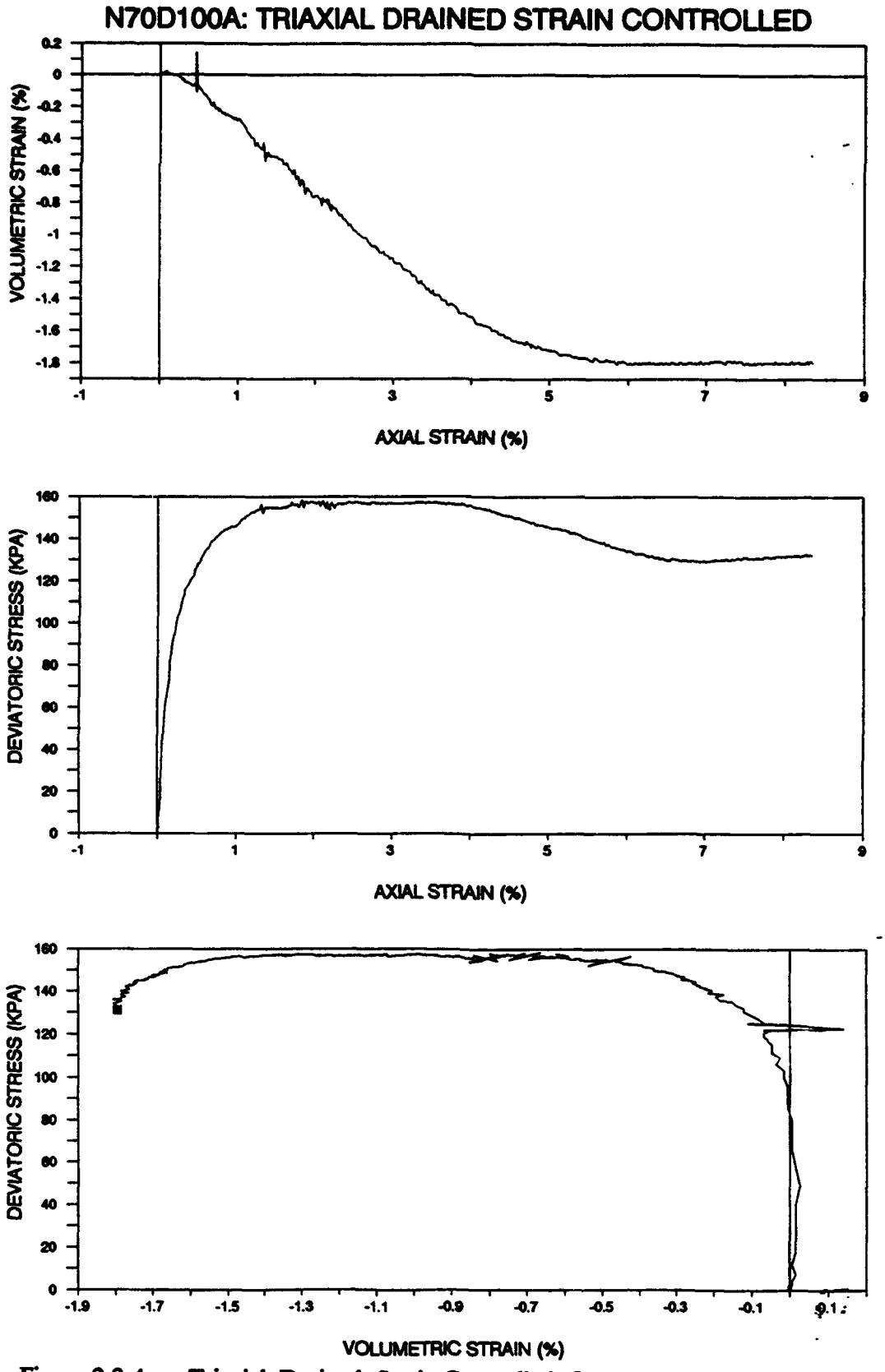

Figure 2.3.4 : Triaxial, Drained, Strain Controlled, Constant p' Test (N70D100A)

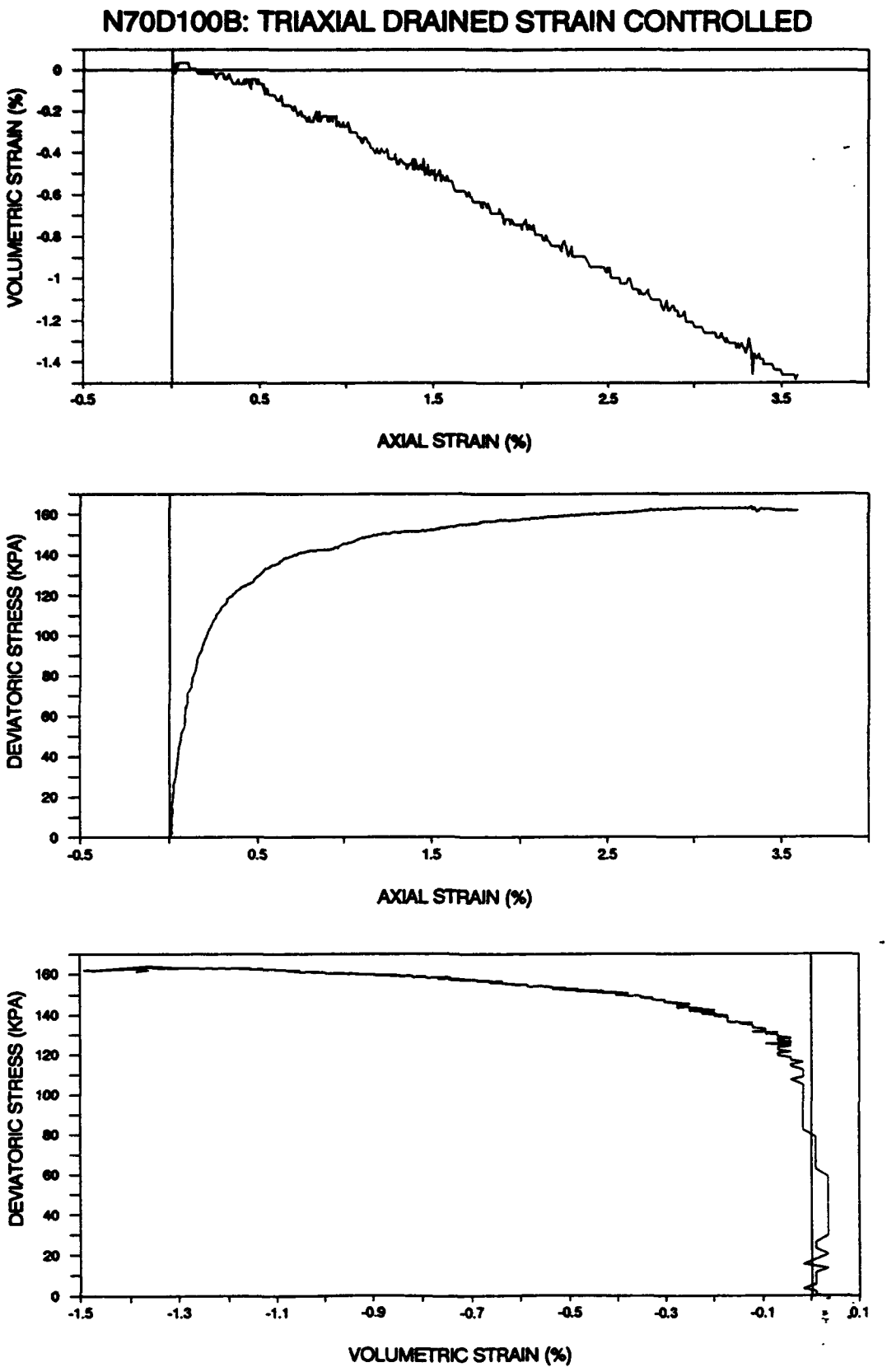

Figure 2.3.5 : Triaxial, Drained, Strain Controlled, Constant p' Test (N70D100B)

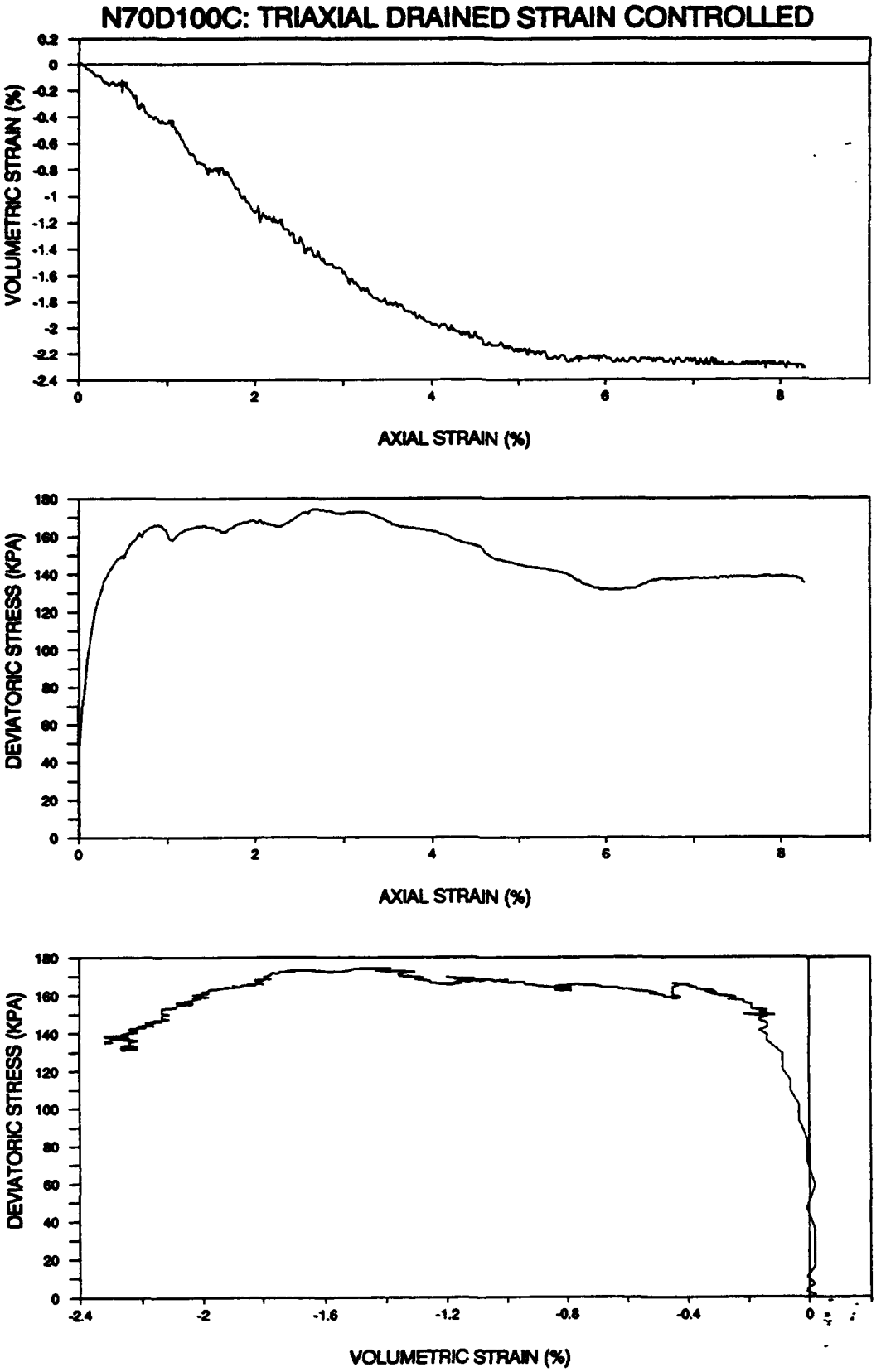

Figure 2.3.6 : Triaxial, Drained, Strain Controlled, Constant p' Test (N70D100C)

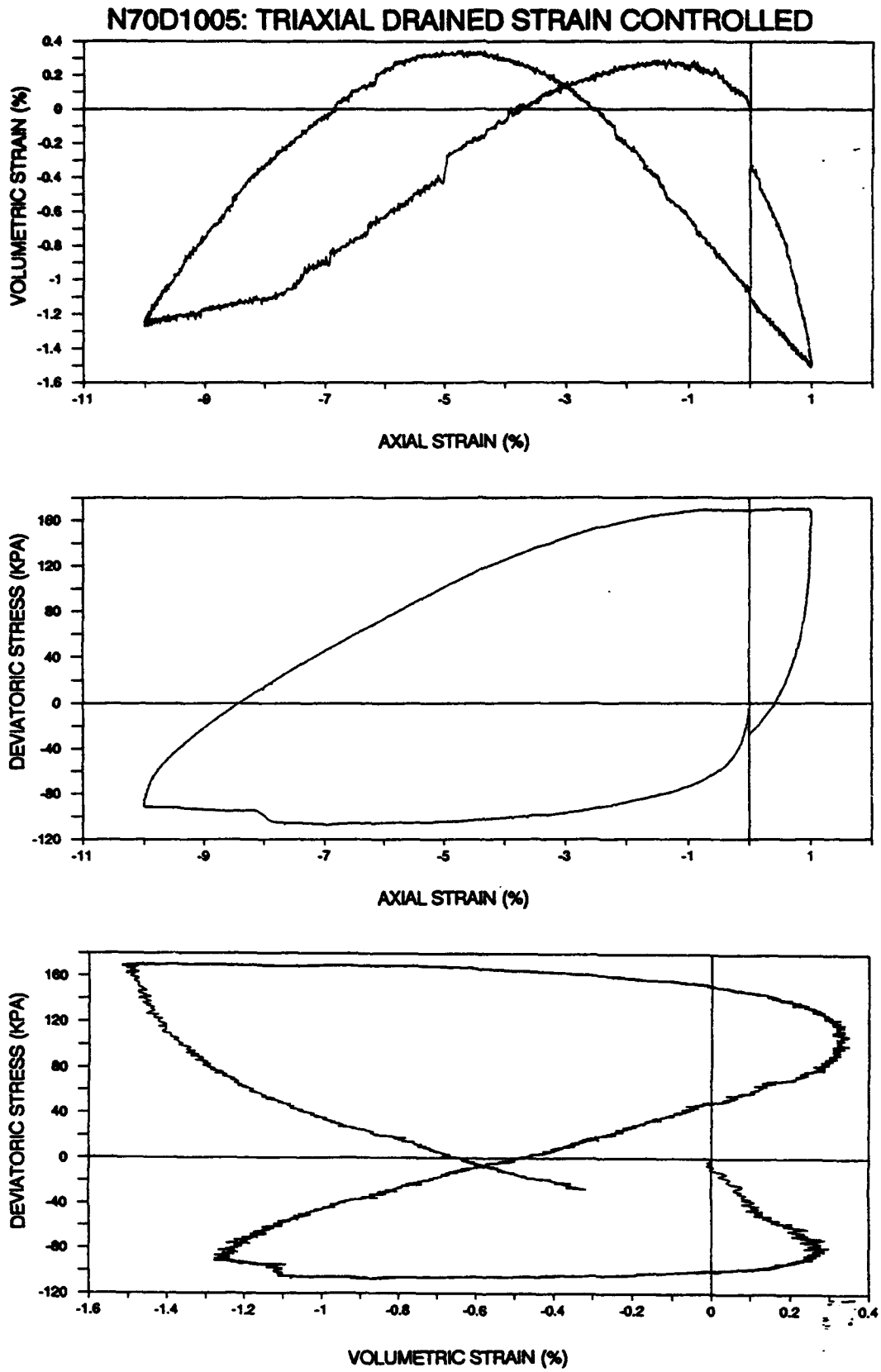

Figure 2.3.7 : Triaxial, Drained, Strain Controlled, Constant p' Test (N70D1005)

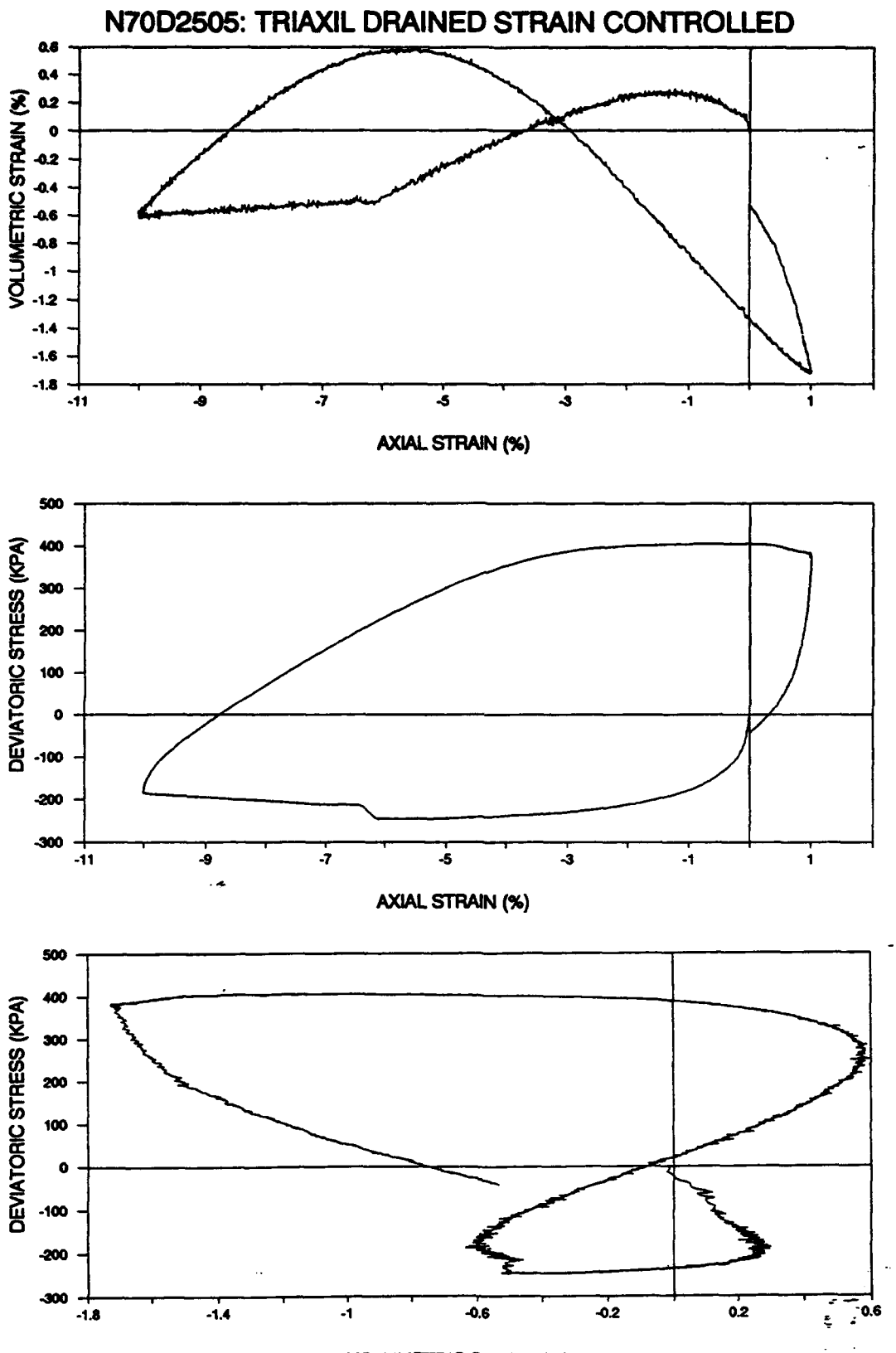

Figure 2.3.8 : Triaxial, Drained, Strain Controlled, Constant p' Test (N70D2505)

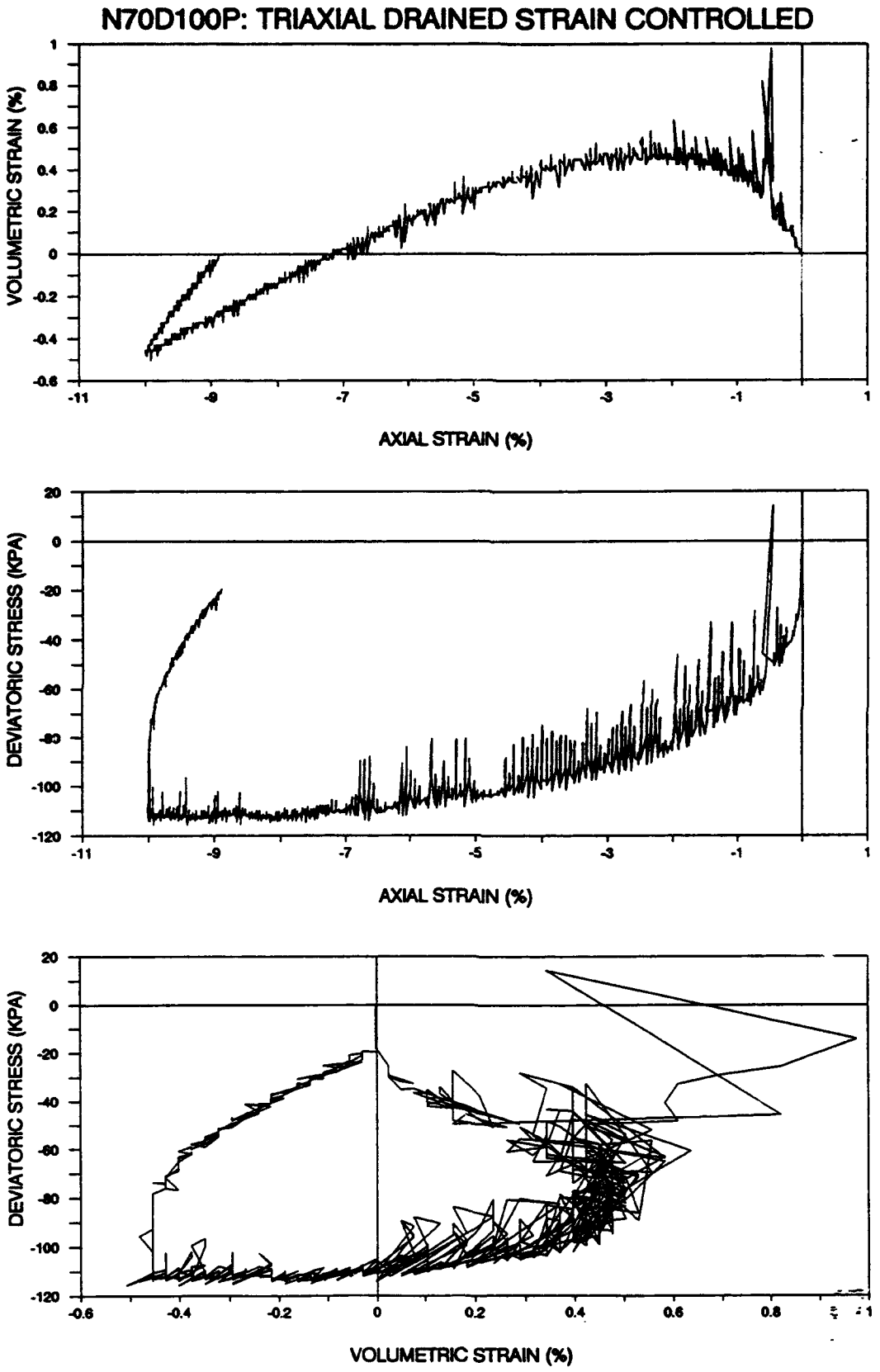

Figure 2.3.9 : Triaxial, Drained, Strain Controlled, Constant p' Test (N70D100P)

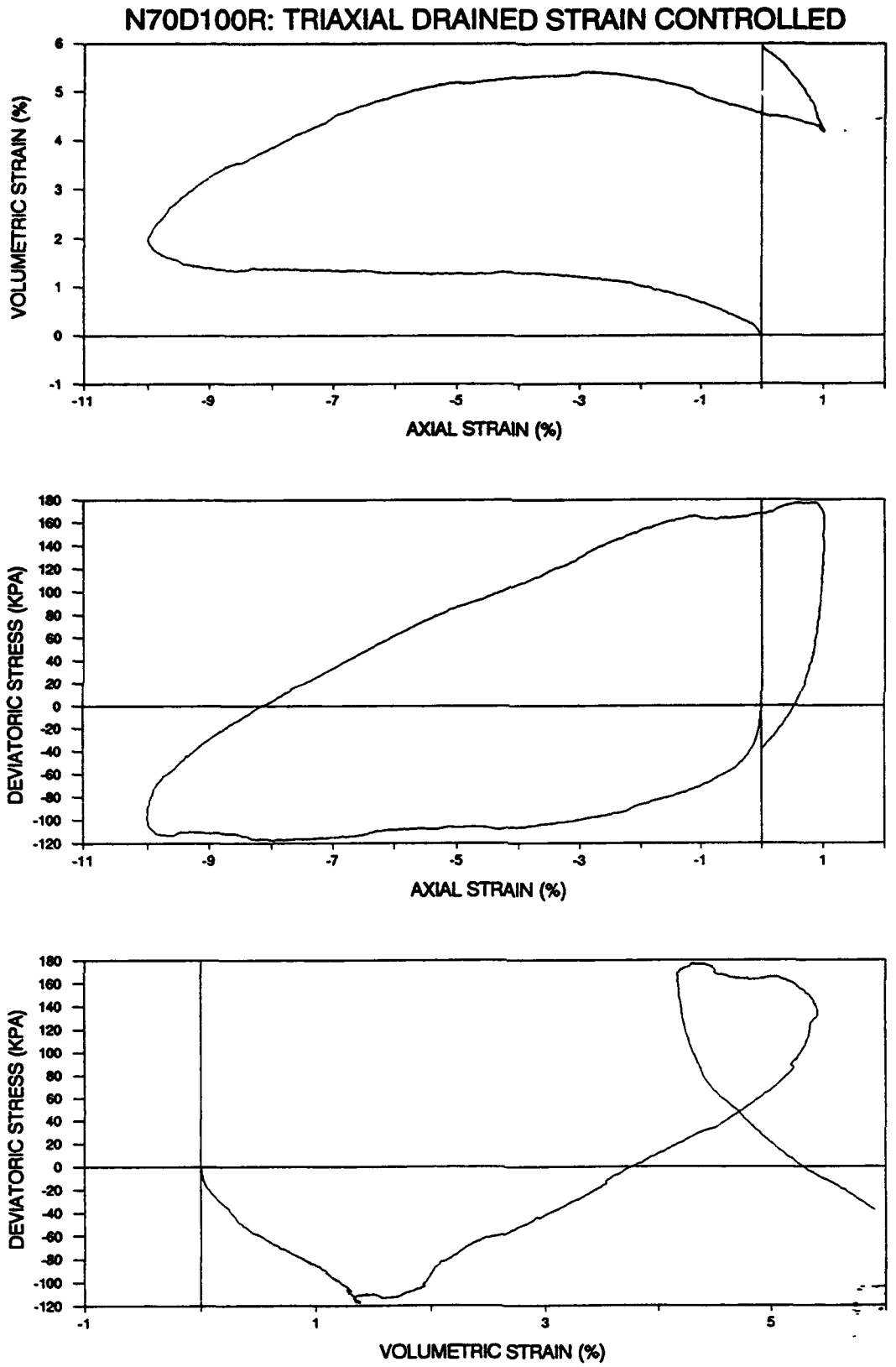

Figure 2.3.10 : Triaxial, Drained, Strain Controlled, Constant p' Test (N70D100R)

TEST RESULTS
ON
TRIAXIAL UNDRAINED, STRESS CONTROLLED, CYCLIC TESTS

Figure 2.4.1 : Triaxial, Undrained, Stress Controlled, Cyclic Test (CY50N1)
Figure 2.4.2 : Triaxial, Undrained, Stress Controlled, Cyclic Test (CY100N1)
Figure 2.4.3 : Triaxial, Undrained, Stress Controlled, Cyclic Test (CY100N2)
Figure 2.4.4 : Triaxial, Undrained, Stress Controlled, Cyclic Test (CY100N3)
Figure 2.4.5 : Triaxial, Undrained, Stress Controlled, Cyclic Test (CY100N4)
Figure 2.4.6 : Triaxial, Undrained, Stress Controlled, Cyclic Test (CY100N5)
Figure 2.4.7 : Triaxial, Undrained, Stress Controlled, Cyclic Test (CY100N6)
Figure 2.4.8 : Triaxial, Undrained, Stress Controlled, Cyclic Test (CY250N1)
Figure 2.4.9 : Triaxial, Undrained, Stress Controlled, Cyclic Test (CY250N2)
Figure 2.4.10 : Triaxial, Undrained, Stress Controlled. Cyclic Test (CY250N3)
Figure 2.4.11 : Triaxial, Undrained, Stress Controlled, Cyclic Test (CY250N4)
Figure 2.4.12 : Triaxial, Undrained, Stress Controlled, Cyclic Test (CY250N5)
Figure 2.4.13 : Triaxial, Undrained, Stress Controlled, Cyclic Test (CY250N6)
Figure 2.4.14 : Triaxial, Undrained, Stress Controlled, Cyclic Test (CY250N7)
Figure 2.4.15 : Triaxial, Undrained, Stress Controlled, Cyclic Test (CY250N8)
Figure 2.4.16 : Triaxial, Undrained, Stress Controlled, Cyclic Test (CY250N9)
Figure 2.4.17 : Triaxial, Undrained, Stress Controlled, Cyclic Test (CY250N10)
Figure 2.4.18 : Triaxial, Undrained, Stress Controlled, Cyclic Test (CY250N11)
Figure 2.4.19 : Triaxial, Undrained, Stress Controlled, Cyclic Test (CY250N12)
Figure 2.4.20 : Triaxial, Undrained, Stress Controlled, Cyclic Test (CY250N13)
Figure 2.4.21 : Triaxial, Undrained, Stress Controlled, Cyclic Test (CY250N14)
Figure 2.4.22 : Triaxial, Undrained, Stress Controlled, Cyclic Test (CY50O1)
Figure 2.4.23 : Triaxial, Undrained, Stress Controlled, Cyclic Test (CY100O1)
Figure 2.4.24 : Triaxial, Undrained, Stress Controlled, Cyclic Test (CY100O21)
Figure 2.4.25 : Triaxial, Undrained, Stress Controlled, Cyclic Test (CY100O22)
Figure 2.4.26 : Triaxial, Undrained, Stress Controlled, Cyclic Test (CY200O1X)
Figure 2.4.27 : Triaxial, Undrained, Stress Controlled, Cyclic Test (CY200O21)
Figure 2.4.28 : Triaxial, Undrained, Stress Controlled, Cyclic Test (CY100O2)
Figure 2.4.29 : Triaxial, Undrained, Stress Controlled, Cyclic Test (CY100O3X)
Figure 2.4.30 : Triaxial, Undrained, Stress Controlled, Cyclic Test (CY100O4)
Figure 2.4.31 : Triaxial, Undrained, Stress Controlled, Cyclic Test (CY100O46
Figure 2.4.32 : Triaxial, Undrained, Stress Controlled, Cyclic Test (CY100O47

Figure 2.4.33 : Triaxial, Undrained, Stress Controlled, Cyclic Test (CY100O48)

Figure 2.4.34 : Triaxial, Undrained, Stress Controlled, Cyclic Test (CY100O49)

Figure 2.4.35 : Triaxial, Undrained, Stress Controlled, Cyclic Test (CY50O2)

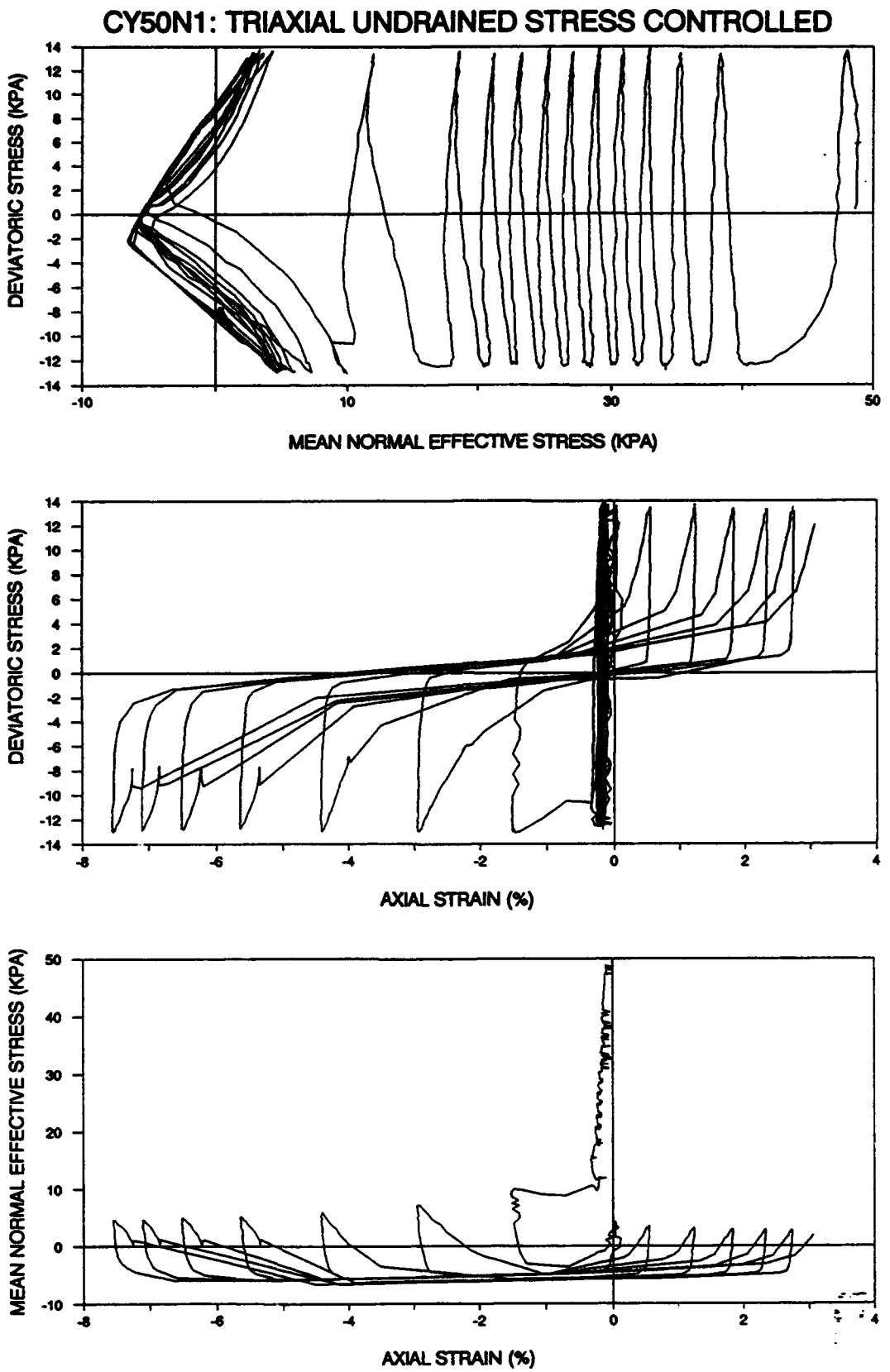

Figure 2.4.1 : Triaxial, Undrained, Stress Controlled, Cyclic Test (CY50N1)

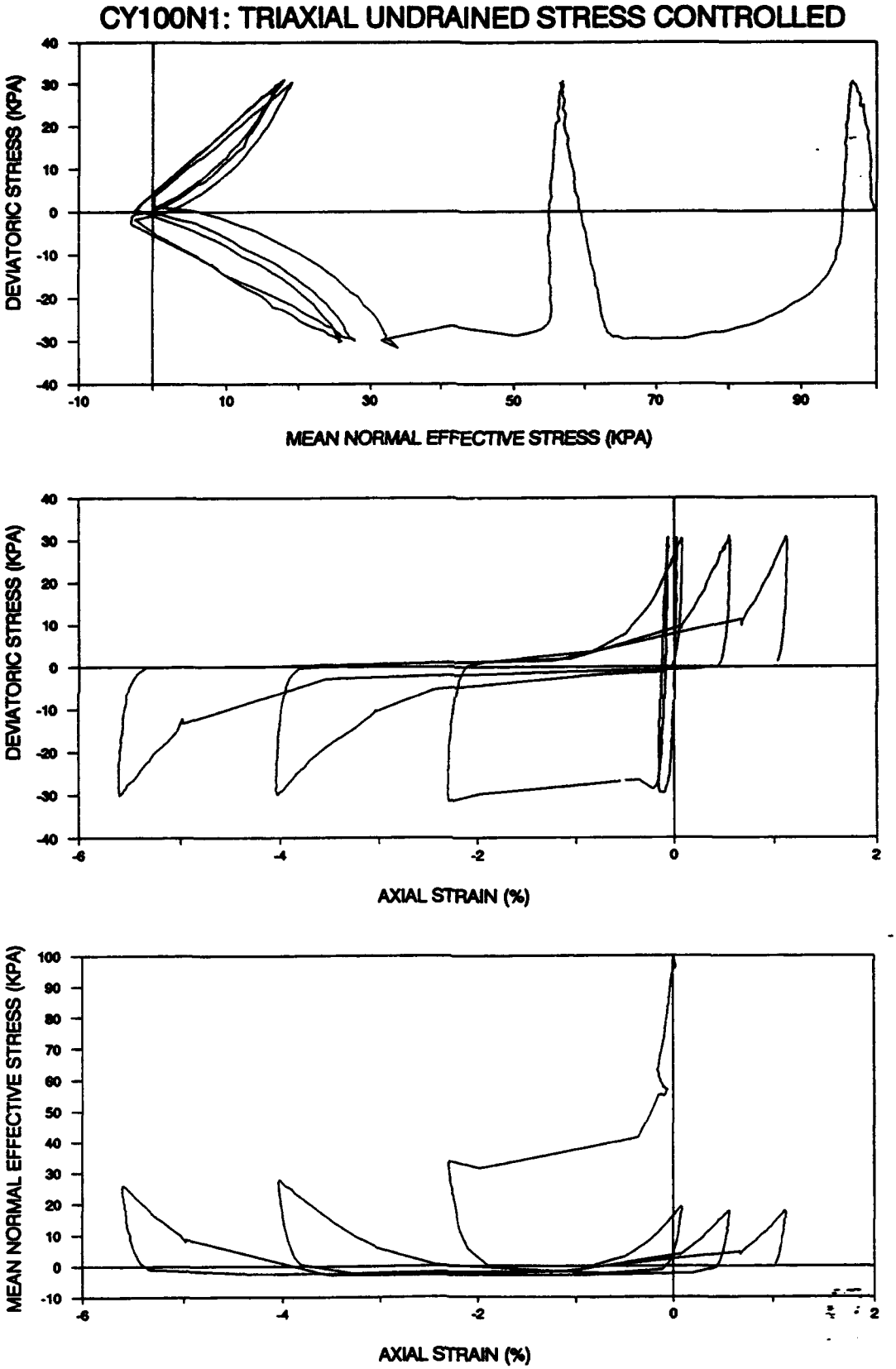

Figure 2.4.2 : Triaxial, Undrained, Stress Controlled, Cyclic Test (CY100N1)

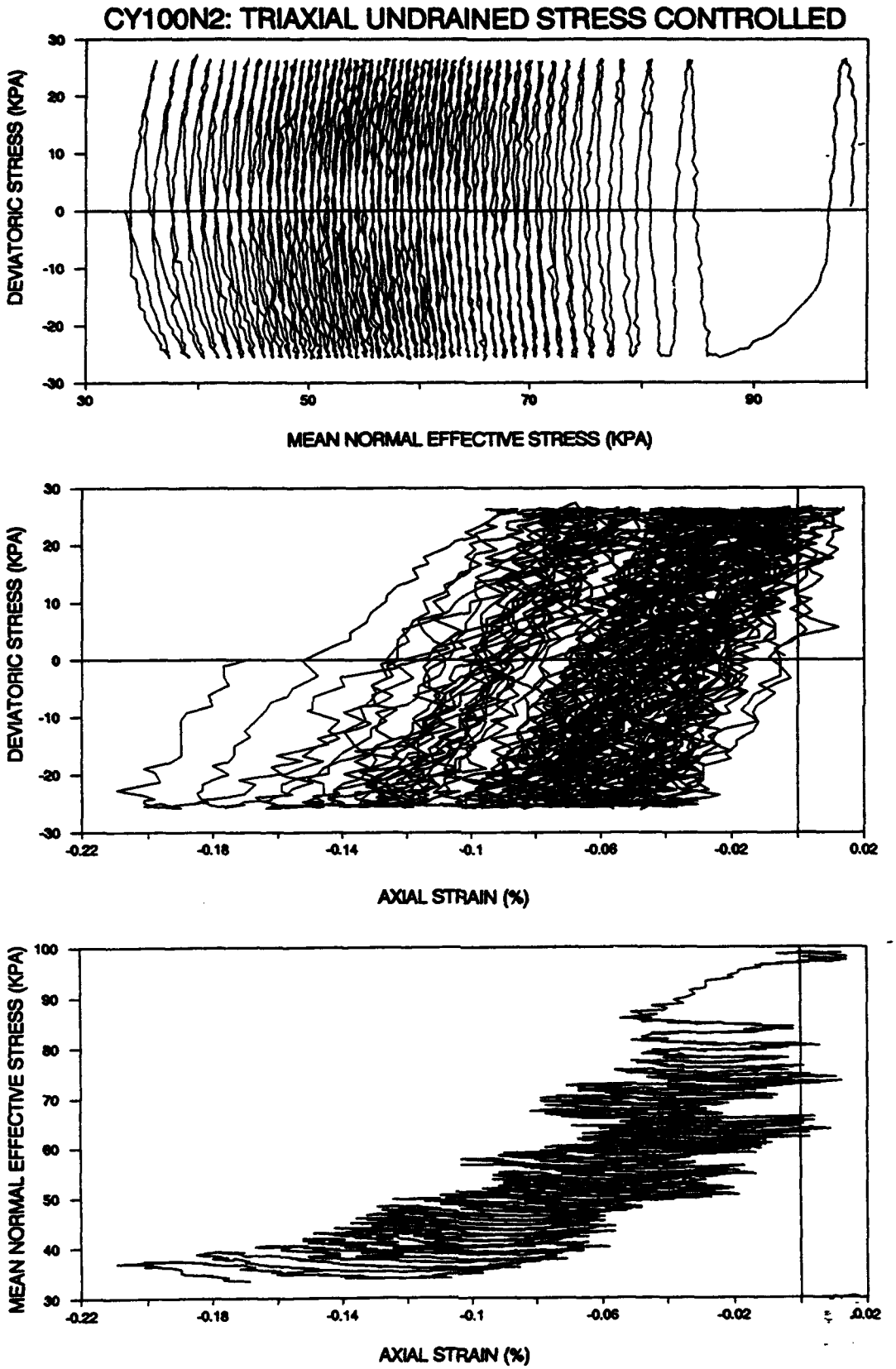

Figure 2.4.3 : Triaxial, Undrained, Stress Controlled, Cyclic Test (CY100N2)

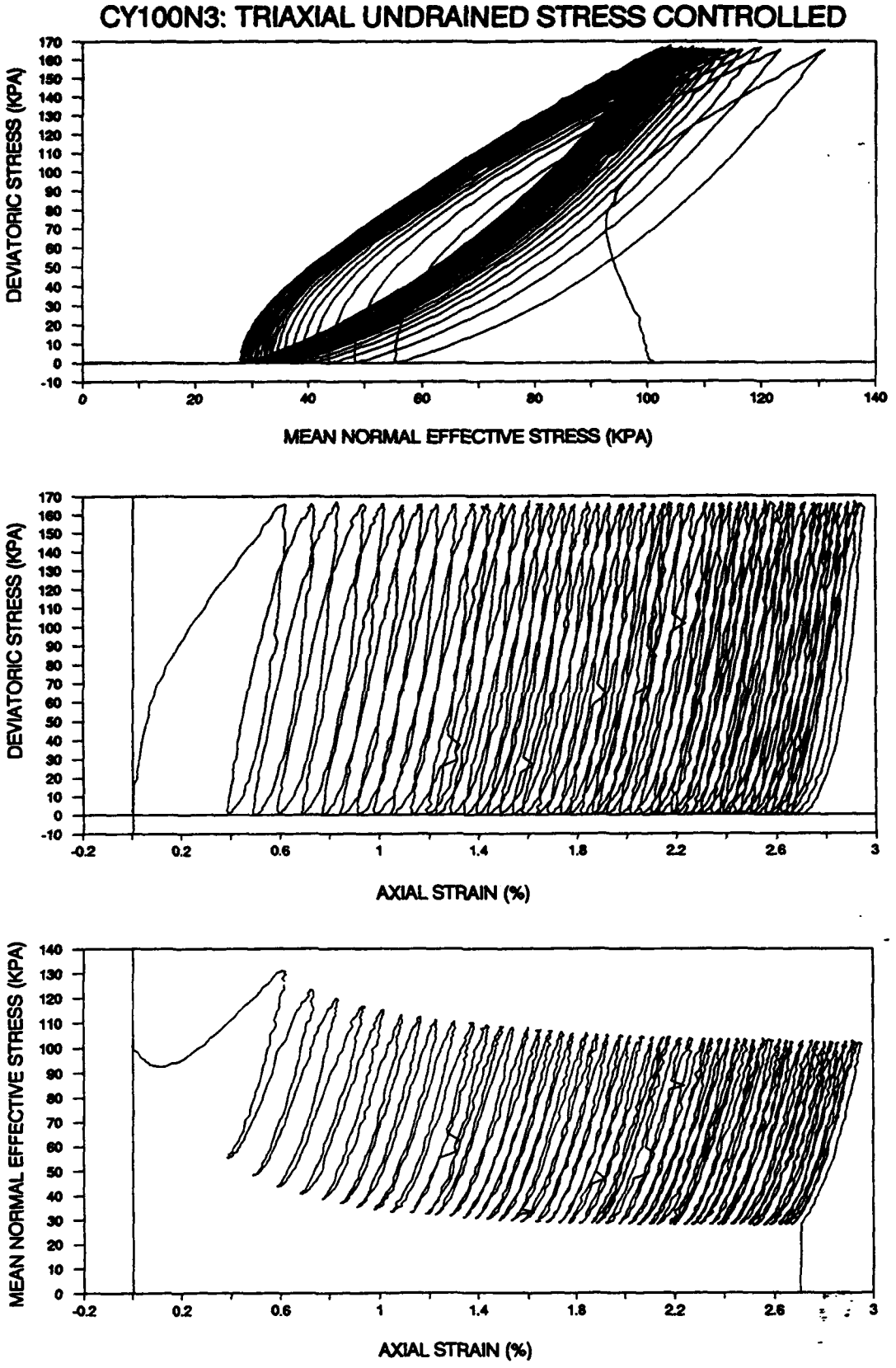

Figure 2.4.4 : Triaxial, Undrained, Stress Controlled, Cyclic Test (CY100N3)

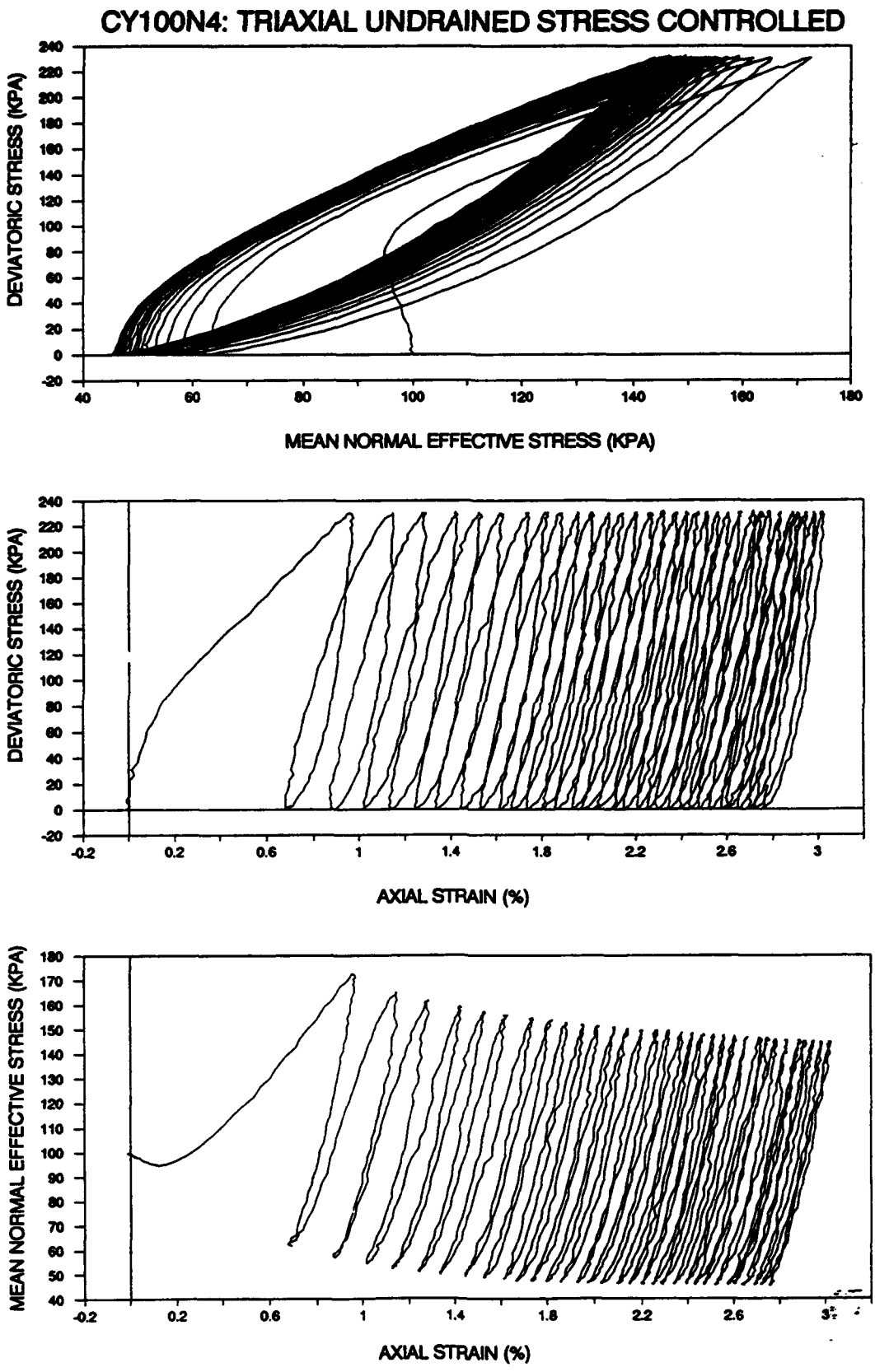

Figure 2.4.5 : Triaxial, Undrained, Stress Controlled, Cyclic Test (CY100N4)

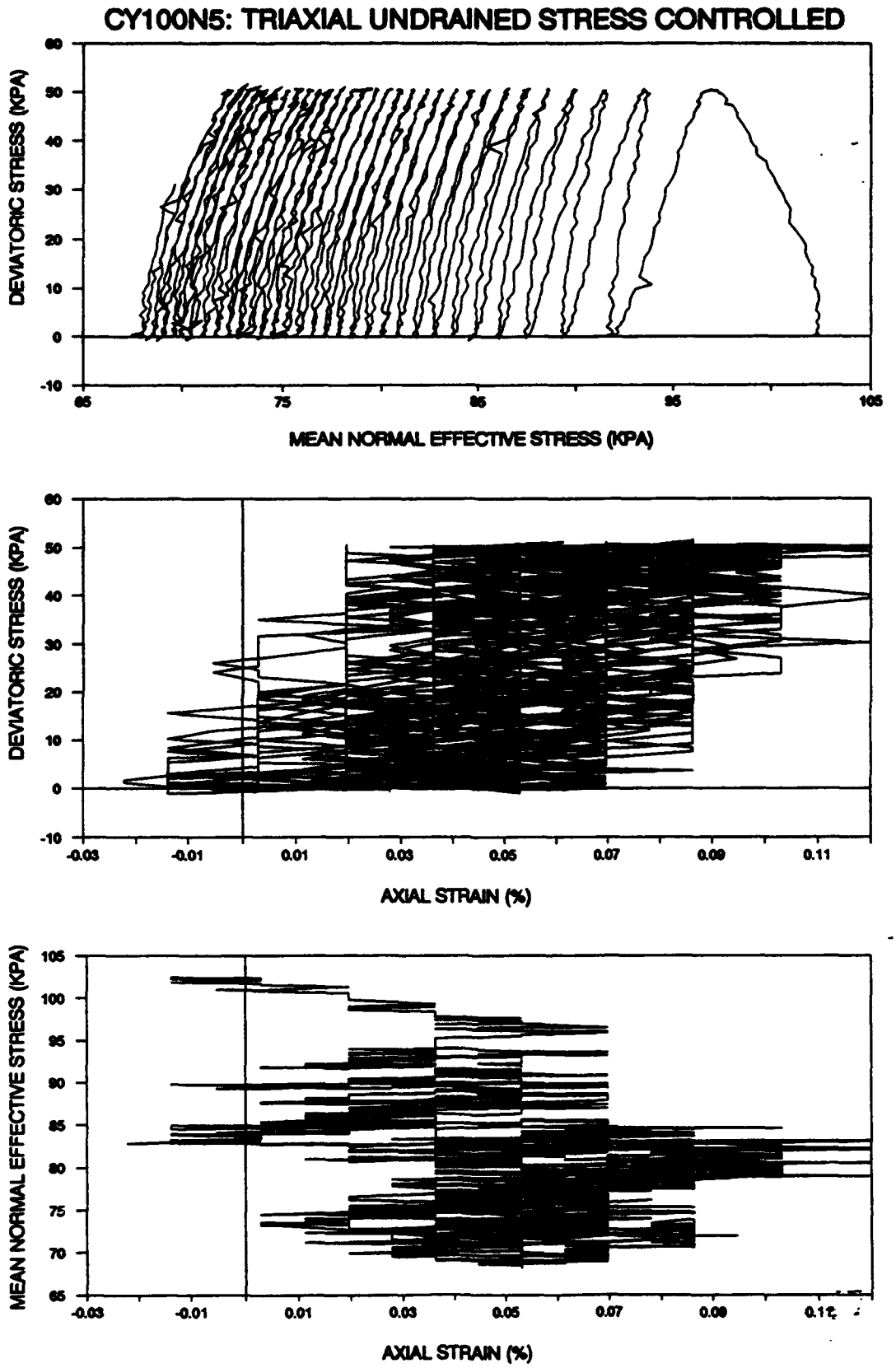

Figure 2.4.6 : Triaxial, Undrained, Stress Controlled, Cyclic Test (CY100N5)

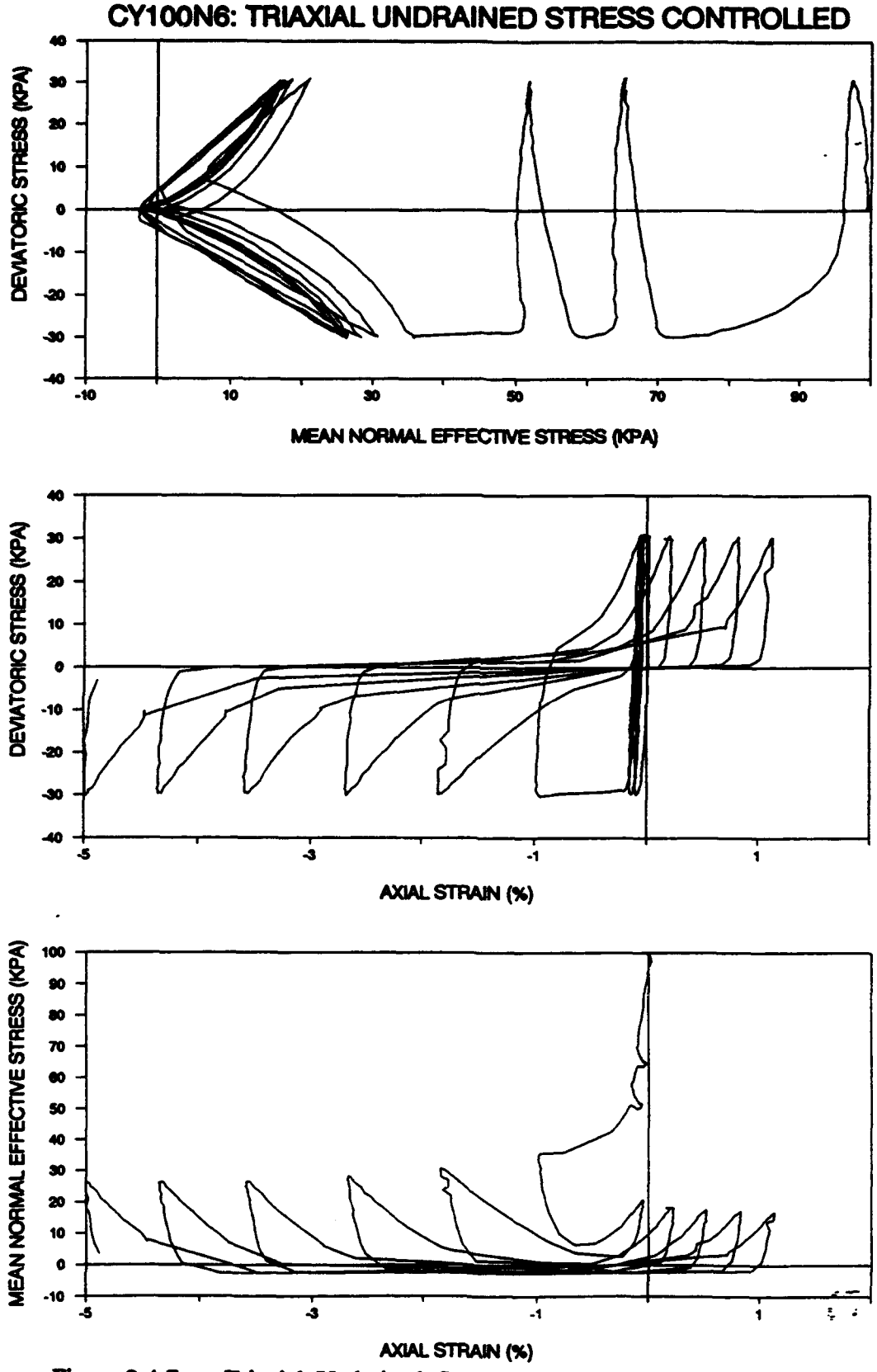

Figure 2.4.7 : Triaxial, Undrained, Stress Controlled, Cyclic Test (CY100N6)

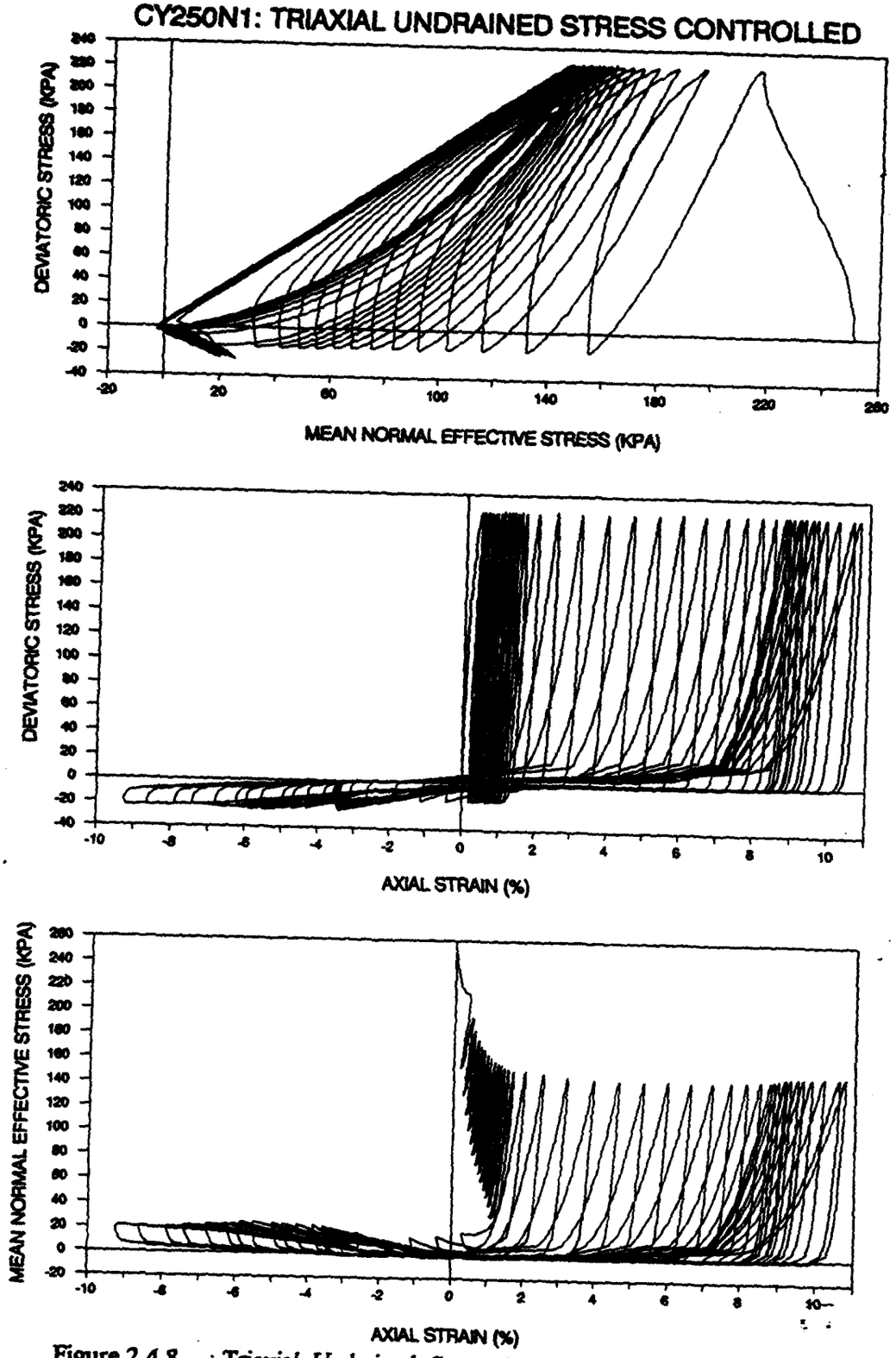

Figure 2.4.8 : Triaxial, Undrained, Stress Controlled, Cyclic Test (CY250N1)

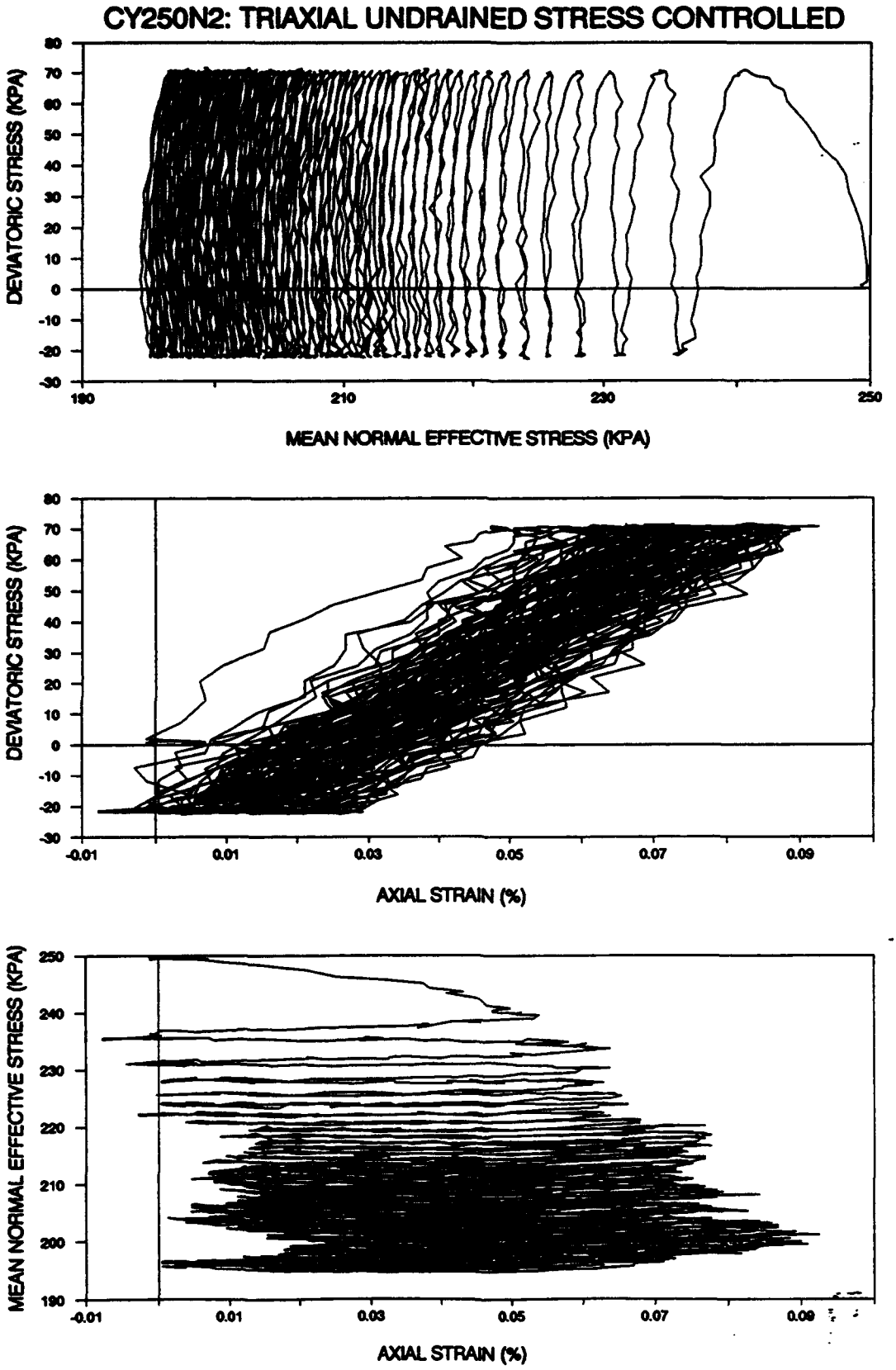

Figure 2.4.9 : Triaxial, Undrained, Stress Controlled, Cyclic Test (CY250N2)

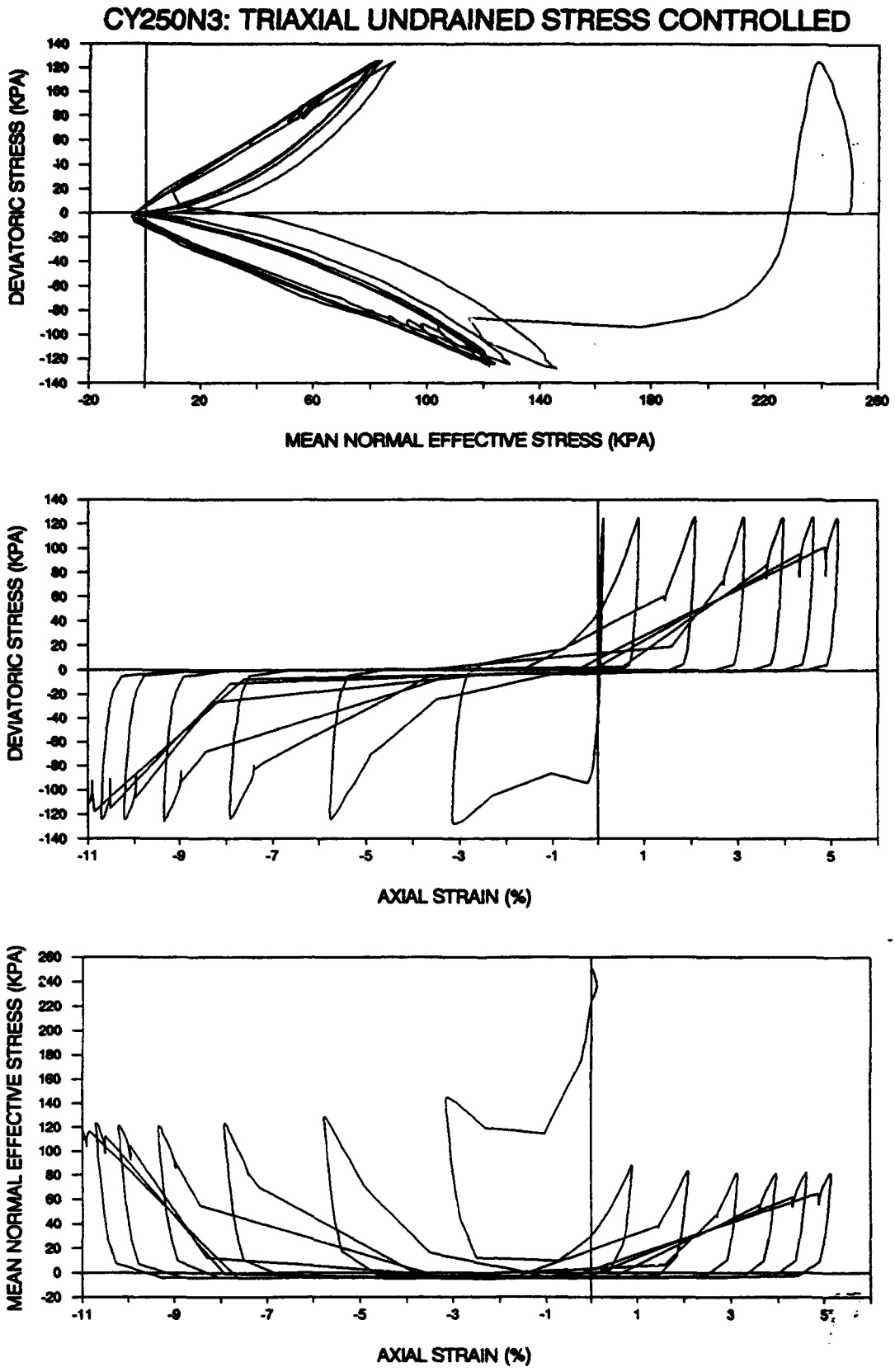

Figure 2.4.10 : Triaxial, Undrained, Stress Controlled, Cyclic Test (CY250N3)

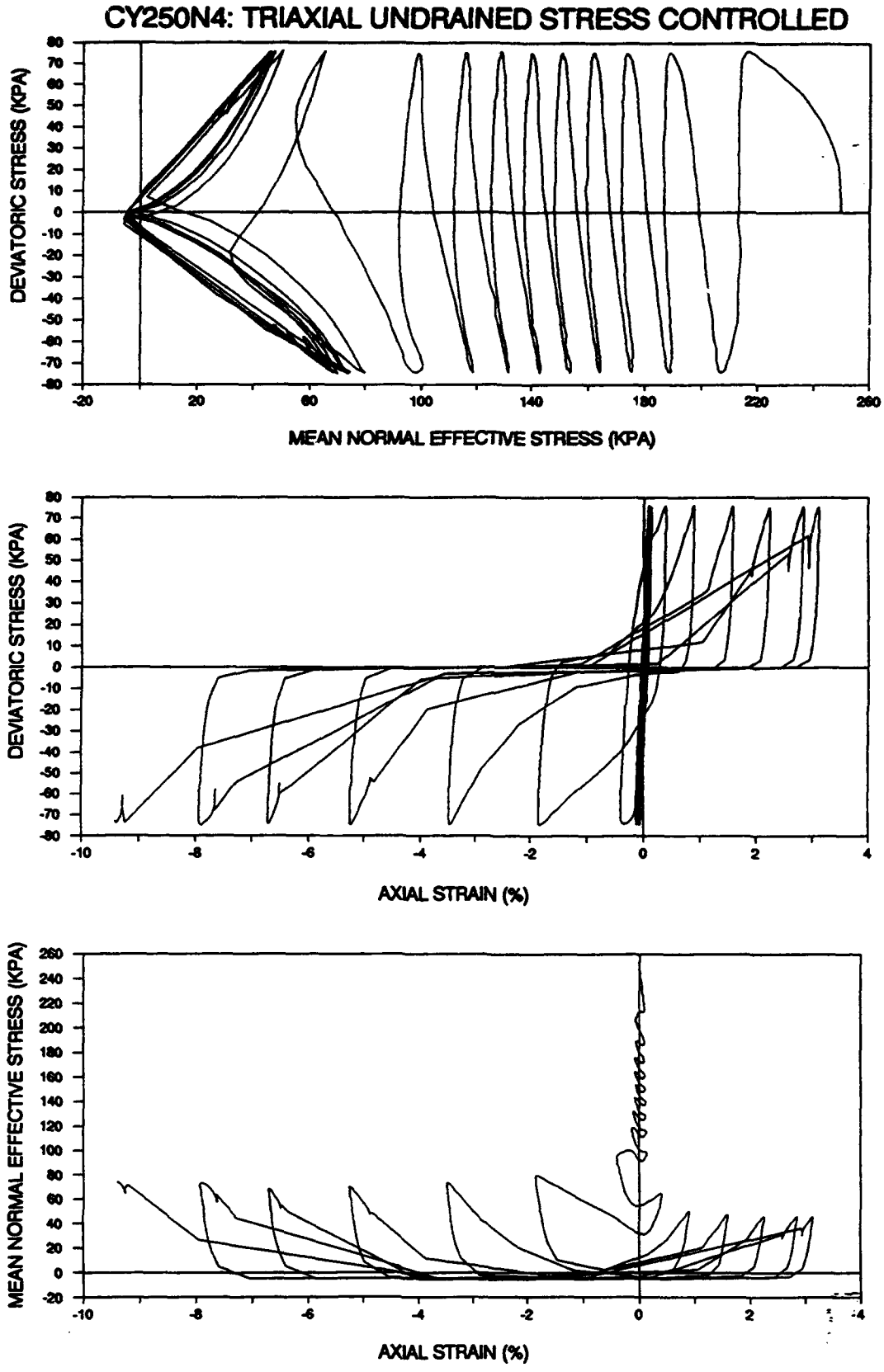

Figure 2.4.11 : Triaxial, Undrained, Stress Controlled, Cyclic Test (CY250N4)

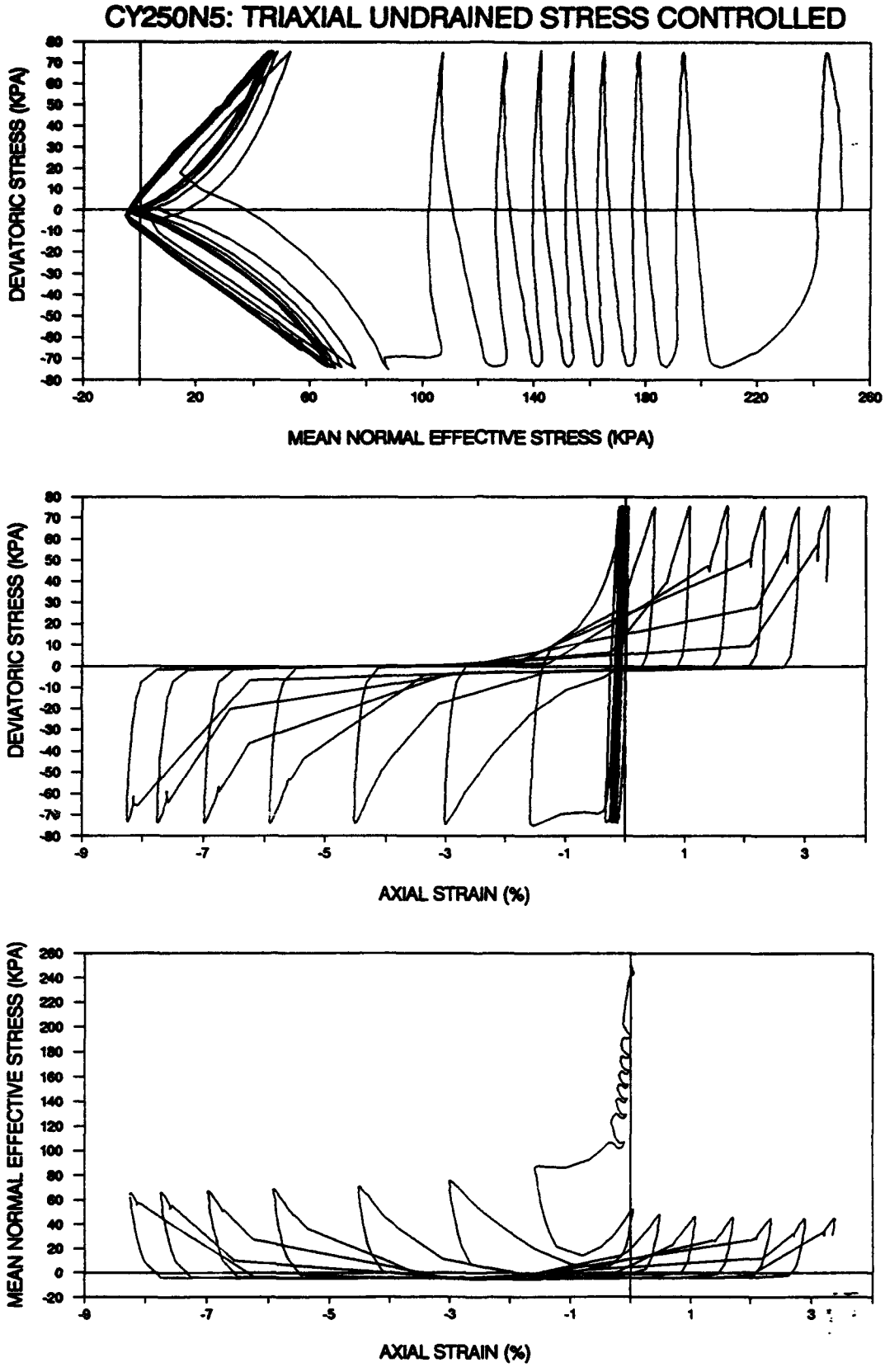

Figure 2.4.12 : Triaxial, Undrained, Stress Controlled, Cyclic Test (CY250N5)

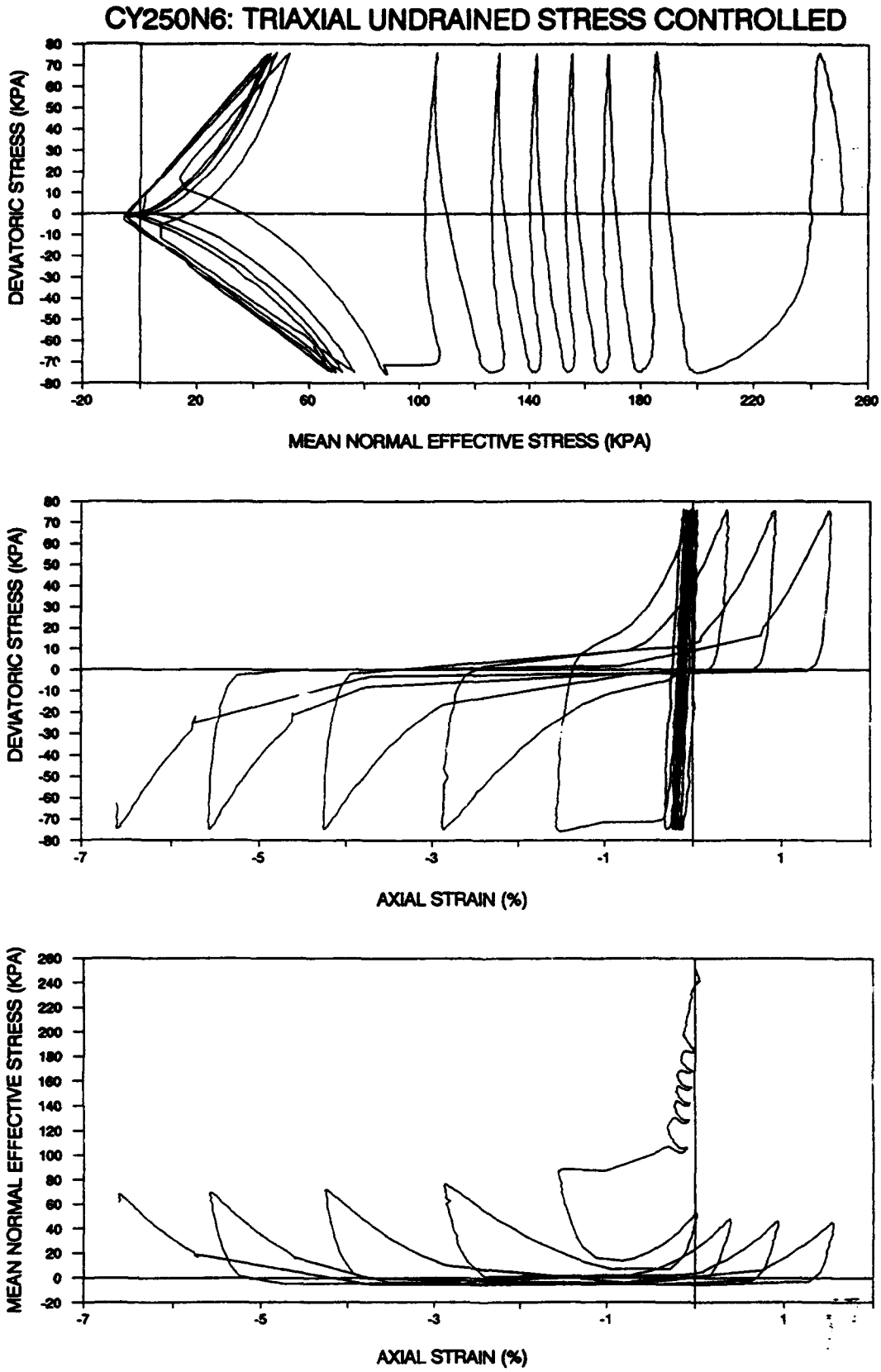

Figure 2.4.13 : Triaxial, Undrained, Stress Controlled, Cyclic Test (CY250N6)

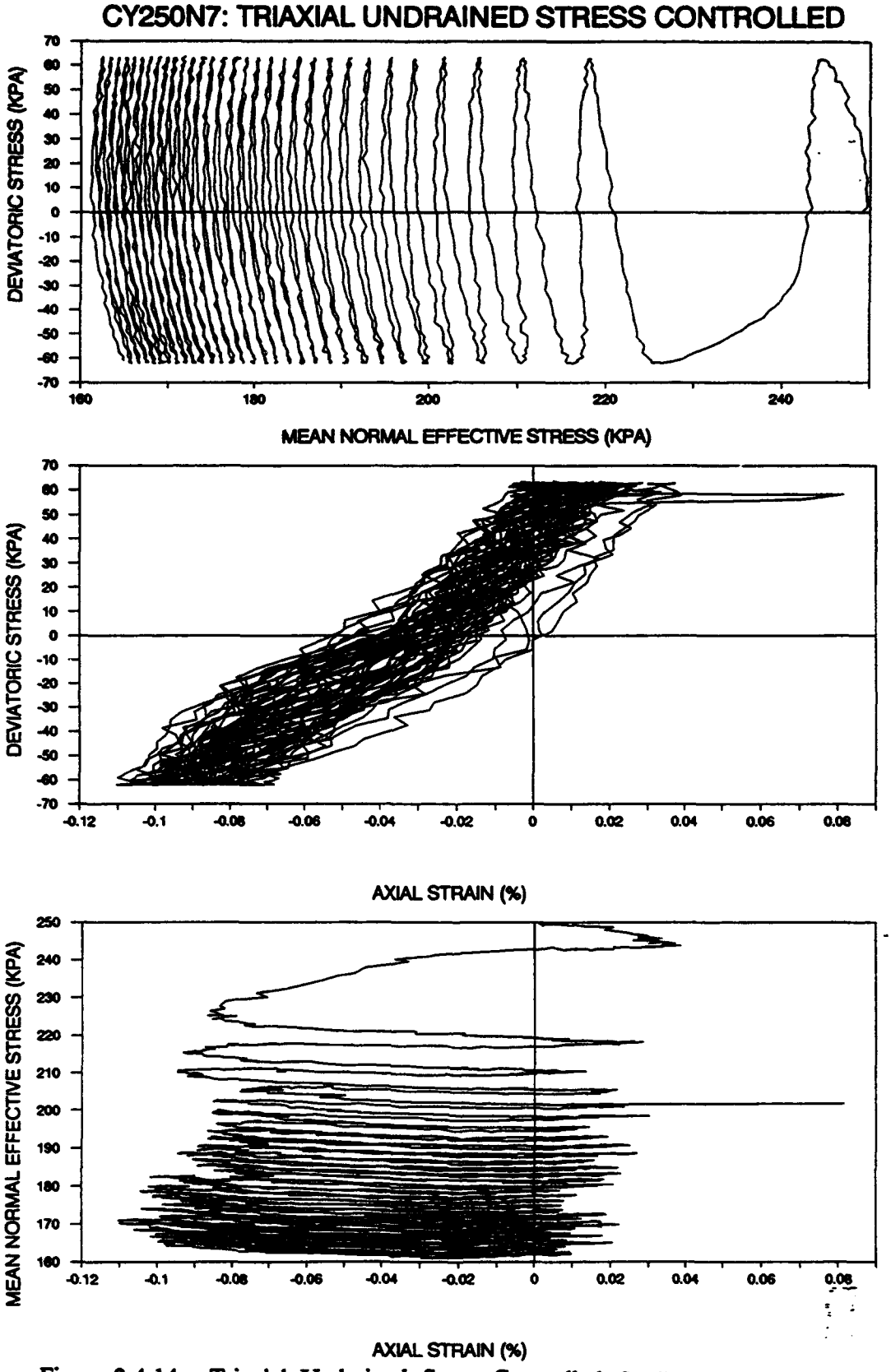

Figure 2.4.14 : Triaxial, Undrained, Stress Controlled, Cyclic Test (CY250N7)

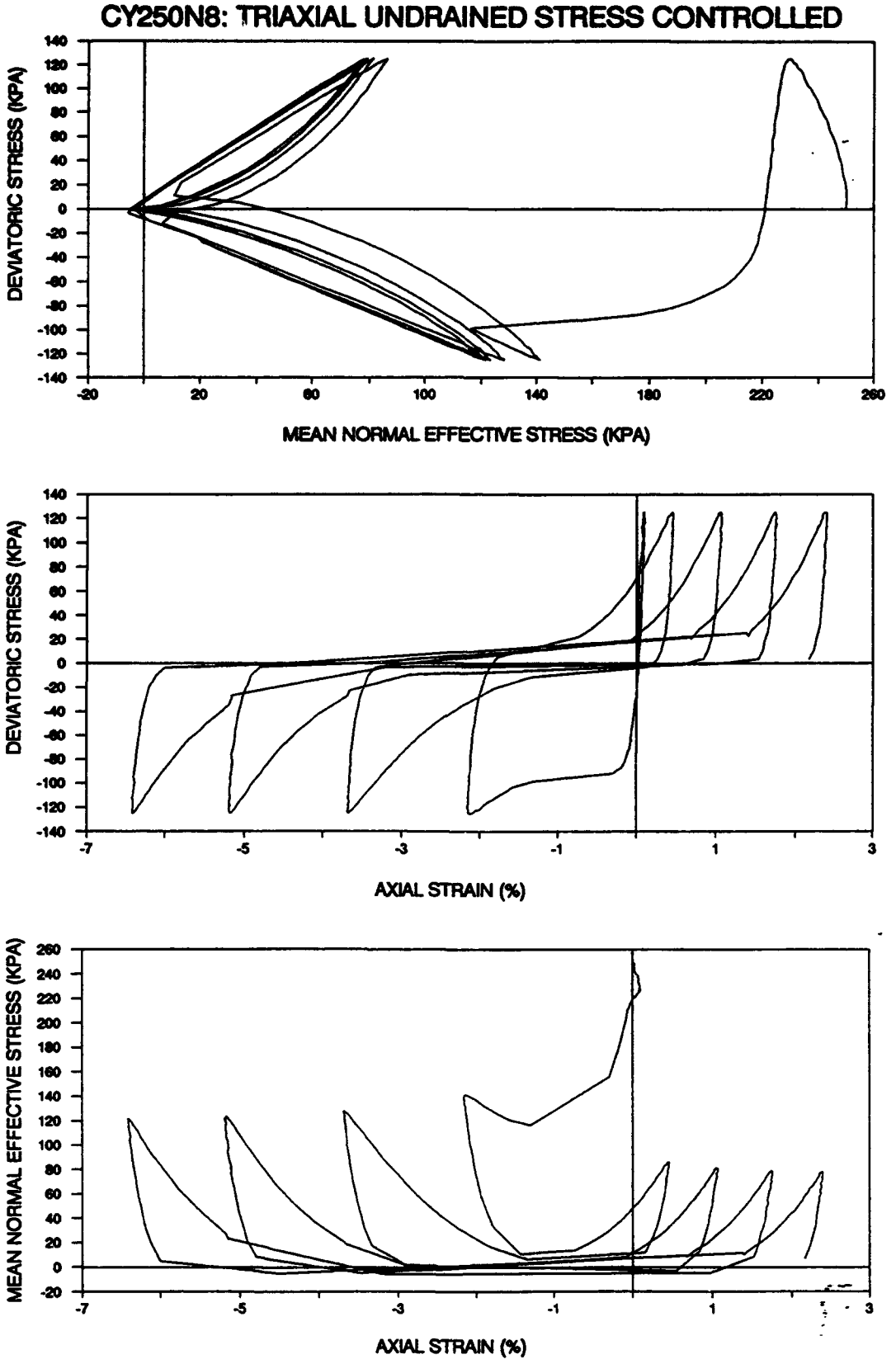

Figure 2.4.15 : Triaxial, Undrained, Stress Controlled, Cyclic Test (CY250N8)

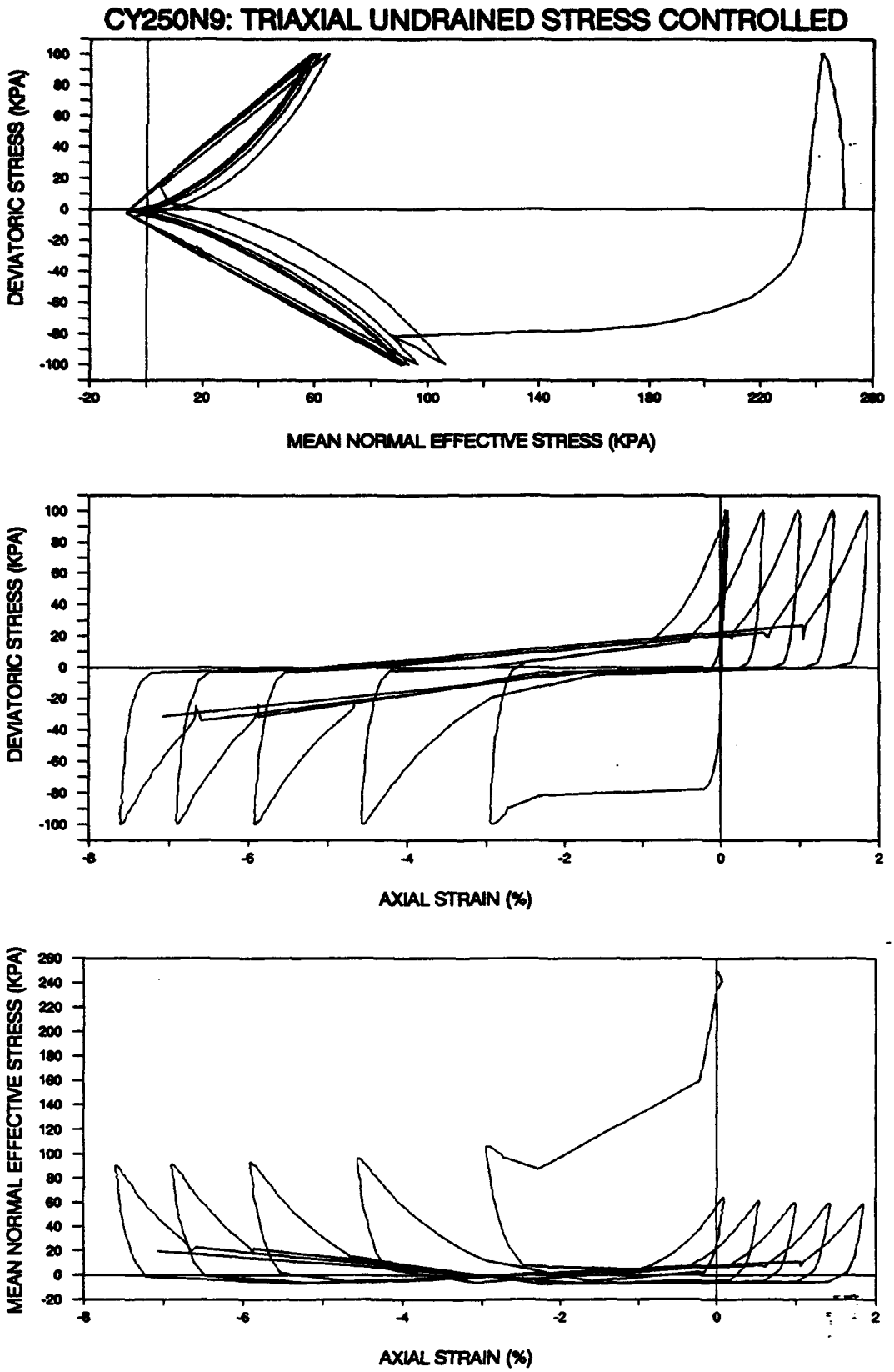

Figure 2.4.16 : Triaxial, Undrained, Stress Controlled, Cyclic Test (CY250N9)

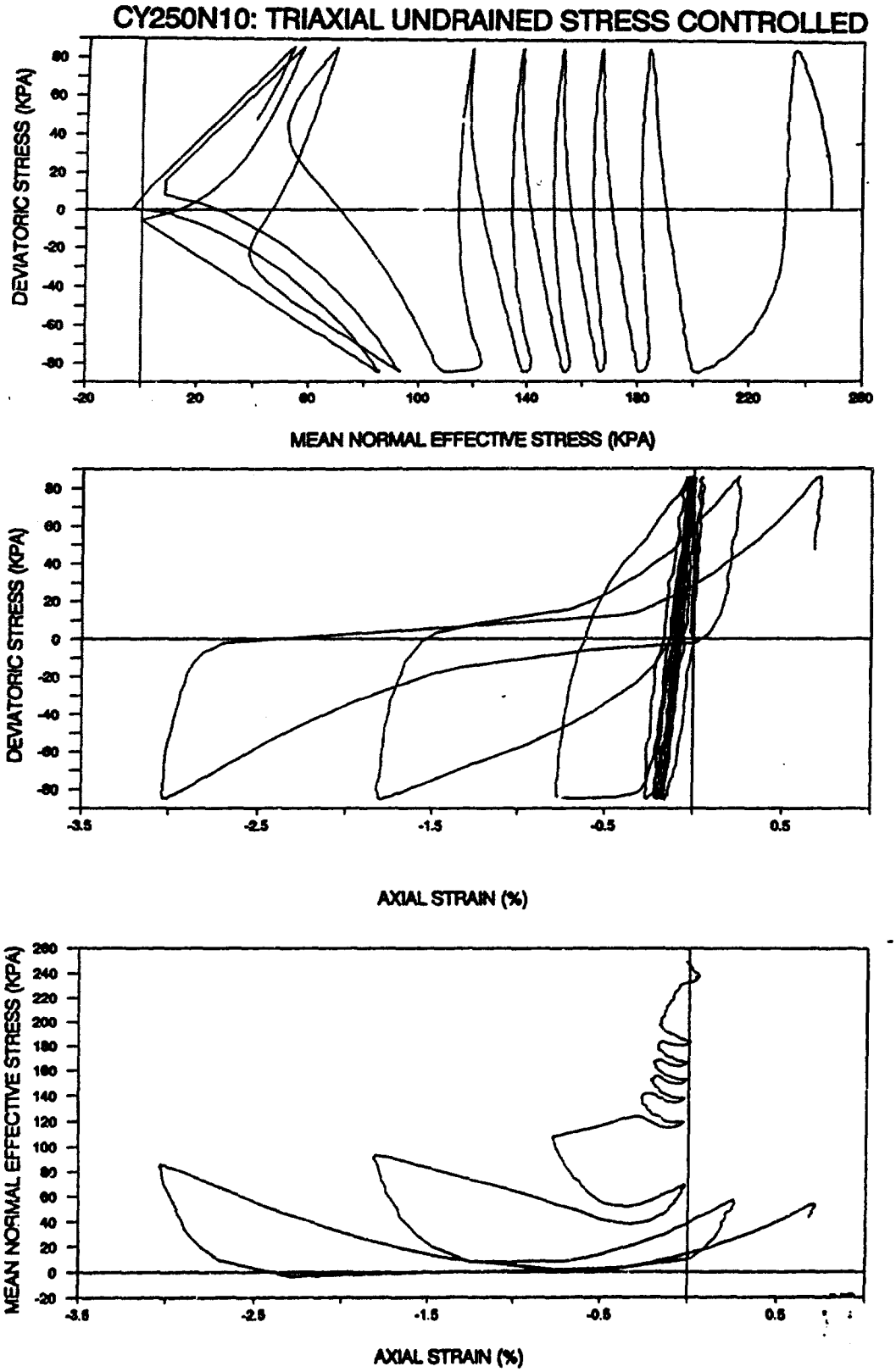

Figure 2.4.17 : Triaxial, Undrained, Stress Controlled, Cyclic Test (CY250N10)

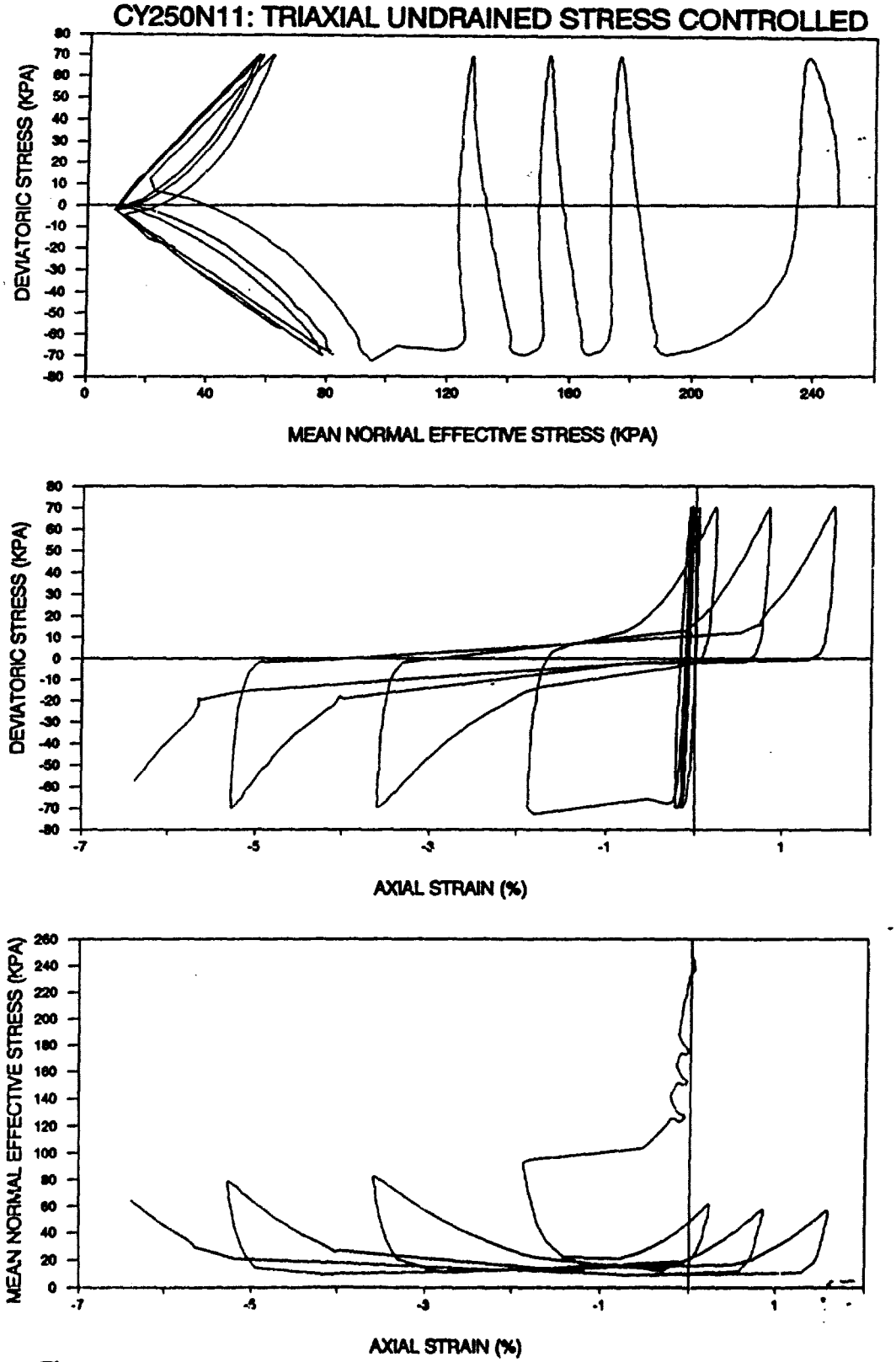

Figure 2.4.18 : Triaxial, Undrained, Stress Controlled, Cyclic Test (CY250N11)

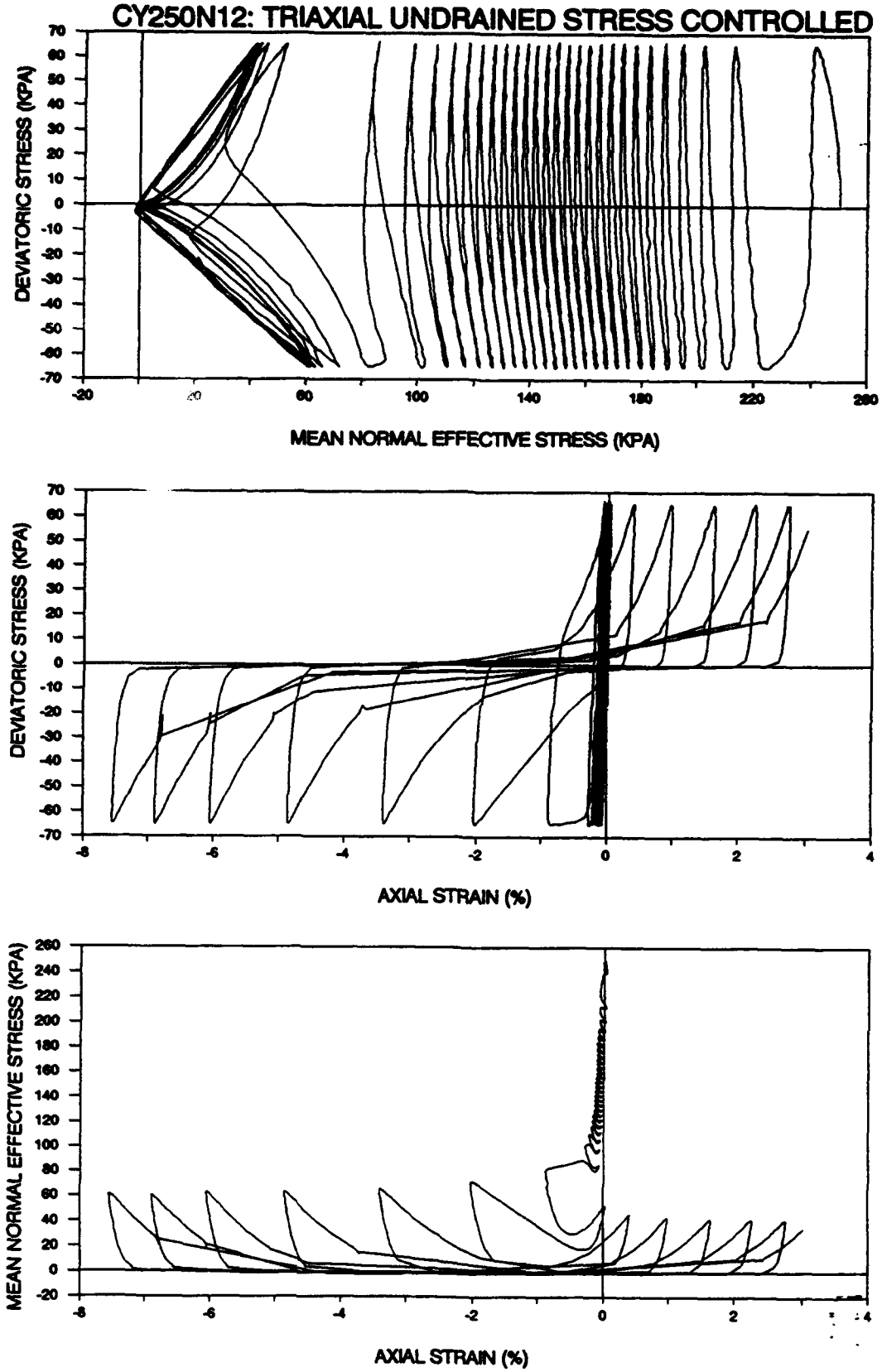

Figure 2.4.19 : Triaxial, Undrained, Stress Controlled, Cyclic Test (CY250N12)

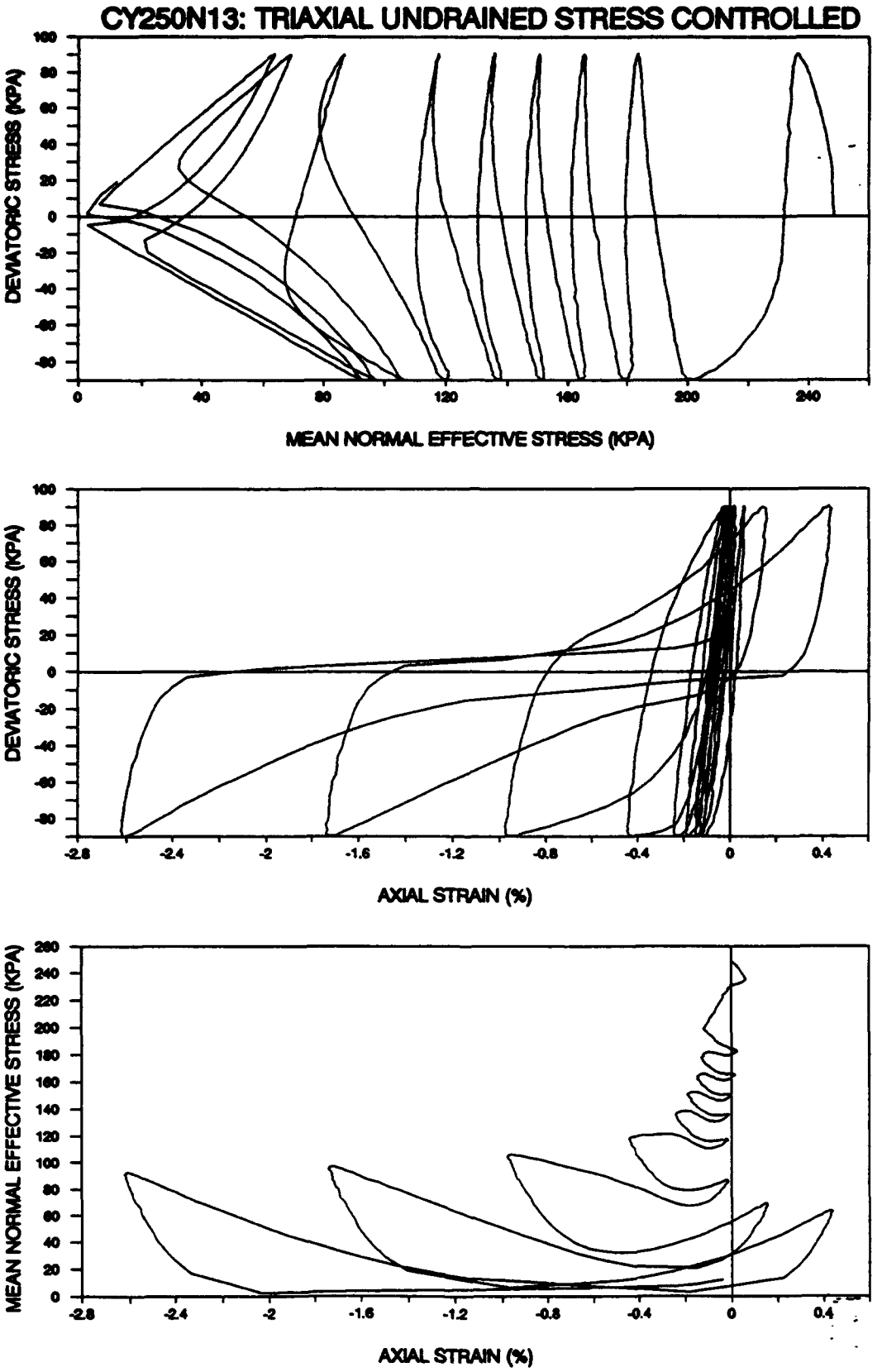

Figure 2.4.20 : Triaxial, Undrained, Stress Controlled, Cyclic Test (CY250N13)

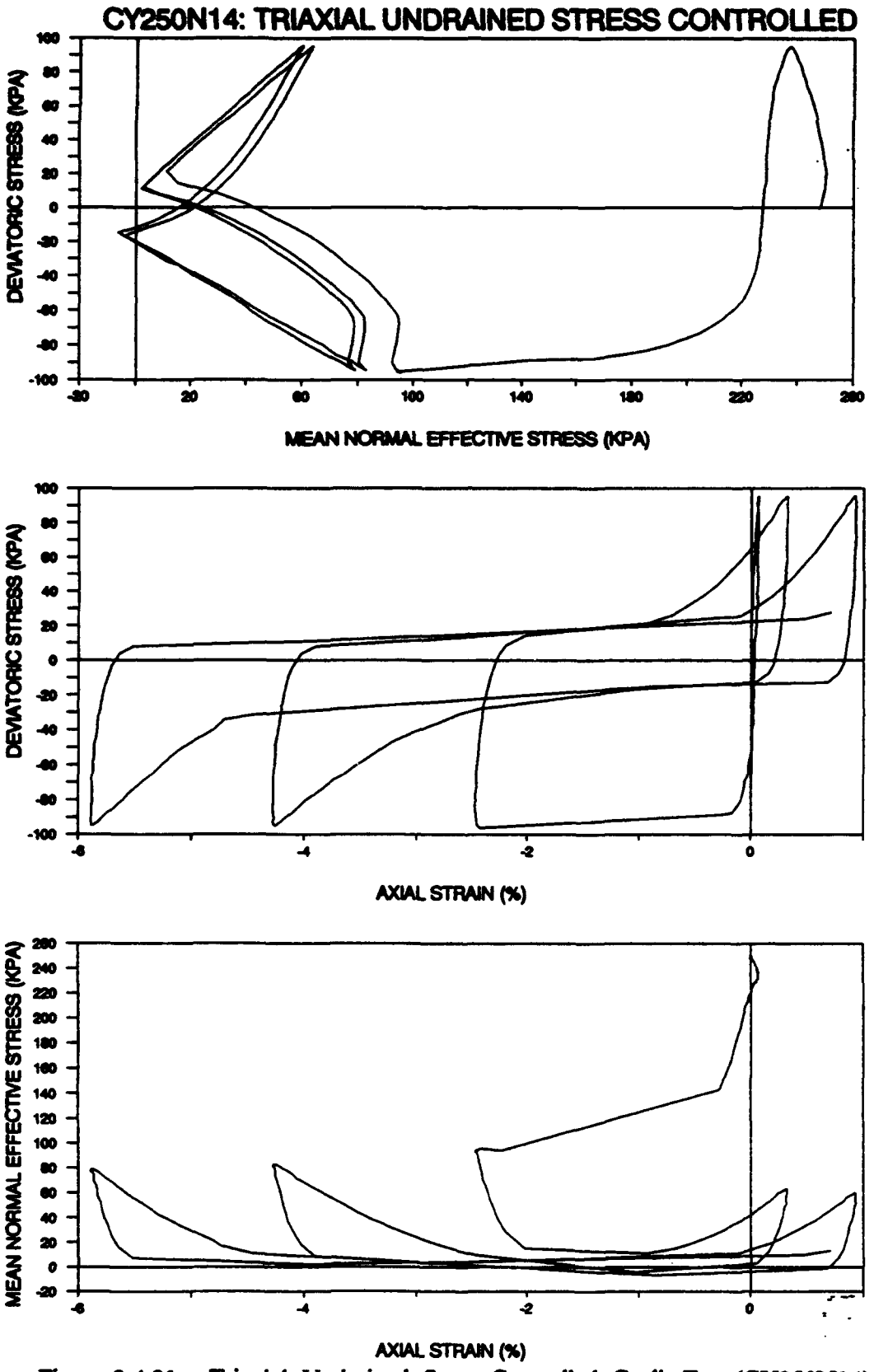

Figure 2.4.21 : Triaxial, Undrained, Stress Controlled, Cyclic Test (CY250N14)

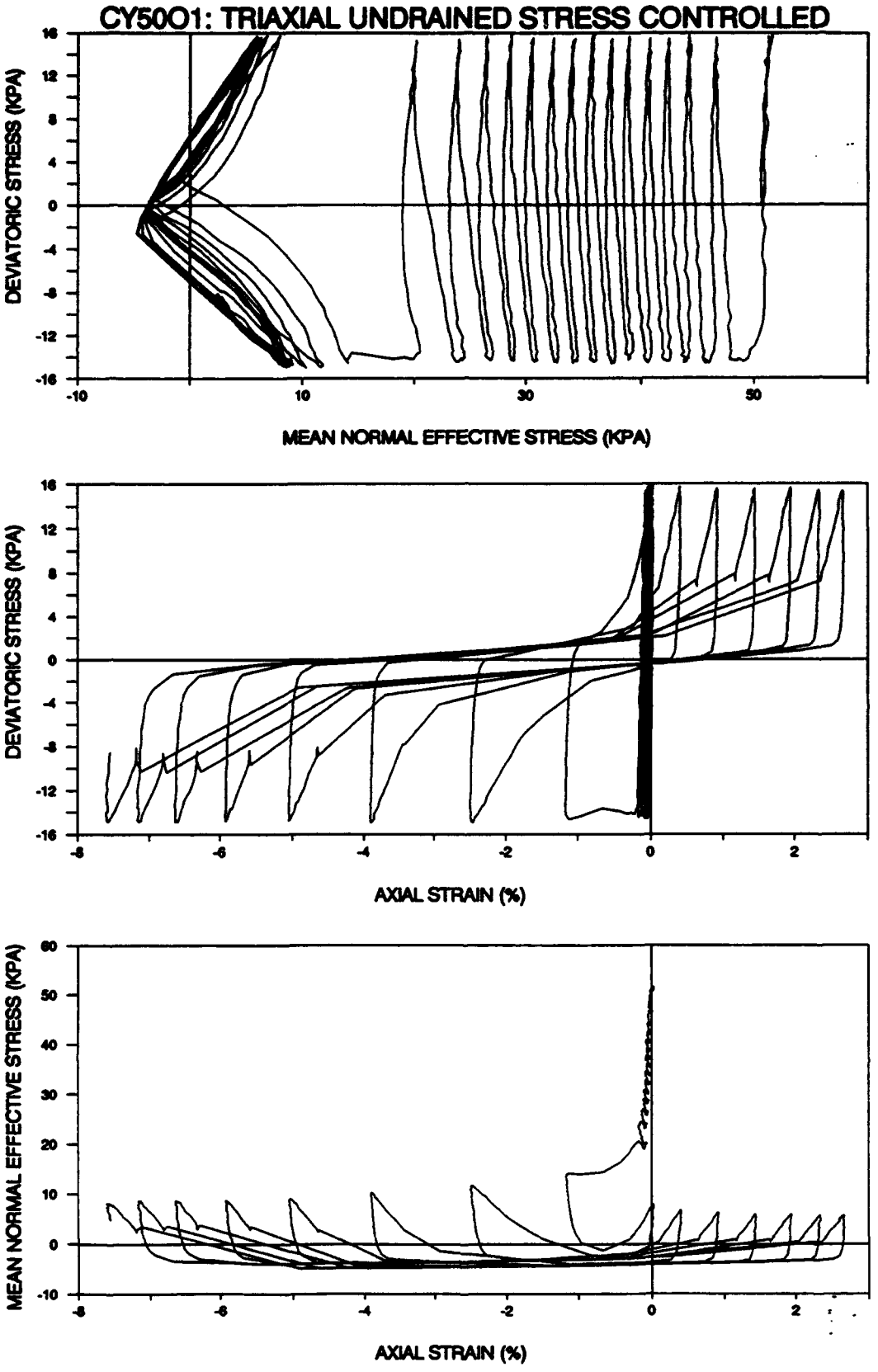

Figure 2.4.22 : Triaxial, Undrained, Stress Controlled, Cyclic Test (CY50O1)

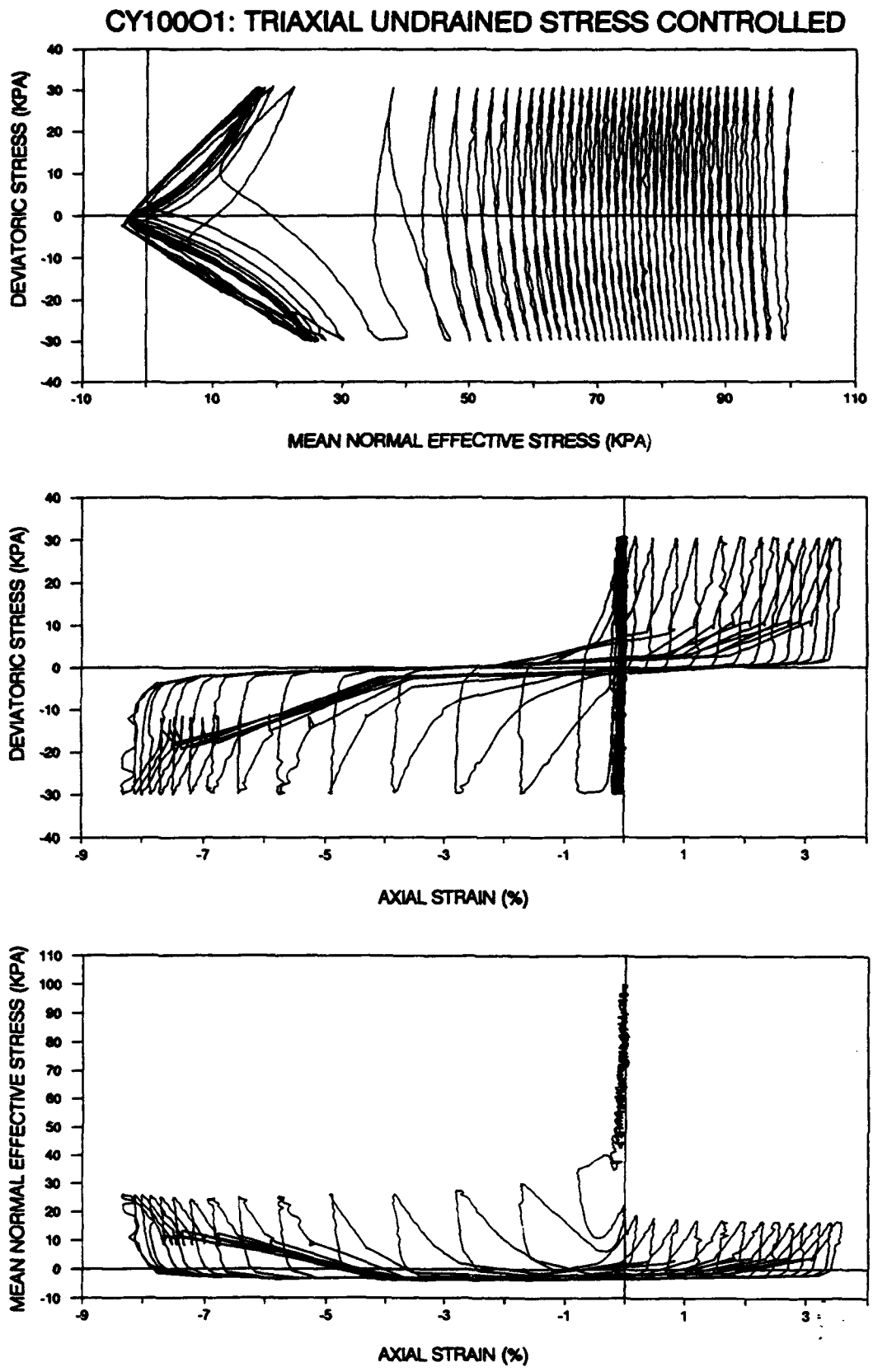

Figure 2.4.23 : Triaxial, Undrained, Stress Controlled, Cyclic Test (CY100O1)

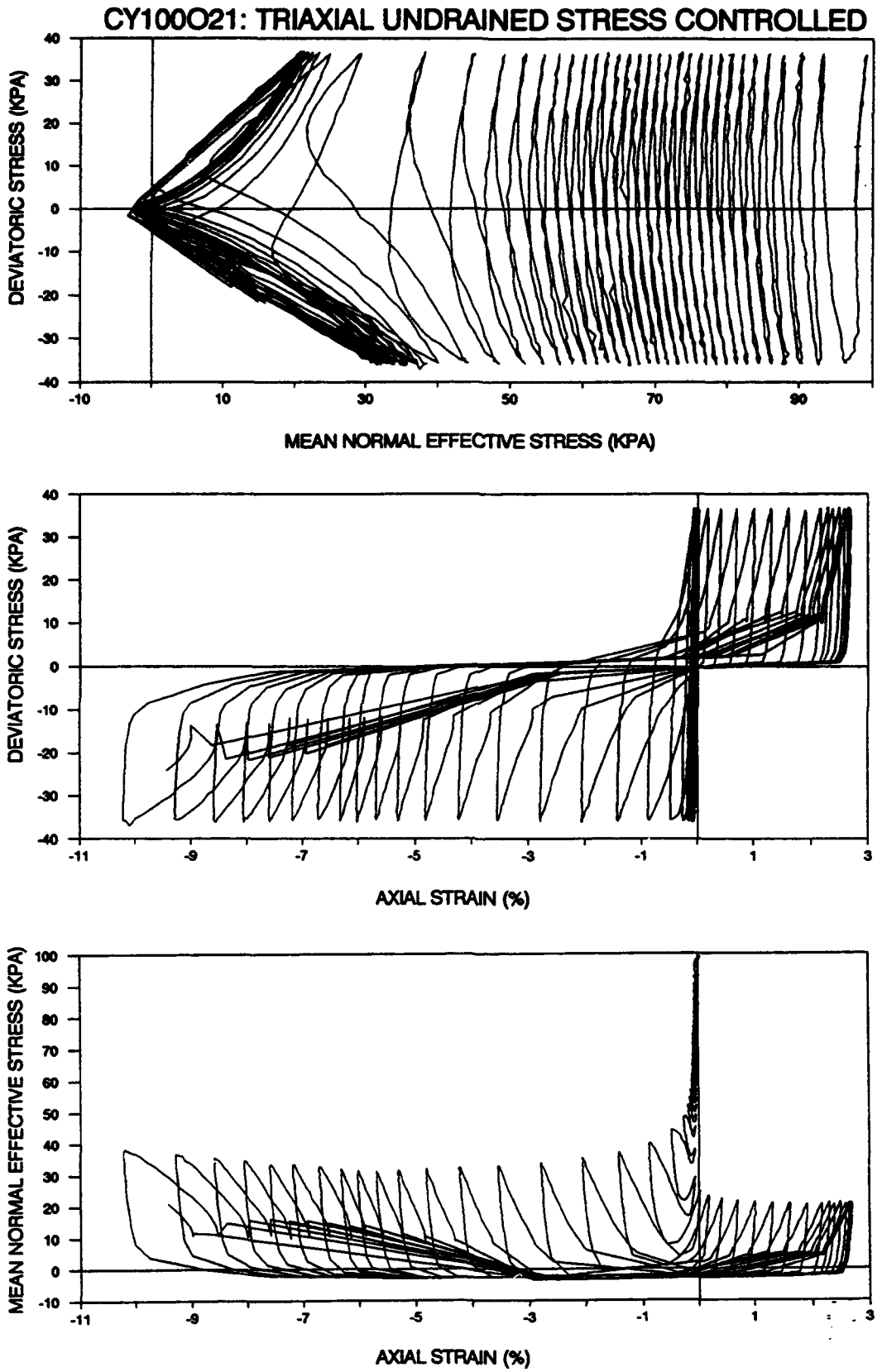

Figure 2.4.24 : Triaxial, Undrained, Stress Controlled, Cyclic Test (CY100O21)

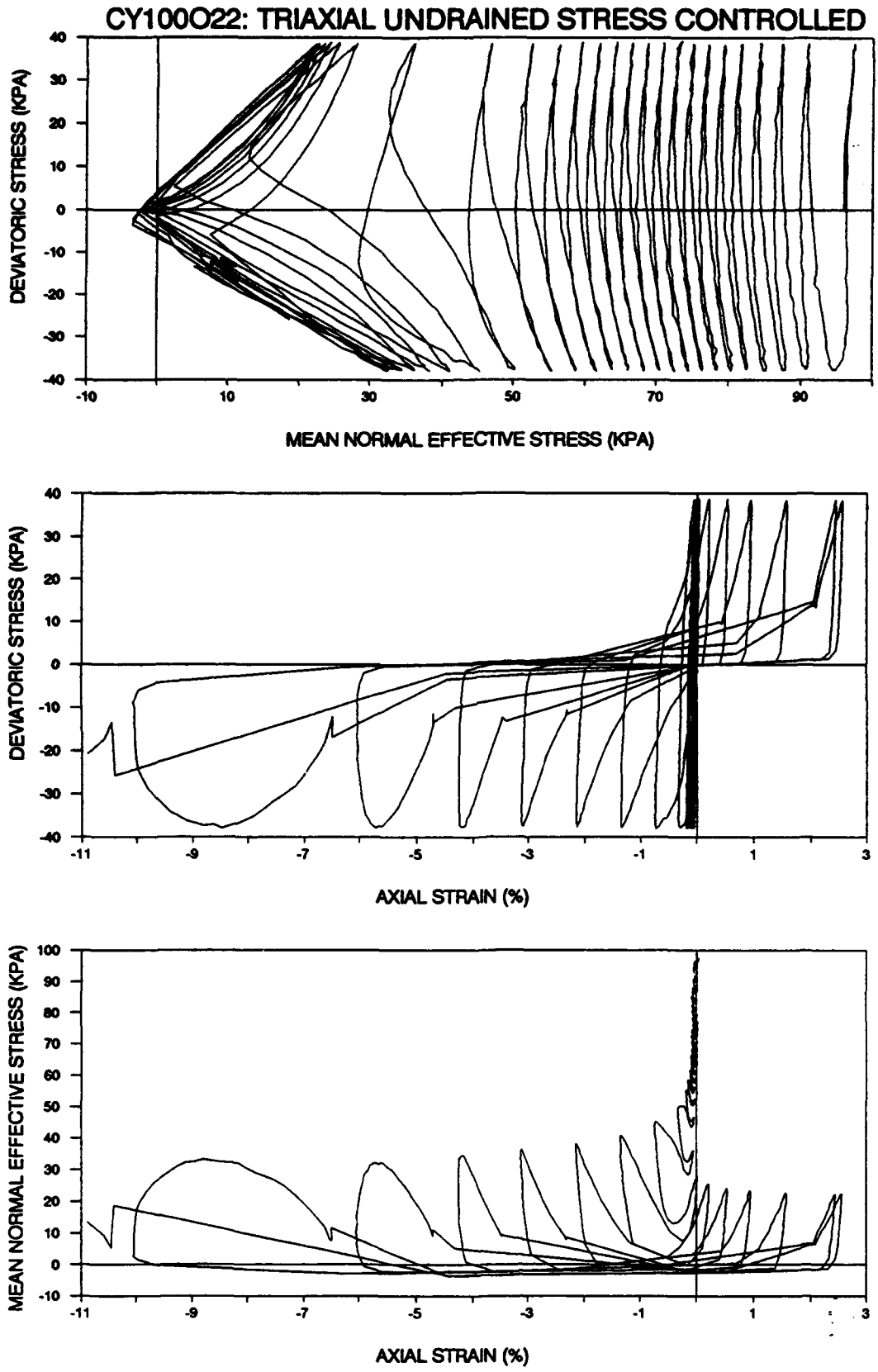

Figure 2.4.25 : Triaxial, Undrained, Stress Controlled, Cyclic Test (CY100O22)

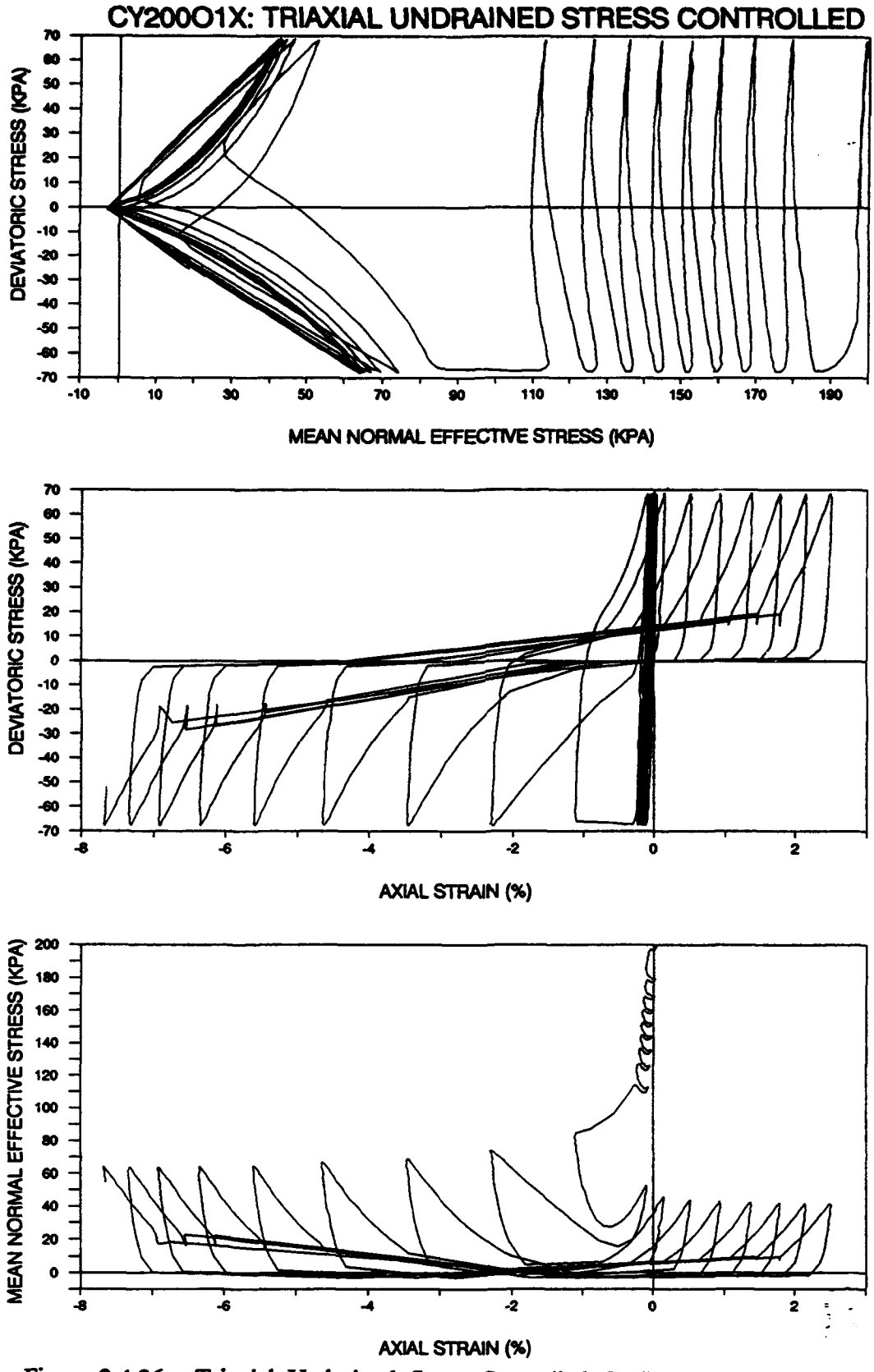

Figure 2.4.26 : Triaxial, Undrained, Stress Controlled, Cyclic Test (CY200O1X)

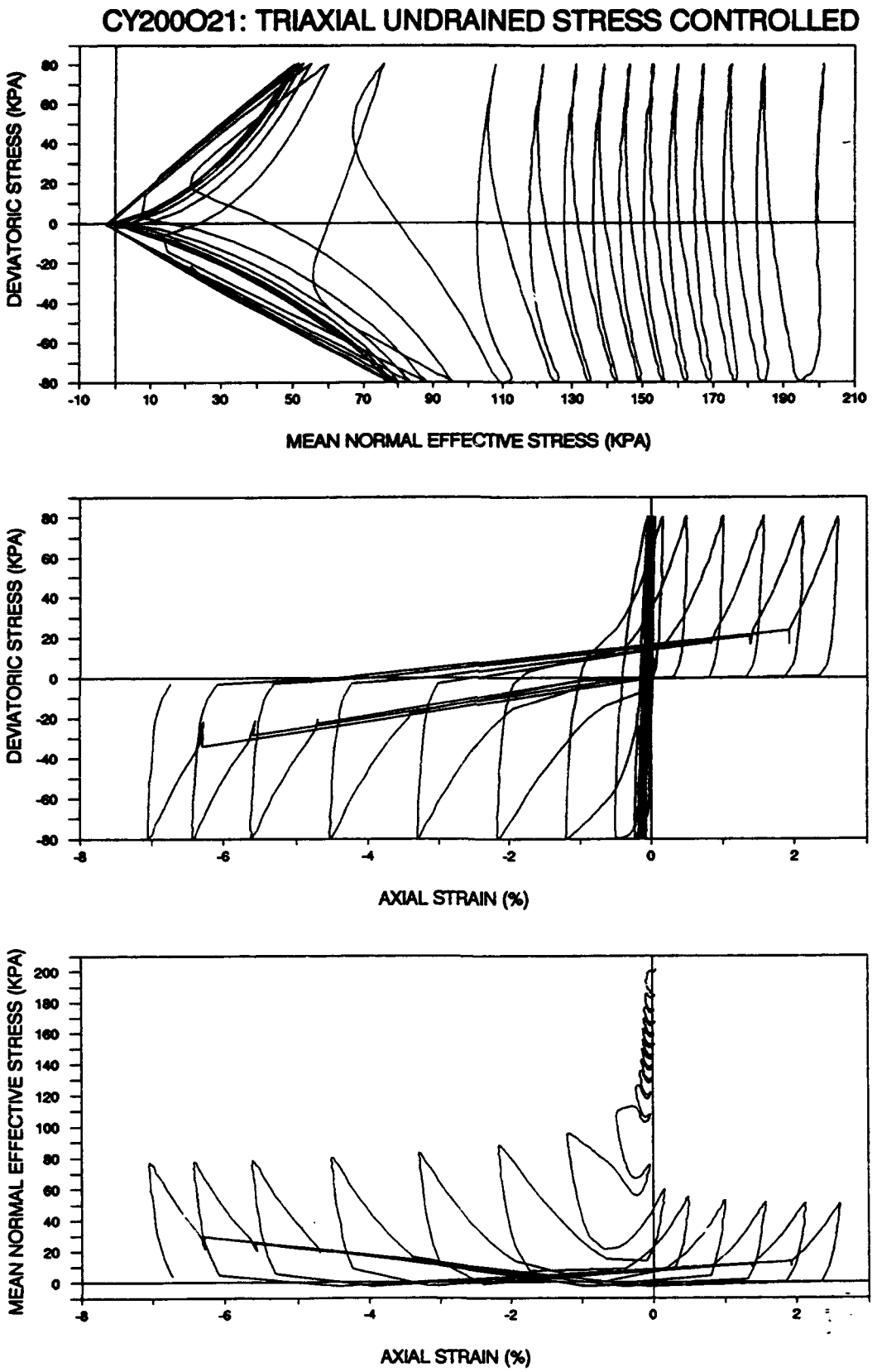

Figure 2.4.27 : Triaxial, Undrained, Stress Controlled, Cyclic Test (CY200O21)

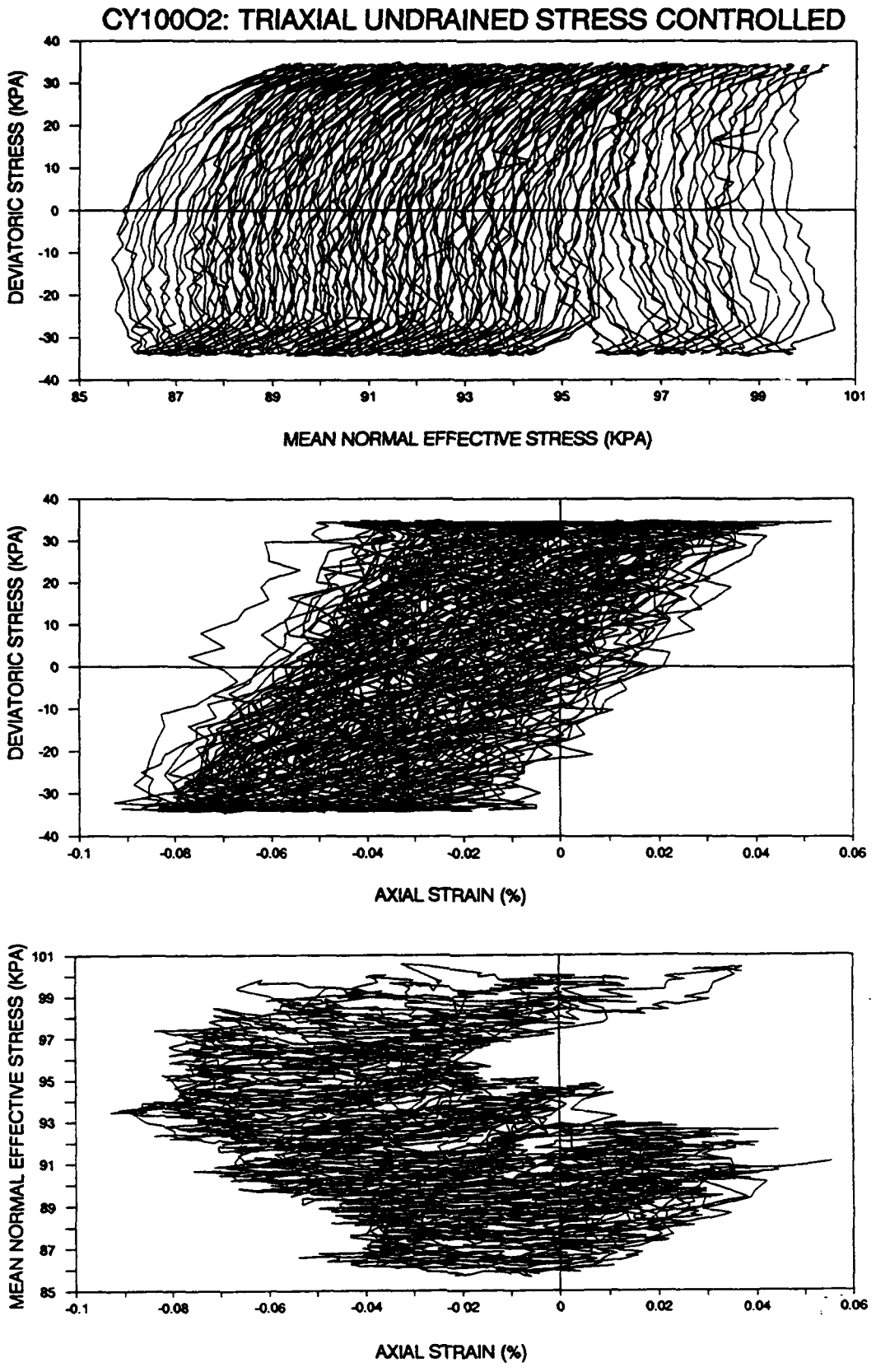

Figure 2.4.28 : Triaxial, Undrained, Stress Controlled, Cyclic Test (CY100O2)

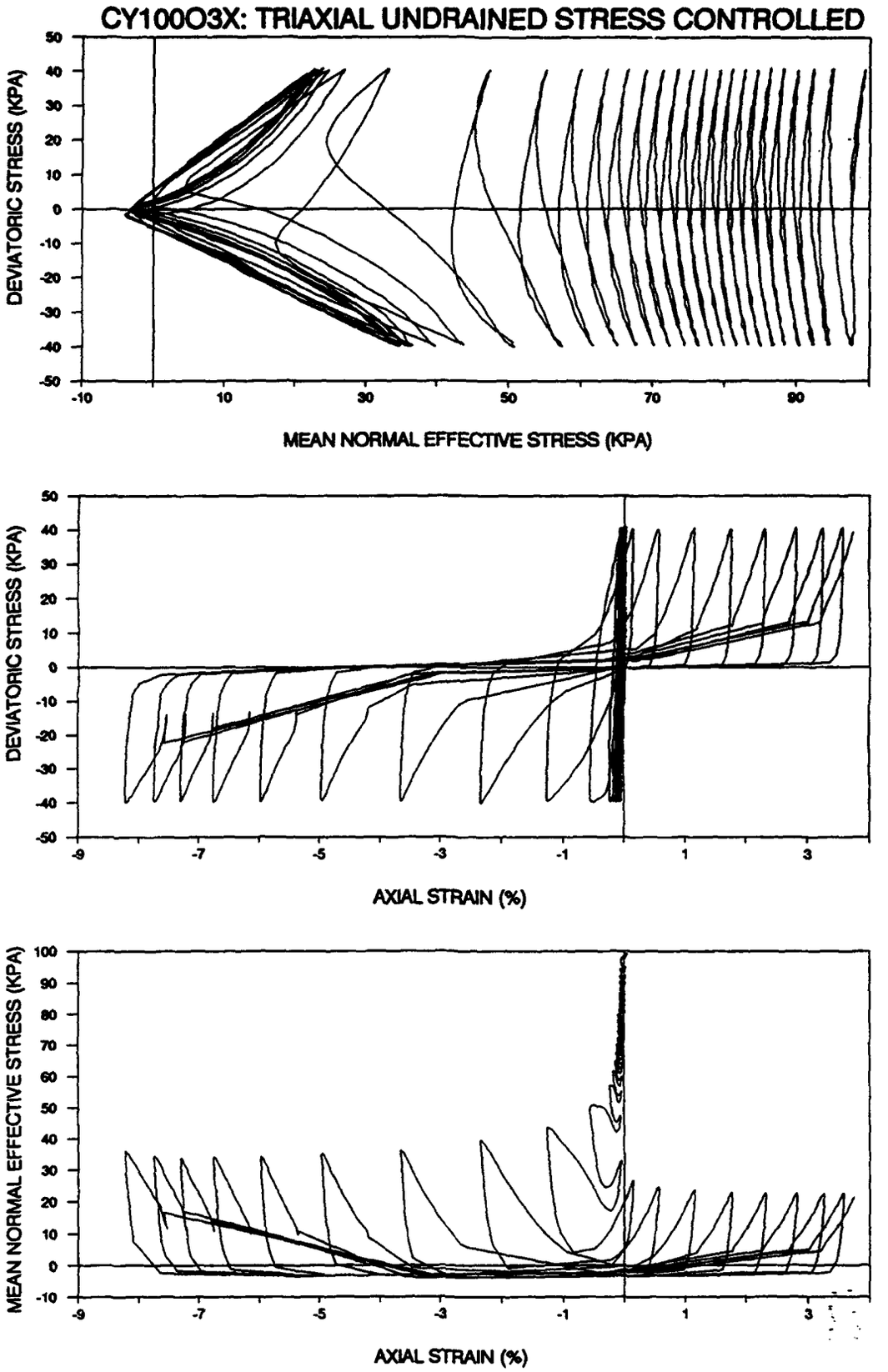

Figure 2.4.29 : Triaxial, Undrained, Stress Controlled, Cyclic Test (CY100O3X)

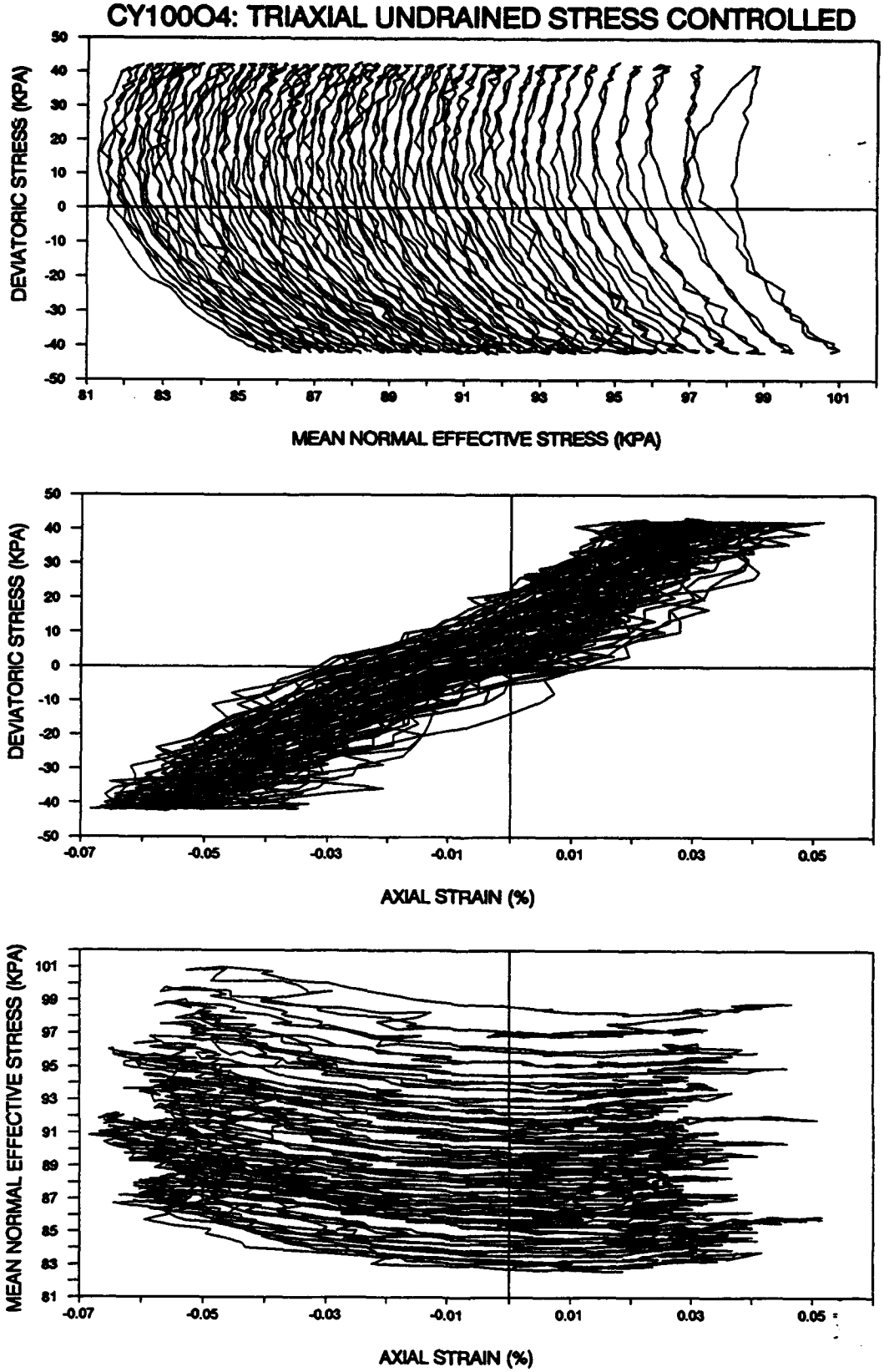

Figure 2.4.30 : Triaxial, Undrained, Stress Controlled, Cyclic Test (CY100O4)

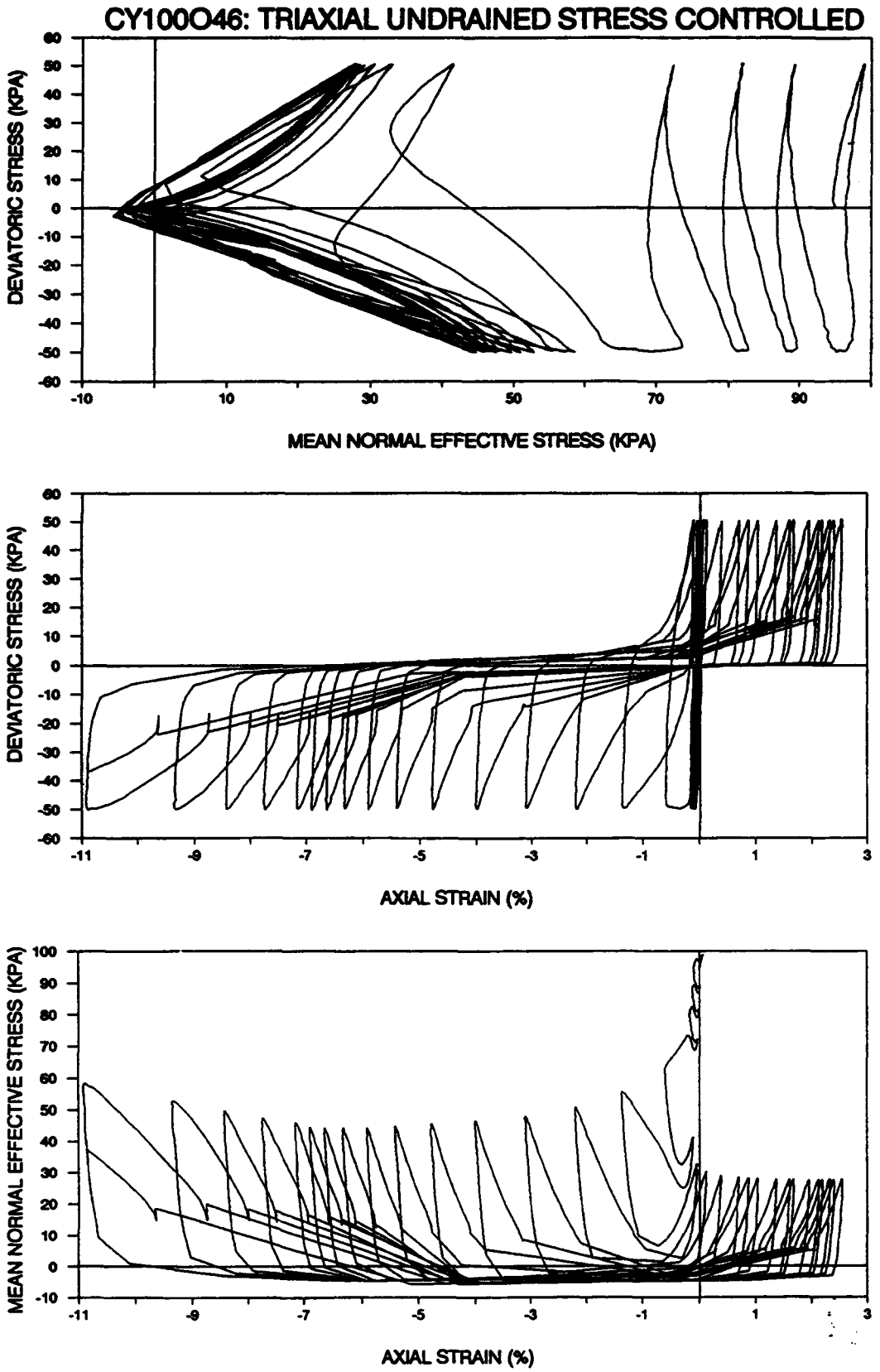

Figure 2.4.31 : Triaxial, Undrained, Stress Controlled, Cyclic Test (CY100O46

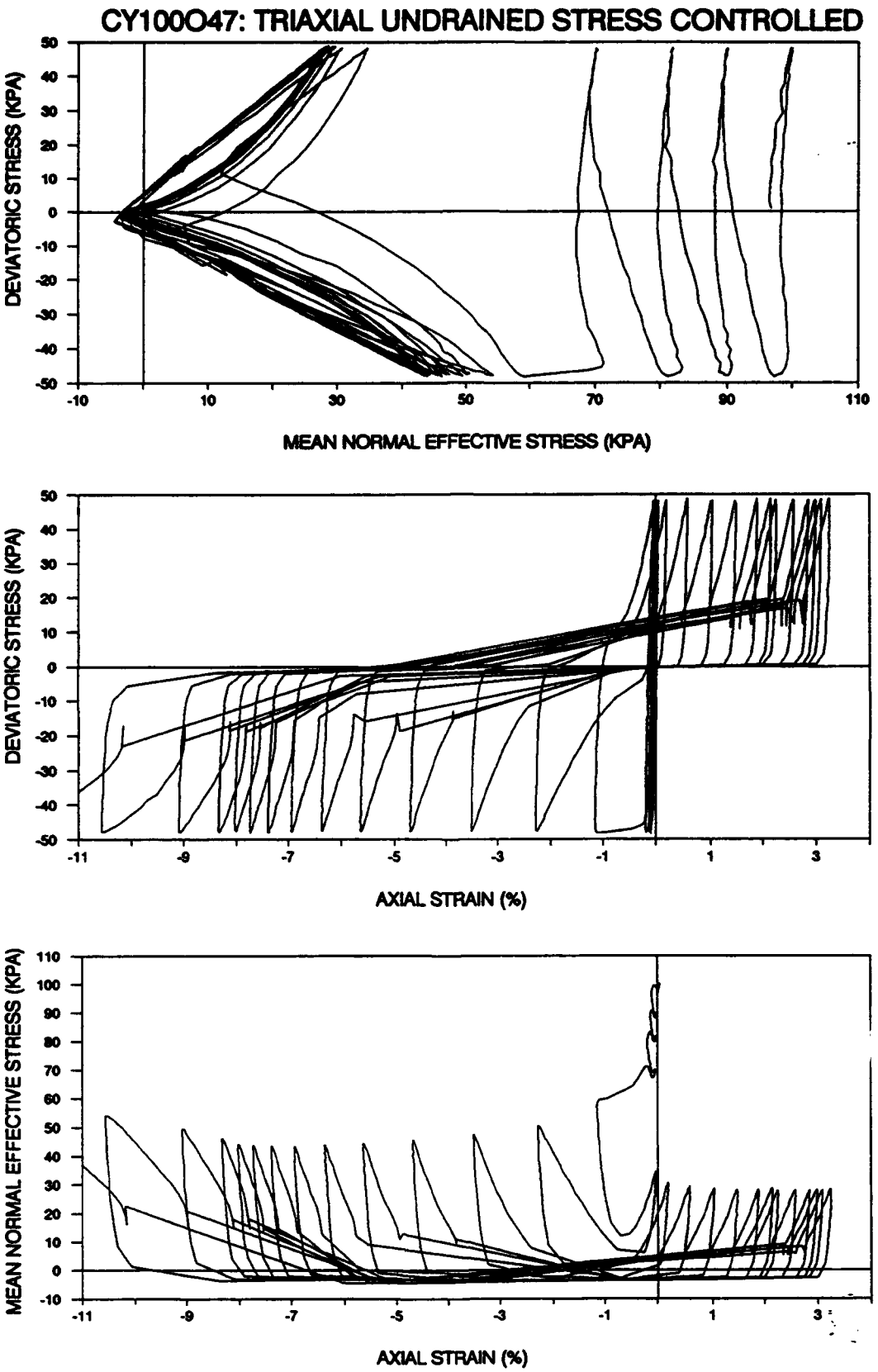

Figure 2.4.32 : Triaxial, Undrained, Stress Controlled, Cyclic Test (CY100O47

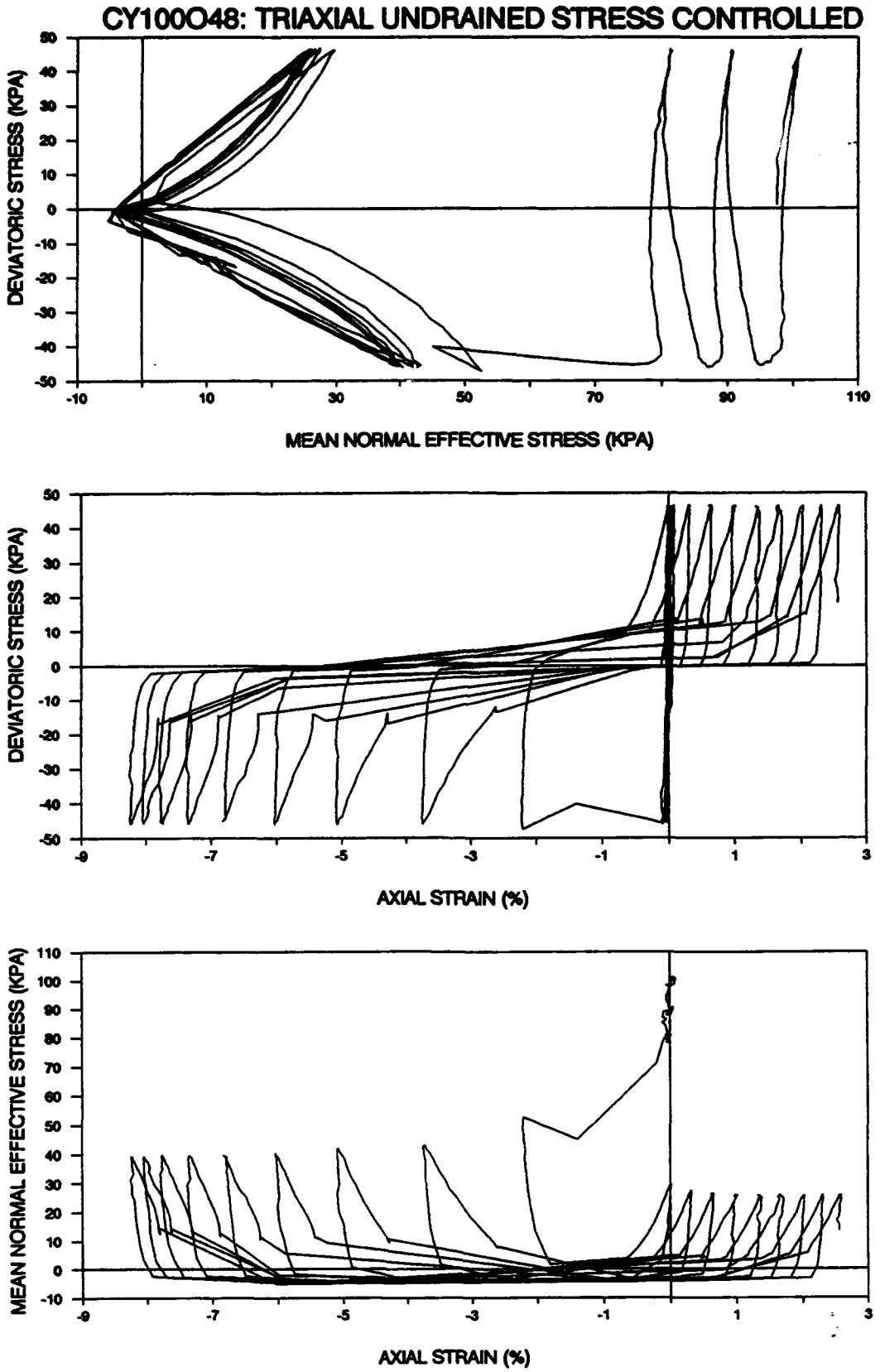

Figure 2.4.33 : Triaxial, Undrained, Stress Controlled, Cyclic Test (CY100O48)

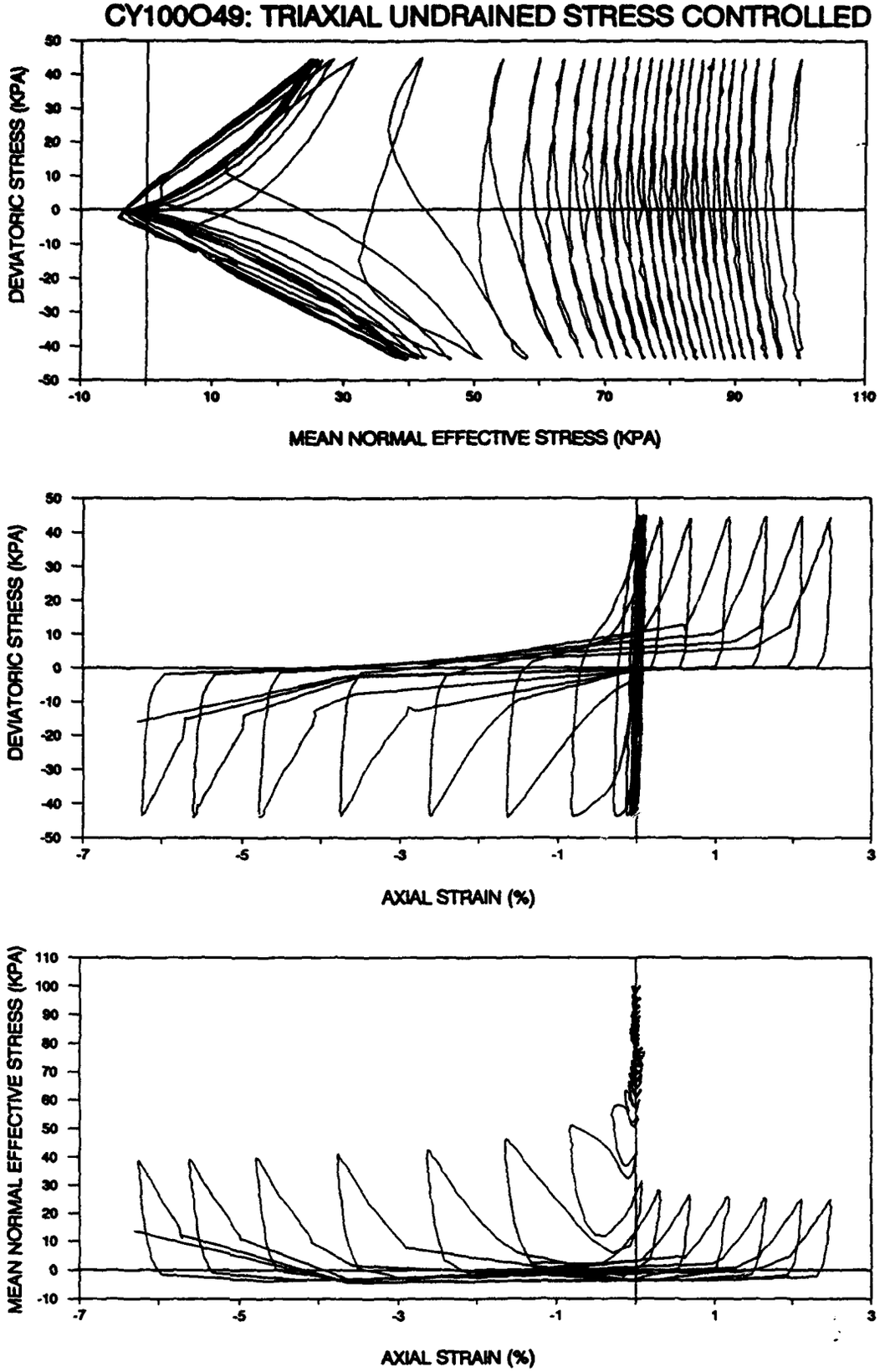

Figure 2.4.34 : Triaxial, Undrained, Stress Controlled, Cyclic Test (CY100O49)

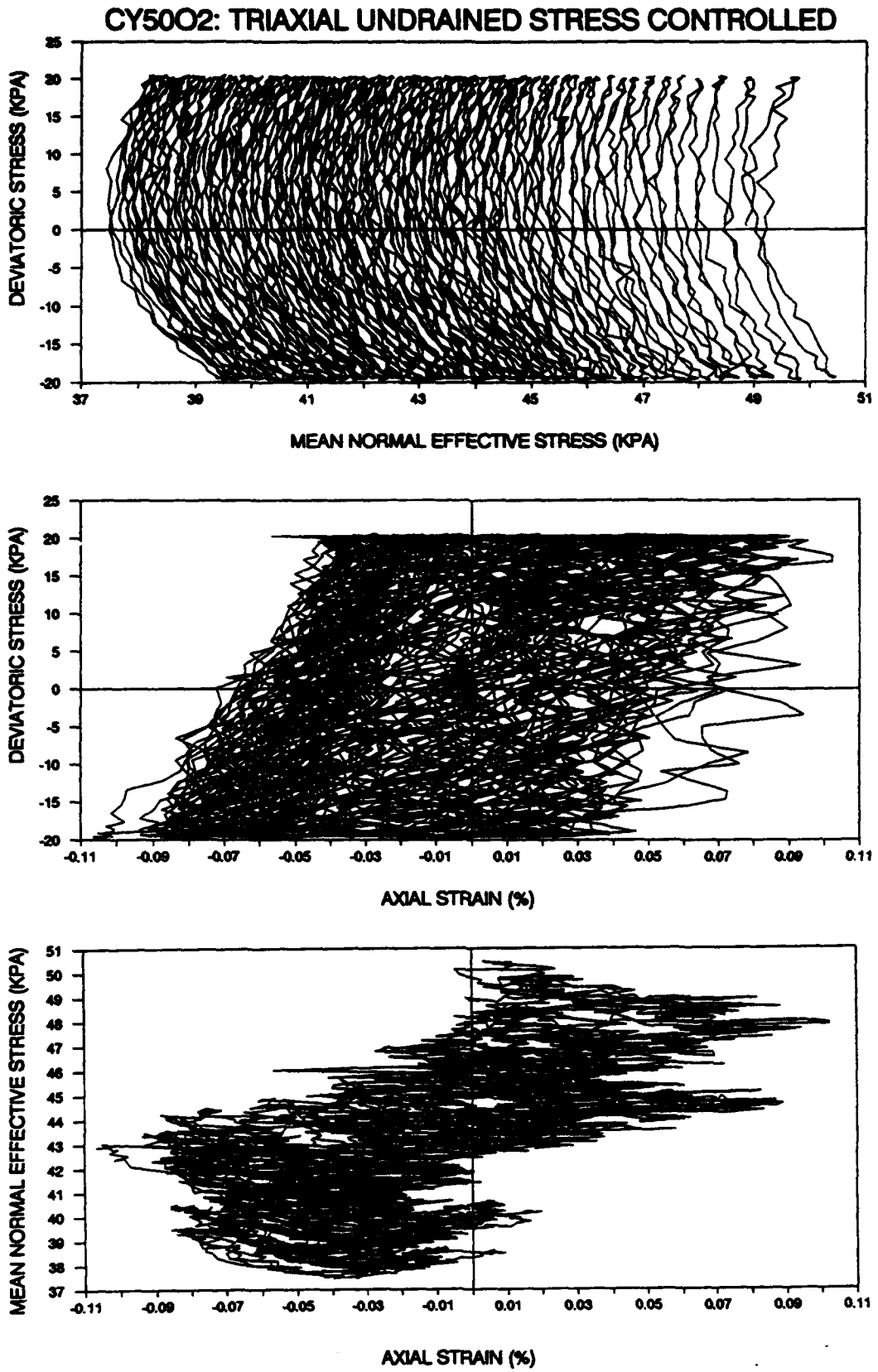

Figure 2.4.35 : Triaxial, Undrained, Stress Controlled, Cyclic Test (CY50O2)

TEST RESULTS
ON
TRIAXIAL CONSOLIDATION AND REBOUND TESTS

Figure 2.5.1 : Triaxial Consolidation Test (CY50O2C)
Figure 2.5.2 : Triaxial Consolidation Test (CY100O3C)
Figure 2.5.3 : Triaxial Consolidation Test (CY100C46)
Figure 2.5.4 : Triaxial Consolidation Test (CY100C48)
Figure 2.5.5 : Triaxial Consolidation Test (CY100C49)
Figure 2.5.6 : Triaxial Consolidation Test (O60C1001)
Figure 2.5.7 : Triaxial Consolidation Test (O60C1002)
Figure 2.5.8 : Triaxial Consolidation Test (O60C1006)

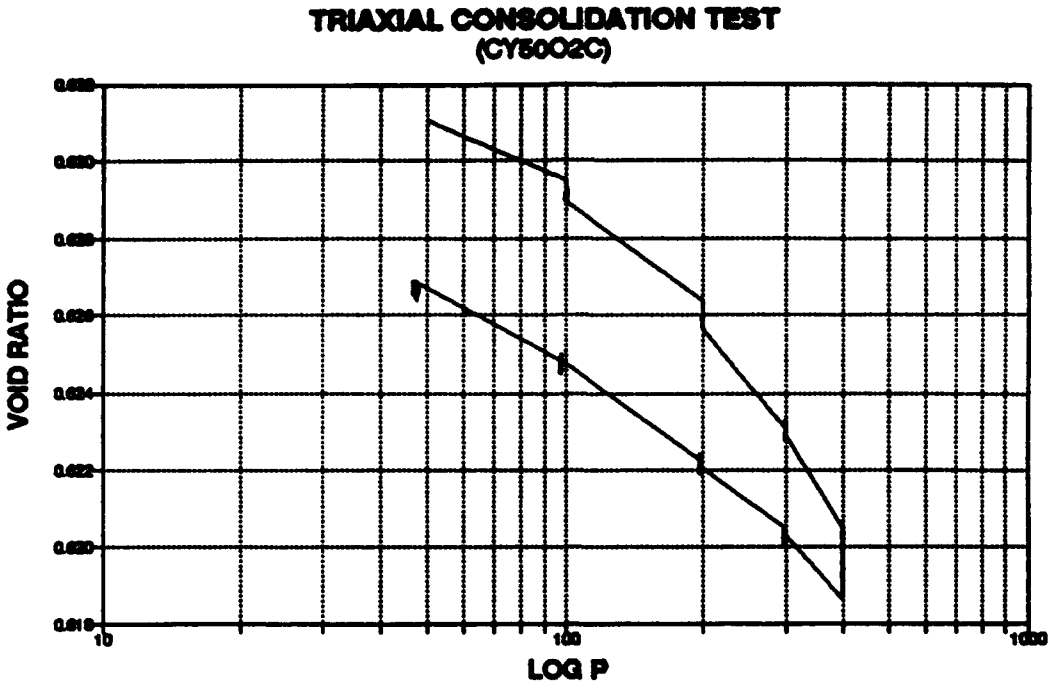

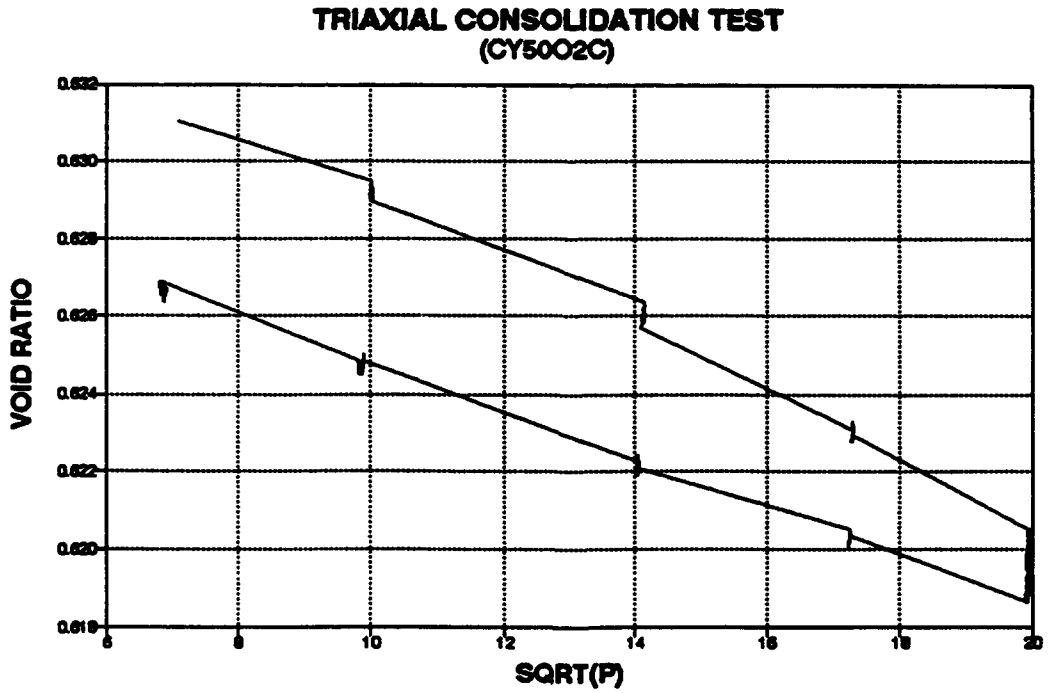

Figure 2.5.1 : Triaxial Consolidation Test (CY50O2C)

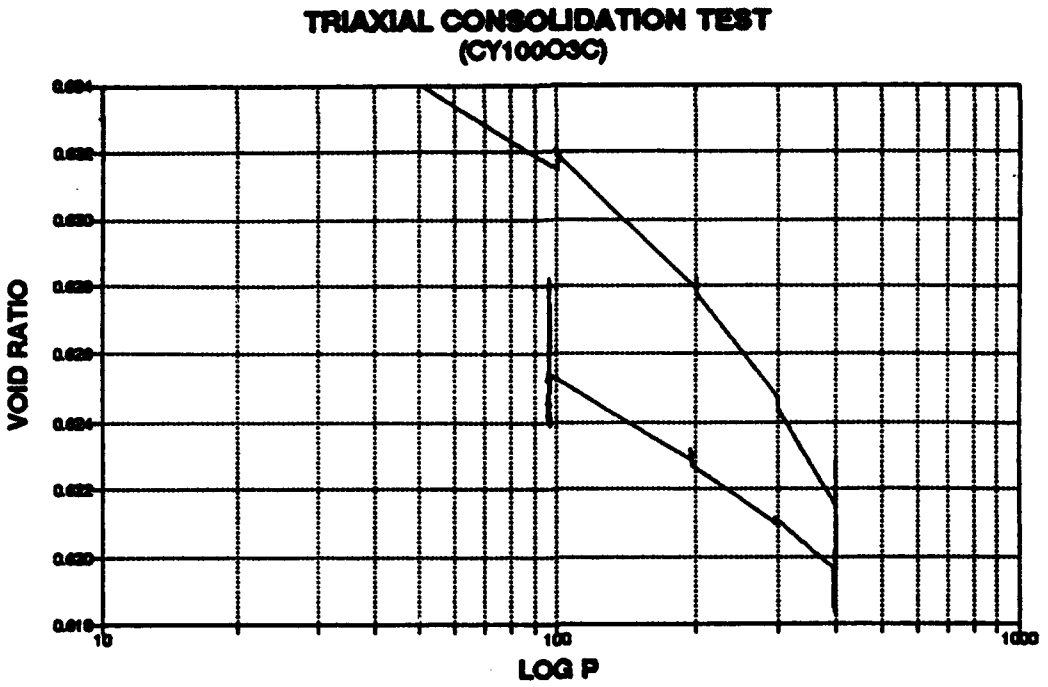

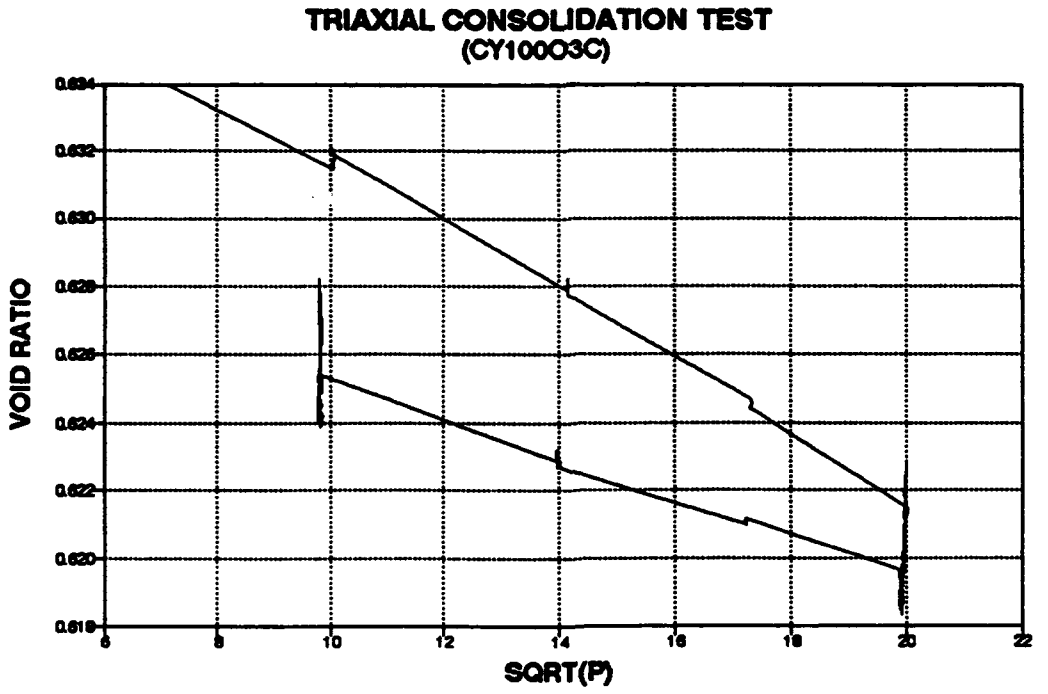

Figure 2.5.2 : Triaxial Consolidation Test (CY100O3C)

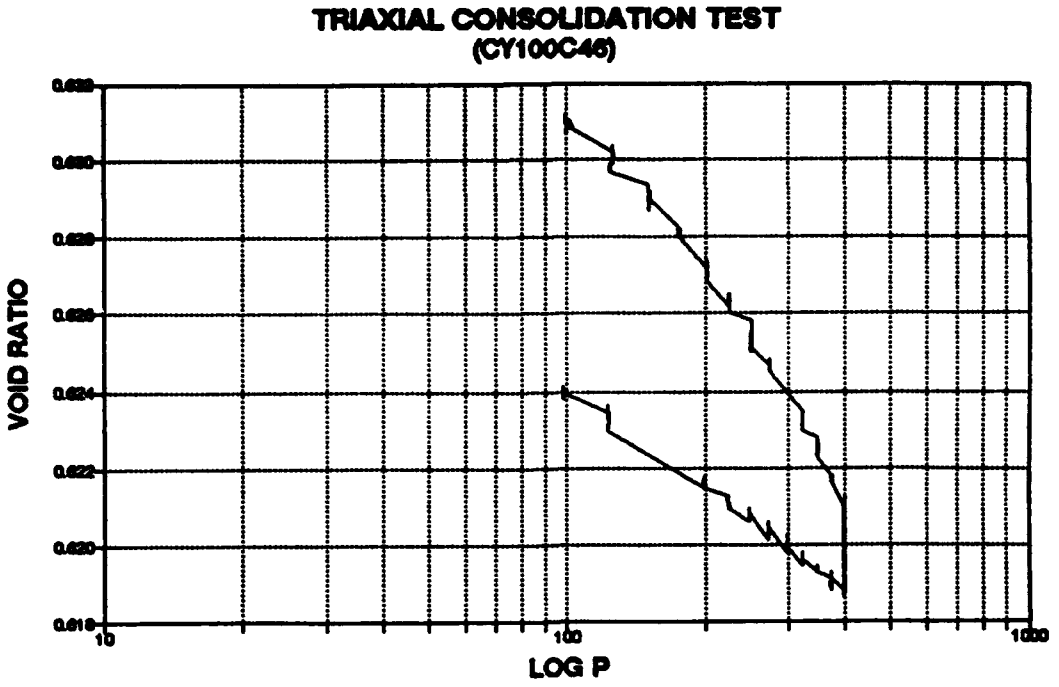

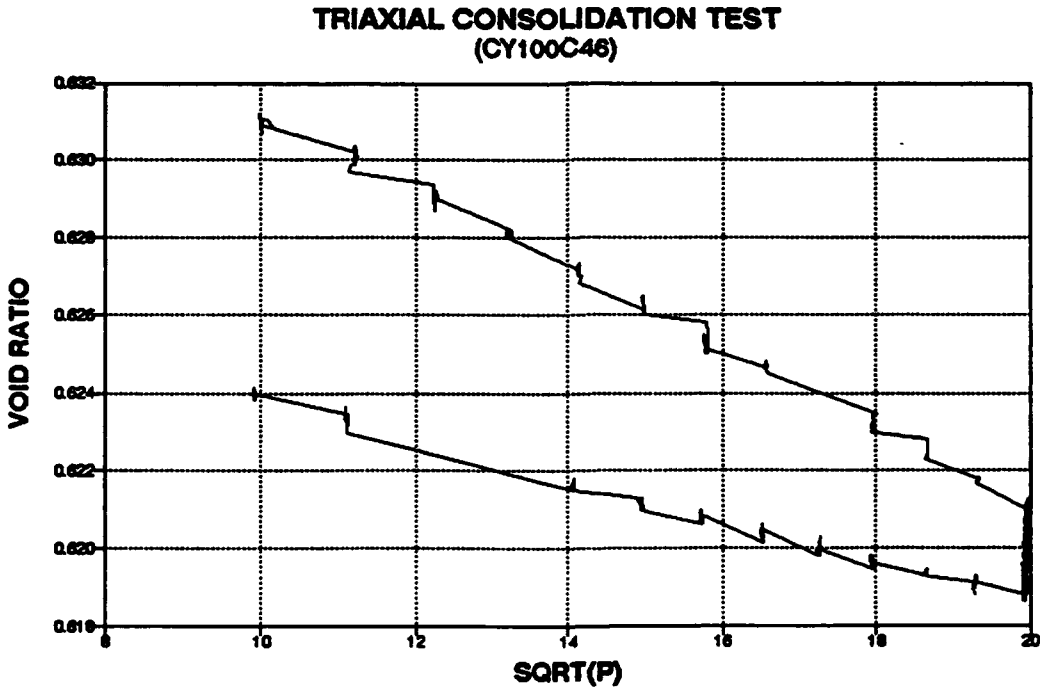

Figure 2.5.3 : Triaxial Consolidation Test (CY100C46)

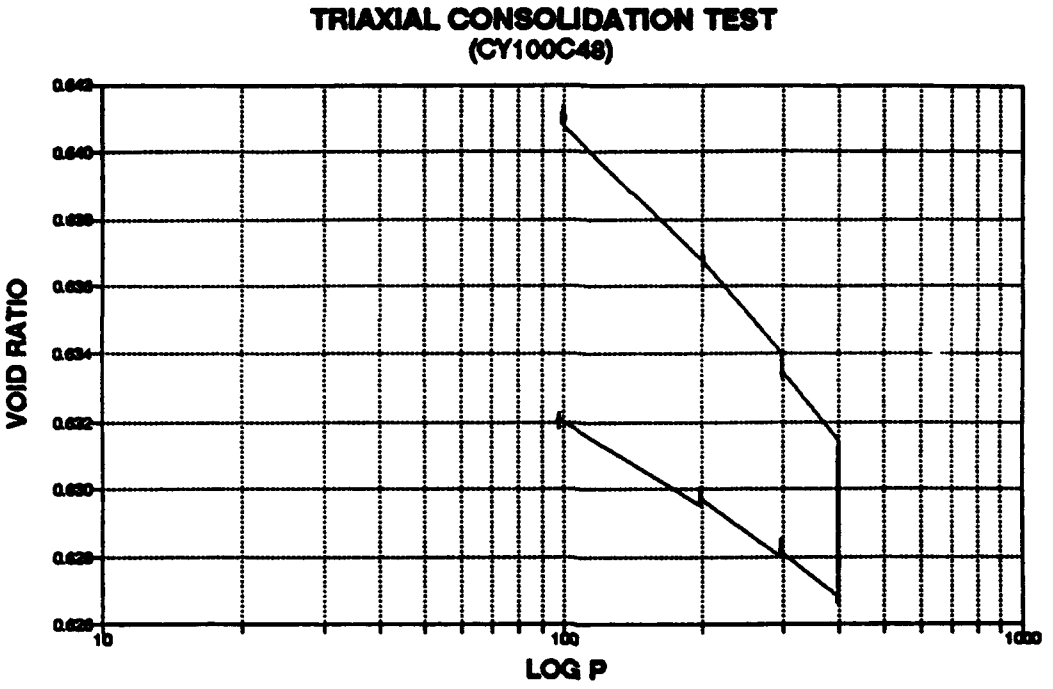

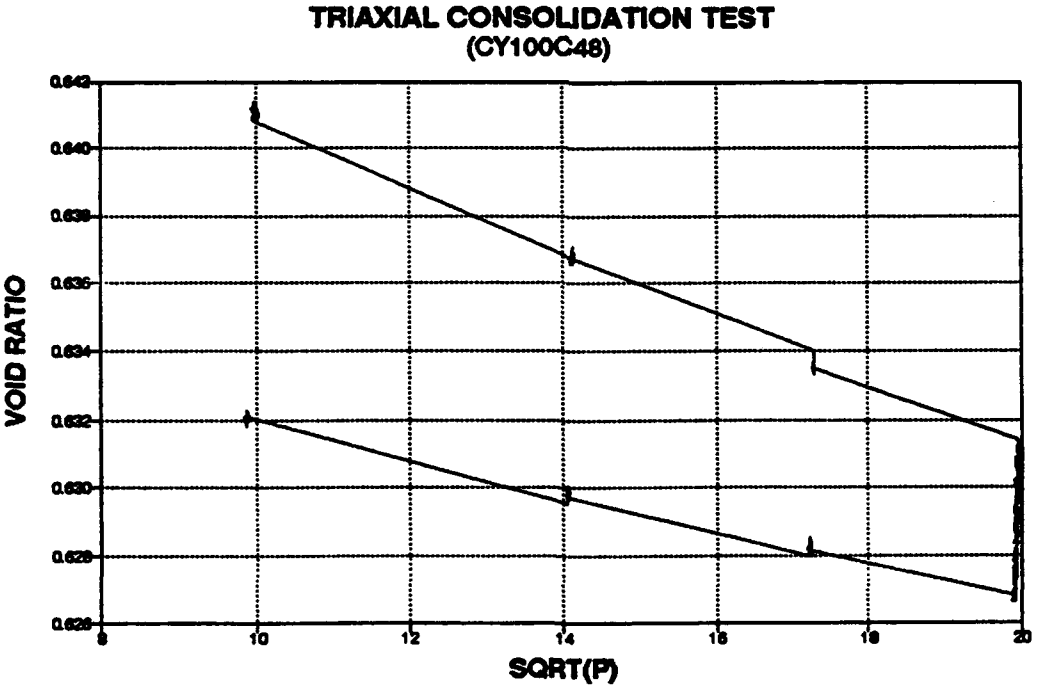

Figure 2.5.4 : Triaxial Consolidation Test (CY100C48)

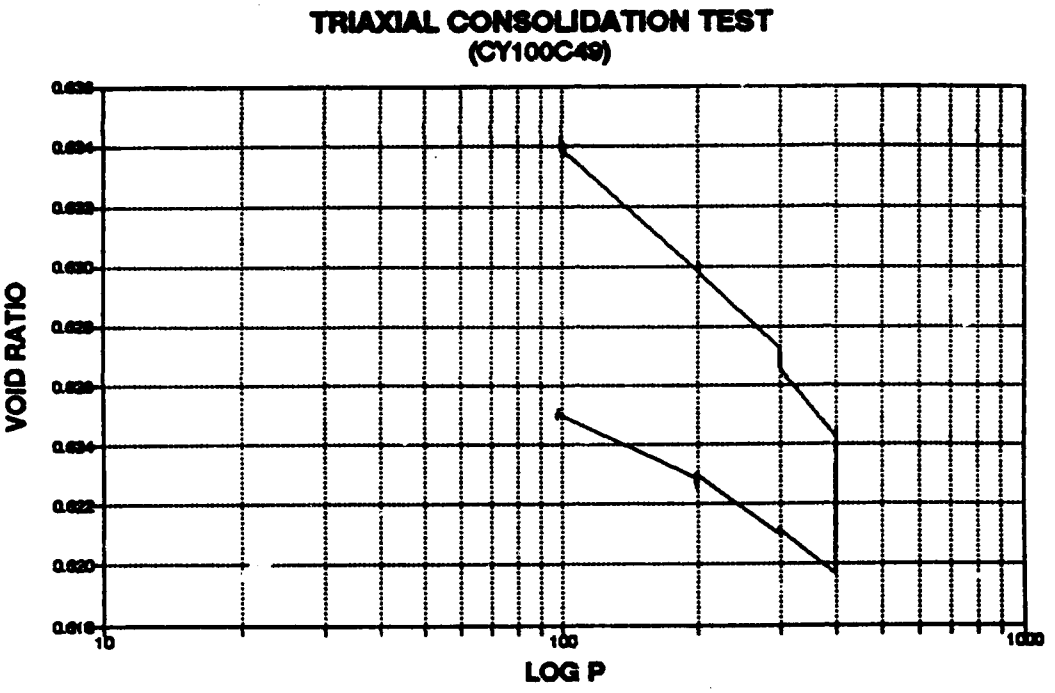

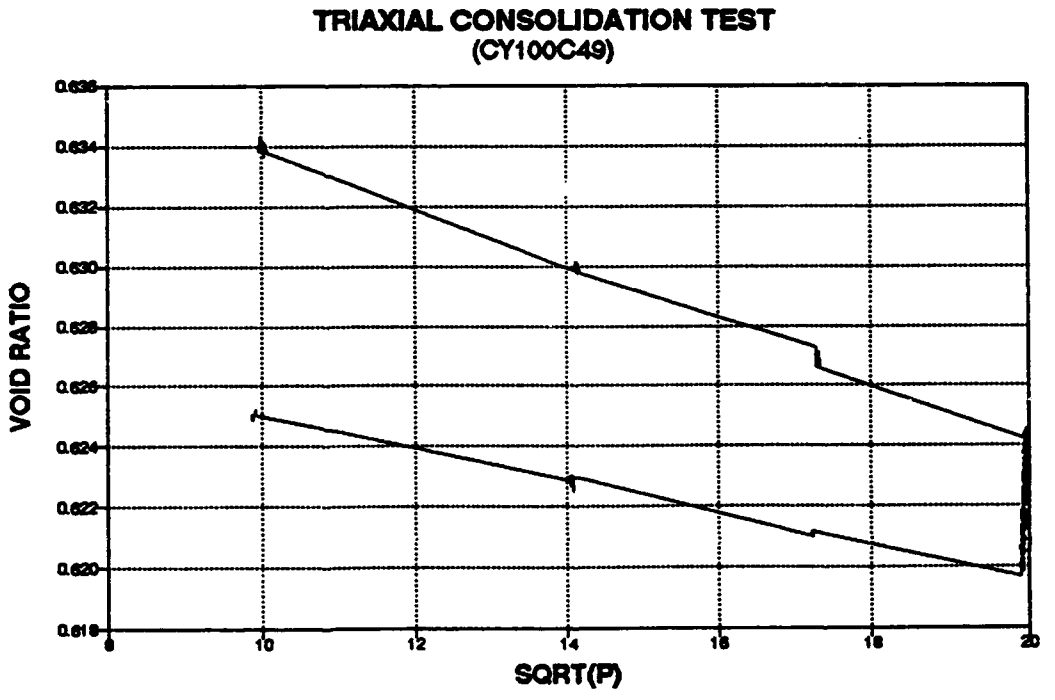

Figure 2.5.5 : Triaxial Consolidation Test (CY100C49)

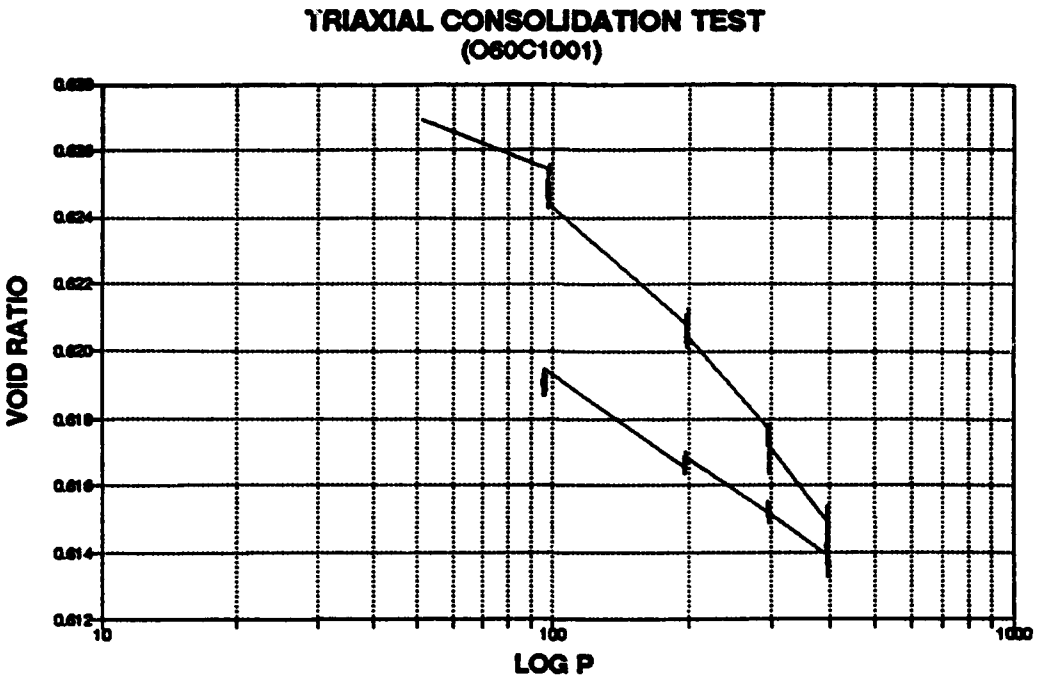

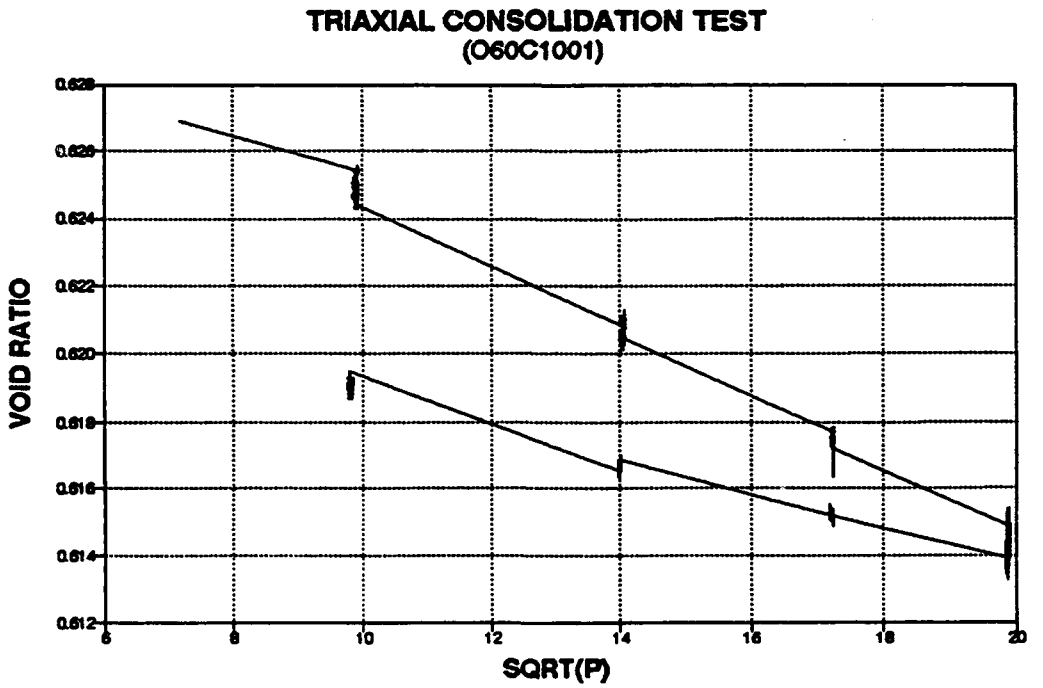

Figure 2.5.6 : Triaxial Consolidation Test (O60C1001)

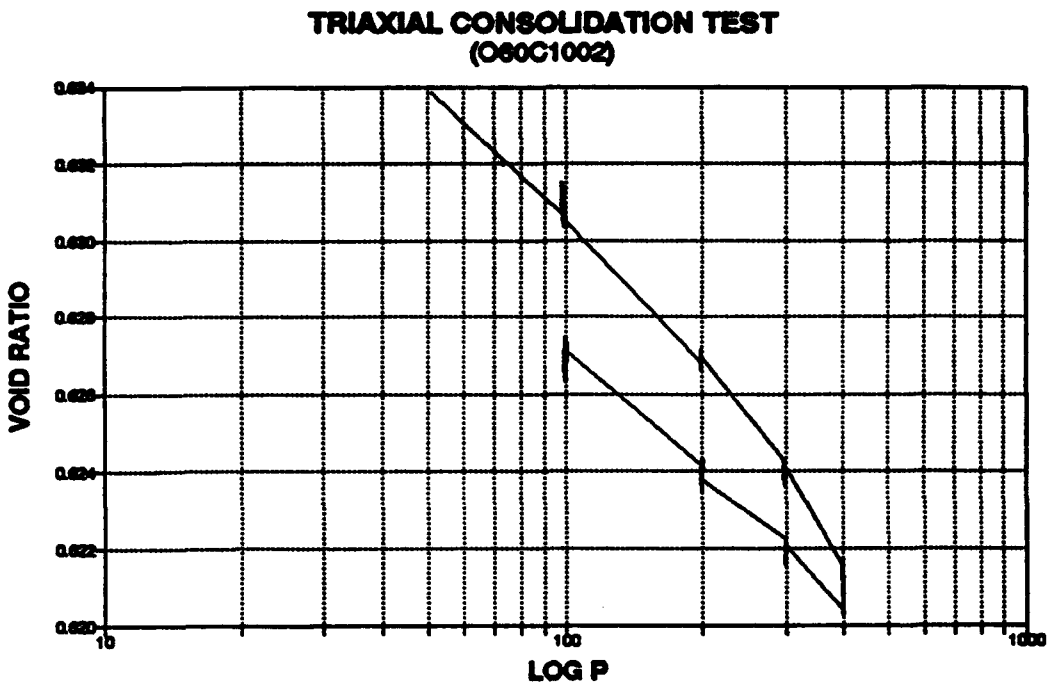

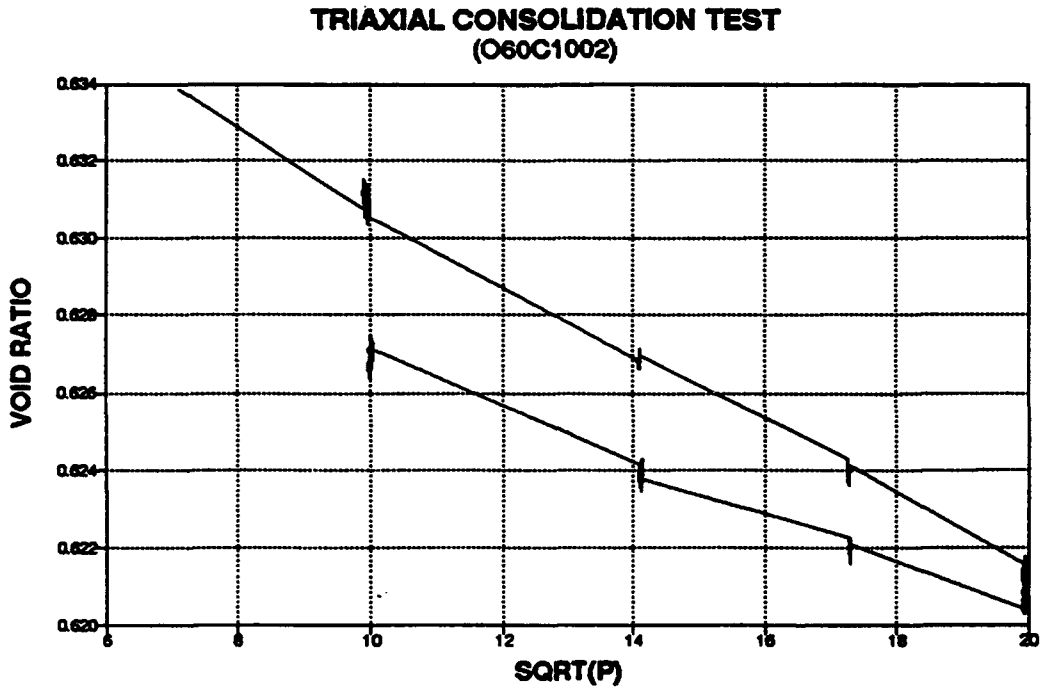

Figure 2.5.7 : Triaxial Consolidation Test (O60C1002)

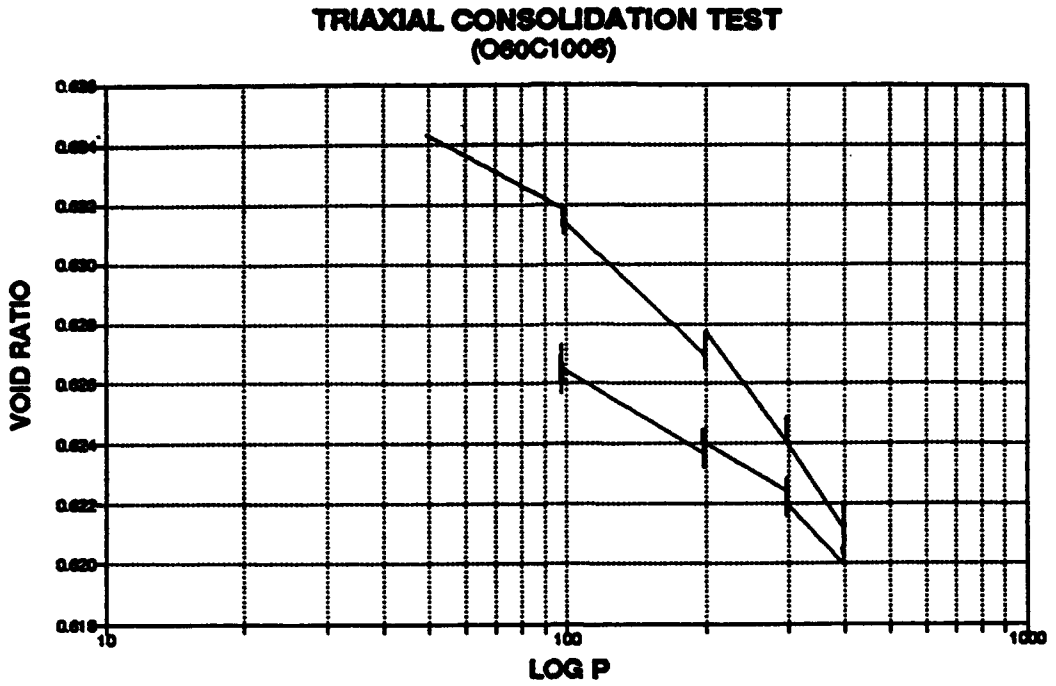

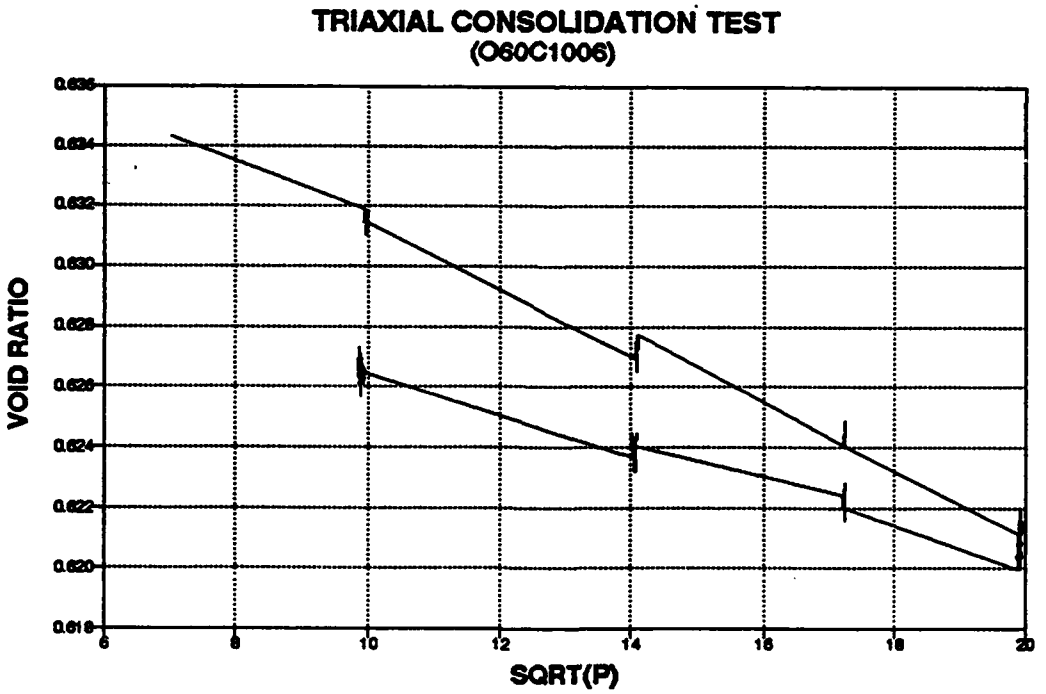

Figure 2.5.8 : Triaxial Consolidation Test (O60C1006)

TEST RESULTS
ON
UNDRAINED, STRESS CONTROLLED, TORSIONAL SHEAR TESTS

Figure 3.2.1 : Hollow Cylinder Cyclic Torsional Shear Test (NK41CU50)
Figure 3.2.2 : Hollow Cylinder Cyclic Torsional Shear Test (NK41CU50)
Figure 3.2.3 : Hollow Cylinder Cyclic Torsional Shear Test (NK41CU50)
Figure 3.2.4 : Hollow Cylinder Cyclic Torsional Shear Test (NK41CU50)
Figure 3.2.5 : Hollow Cylinder Cyclic Torsional Shear Test (NK41CU50)
Figure 3.2.6 : Hollow Cylinder Cyclic Torsional Shear Test (NK63CU50)
Figure 3.2.7 : Hollow Cylinder Cyclic Torsional Shear Test (NK63CU50)
Figure 3.2.8 : Hollow Cylinder Cyclic Torsional Shear Test (NK63CU50)
Figure 3.2.9 : Hollow Cylinder Cyclic Torsional Shear Test (NK63CU50)
Figure 3.2.10 : Hollow Cylinder Cyclic Torsional Shear Test (NK63CU50)
Figure 3.2.11 : Hollow Cylinder Cyclic Torsional Shear Test (NK10CU50)
Figure 3.2.12 : Hollow Cylinder Cyclic Torsional Shear Test (NK10CU50)
Figure 3.2.13 : Hollow Cylinder Cyclic Torsional Shear Test (NK10CU50)
Figure 3.2.14 : Hollow Cylinder Cyclic Torsional Shear Test (NK10CU50)
Figure 3.2.15 : Hollow Cylinder Cyclic Torsional Shear Test (NK10CU50)
Figure 3.2.16 : Hollow Cylinder Cyclic Torsional Shear Test (NK138U51)
Figure 3.2.17 : Hollow Cylinder Cyclic Torsional Shear Test (NK138U51)
Figure 3.2.18 : Hollow Cylinder Cyclic Torsional Shear Test (NK138U51)
Figure 3.2.19 : Hollow Cylinder Cyclic Torsional Shear Test (NK138U51)
Figure 3.2.20 : Hollow Cylinder Cyclic Torsional Shear Test (NK138U51)

NK41CU50 : UNDRAINED STRESS CONTROLLED TORSIONAL SHEAR TEST

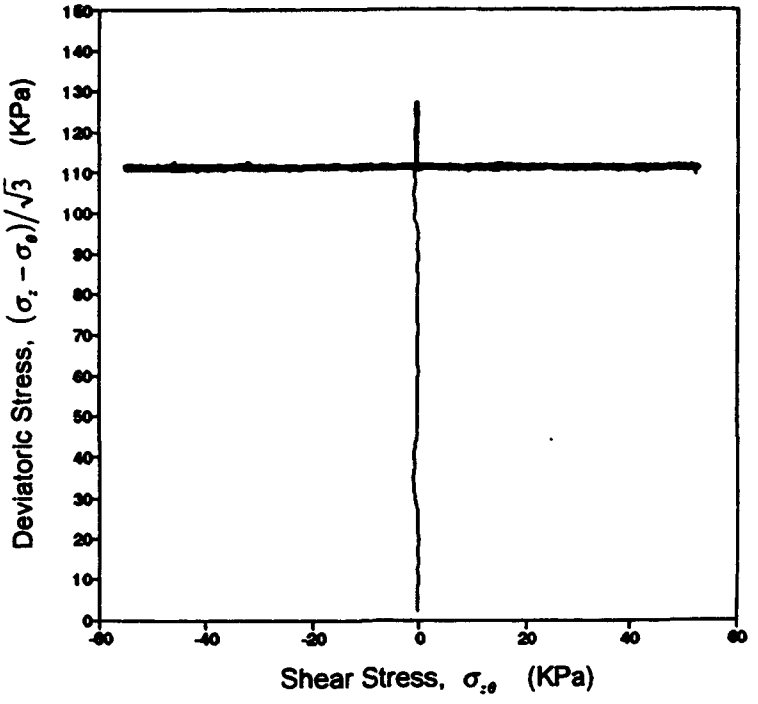

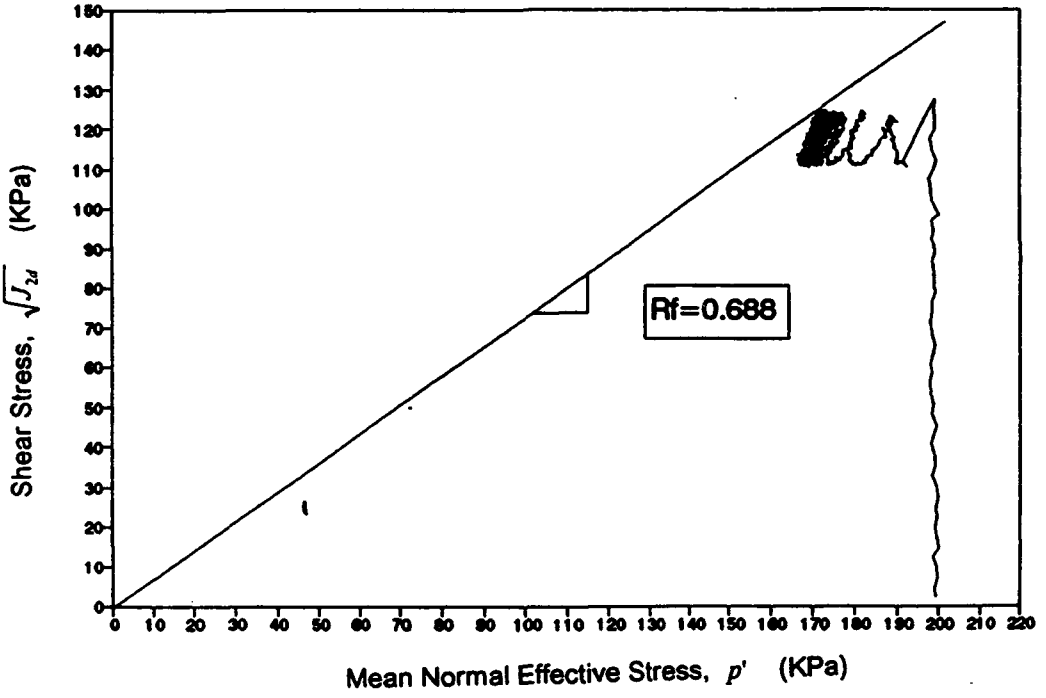

Figure 3.2.1 : Hollow Cylinder Cyclic Torsional Shear Test (NK41CU50)

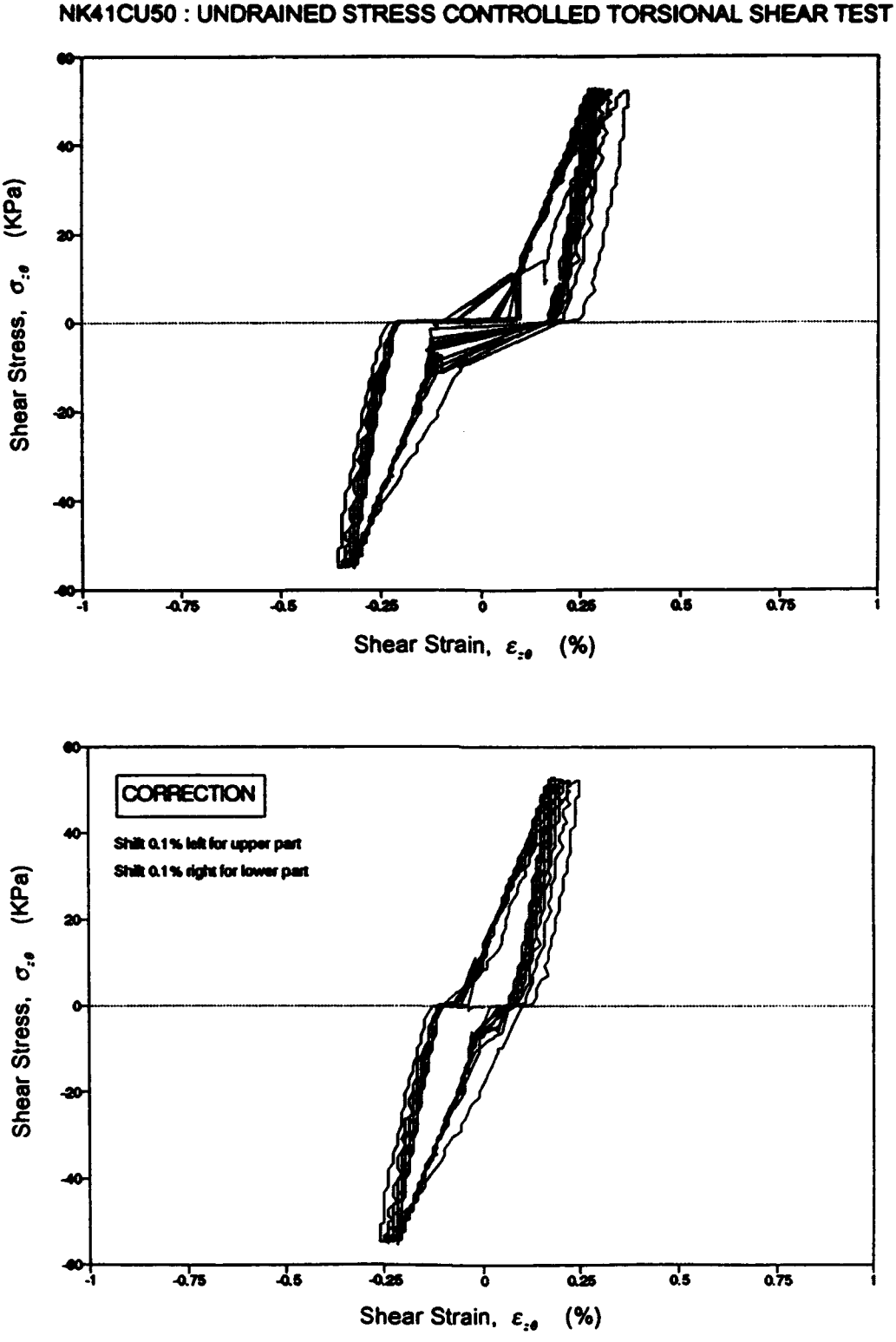

Figure 3.2.2 : Hollow Cylinder Cyclic Torsional Shear Test (NK41CU50)

NK41CU50 : UNDRAINED STRESS CONTROLLED TORSIONAL SHEAR TEST

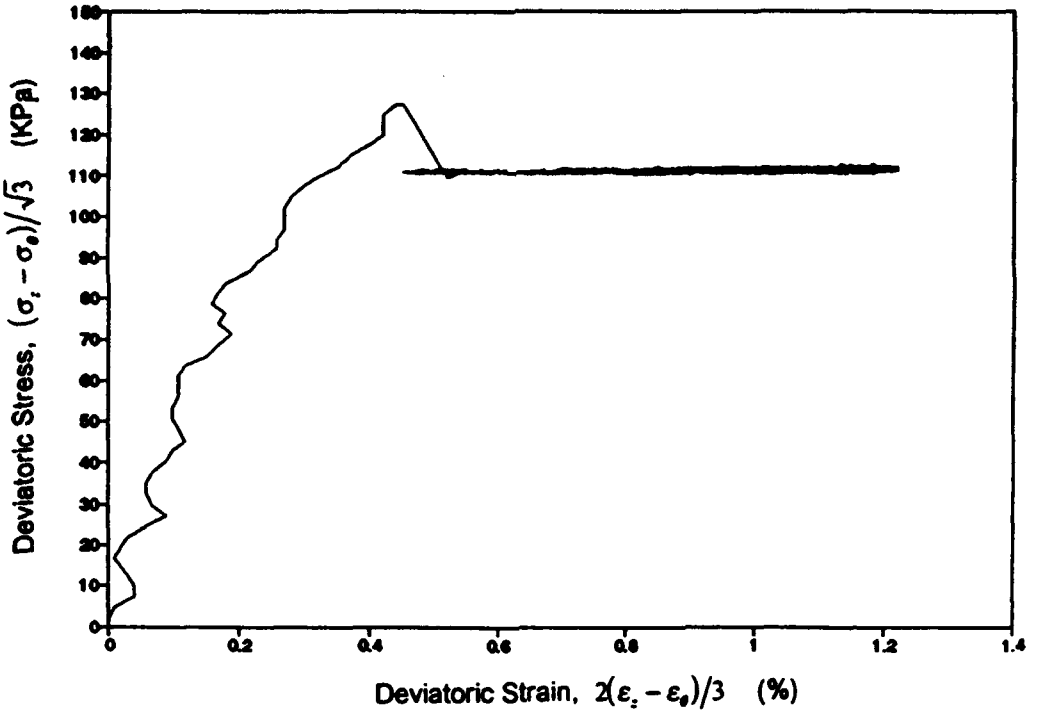

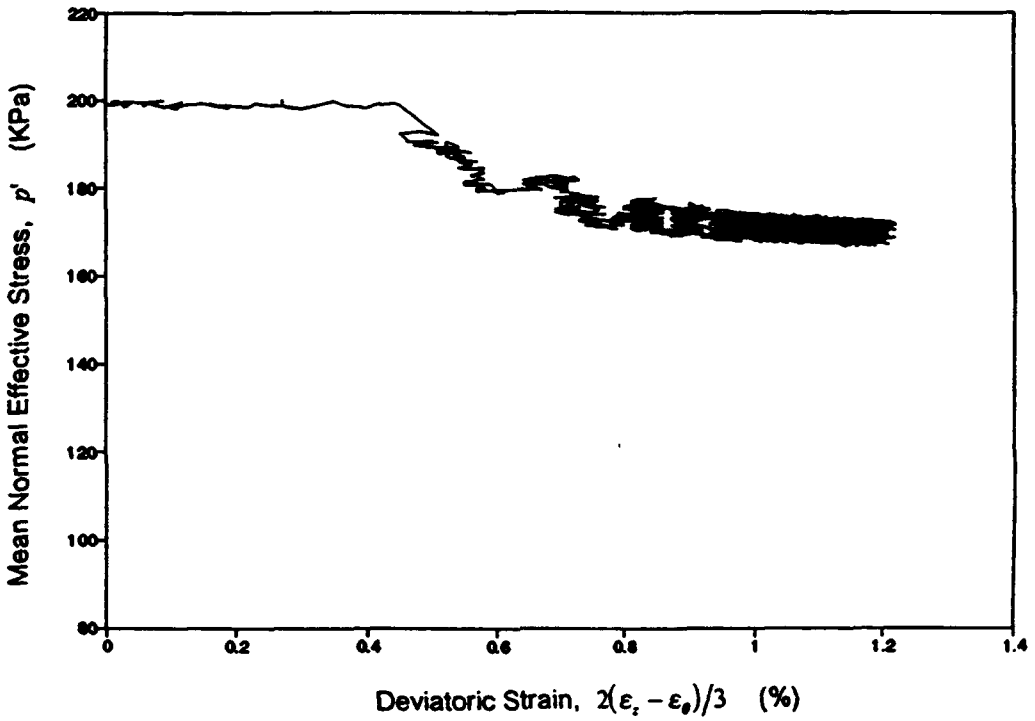

Figure 3.2.3 : Hollow Cylinder Cyclic Torsional Shear Test (NK41CU50)

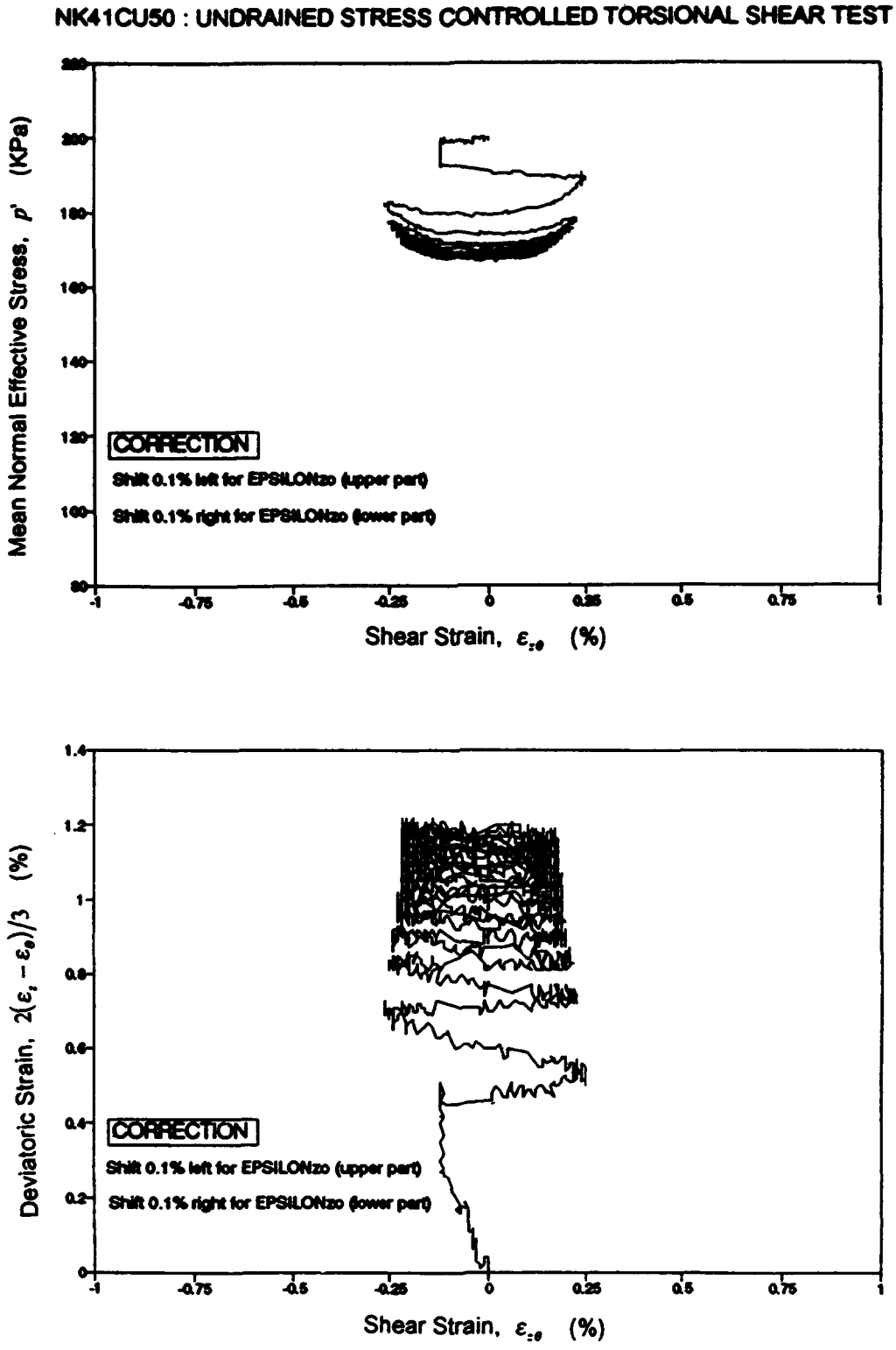

Figure 3.2.4 : Hollow Cylinder Cyclic Torsional Shear Test (NK41CU50)

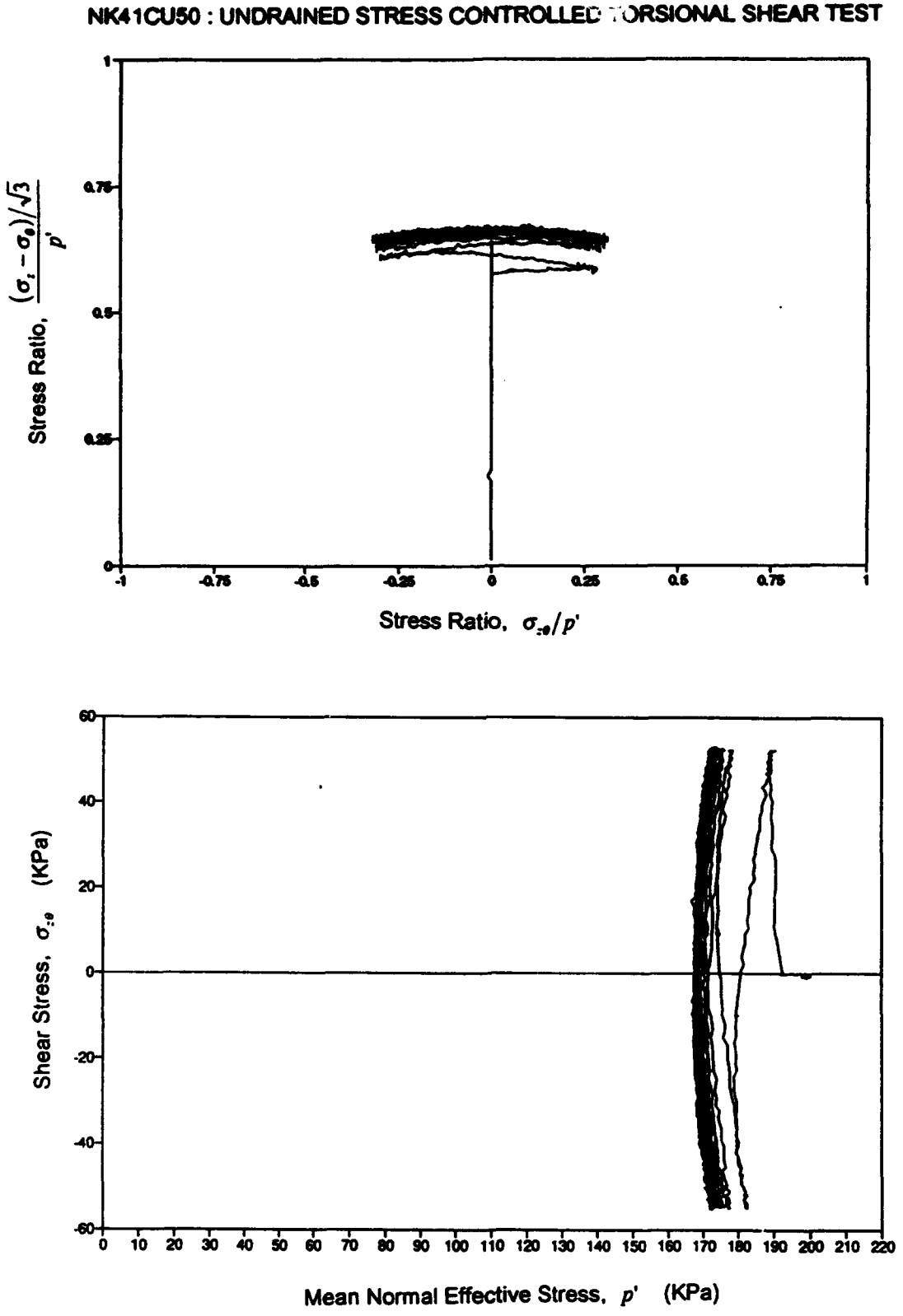

Figure 3.2.5 : Hollow Cylinder Cyclic Torsional Shear Test (NK41CU50)

NK63CU50 : UNDRAINED STRESS CONTROLLED TORSIONAL SHEAR TEST

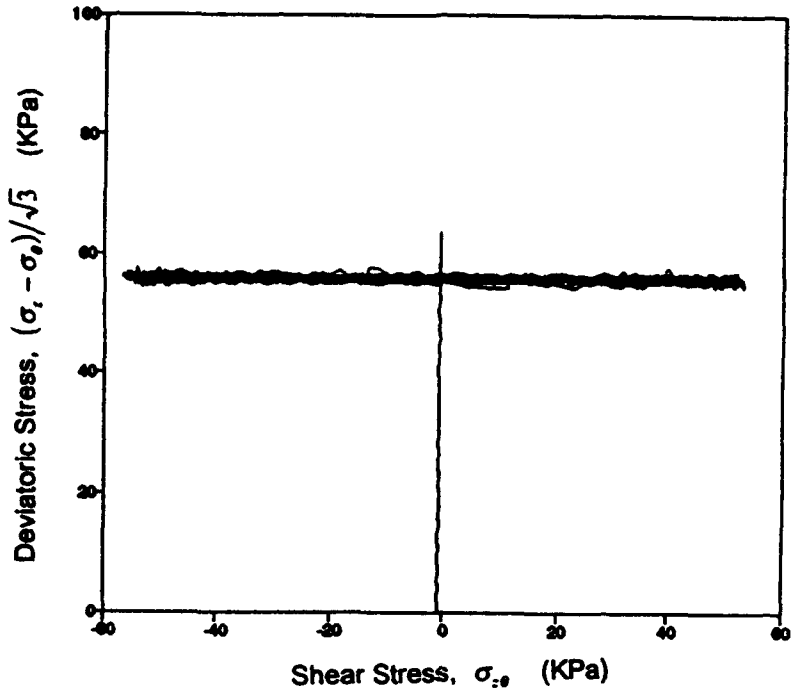

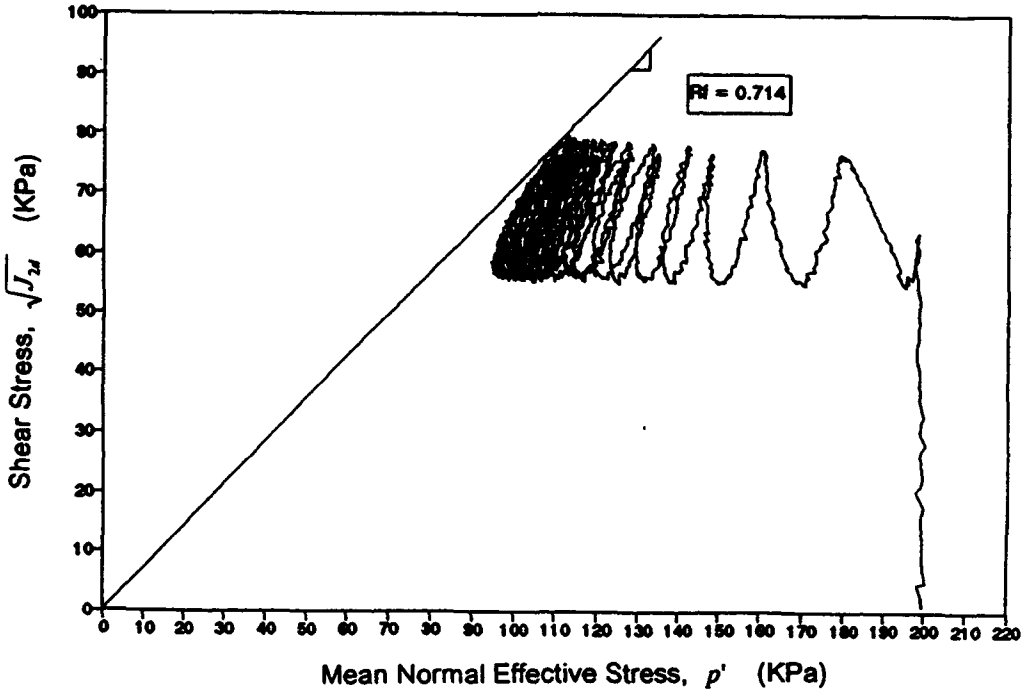

Figure 3.2.6 : Hollow Cylinder Cyclic Torsional Shear Test (NK63CU50)

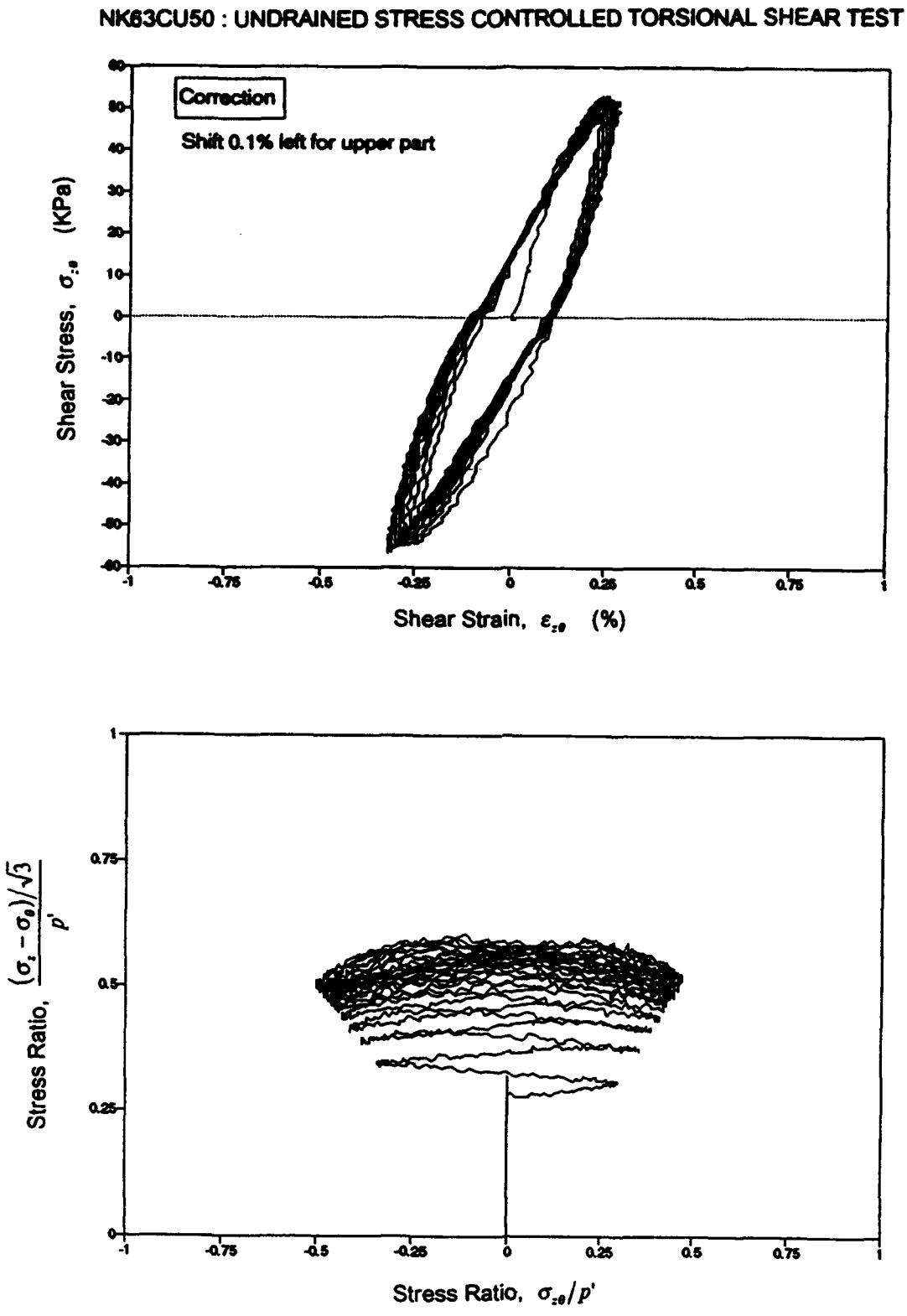

Figure 3.2.7 : Hollow Cylinder Cyclic Torsional Shear Test (NK63CU50)

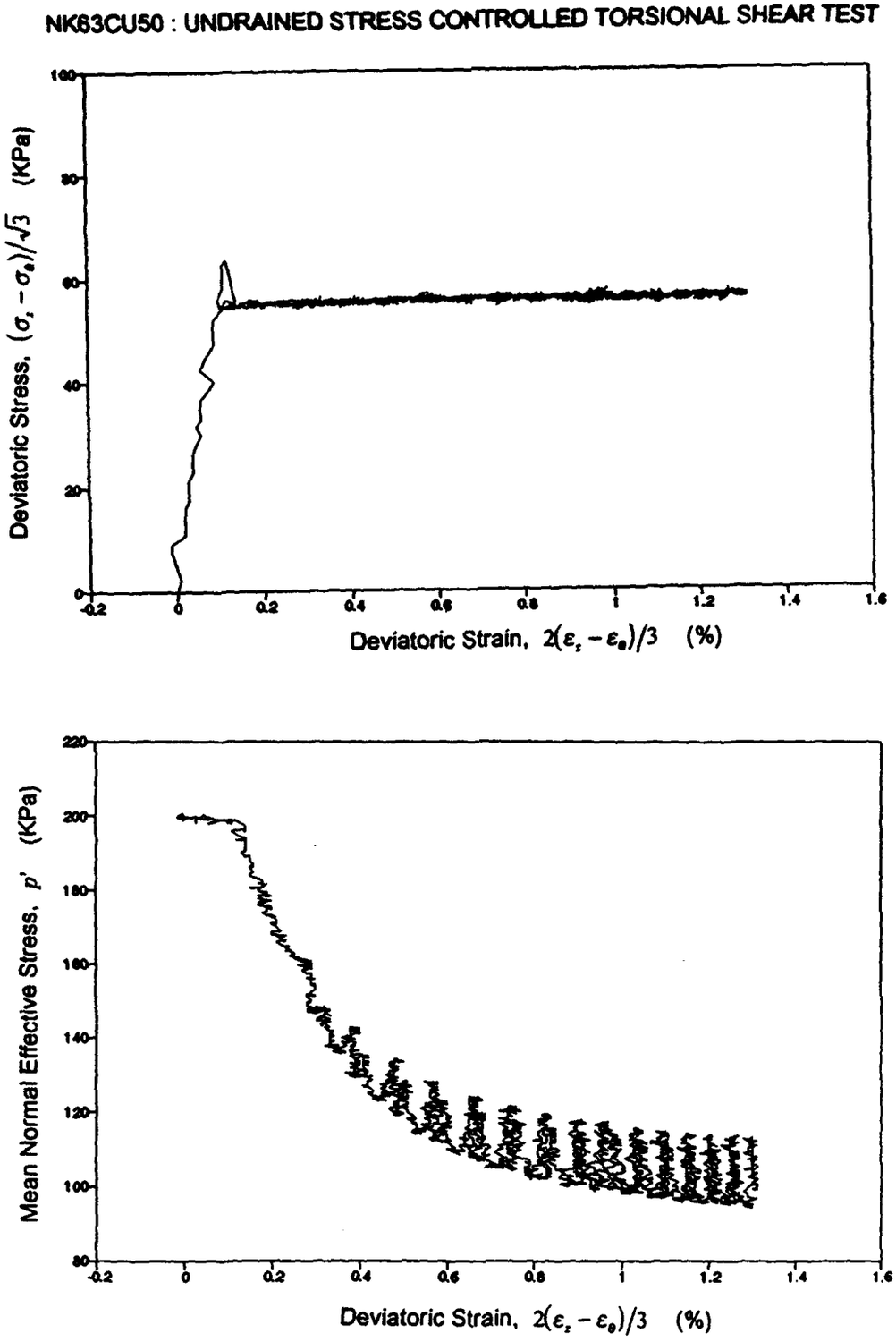

Figure 3.2.8 : Hollow Cylinder Cyclic Torsional Shear Test (NK63CU50)

NK63CU50 : UNDRAINED STRESS CONTROLLED TORSIONAL SHEAR TEST

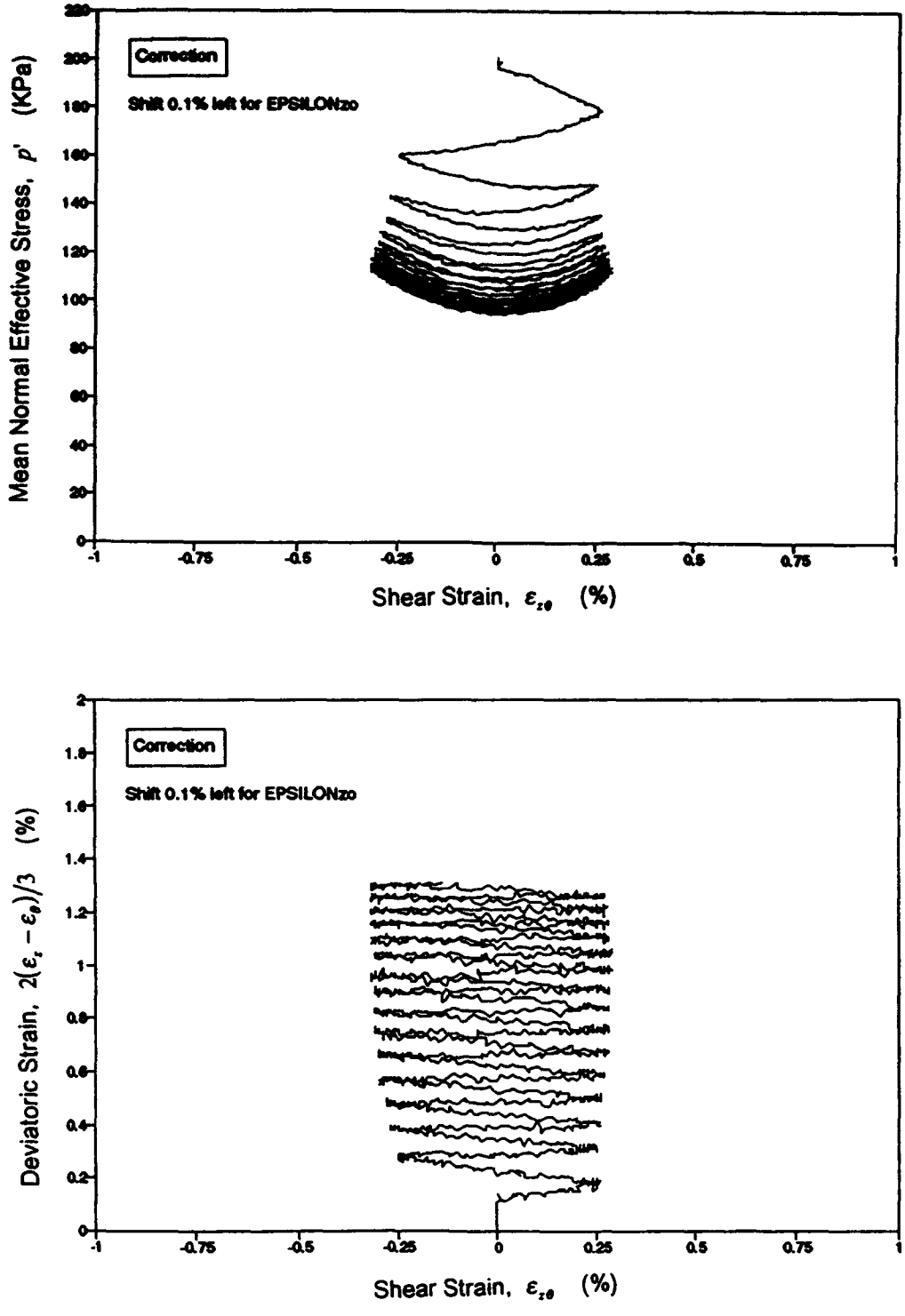

Figure 3.2.9 : Hollow Cylinder Cyclic Torsional Shear Test (NK63CU50)

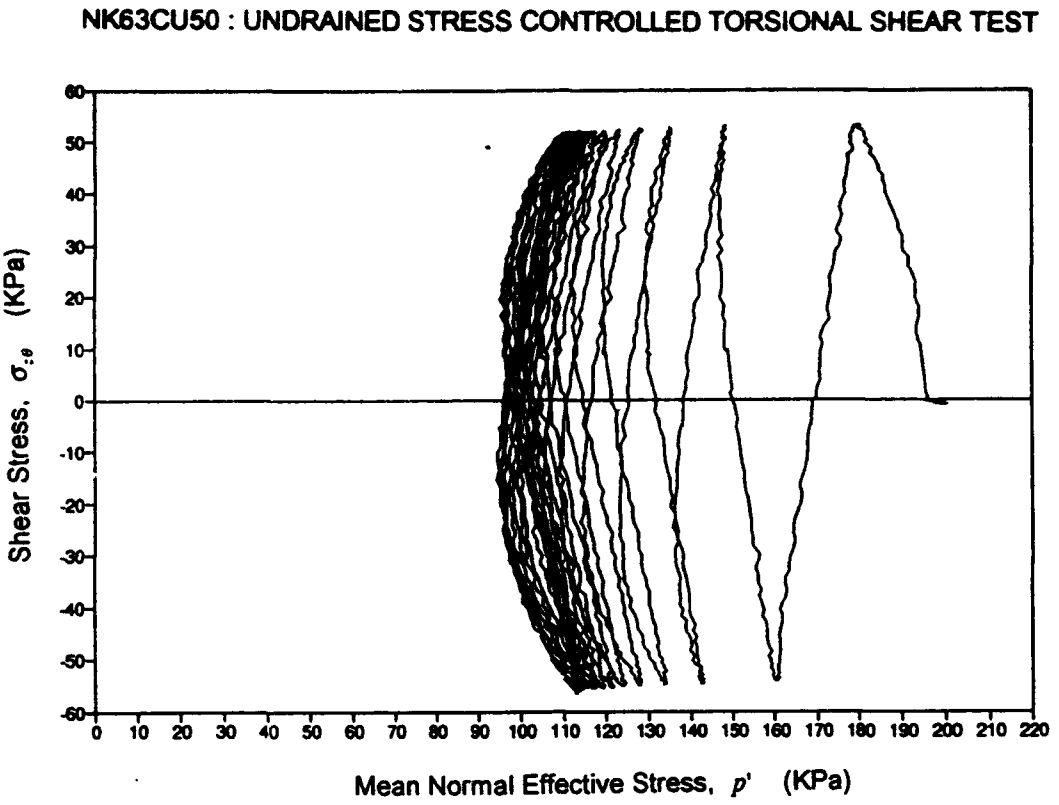

Figure 3.2.10 : Hollow Cylinder Cyclic Torsional Shear Test (NK63CU50)

NK10CU50 : UNDRAINED STRESS CONTROLLED TORSIONAL SHEAR TEST

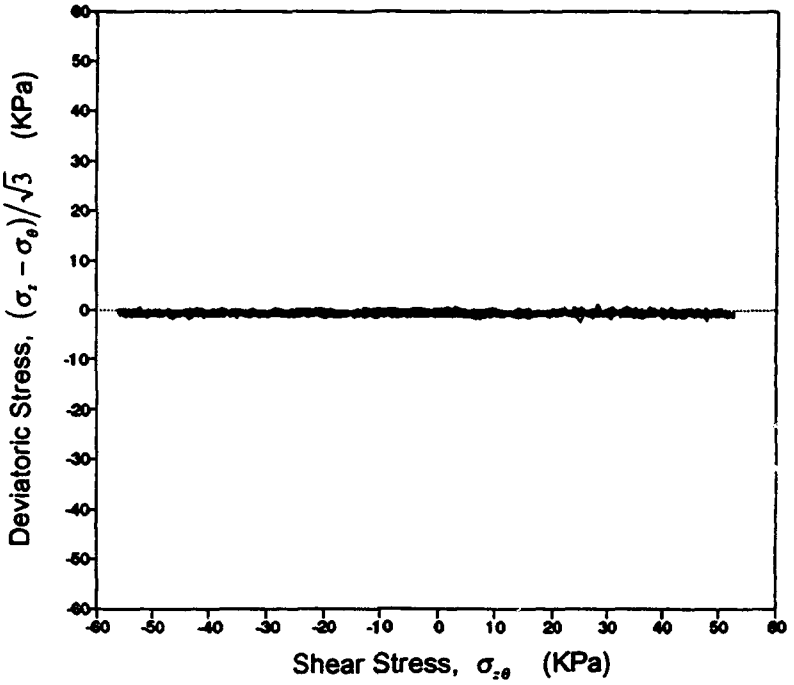

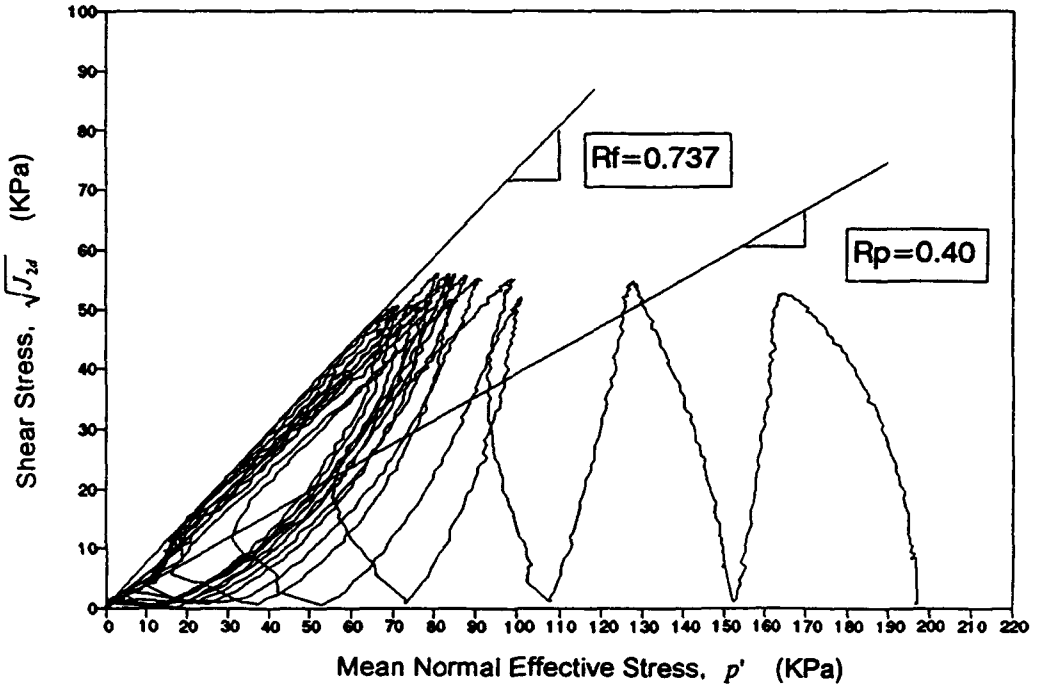

Figure 3.2.11 : Hollow Cylinder Cyclic Torsional Shear Test (NK10CU50)

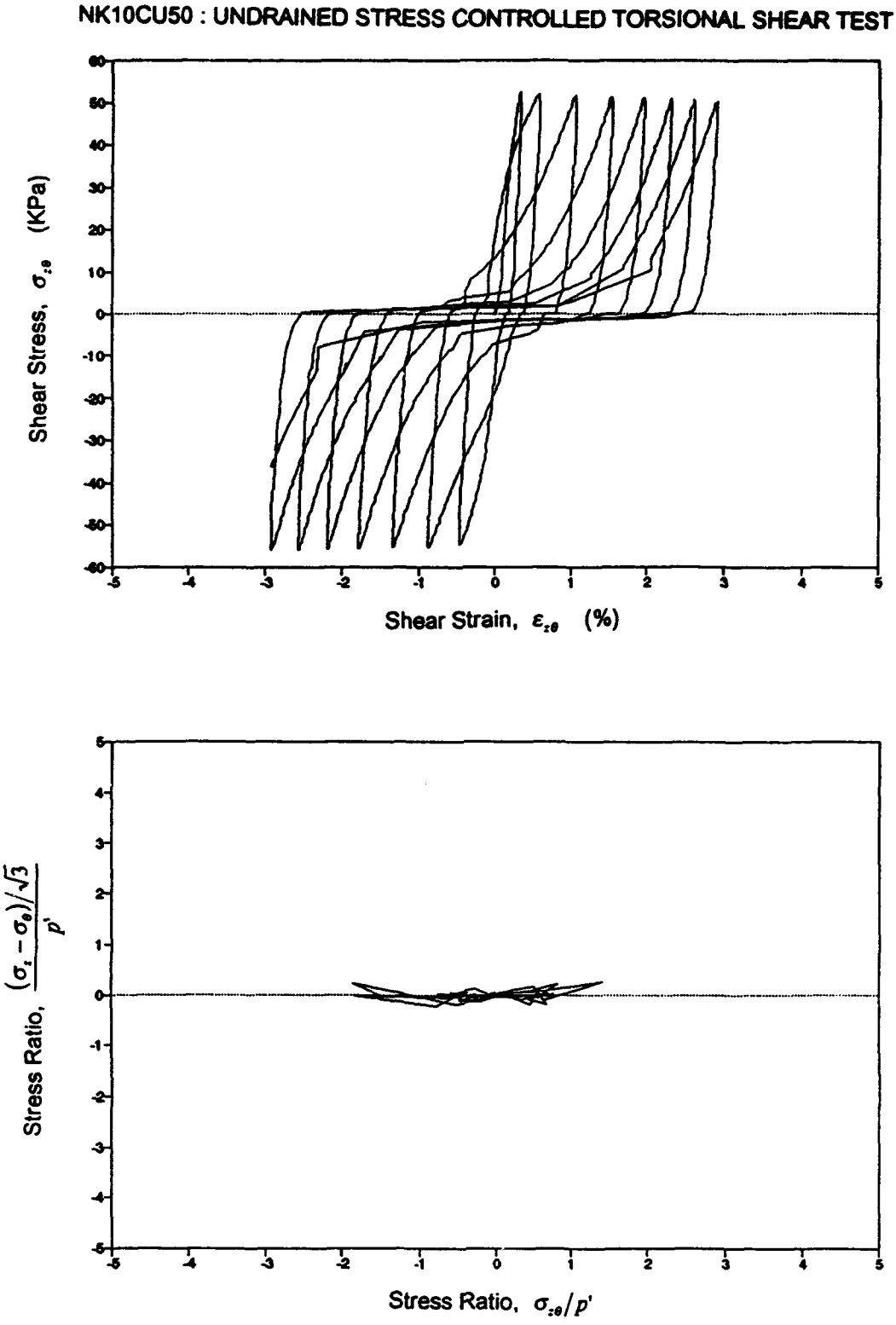

Figure 3.2.12 : Hollow Cylinder Cyclic Torsional Shear Test (NK10CU50)

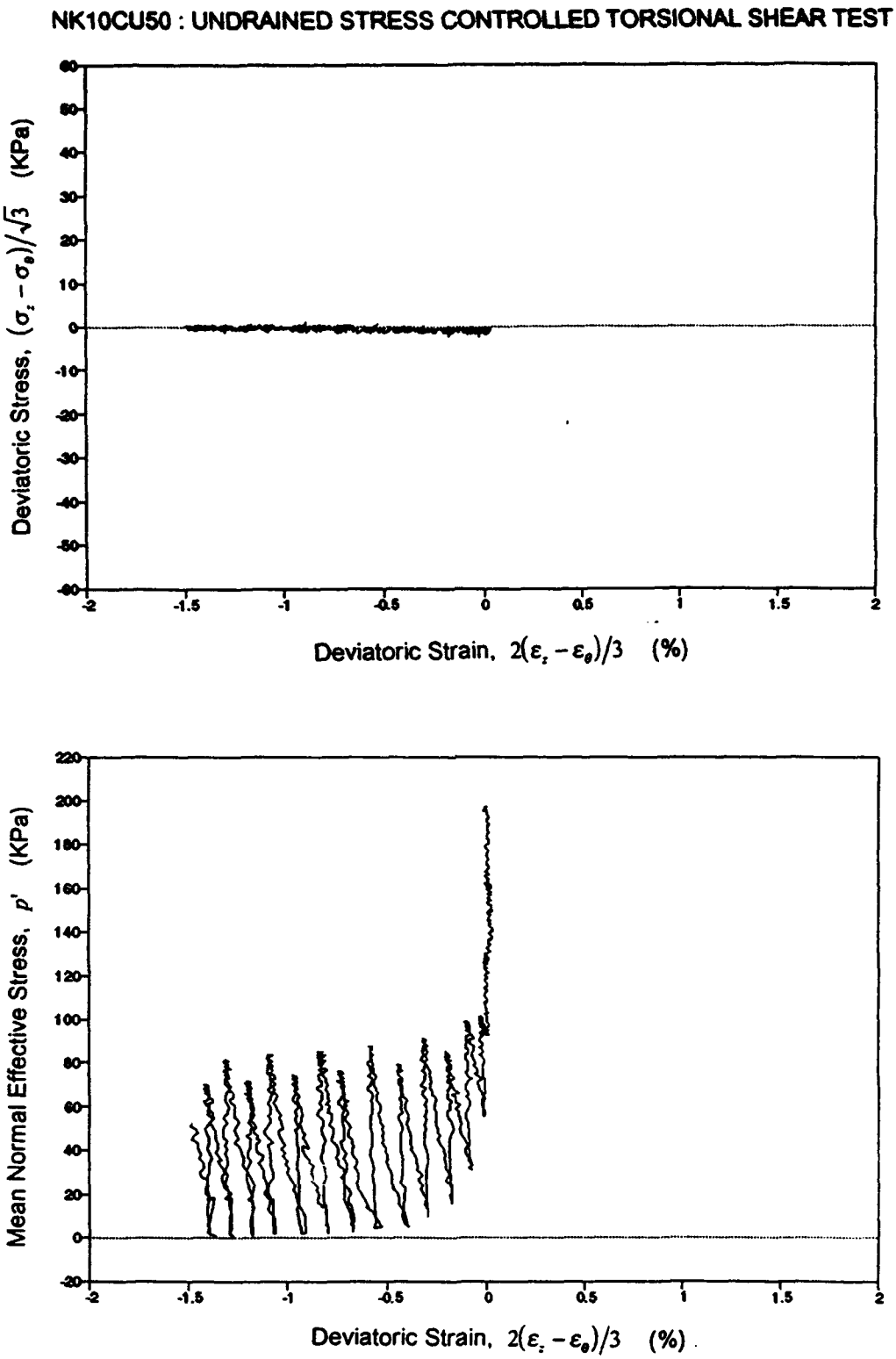

Figure 3.2.13 : Hollow Cylinder Cyclic Torsional Shear Test (NK10CU50)

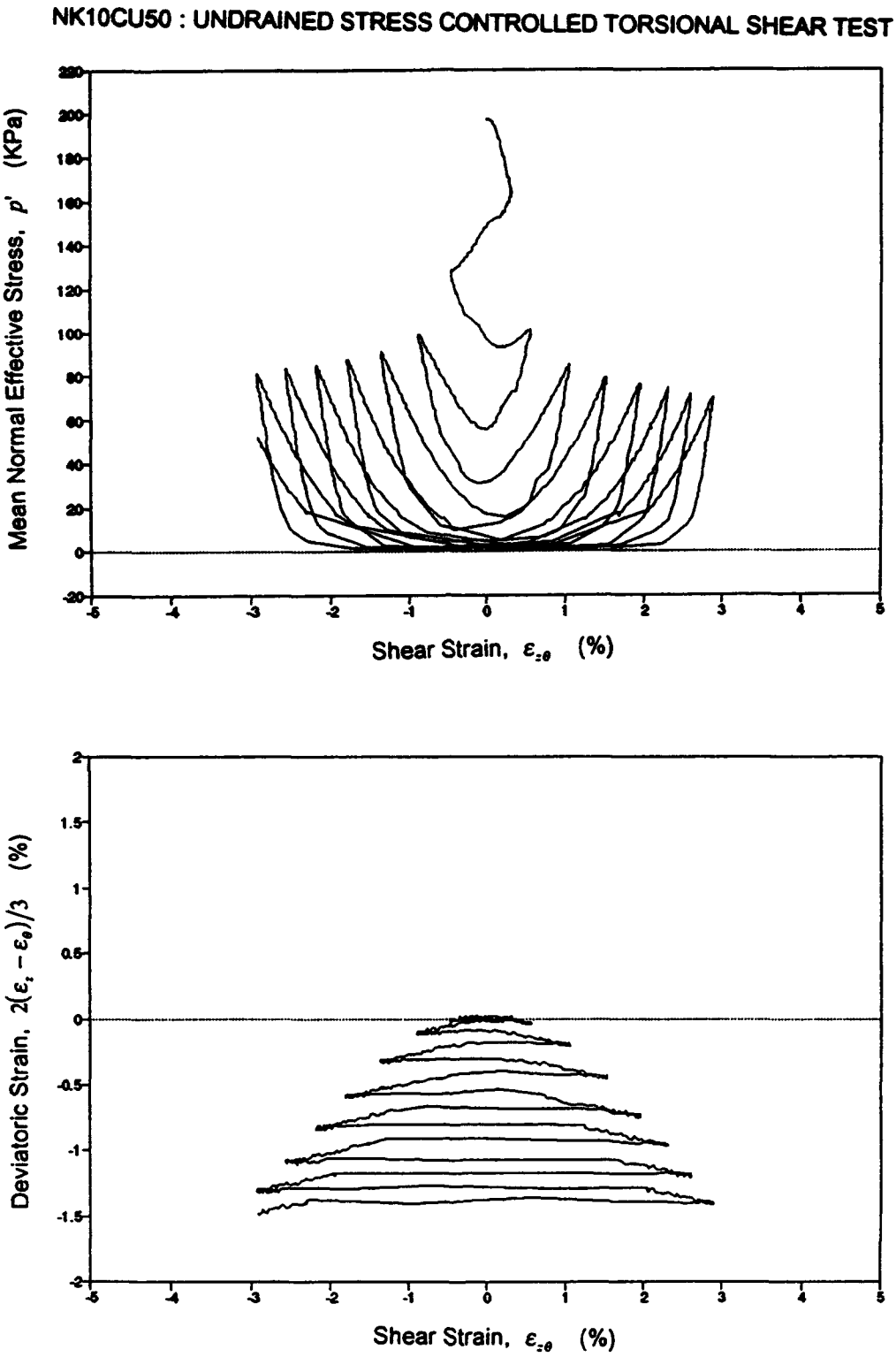

Figure 3.2.14 : Hollow Cylinder Cyclic Torsional Shear Test (NK10CU50)

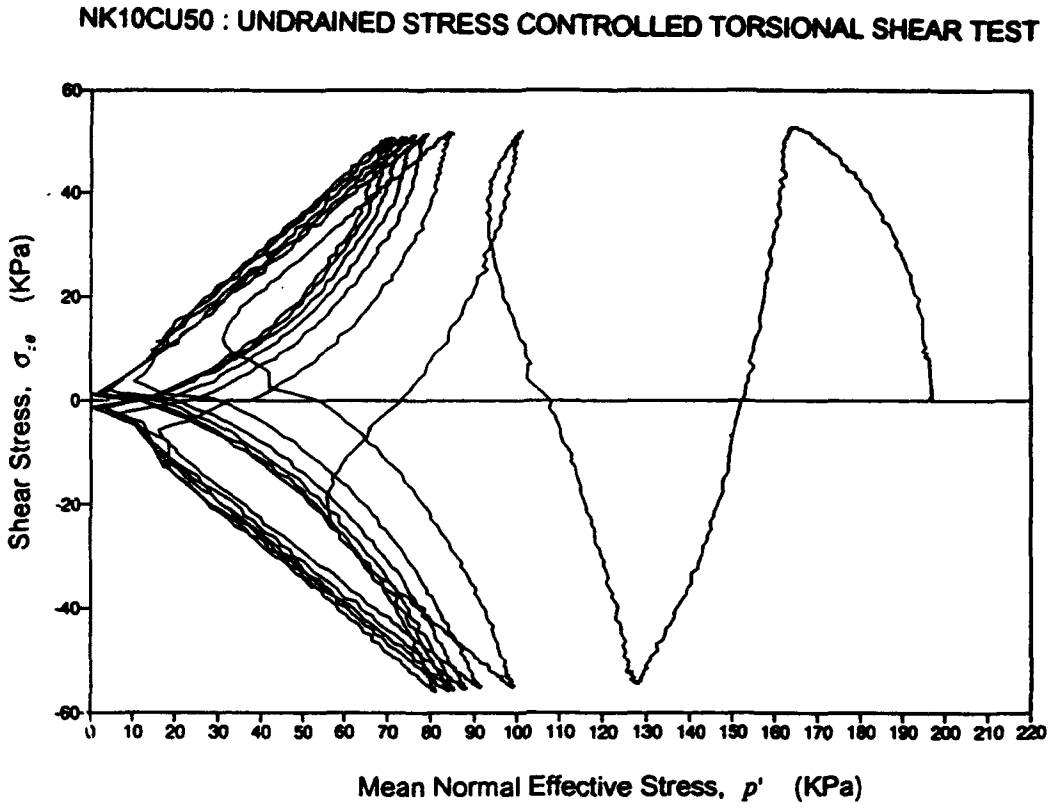

Figure 3.2.15 : Hollow Cylinder Cyclic Torsional Shear Test (NK10CU50)

NK138U51 : UNDRAINED STRESS CONTROLLED TORSIONAL SHEAR TEST

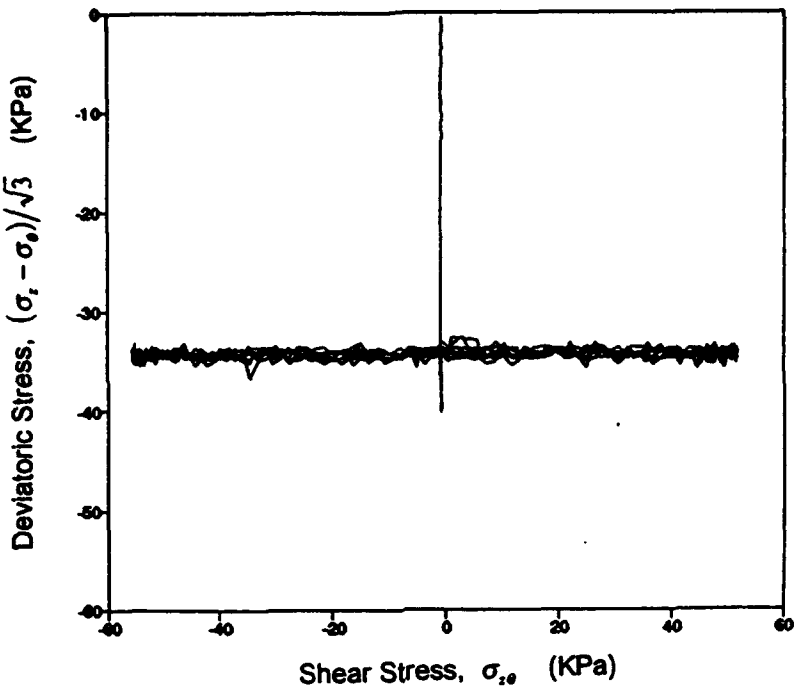

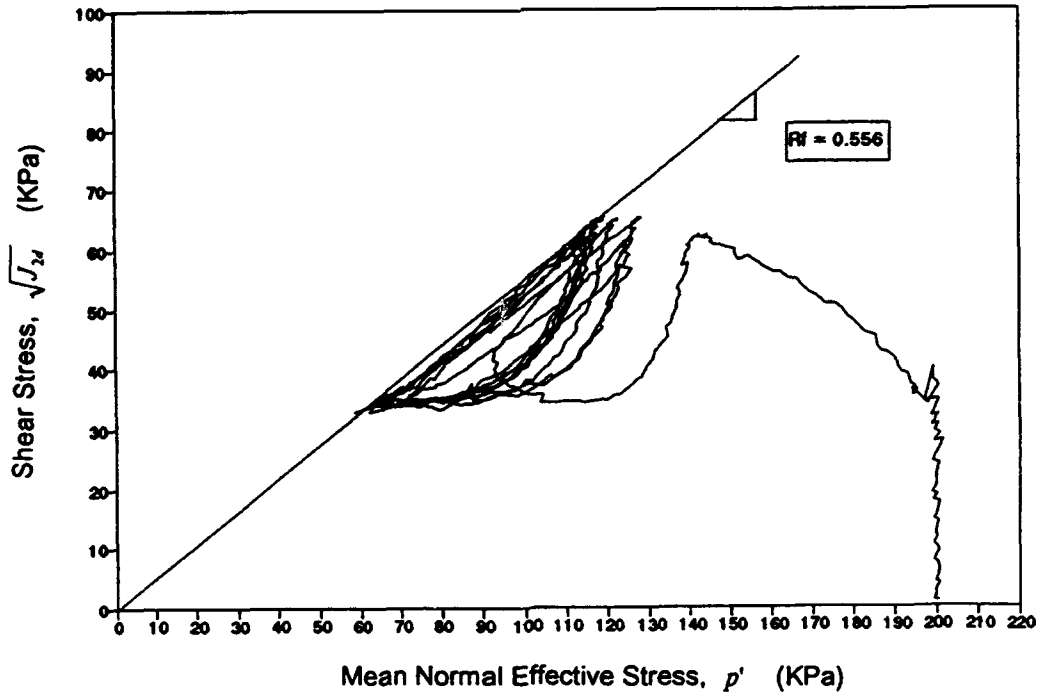

Figure 3.2.16 : Hollow Cylinder Cyclic Torsional Shear Test (NK138U51)

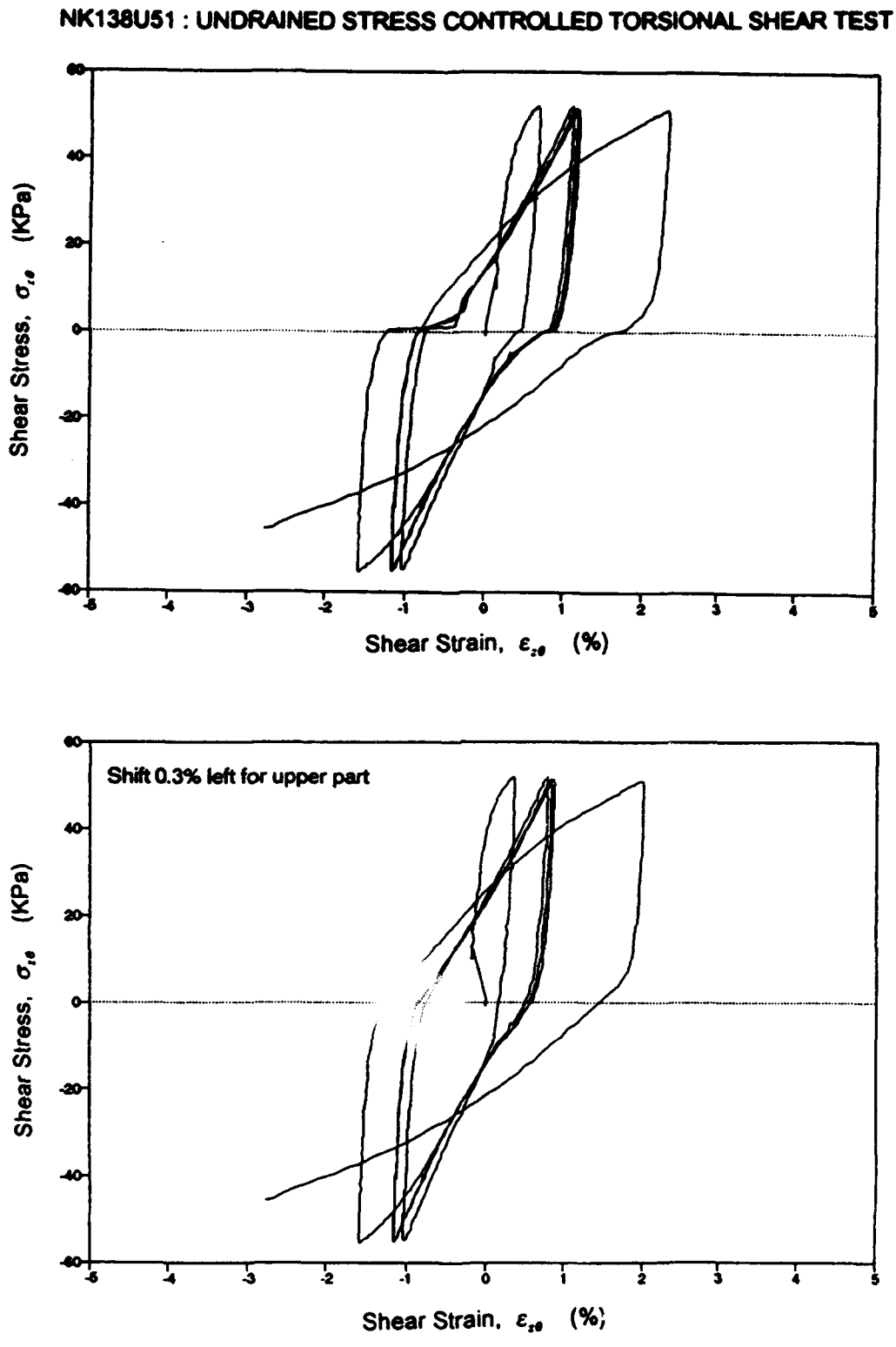

Figure 3.2.17 : Hollow Cylinder Cyclic Torsional Shear Test (NK138U51)

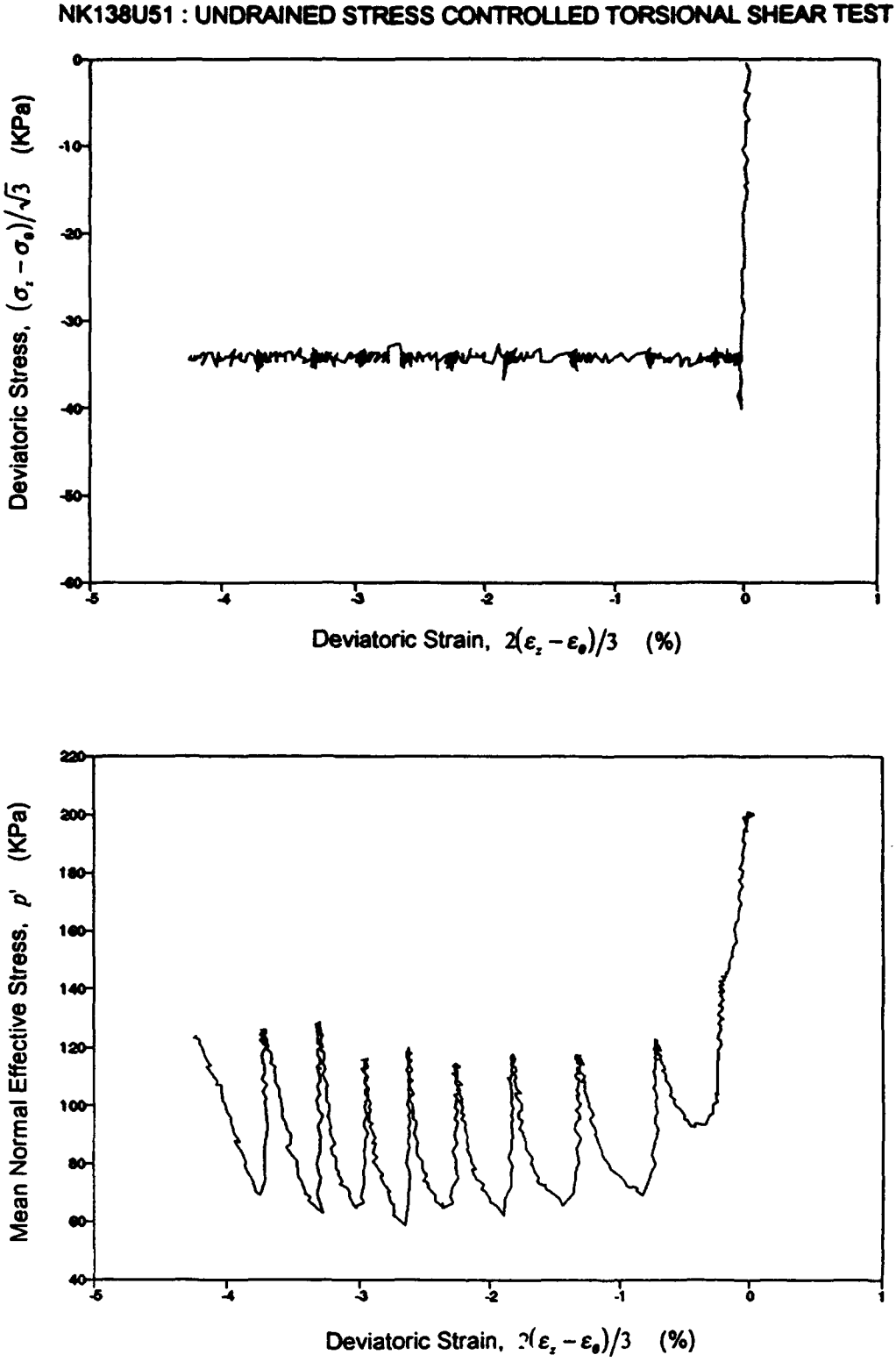

Figure 3.2.18 : Hollow Cylinder Cyclic Torsional Shear Test (NK138U51)

NK138U51 : UNDRAINED STRESS CONTROLLED TORSIONAL SHEAR TEST

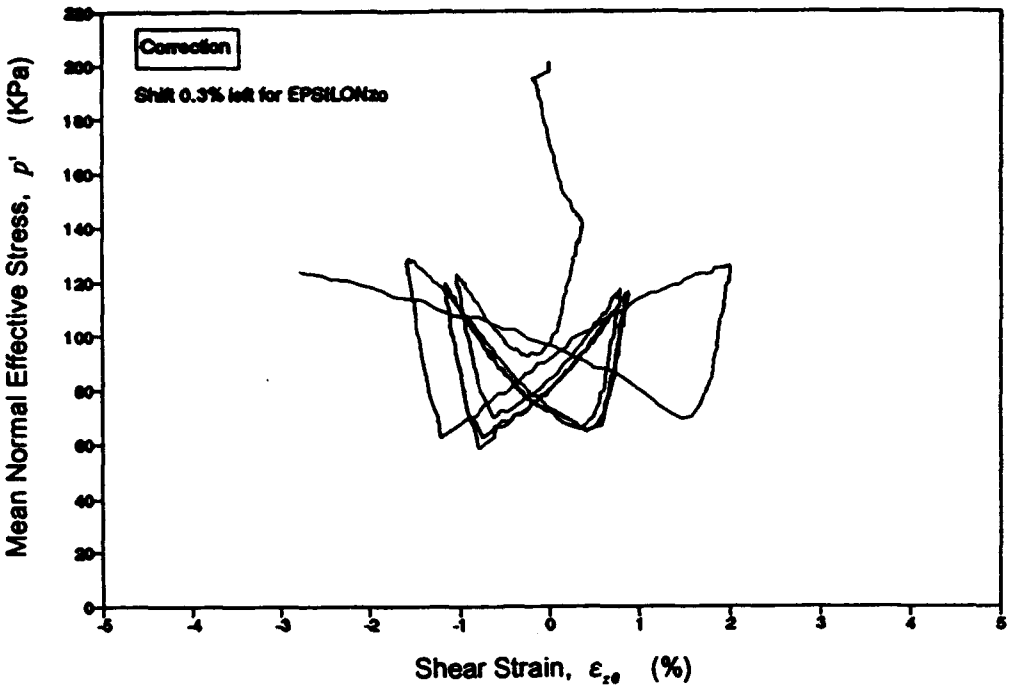

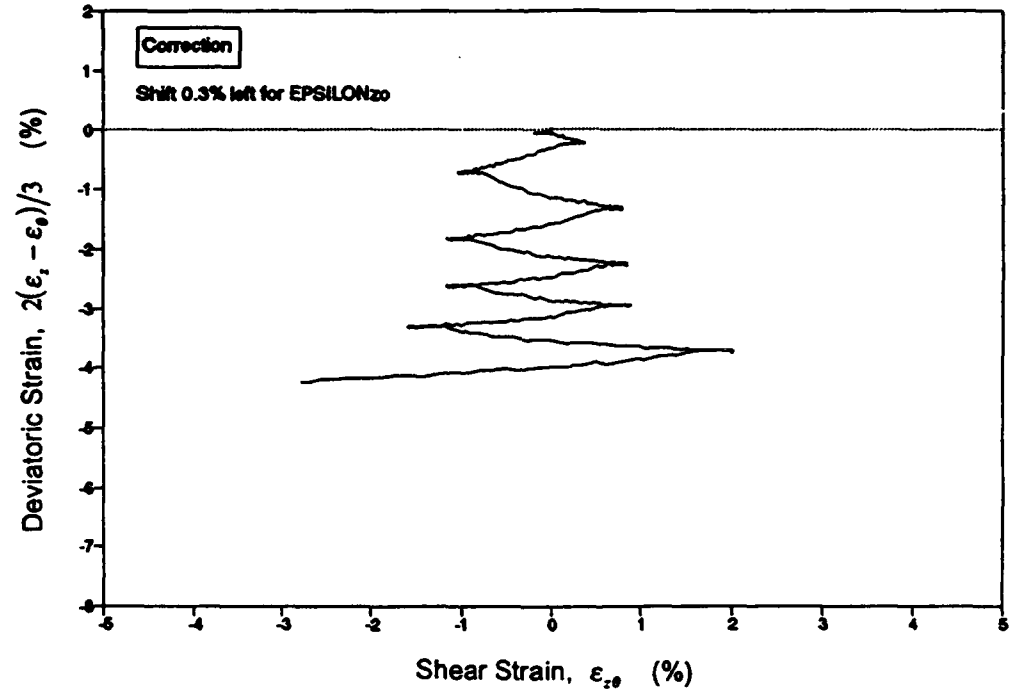

Figure 3.2.19 : Hollow Cylinder Cyclic Torsional Shear Test (NK138U51)

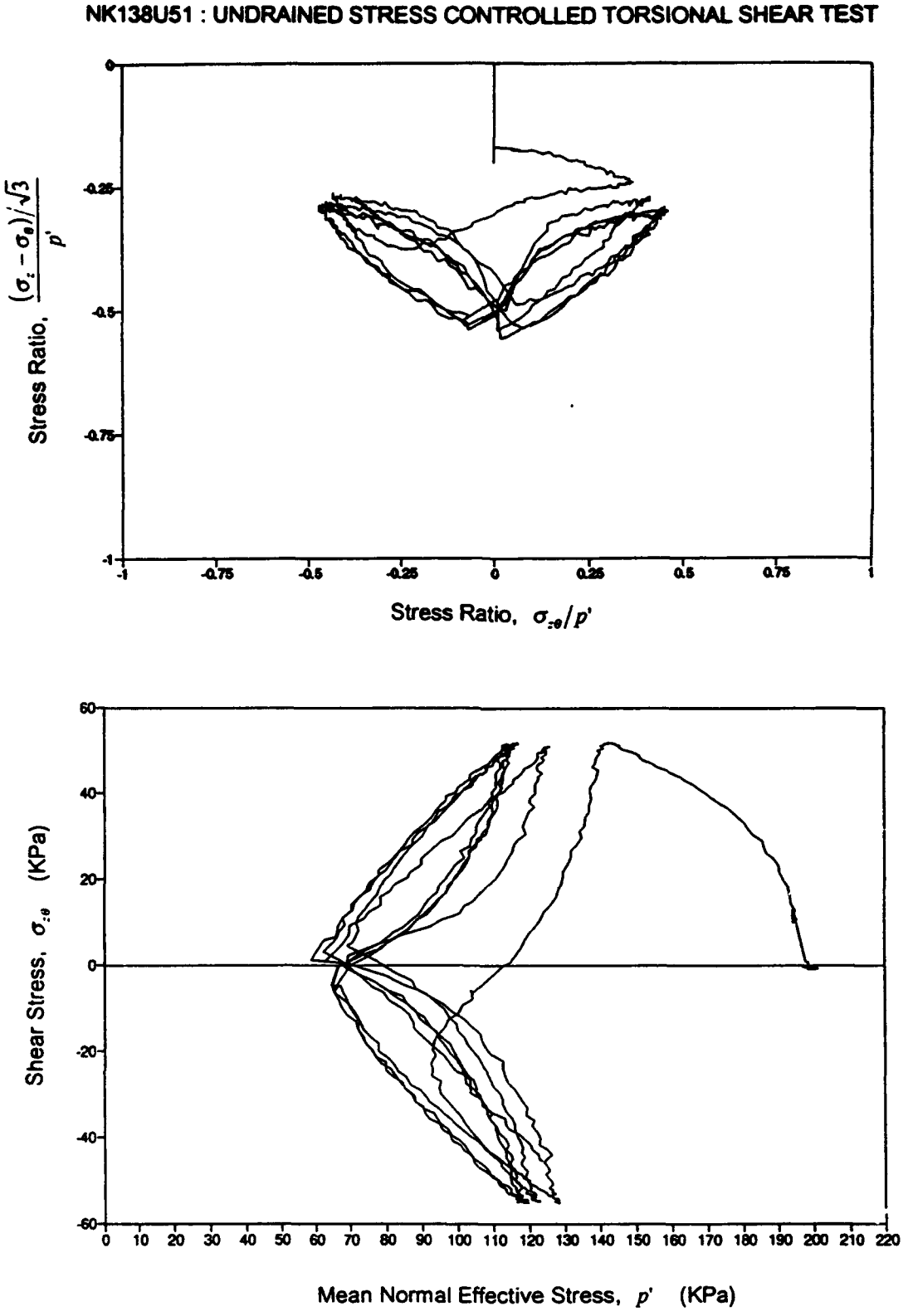

Figure 3.2.20 : Hollow Cylinder Cyclic Torsional Shear Test (NK138U51)

TEST RESULTS
ON
UNDRAINED, STRESS CONTROLLED, ROTATIONAL SHEAR TESTS

Figure 3.3.1 : Hollow Cylinder Rotational Shear Test (NR40CU50)
Figure 3.3.2 : Hollow Cylinder Rotational Shear Test (NR40CU50)
Figure 3.3.3 : Hollow Cylinder Rotational Shear Test (NR40CU50)
Figure 3.3.4 : Hollow Cylinder Rotational Shear Test (NR40CU50)
Figure 3.3.5 : Hollow Cylinder Rotational Shear Test (NR40CU50)
Figure 3.3.6 : Hollow Cylinder Rotational Shear Test (NR56CU50)
Figure 3.3.7 : Hollow Cylinder Rotational Shear Test (NR56CU50)
Figure 3.3.8 : Hollow Cylinder Rotational Shear Test (NR56CU50)
Figure 3.3.9 : Hollow Cylinder Rotational Shear Test (NR56CU50)
Figure 3.3.10 : Hollow Cylinder Rotational Shear Test (NR56CU50)

NR40CU50 : UNDRAINED STRESS CONTROLLED ROTATIONAL SHEAR TEST

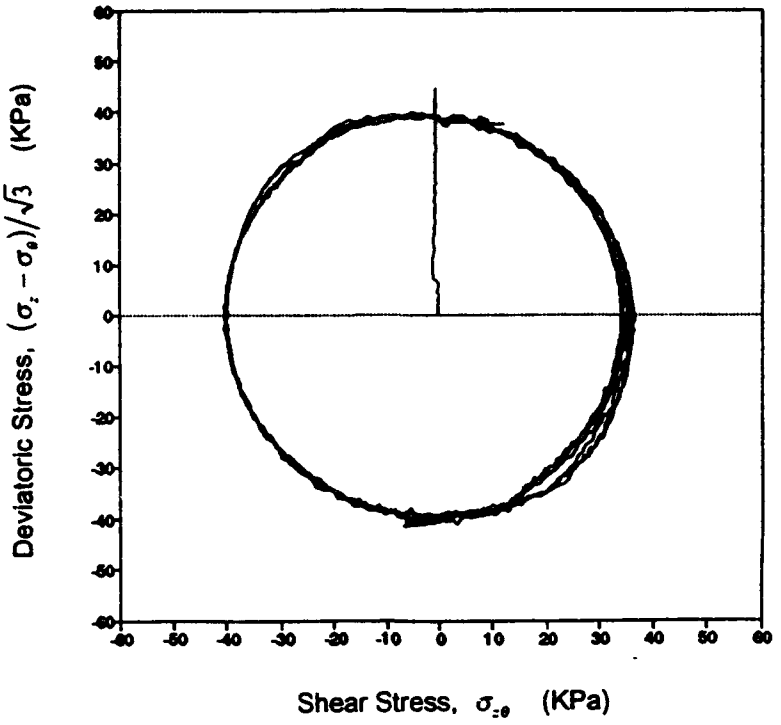

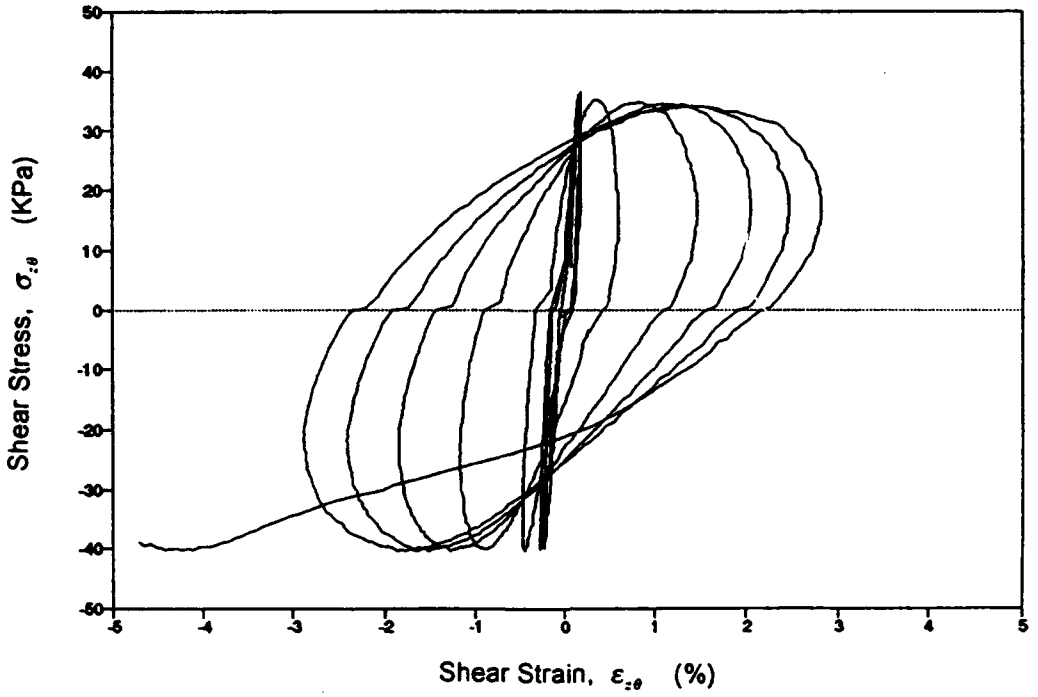

Figure 3.3.1 : Hollow Cylinder Rotational Shear Test (NR40CU50)

NR40CU50 : UNDRAINED STRESS CONTROLLED ROTATIONAL SHEAR TEST

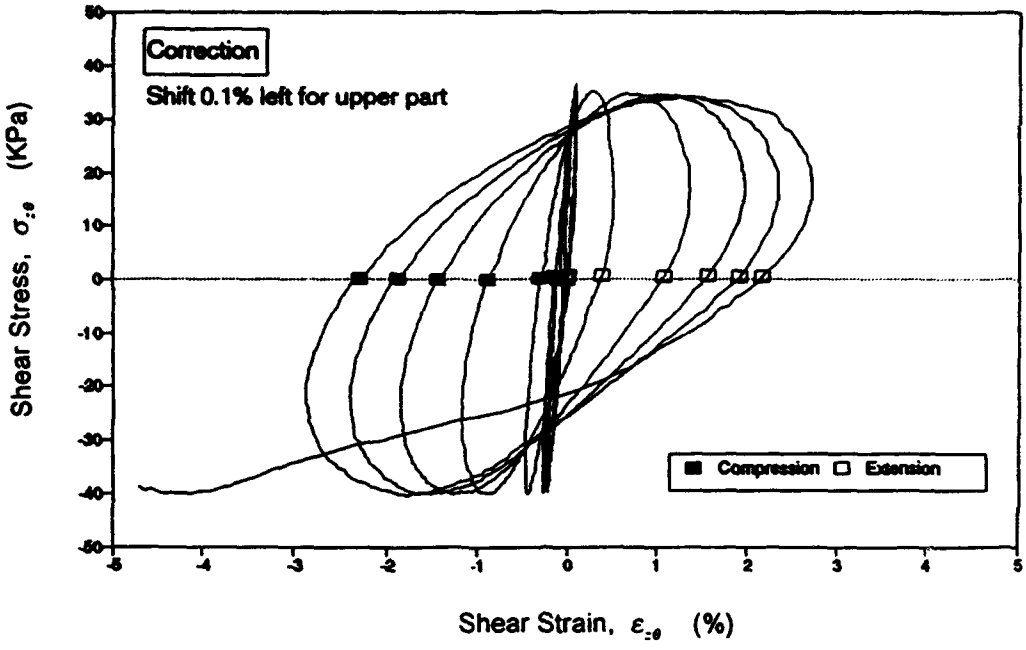

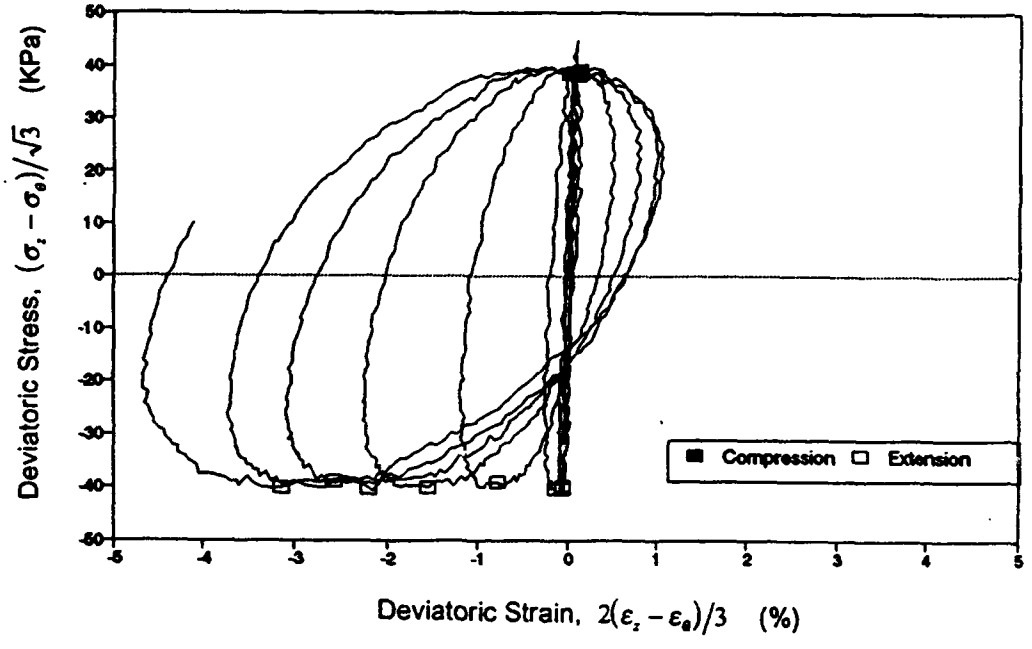

Figure 3.3.2 : Hollow Cylinder Rotational Shear Test (NR40CU50)

NR40CU50 : UNDRAINED STRESS CONTROLLED ROTATIONAL SHEAR TEST

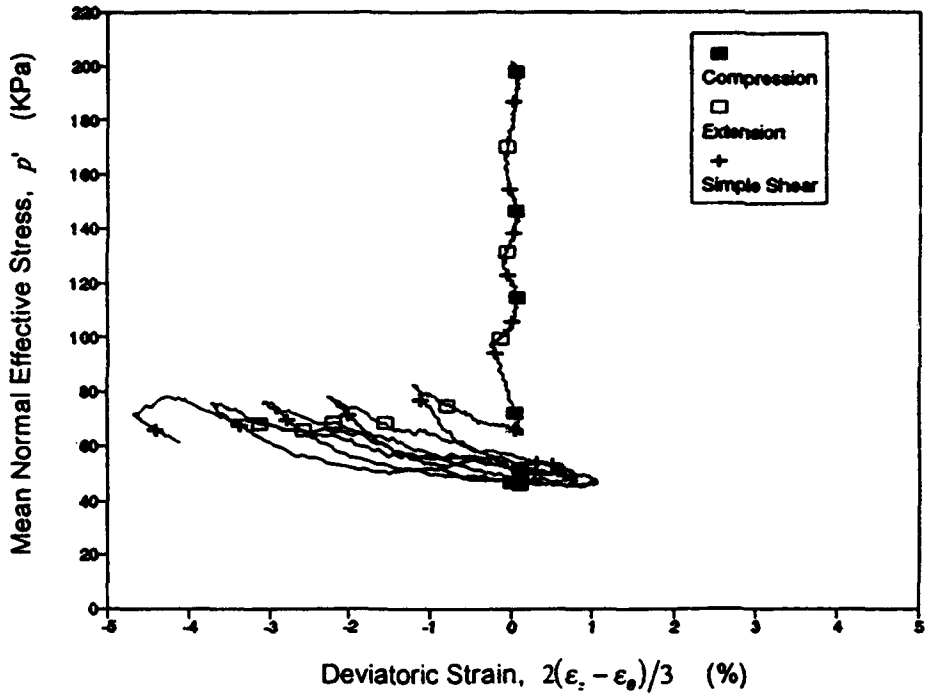

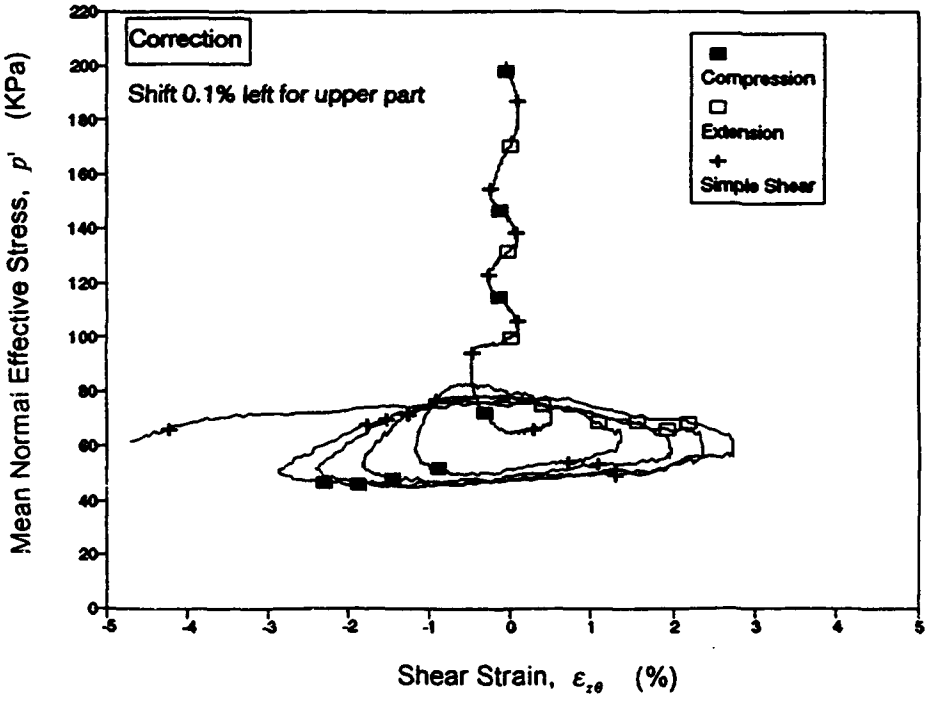

Figure 3.3.3 : Hollow Cylinder Rotational Shear Test (NR40CU50)

NR40CU50 : UNDRAINED STRESS CONTROLLED ROTATIONAL SHEAR TEST

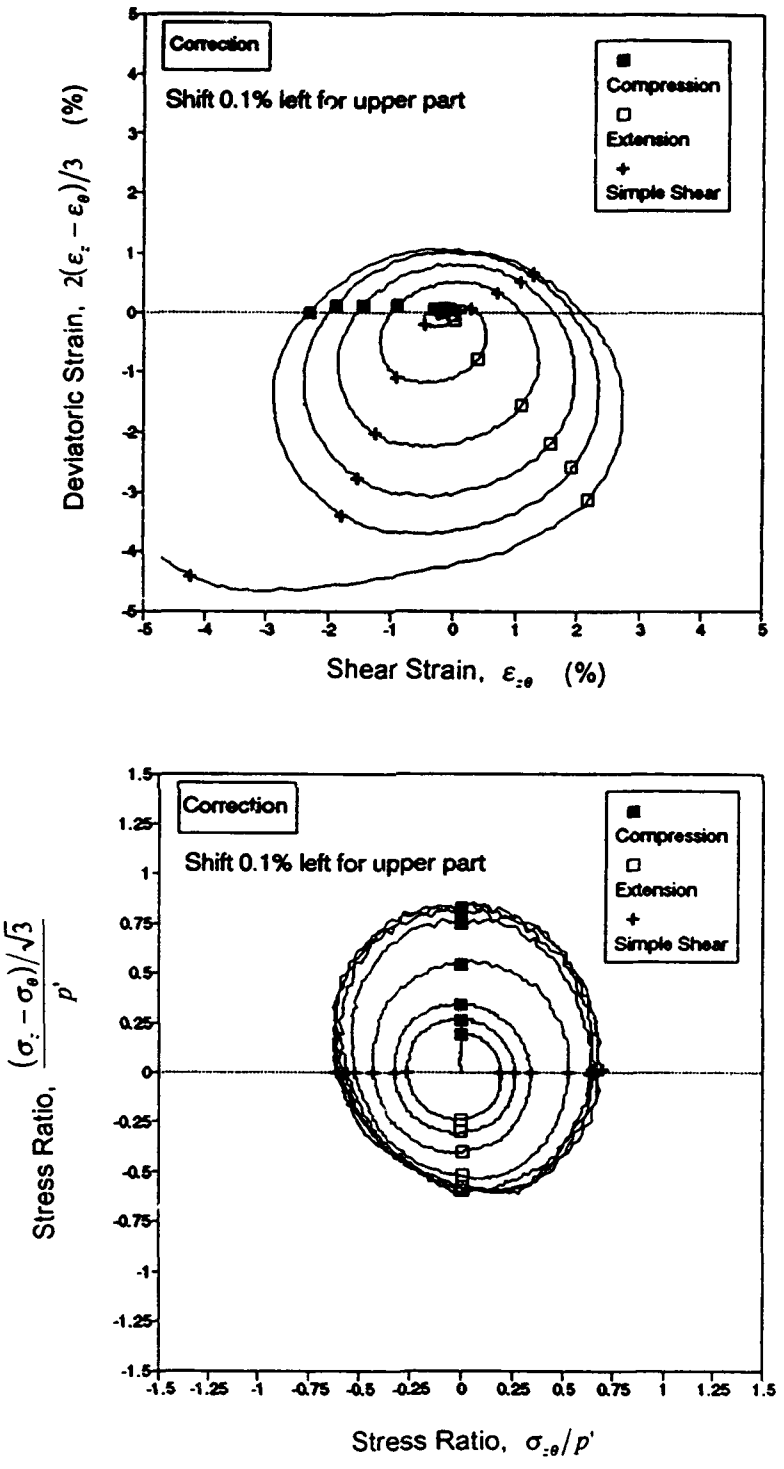

Figure 3.3.4 : Hollow Cylinder Rotational Shear Test (NR40CU50)

NR40CU50 : UNDRAINED STRESS CONTROLLED ROTATIONAL SHEAR TEST

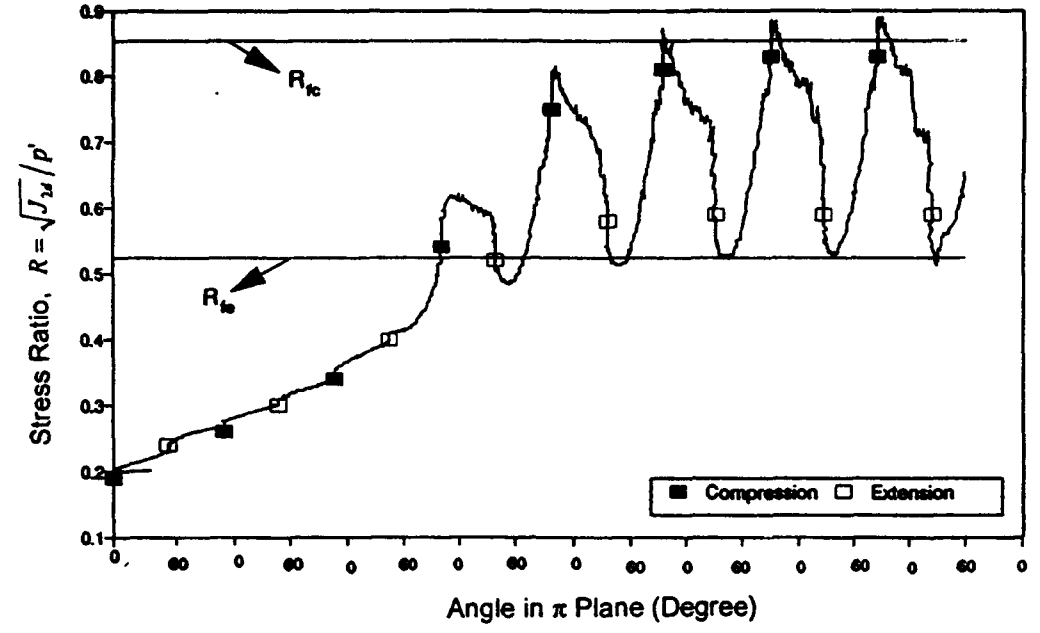

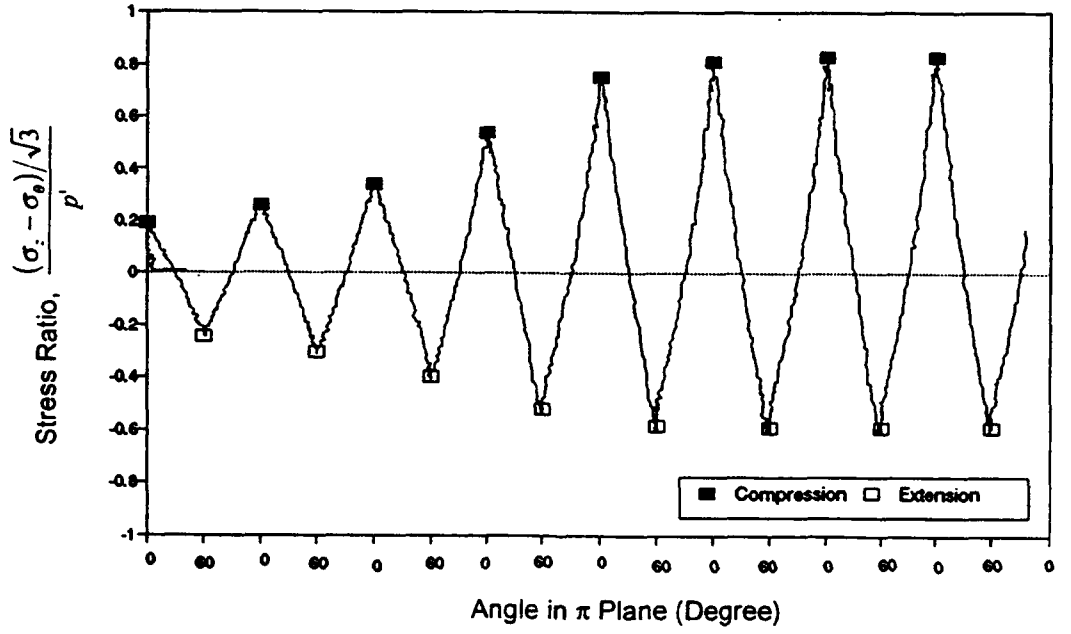

Figure 3.3.5 : Hollow Cylinder Rotational Shear Test (NR40CU50)

NR56CU50 : UNDRAINED STRESS CONTROLLED ROTATIONAL SHEAR TEST

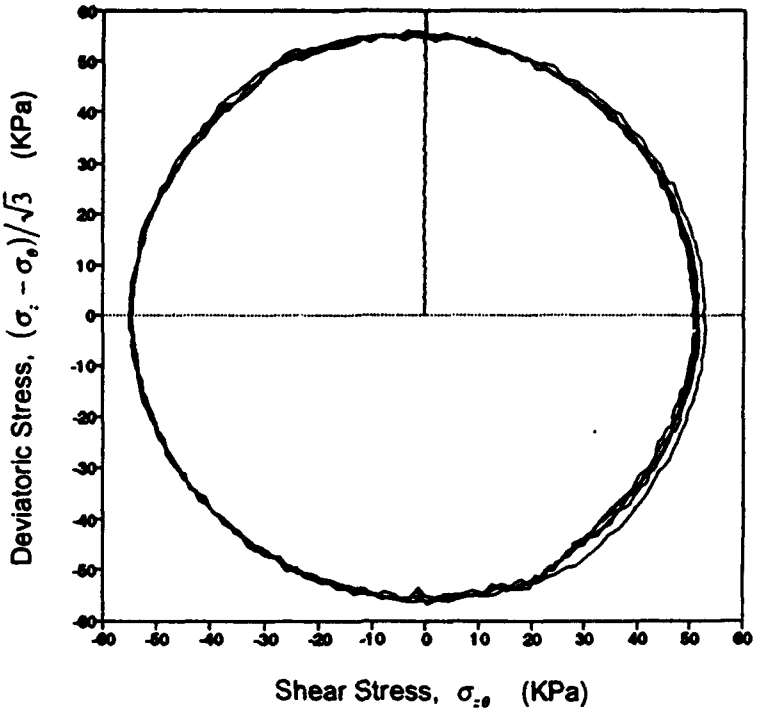

Figure 3.3.6 : Hollow Cylinder Rotational Shear Test (NR56CU50)

NR56CU50 : UNDRAINED STRESS CONTROLLED ROTATIONAL SHEAR TEST

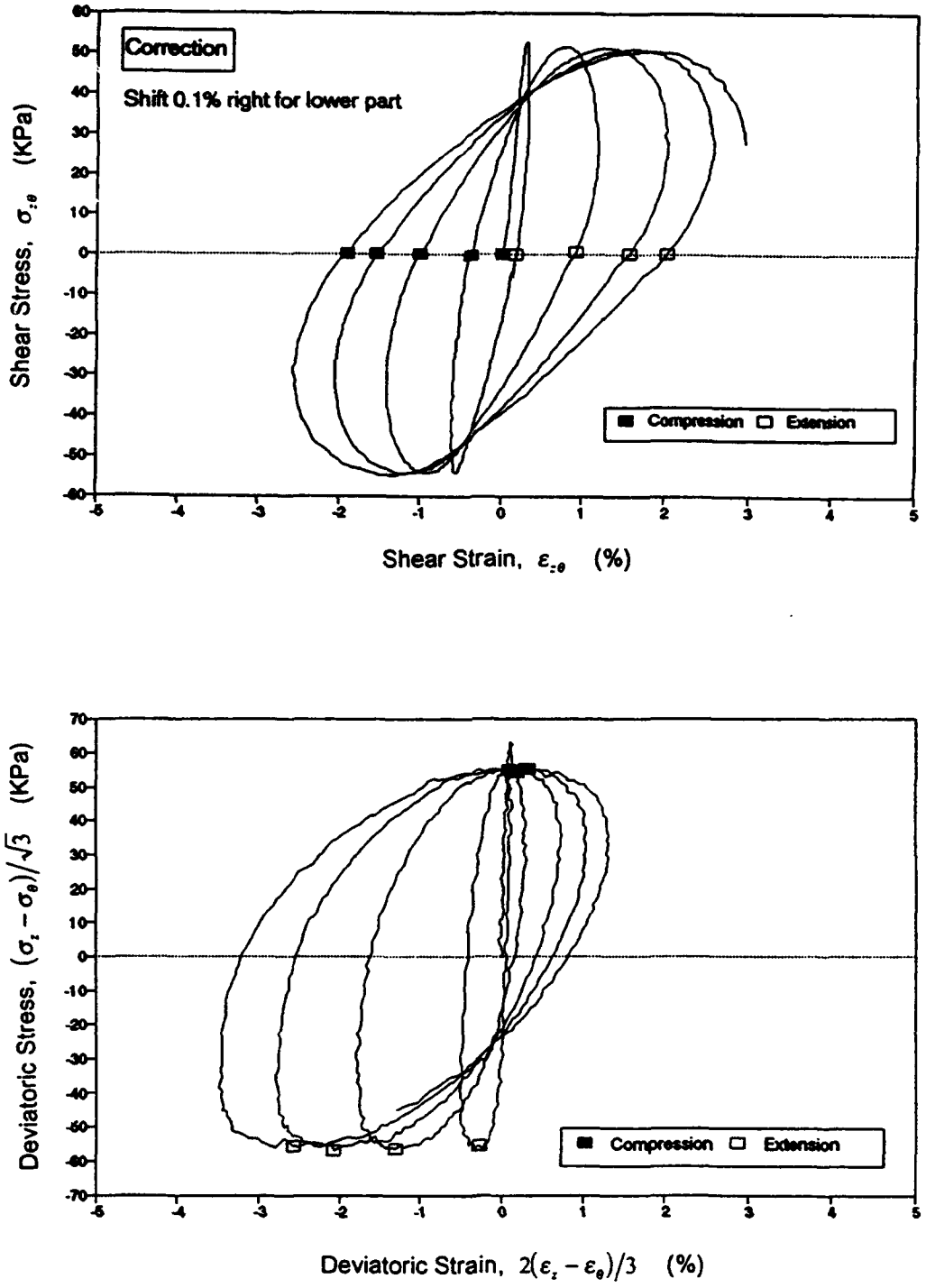

Figure 3.3.7 : Hollow Cylinder Rotational Shear Test (NR56CU50)

NR56CU50 : UNDRAINED STRESS CONTROLLED ROTATIONAL SHEAR TEST

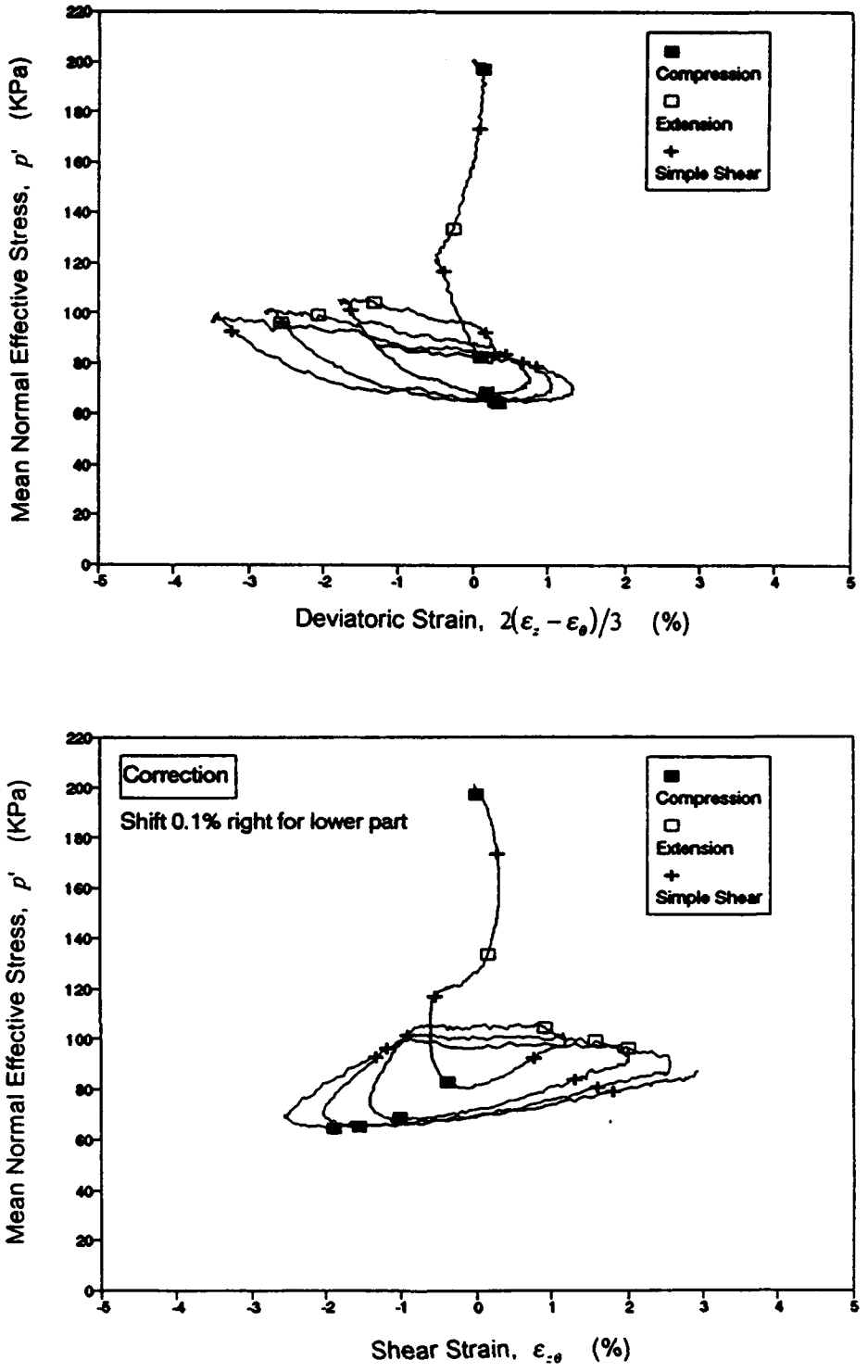

Figure 3.3.8 : Hollow Cylinder Rotational Shear Test (NR56CU50)

NR56CU50 : UNDRAINED STRESS CONTROLLED ROTATIONAL SHEAR TEST

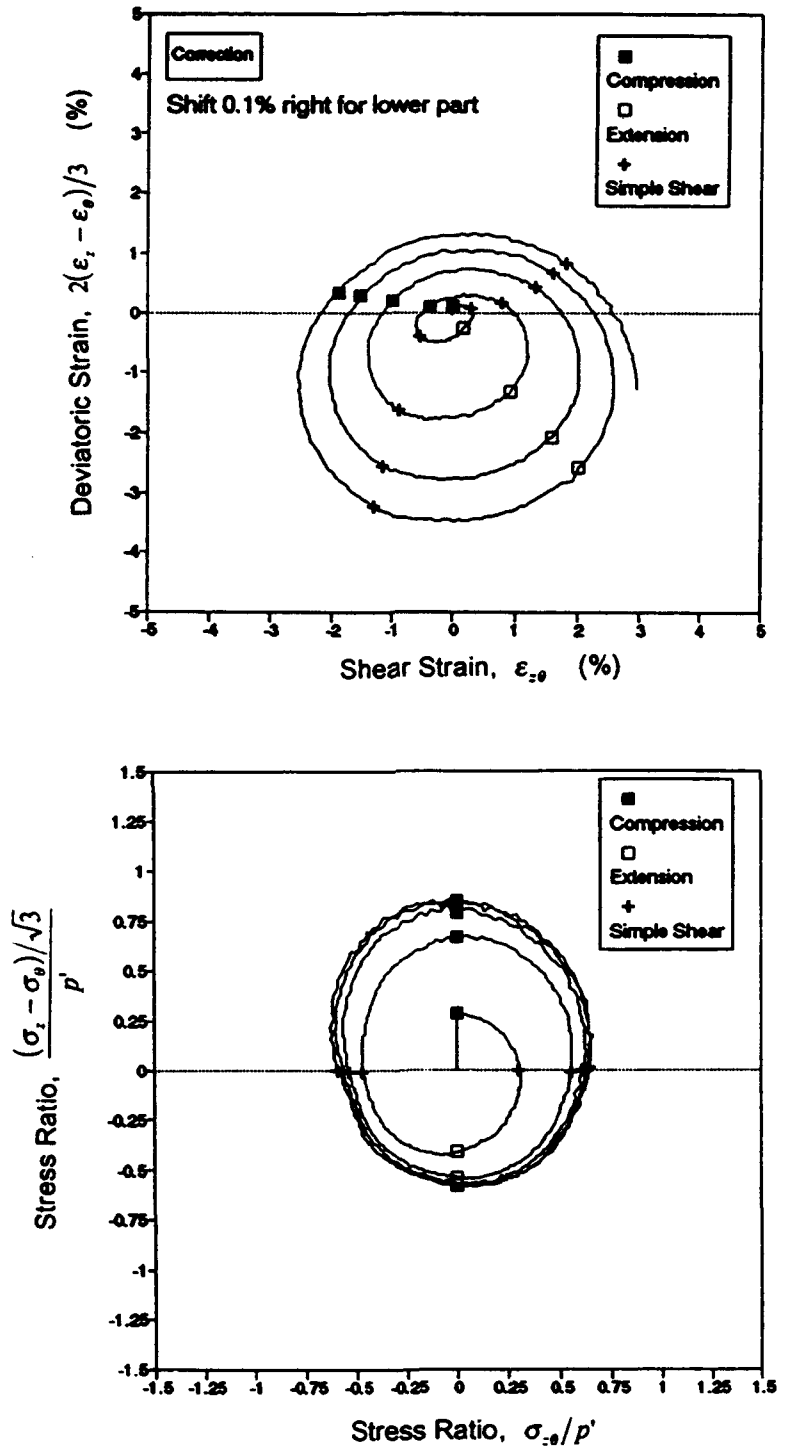

Figure 3.3.9 : Hollow Cylinder Rotational Shear Test (NR56CU50)

NR56CU50 : UNDRAINED STRESS CONTROLLED ROTATIONAL SHEAR TEST

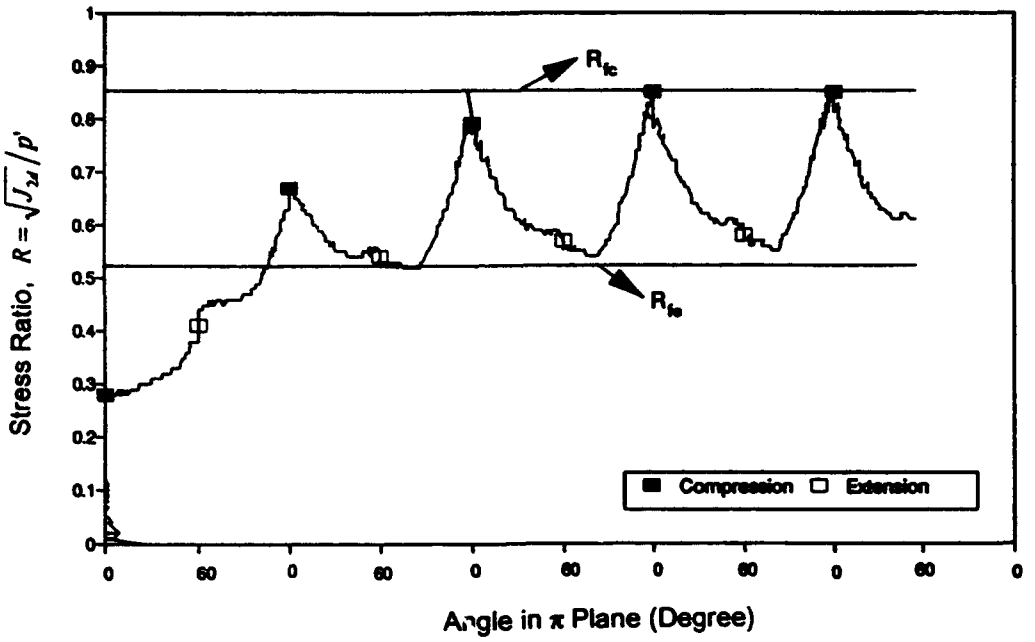

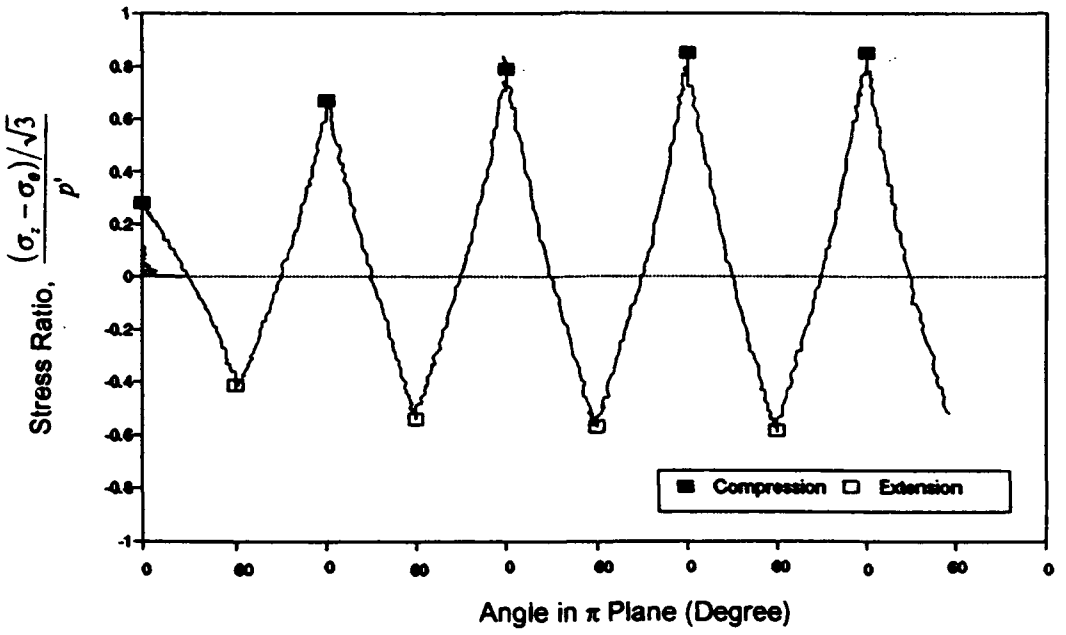

Figure 3.3.10 : Hollow Cylinder Rotational Shear Test (NR56CU50)

SUMMARY PLOTS
ON
TRIAXIAL, TORSIONAL AND ROTATIONAL SHEAR TESTS

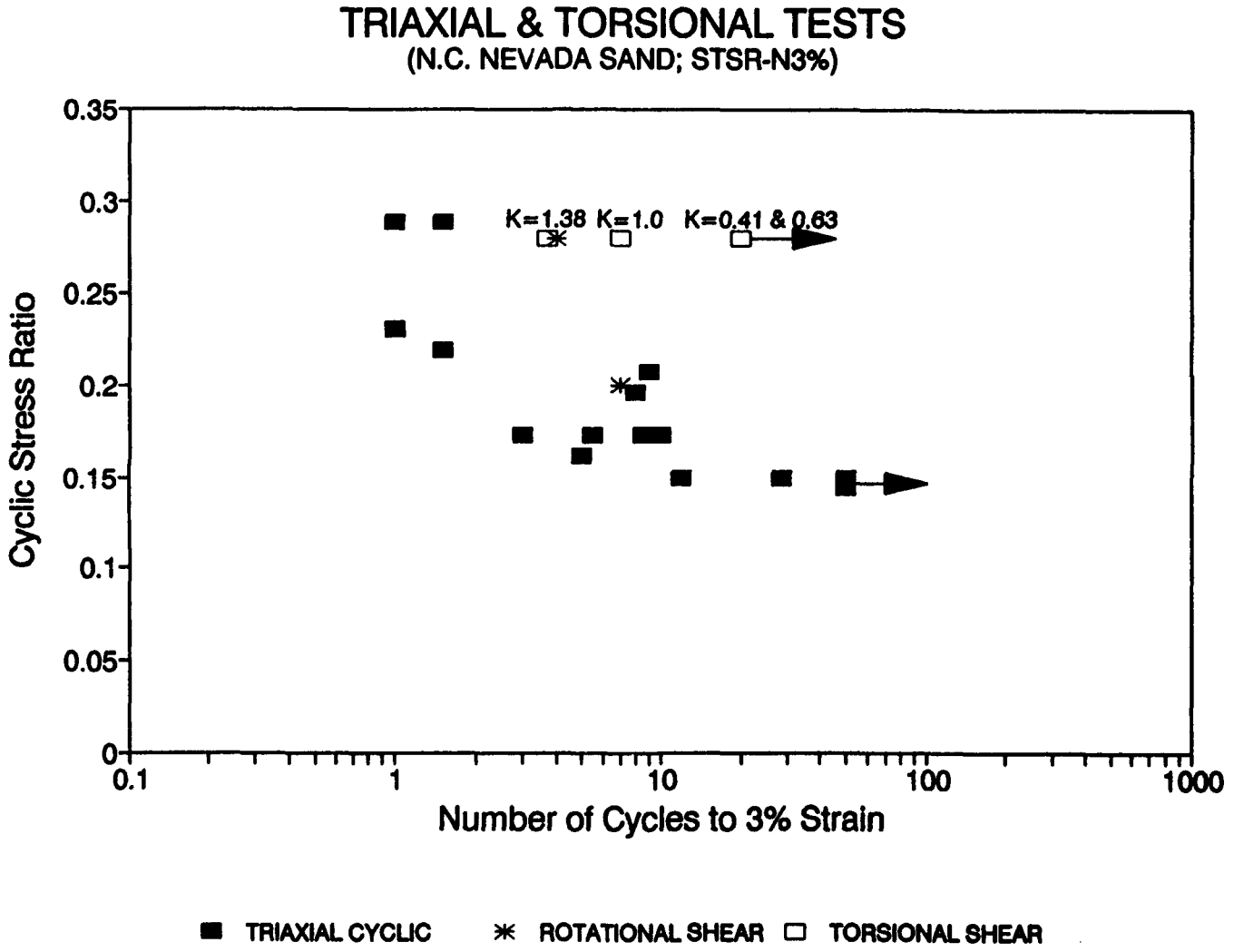

Figure 4.1 : Summary Data for Cyclic Stress Ratio Versus Number of Cycles to Cause 3% Strain in Triaxial, Torsional and Rotational Shear Tests

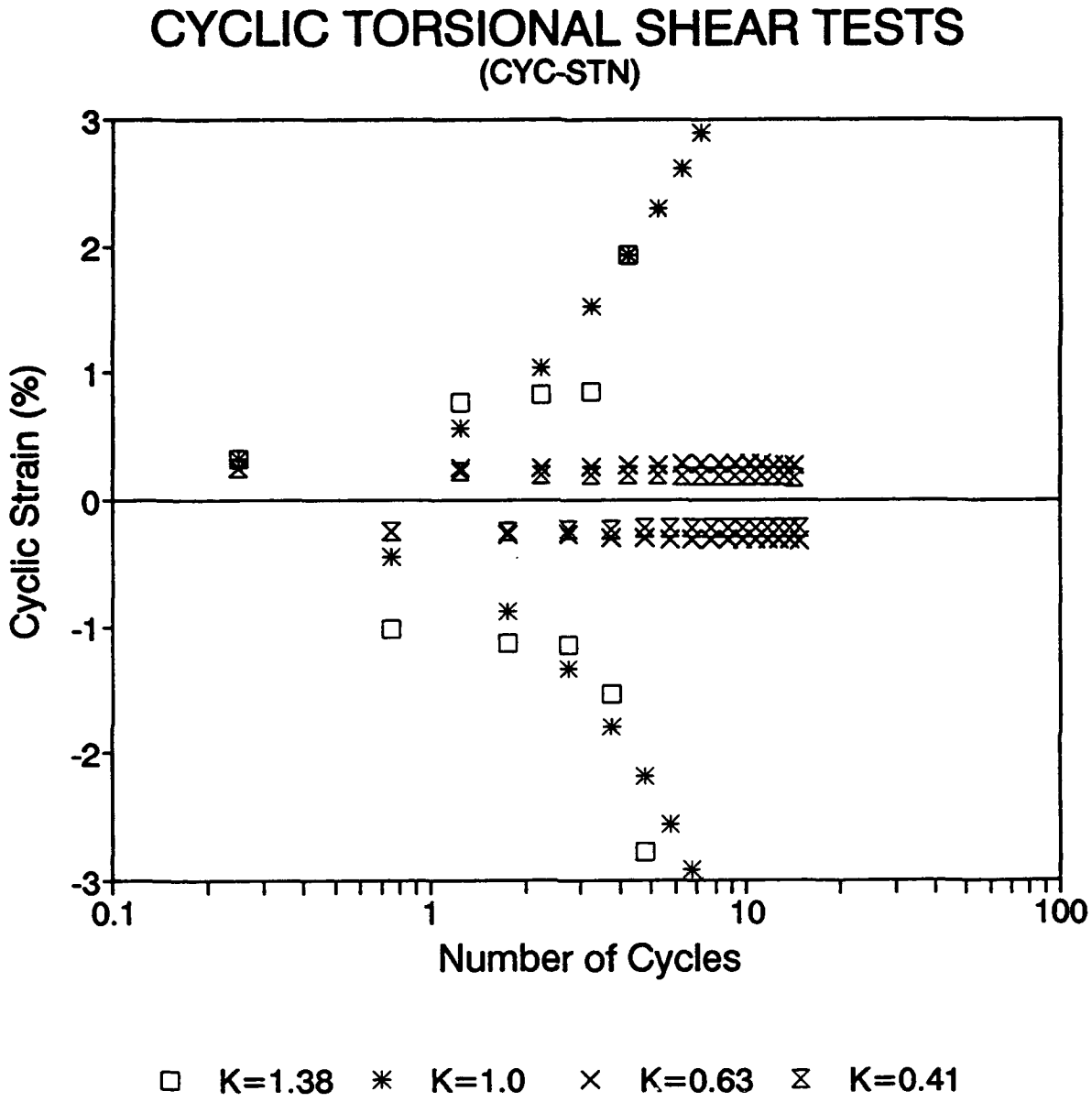

Figure 4.2 : Relationship Between Cyclic Strain and Number of Cycles in Hollow Cylinder Cyclic Torsion Shear Tests

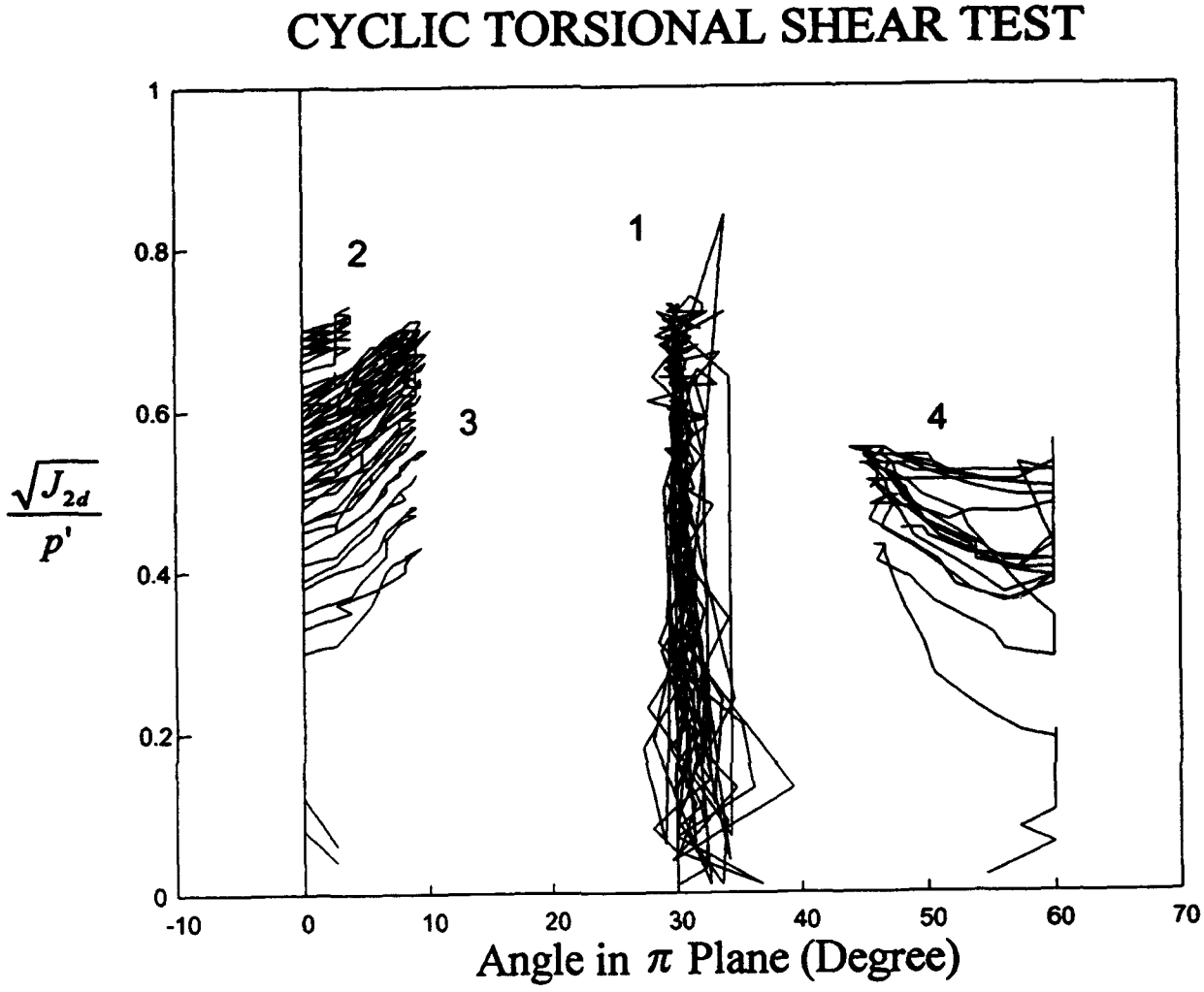

Figure 4.3 : Relationship Between Stress Ratio and Angle in π Plane for Hollow Cylinder Cyclic Torsion Shear Tests

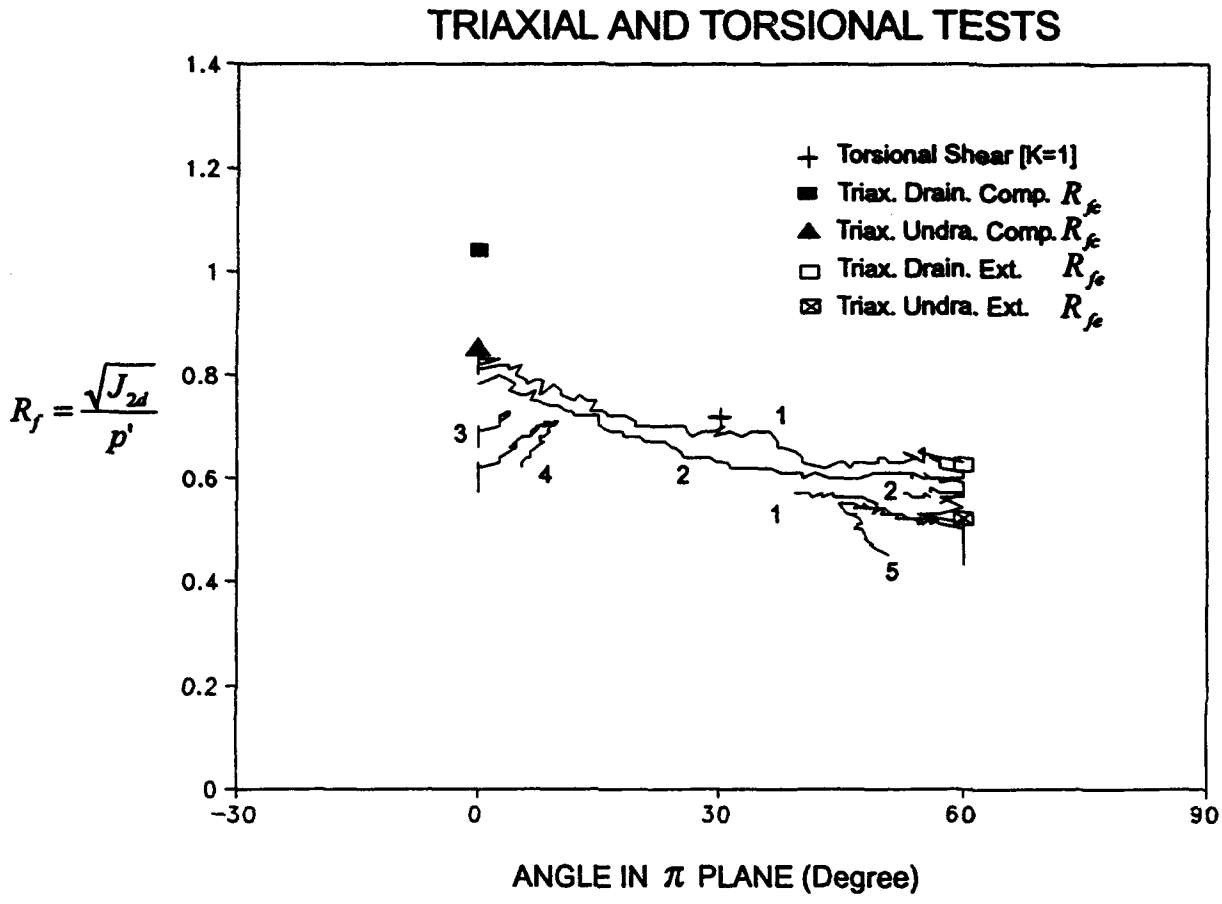

"1" : Rotational Shear ($\sqrt{J_{2d}}$ = 40 kPa)

"2" : Rotational Shear ($\sqrt{J_{2d}}$ = 56 kPa)

"3" : Torsional Shear [K=0.41]

"4" : Torsional Shear [K=0.63]

"5" : Torsional Shear [K=1.38]

(File: COMB1)

Figure 4.4 : Summary Plot for Peak Stress Ratio Versus Angle in π Plane in Triaxial and Cyclic Simple Shear Tests with Stress Paths of the Last Cycl e of Torsional and Rotational Shear Tests

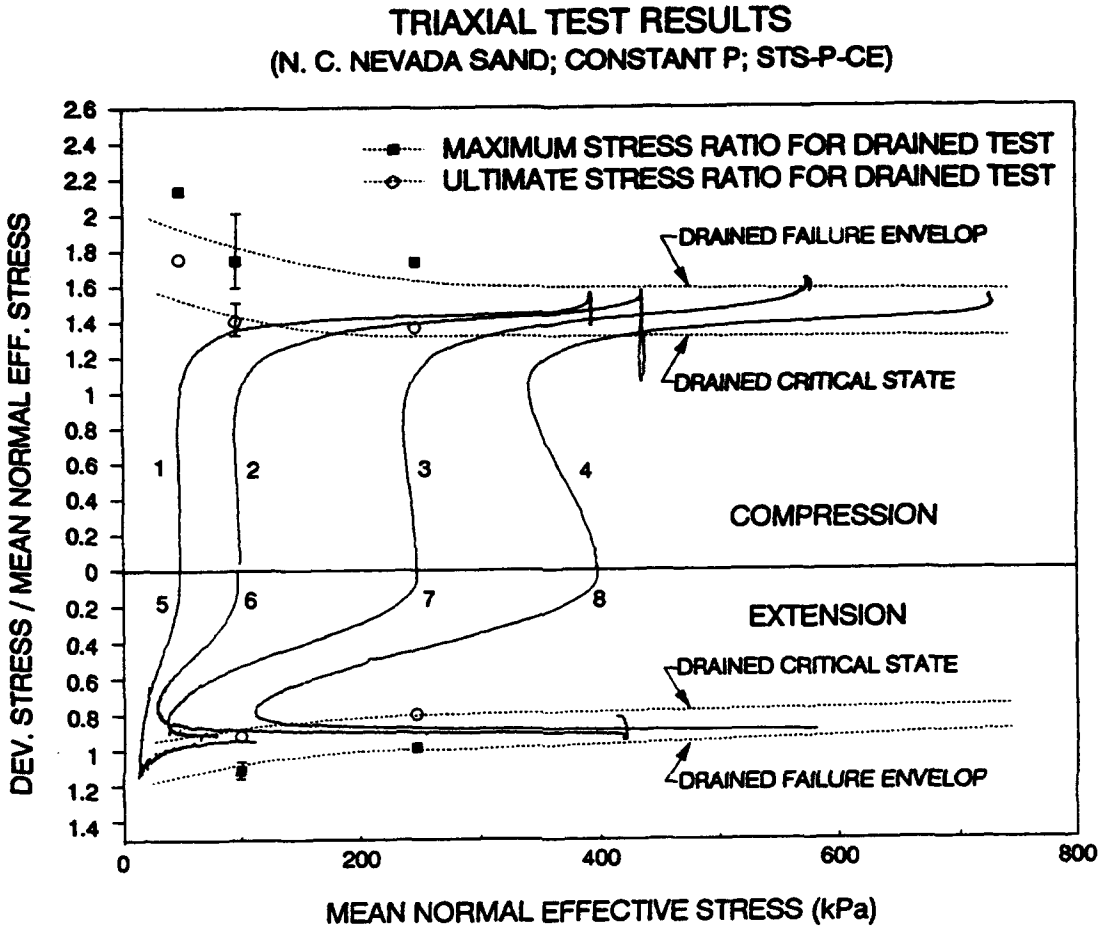

"1" : UNDRAINED STRAIN CONTROLLED TEST N50U1
"2" : UNDRAINED STRAIN CONTROLLED TEST N60U1002
"3" : UNDRAINED STRAIN CONTROLLED TEST N60U2501
"4" : UNDRAINED STRAIN CONTROLLED TEST N60U4002
"5" : UNDRAINED STRAIN CONTROLLED TEST N50U2
"6" : UNDRAINED STRAIN CONTROLLED TEST N60U1009
"7" : UNDRAINED STRAIN CONTROLLED TEST N60U2506
"8" : UNDRAINED STRAIN CONTROLLED TEST N60U4006

Figure 4.5 : Summary Plot for Stress Ratio Versus Mean Normal Effective Stress in Triaxial Compression and Extension Tests

DISTRIBUTION LIST

ADINA ENGRG, INC / WALCZAK, WATERTOWN, MA
AFOSR / NA (WU), WASHINGTON, DC
APPLIED RSCH ASSOC, INC / HIGGINS, ALBUQUERQUE, NM
APPLIED TECHNOLOGY AND MANAGEMENT / C. JONES, CHARLESTON, SC
APTEK / SCHWER, SAN JOSE, CA
ARMY / ENGR CEN, ATSE-DAC-LC, (ALLAN), FORT LEONARD WOOD, MO
ARMY BELVOIR R&D CEN / STRBE-AALO, FORT BELVOIR, VA
ARMY CECOM R&D TECH LIBRARY / ASNC-ELC-I-T, FORT MONMOUTH, NJ
ARMY CERL / CECER-FME (HAYES), CHAMPAIGN, IL
ARMY CERL / ENERGY SYS DIV, CHAMPAIGN, IL
ARMY CERL / LIB, CHAMPAIGN, IL
ARMY CORPS OF ENGRS / HQ, DAEN-ECE-D, WASHINGTON, DC
ARMY CRREL / CRREL-IC, HANOVER, NH
ARMY CRREL / ISKANDAR, HANOVER, NH
ARMY EWES / CEWES-CD-P, VICKSBURG, MS
ARMY EWES / FRANKLIN, VICKSBURG, MI
ARMY EWES / GP-EC (WEBSTER), VICKSBURG, MS
ARMY EWES / LIBRARY, VICKSBURG, MS
ARMY EWES / PERRY, VICKSBURG, MS
ARMY EWES / WES (NORMAN), VICKSBURG, MS
ARMY EWES / WES (PETERS), VICKSBURG, MS
ARMY EWES / WESCD-P (MELBY), VICKSBURG, MS
ARMY EWES / WESCP-D (VALLIANOS), VICKSBURG, MS
ARMY EWES / WESCV-Z (WHALIN), VICKSBURG, MS
ASSOCIATED SCIENTISTS / MCCOY, WOODS HOLE, MA
ATLANTIC RICHFIELD CO / RE SMITH, DALLAS, TX
BATTELLE / D. FRINK, COLUMBUS, OH
BATTELLE / RAHMAN, COLUMBUS, OH
BATTELLE NEW ENGLAND MARINE RSCH LAB / LIB, DUXBURY, MA
BECHTEL CIVIL, INC / K. MARK, SAN FRANCISCO, CA
BEN C GERWICK INC / FOTINOS, SAN FRANCISCO, CA
BING YEN AND ASSOCIATES, INC / IRVINE, CA
BRITISH EMBASSY / SCI & TECH DEPT (WILKINS), WASHINGTON, DC
BUREAU OF RECLAMATION / D-1512 (GS DEPUY), DENVER, CO
BUREAU OF RECLAMATION / MCLEAN, DENVER, CO
BUREAU OF RECLAMATION / SMOAK, DENVER, CO
CAL STATE UNIV FULLERTON / RAMSAMOOJ, FULLERTON, CA
CAL. STATE UNIV LONG BEACH / C.V. CHELAPATI, LONG BEACH, CA
CAL TECH / HUSHMAND, PASADENA, CA
CAL TECH / SCOTT, PASADENA, CA
CALTRANS / HOLLAND, SACRAMENTO, CA
CASE WESTERN RESERVE UNIV / CE DEPT (PERDIKARIS), CLEVELAND, OH
CATHOLIC UNIV / CE DEPT (KIM) WASHINGTON, DC
CENTRIC ENGINEERING SYSTEMS INC / TAYLOR, PALO ALTO, CA
CHEVRON OIL FLD RSCH CO / ALLENDER, LA HABRA, CA
CNO / DCNO, LOGS, OP-424C, WASHINGTON, DC
COGUARD / SUPERINTENDENT, NEW LONDON, CT
COLLEGE OF ENGINEERING / CE DEPT (AKINMUSURU), SOUTHFIELD, MI
COLLEGE OF ENGINEERING / CE DEPT (GRACE), SOUTHFIELD, MI

COLORADO SCHOOL OF MINES / DEPT OF ENGRG (CHUNG), GOLDEN, CO
COLORADO STATE UNIV / CE DEPT (CHARLIE), FORT COLLINS, CO
COLORADO STATE UNIV / CE DEPT (CRISWELL), FORT COLLINS, CO
CONSTRUCTION TECH LABS, INC / G. CORLEY, SKOKIE, IL
CORNELL UNIV / CIVIL & ENVIRON ENGRG, ITHACA, NY
CORNELL UNIV / LIB, ITHACA, NY
DAMES & MOORE / LIB, LOS ANGELES, CA
DOD / EXPLOS SAFETY BRD, ALEXANDRIA, VA
DOT / TRANSP SYS CEN (TONG), CAMBRIDGE, MA
DTIC / ALEXANDRIA, VA
DTRCEN / CODE 172, BETHESDA, MD
DTRCEN / CODE 1760, BETHESDA, MD
EARTH TECH / MURALEETHARAN, IRVINE, CA
EXXON PRODUCTION RSCH CO / OFFSHORE OP DIV, HOUSTON, TX
FLORIDA ATLANTIC UNIV / OCEAN ENGRG DEPT (MARTIN), BOCA RATON, FL
FLORIDA ATLANTIC UNIV / OCEAN ENGRG DEPT (SU), BOCA RATON, FL
FLORIDA ATLANTIC UNIV / OCEAN ENGRG DEPT (WOLF) BOCA RATON, FL
FLORIDA INST OF TECH / CE DEPT (KALAJIAN), MELBOURNE, FL
GEORGE WASHINGTON UNIV / ENGRG & APP SCI SCHL, WASHINGTON, DC
GEORGIA INST OF TECH / ARCH COLL (BENTON), ATLANTA, GA
GEORGIA INST OF TECH / CE SCHL (KAHN), ATLANTA, GA
GEORGIA INST OF TECH / CE SCHL (SWANGER), ATLANTA, GA
GEORGIA INST OF TECH / CE SCHL (ZURUCK), ATLANTA, GA
GEORGIA TECH / CHAMEAU, ATLANTA, GA
GEOTECHNICAL ENGRS, INC / MURDOCK, WINCHESTER, MA
GRE INC / GAFFNEY, ALBUQUERQUE, NM
HKS INC / RESENDE, PAWTUCKET, RI
HQ AFESC / RDC (DR. M. KATONA), TYNDALL AFB, FL
HUS INC / NAGTEGAAL, PAWTUCKET, RI
IOWA STATE UNIVE / CE DEPT, AMES, IA
JOHN J MC MULLEN ASSOC / LIB, NEW YORK, NY
JOHNS HOPKINS UNIV / CE DEPT, COX, BALTIMORE, MD
JOHNS HOPKINS UNIV / CE DEPT, JONES, BALTIMORE, MD
KARAGOZIAN & CASE / CRAWFORD, GLENDALE, CA
KING SAUD UNIV / AL-SHAURANI, RIYADH,
KSU / FRITCHEN, MANHATTAN, KS
LAWRENCE LIVERMORE NATIONAL LAB / MCCULLEN, LIVERMORE, CA
LAWRENCE LIVERMORE NATL LAB / FJ TOKARZ, LIVERMORE, CA
LAWRENCE LIVERMORE NATL LAB / PLANT ENGRG LIB, LIVERMORE, CA
LIN OFFSHORE ENGRG / P. CHOW, SAN FRANCISCO, CA
LOCKHEED / RSCH LAB (M. JACOBY), PALO ALTO, CA
LOCKHEED / RSCH LAB (P UNDERWOOD), PALO ALTO, CA
MC CLELLAND ENGRS, INC / LIB, HOUSTON, TX
MICHIGAN TECH UNIV / CO DEPT (HAAS), HOUGHTON, MI
MIT / WHITMAN, CAMBRIDGE, MA
NATL ACADEMY OF SCIENCES / NRC, DR. CHUNG, WASHINGTON, DC
NAVAIRWPNSTA / CODE 1018, POINT MUGU, CA
NAVCOASTSYSCEN / CO, PANAMA CITY, FL
NAVFACENGCOM / CODE 04A1D, ALEXANDRIA, VA
NAVFACENGCOM / CODE 04A3, ALEXANDRIA, VA
NAVFACENGCOM / CODE 04C2, ALEXANDRIA, VA
NAVPGSCOL / CODE 61WL (O WILSON), MONTEREY, CA
NAVSURFWARCEN COASTSYSTA / CODE 0222, PANAMA CITY, FL
NAVSWC / CODE W42 (GS HAGA), DAHLGREN, VA

NFESC / CODE ESC20, PORT HUENEME, CA
NFESC ECDET / CECILIO, WASHINGTON, DC
NOARL / CODE 440, NSTL, MS
NORDA / CODE 1121SP, NSTL, MS
NORDA / CODE 352, NSTL, MS
NORDA / CODE 363, NSTL, MS
NORDA / CODE 440, NSTL, MS
NORTHWESTERN UNIVERSITY / BAZANT, EVANSTON, IL
NRL / CODE 4430, WASHINGTON, DC
NSF / STRUC & BLDG SYSTEMS (KP CHONG), WASHINGTON, DC
NUSC DET / NEWPORT, RI
NUSC DET / CODE 44 (MUNN), NEW LONDON, CT
NUSC DET / DOC LIB, NEW LONDON, CT
OCNR / CODE 10P4 (KOSTOFF), ARLINGTON, VA
OCNR / CODE 1121 (EA SILVA), ARLINGTON, VA
OHIO STATE UNIV / BYRD POLAR RESEARCH CENTER, COLUMBUS, OH
OHIO STATE UNIVERSITY / WU, COLUMBUS, OH
ONR / CODE 1132SM, ARLINGTON, VA
OREGON STATE UNIV / CE DEPT (LEONARD), STORRS, CT
OREGON STATE UNIV / CE DEPT (YIM), CORVALLIS, OR
PENNSYLVANIA STATE UNIV / APPLIED RSCH LAB, STATE COLLEGE, PA
PMB ENGRG / LUNDBERG, SAN FRANCISCO, CA
PORT OF LA / WITTKOP, SAN PEDRO, CA
PRINCETON UNIV / PREVOST, PRINCETON, NJ
PURDUE UNIV / CE SCOL (CHEN), WEST LAFAYETTE, IN
SAN DIEGO STATE UNIV / CE DEPT (KRISHNAMOORTHY), SAN DIEGO, CA
SAN DIEGO STATE UNIV / CE DEPT (NOORANY), SAN DIEGO, CA
SANDIA NATIONAL LAB / WEINGARTEN, LIVERMORE, CA
SANDIA NATL LABS / LIB, LIVERMORE, CA
SCOPUS TECHNOLOGY INC / (B NOUR-OMID), EMERYVILLE, CA
SCRIPPS INST OF OCEANOGRAPHY / LIB, LA JOLLA, CA
SHANNON & WILSON, INC / LIB, SEATTLE, WA
SHELL OIL CO / E. DOYLE, HOUSTON, TX
SHUGAR, T A / VENTURA, CA
SOUTHWEST RSCH INST / MARCHAND, SAN ANTONIO, TX
SRI INTL / ENGRG MECH DEPT (GRANT), MENLO PARK, CA
STANFORD UNIV / CE DEPT (PENSKY), STANFORD, CA
STANFORD UNIV / DIV OF APP MECH (SIMO), STANFORD, CA
STANFORD UNIV / KIREMIDJIAM, STANFORD, CA
STATE UNIV OF NEW YORK / CE DEPT, BUFFALO, NY
TEXAS A&M UNIV / CE DEPT (NIEDZWECKI), COLLEGE STATION, TX
TEXAS A&M UNIV / OCEAN ENGR PROJ, COLLEGE STATION, TX
TRW INC / ENGR LIB, CLEVELAND, OH
TUFTS UNIV / SANAYEI, MEDFORD, MA
UNIV OF CALIFORNIA / CE DEPT (FENVES), BERKELEY, CA
UNIV OF CALIFORNIA / CE DEPT (HERRMANN), DAVIS, CA
UNIV OF CALIFORNIA / CE DEPT (KUTTER), DAVIS, CA
UNIV OF CALIFORNIA / CE DEPT (MITCHELL), BERKELEY, CA
UNIV OF CALIFORNIA / CE DEPT (RAMEY), DAVIS, CA
UNIV OF CALIFORNIA / CE DEPT (ROMSTAD), DAVIS, CA
UNIV OF CALIFORNIA / CTR FOR GEOTECH MODEL (IDRISS), DAVIS, CA
UNIV OF CALIFORNIA / INMAN, LA JOLLA, CA
UNIV OF CALIFORNIA / MECH ENGRG DEPT (TULIN), SANTA BARBARA, CA
UNIV OF CALIFORNIA / SEED, BERKELEY, CA

UNIV OF COLORADO / CE DEPT (HON-YIM KO), BOULDER, CO
UNIV OF COLORADO / STURE, BOULDER, CO
UNIV OF CONN / ACCORSI, STORRS, CT
UNIV OF CONNECTICUT / LIB, GROTON, CT
UNIV OF DELAWARE / CE DEPT, NEWARK, DE
UNIV OF HAWAII / CE DEPT (CHIU), HONOLULU, HI
UNIV OF HAWAII / MANOA, LIB, HONOLULU, HI
UNIV OF HAWAII / OCEAN ENGRG DEPT (ERTEKIN), HONOLULU, HI
UNIV OF HAWAII / RIGGS, HONOLULU, HI
UNIV OF ILLINOIS / GHABOUSSI, URBANA, IL
UNIV OF ILLINOIS / METZ REF RM, URBANA, IL
UNIV OF N CAROLINA / CE DEPT (GUPTA), RALEIGH, NC
UNIV OF N CAROLINA / CE DEPT (TUNG), RALEIGH, NC
UNIV OF NEVADA / SIDDHARTAN, RENO, NV
UNIV OF NEW MEXICO / NMERI, HL SCHREYER, ALBUQUERQUE, NM
UNIV OF RHODE ISLAND / CE DEPT (KARAMANLIDIS), KINGSTON, RI
UNIV OF RHODE ISLAND / CE DEPT (KOVACS), KINGSTON, RI
UNIV OF RHODE ISLAND / CE DEPT (LEE), KINGSTON, RI
UNIV OF RHODE ISLAND / CE DEPT (TSIATAS), KINGSTON, RI
UNIV OF SOUTHERN CALIFORNIA / JEAN-PIERRE BARDET, LOS ANGELES, CA
UNIV OF TEXAS / CE DEPT (STOKOE), AUSTIN, TX
UNIV OF TEXAS / ROESSET, AUSTIN, TX
UNIV OF WASHINGTON / CE DEPT (KRAMER), SEATTLE, WA
UNIV OF WASHINGTON / CE DEPT (MATTOCK), SEATTLE, WA
UNIV OF WISCONSIN / GREAT LAKES STUDIES CEN, MILWAUKEE, WI
UNIV OF WYOMING / CIVIL ENGRG DEPT, LARAMIE, WY
US COE / WALZ, WASHINGTON, DC
US GEOLOGICAL SURVEY / MARINE GEOLOGICAL OFFC, RESTON, VA
US NUCLEAR REGULATORY COMMISSION / KIM, WASHINGTON, DC
USA CERL / WALASZEK, CHAMPAIGN, IL
USACOE / CESPD-CO-EQ, SAN FRANCISCO, CA
USNA / OCEAN ENGRG DEPT, ANNAPOLIS, MD
WEIDLINGER ASSOC / F.S. WONG, LOS ALTOS, CA
WISS, JANNEY, ELSTNER, & ASSOC / DW PFEIFER, NORTHBROOK, IL
WOODWARD CLYDE CONSULTANTS / MORIWAKI, SANTA ANA, CA
WOODWARD-CLYDE CONSULTANTS / R. CROSS, OAKLAND, CA
WOODWARD-CLYDE CONSULTANTS / SCOTT, DENVER, CO
WOODWARD-CLYDE CONSULTANTS / WEST REG, LIB, OAKLAND, CA